NNLO QCD Corrections to Higgs Plus One Jet Production

Dissertation

zur

Erlangung der naturwissenschaftlichen Doktorwürde
(Dr. sc. nat.)

vorgelegt der

Mathematisch-naturwissenschaftlichen Fakultät

der

Universität Zürich

von

Matthieu Jaquier

aus

Villars-Le-Comte VD

Promotionskomitee

Prof. Dr. Thomas Gehrmann (Vorsitz)
Prof. Dr. Stefano Pozzorini
PD. Dr. Massimiliano Grazzini

Zürich,2015

Contents

1 Introduction **4**

2 Theory **8**
2.1 Elements of QCD . . . 9
2.2 Higgs mechanism . . . 10
2.3 Higgs effective field theory . . . 12
2.4 Experimental setup . . . 13
2.4.1 Colliders . . . 13
2.4.2 Detectors and kinematic variables . . . 14
2.5 Collider observables . . . 15
2.5.1 Partial amplitudes and colour ordering . . . 16
2.5.2 Jet selection . . . 17
2.6 Higher orders . . . 18
2.7 Renormalisation . . . 19
2.8 Infrared divergences of colour ordered QCD matrix elements . . . 20
2.8.1 Infrared behaviour in unresolved phase-space regions . . . 21
2.8.2 Infrared behaviour in loop diagrams . . . 23
2.8.3 Infrared cancellation . . . 24
2.9 Mass factorisation . . . 24
2.10 Subtraction terms . . . 26
2.11 Monte-Carlo integration . . . 27

3 Two-loop helicity amplitudes for H $\to$ 3 partons **29**
3.1 Tensor structures, helicity amplitudes and projectors . . . 30
3.1.1 The general tensor for $H \to ggg$ . . . 30
3.1.2 The general tensor for $H \to q\bar{q}g$ . . . 32
3.1.3 Helicity amplitudes . . . 33
3.2 REDUZE and master integrals . . . 34
3.3 Feynman diagrammatic calculation . . . 36
3.4 Results . . . 37
3.4.1 Infrared factorisation . . . 38
3.5 Application to two-loop splitting amplitudes . . . 39

4 Antenna subtraction **41**
4.1 Antenna functions . . . 41
4.2 Real subtraction term . . . 42
4.2.1 Final-final kinematics . . . 43
4.2.2 Initial-final kinematics . . . 44
4.2.3 Initial-initial kinematics . . . 46

4.3 Integrated subtraction terms and mass factorisation . . . 47
4.4 NLO subtraction for N_F=0 $H + 1J$ . . . 48
4.5 NNLO subtraction . . . 51
4.5.1 Double-real contribution . . . 52
4.5.2 Real-virtual contribution . . . 54
4.5.3 Double-virtual contribution . . . 57
4.6 Subtraction terms for $H + 1J$ . . . 58

5 Implementation **61**
5.1 Code . . . 61
5.1.1 Phase-space generator . . . 62
5.1.2 Matrix elements . . . 63
5.1.3 Antennae . . . 66
5.1.4 Jet function, coupling and PDF's . . . 66
5.1.5 Convolutions . . . 67
5.1.6 Scale variation . . . 69
5.1.7 Binning . . . 71
5.2 Experimental setup and runs . . . 72
5.2.1 Experimental parameters . . . 72
5.2.2 Warmup runs . . . 72
5.2.3 Run parameters . . . 73
5.2.4 Post processing . . . 73

6 Validation **74**
6.1 Internal checks . . . 74
6.2 Comparison with Madgraph5/MCFM-6.6 . . . 76

7 Results **77**
7.1 Total cross section . . . 77
7.1.1 Differential distributions . . . 78
7.2 Comparison with ATLAS . . . 80

8 Conclusions and outlook **84**

A NNLO subtraction terms **86**
A.1 The double-real IIFFF terms . . . 86
A.2 The double-real IFIFF terms . . . 87
A.3 The IIFFF large angle soft terms . . . 89
A.4 The IFIFF large angle soft terms . . . 90
A.5 The real-virtual IIFF subtraction terms . . . 91
A.6 The real-virtual IFIF subtraction terms . . . 92
A.7 The double-virtual term . . . 94
A.7.1 The full subtraction term . . . 94
A.7.2 The $\mathbf{J}_3^{(1)}$ term . . . 94
A.7.3 The $\mathbf{J}_3^{(1)} \otimes \mathbf{J}_3^{(1)}$ term . . . 95
A.7.4 The $\mathbf{J}_3^{(2)}$ term . . . 96

B Integrated LAS **97**

C PDF weights **98**

Chapter 1

Introduction

The comissioning of the large hadron collider (LHC) has marked the onset of a new era of precision in high-energy physics. In 2010-2013, the general-purpose experiments CMS and ATLAS have each delivered ~ 5 fb^{-1} of data at a center-of-mass energy of 7 TeV and ~ 20 fb^{-1} at 8 TeV. This has allowed to probe the standard model (SM) of particle physics and deviations thereof at an unprecedented level of precision and lifted the energy frontier for searches for new physics. Most notably, it has led to the discovery of a new neutral scalar boson with a mass of 125 GeV [1, 2]. The compatibility of this new particle with the SM Higgs boson has been established [3] and later confirmed by refined analyses [4–6].

The Higgs boson emerges as a byproduct of the mechanism of spontaneous symmetry breaking, which confers a mass to the SM particles in a gauge invariant way [7]. Its discovery completes the SM and ensures its validity as a predictive theory. Some questions however remain unanswered by now which call for new physical content. Various observations indicate that visible matter constitutes only a small fraction of the total mass present in the universe [8]. The exact nature of the remaining 'dark matter' is the object of active research and many models which provide a candidate particle are under investigation [9–11]. Another issue is the difference between the weak mass scale $m_{\mathrm{EW}} \sim 10^3$ GeV and the other fundamental mass scale, $M_{\mathrm{Planck}} \sim 10^{18}$ GeV, at which gravity becomes strongly interacting. In absence of new physics, the squared Higgs boson mass receives virtual corrections proportional to M^2_{Planck}. To obtain the measured Higgs boson mass would require an amount of fine-tuning between the bare mass and the quantum corrections which appears hardly justifiable [12]. One therefore expects the onset of physics beyond the standard model (BSM) around the electroweak scale to protect the Higgs boson mass from such large corrections. A variety of models has been proposed to implement such interactions, amongst which supersymmetric models [9] and composite Higgs models, which are extensions of technicolor models [11], are the most promising. These BSM models feature additional particles which carry the new interactions and fix their properties such as to achieve consistence with the SM at low energies. Such particles are expected at energies around 1 TeV and their observation would be a breakthrough towards a more fundamental theory. On the other hand new physics models differ in particular in the way electroweak symmetry breaking is implemented, sometimes involving several Higgs bosons. Precision studies of the properties of the newly discovered boson might therefore yield hints regarding the nature of BSM physics. In particular, measurements of its spin, charge and parity as well as its coupling to other SM particles can lead to a better understanding of the mechanism of spontaneous symmetry breaking and have become a priority in the LHC research programme.

A major obstacle for Higgs studies at the LHC is that the signal is overwhelmed by the background from quantum chromodynamics (QCD) processes. In order to increase the signal-to-background ratio, increasingly sophisticated techniques have been developed which rely on the

knowledge of the kinematical characteristics of the relevant processes. These techniques consist on one hand in investigating production and decay channels whose specific signature allow for a better detection and event reconstruction, and on the other hand in restricting the scrutiny to phase-space regions where the background is known to be more modest w.r.t. the signal. One of the most common variables used in this respect is the transverse momentum $p_{\mathrm{T,H}}$ of the Higgs boson. In the vector boson fusion (VBF) production channel $VV \to H$, the V bosons are recoiling against a quark pair and the Higgs boson receives a p_{T} of the order of M_{V}. In the gluon fusion channel the initial state gluons have a negligible transverse momentum, and the p_{T} of the Higgs boson is associated with its production together with a QCD jet against which it recoils. The applications of the $p_{\mathrm{T,H}}$ spectrum in the background rejection for Higgs studies are manifold. For instance, when considering the production of a Higgs boson via vector boson fusion followed by its decay into a W boson pair it has become customary to apply a veto on highly transverse jets in order to get rid of the dominating $t\bar{t}$ background [1, 2, 13]. This restriction on the jet kinematics has of course also an effect on the signal itself. In order to assess this effect, a good understanding of the $H + 1J$ process is essential. A further example is the binning of the signal according to the number of jets as is being done for instance when studying the $H \to WW$ decay channel [1, 2, 14]. Since the final states of distinct jet multiplicity suffer from different backgrounds, the possibility to apply dedicated selection cuts to the individual bins substantially improves the background rejection. It appears however that the samples of different multiplicities are correlated due to migration of events between the jet bins [15]. In order to take account of it in a consistent way in the evaluation of the perturbative uncertainty, it becomes important to know the $H+0J$ and $H+1J$ predictions at the same level of theoretical precision. This is in particular the case since final states with $H + 0J$ and $H + 1J$ contribute to roughly equal amount in many Higgs studies. The Higgs boson p_{T} spectrum also comes into play in situations where it is required to be produced with high transverse momentum. This is the case when investigating $H \to b\bar{b}$ decays, which can be tagged by studying the substructure of the fat jet which emerges in boosted Higgs boson decays [16].

In the SM the different Higgs production channels contribute to final states of different jet multiplicities. While gluon fusion mainly contributes to zero- and one-jet final states, Higgs plus two jets final states receive a significant contribution from VBF and associate Higgs production (VH). For higher jet multiplicities $t\bar{t}H$ production becomes increasingly important. The study of jets and their multiplicities in Higgs boson production thus allows to probe the different Higgs production mechanisms. In the LHC run II, ~ 300 fb^{-1} of data are expected to be recorded. This will lower the statistical uncertainty of the measured observables, and in order to keep track with the increasing precision of experimental measurements, higher orders in the perturbative expansion will be needed on the theory side.

At the LHC, the dominant Higgs boson production mode is gluon fusion, where the interaction is mediated through a quark loop. Since the coupling of the Higgs boson to fermions is proportional to their masses, the interaction effectively amounts to the top quark contribution [17]. In the $m_{\mathrm{t}} \to \infty$ limit, the top quark loop can be integrated out, which yields an effective theory where the loop-induced interaction between the Higgs boson and gluons has been replaced by point-like effective vertices [18]. The use of this effective field theory (EFT) represents a substantial computational gain, since it allows to reduce the number of loops in a calculation by one, however it is only valid as long as the scales involved in the process are smaller than $2m_{\mathrm{t}}$ [19]. The fully inclusive cross section for $pp \to H$ has been calculated in gluon fusion in the full theory up to the next-to-leading order (NLO), where the NLO correction has been observed to be large [20]. Using the EFT, the same computation has been performed at NLO [21] and next-to-next-to-leading order (NNLO) [22] accuracy, which established the convergence of the perturbative prediction. The cross section has also been computed differentially including the

Higgs boson decay to two photons or two weak gauge bosons [23, 25]. On the other hand, the differential cross section for $pp \to H + 1J$ and its contribution to the $p_{\mathrm{T,H}}$ spectrum are known only at LO in the full theory [19]. At NLO its computation has been carried out using the EFT [26] and supplemented by $\frac{1}{m_t^2}$ effects [27], leading again to large NLO corrections.

At leading order in gluon fusion the $pp \to H + 1J$ cross section is given at α_s^3 by the squared $gg \to gH$ and $q\overline{q} \to gH$ amplitudes as well as crossings of the latter. This work documents the computation of its NNLO α_s^5 correction using the EFT, where the cross section is computed inclusively in the number of jets but fully differentially otherwise. At this order in α_s three contributions enter the calculation. The first one is the squared amplitudes for the scattering of a Higgs boson and five partons at tree-level [28] (here and in the following the number of loops refers to the one using the EFT). Compact expressions have been obtained for these using MHV techniques [29]. The second ingredient is the one-loop Higgs plus four partons amplitudes, for which analytical expressions have been obtained using unitarity methods [30]. They contribute to the computation in terms of interferences with their tree-level counterparts. The third contribution encompasses interferences of two-loop and tree-level Higgs plus three parton amplitudes as well as the corresponding squared one-loop amplitudes. The latter are known [31], while the two-loop amplitudes are the genuine new ingredient and one of the main results of this work. The main bottleneck for loop calculations is the integration over the loop momentum. Due to the high tensorial rank of Feynman rules involving gluons, gluonic amplitudes in particular require the evaluation of a large number of integrals. The standard procedure is then to use integration-by-parts identities [32, 33] to relate them to a small basis of master integrals. Recently, all master integrals with three massless and one massive external leg have become available at two loops [34, 35], such as to make possible the computation of the $H \to$ 3 partons amplitudes at this loop order [36].

In order to obtain a cross section out of these three ingredients, the integration over their final state phase-space and the convolution with the parton distribution functions (PDF) needs to be performed. Due to the complexity of the phase-space, itself subjected to constraints from the definition of the experimental observable, an analytical treatment is not appropriate. The integration is thus performed numerically in terms of a parton-level event generator. Its core consists of a FORTRAN implementation of the VEGAS adaptive Monte Carlo (MC) integration algorithm [37]. Based on it a program has been developed which evaluates the fully inclusive cross section and generates distributions in various user-defined kinematical variables on the fly. The decay of the Higgs boson to two photons is built in and the inclusion of other decay modes is feasible. Modifications of the phase-space restrictions can be implemented in a straightforward manner, which confers a great flexibility to the program and allows for the study of various experimental observables to be performed.

It is well-known that the contributions to higher order corrections involving massless particles in the final state are separately infrared (IR) divergent and that only their sum is finite and well-defined. While the UV-renormalised loop amplitudes display an explicit pole structure, the divergent behaviour of real radiation contributions depends on the kinematical configuration and manifests itself only after integration over the phase-space. Since a numerical integration is spoiled by these implicit divergences, a subtraction formalism is needed to extract them from the real matrix elements and add them back in integrated form to the virtual interferences. In this way the individual contributions are rendered finite and integrable over the whole phase-space and the numerical integration may be safely performed. Several subtraction formalisms have been successfully applied to compute NNLO observables. Q_{T}-subtraction [38] is restricted to colourless final states and uses the well known resummation of small-p_{T} contributions to approximate real radiation corrections. It has been applied to Higgs boson production [25], vector boson production [39], associated VH-production [40], photon pair production [41] and

top quark decay [42]. Sector decomposition [43] performs an iterated decomposition of the final state phase-space to disentangle and isolate the loop and unresolved divergences, and numerically cancels their coefficient without the need of actual subtraction terms. This has been applied to Higgs boson production [24,44,45] and vector boson production [46]. STRIPPER [47], combines the ideas of sector decomposition and residue subtraction and has been applied to top quark pair production [48]. The subtraction formalism used in this work is antenna subtraction [49–52], which has been used at NNLO for $e^+e^- \to 3$ jets [53, 54] as well as gluons-only dijet [55] and $H + 1J$ production [56]. Finally, an independent STRIPPER-like formalism [57] has been used at NNLO for fully differential top quark decay [58] as well as an independent computation of $H + 1J$ [59]. This will allow for a benchmarking of the performance of the different subtraction formalisms.

This work is organised as follows. In chapter 2, some important theoretical concepts are reviewed and some notation established. In chapter 3, the computation of the two-loop helicity amplitudes for $H \to 3$ partons is outlined. In chapter 4, the antenna subtraction formalism is explained and its application to the $H + 1J$ process is sketched. In chapter 5, some essential concepts of the implementation of the parton-level event generator are listed. Chapter 6 details the validation of the program. Results are displayed in chapter 7 and chapter 8 concludes.

Chapter 2

Theory

In this chapter the theory underlying to the computation is shortly rewieved and some notation is fixed.
Matter in its microscopic state is described in terms of elementary particles subjected to certain forces. The dynamics are controlled by the Schrödinger equation, in which the physical rules governing the behaviour of matter and its interaction with radiation is implemented in terms of a Hamiltonian (or equivalently a Lagrangian) operator. It is well-known that this equation is not solvable exactly. However, an approximation which captures the dominant features of the solution can be obtained using perturbation theory. This provides a picture in terms of a classical solution and quantum corrections on top of it. The corrections are organised as a series in the coupling which quantifies the strenght of the respective interaction. The validity of the perturbative approach thus depends crucially on the value of the coupling which itself depends on the energy scale of the process. In energy ranges where perturbation theory breaks down, phenomena may still be qualitatively described by nonperturbative models based on reasonable assumptions.
In practical calculations, the perturbative solution of the Schrödinger equation for a certain interaction can either be written as a Dyson series or a Feynman path integral. Both formalisms lead to an expression in terms of spacetime processes involving a definite set of particles. For these, a diagrammatic representation can be given in terms of modular building blocks, called Feynman rules, which can be obtained from the Lagrangian corresponding to the respective interaction. Assembling the Feynman rules correctly ultimately leads to the cross section σ, which describes the probability for that interaction to take place.
The structure of the Lagrangian $\mathcal{L}$ is based on very general principles. Renormalisability (see sec. 2.7) together with dimensional analysis, puts an upper bound on the number of fields which may appear in a particular term of $\mathcal{L}$. It has furthermore turned out that physical laws are invariant under local gauge transformations. These can be understood as rotations in the space spanned by the charges connected with a certain force. Imposing this symmetry on $\mathcal{L}$, together with renormalisability, yields tight constraints which leave only Lagrangians with a particular structure and a finite number of terms. In particular this yields a finite set of Feynman rules.
In the following some aspects of gauge theory and perturbative computations are detailed, with emphasis on the theory of the strong nuclear force, quantum chromodynamics, and the Higgs mechanism. The theory of electroweak (EW) forces, altough mentioned, is not a topic of this work and will not be further treated. Together with QCD and the Higgs mechanism this forms the standard model of particle physics, the by now most successful attempt to describe the fundamental structure of matter and forces.

2.1 Elements of QCD

The idea of a substructure of protons and neutrons appeared around the 1960's. At that time, several new particles had been discovered in scattering experiments, raising the need to organise them into some theoretical structure. It was discovered that this 'particle zoo' could be classified into multiplets of the special unitary Lie group $SU(3)$. Following this insight, three new elementary particles, called 'quarks' (or, initially, 'partons'), were postulated in the fundamental representation of $SU(3)$. The members of the particle zoo were thought of as composed of quarks and called 'hadrons'. These were further classified as 'baryons', fermionic particles being built out of three quarks and to which protons and neutrons belong, and 'mesons', being composed of a quark-antiquark pair and obeying Bose-Einstein statistics. The quarks would carry fractional electrical charges $\pm\frac{1}{3}$ or $\pm\frac{2}{3}$ and have spin $\frac{1}{2}$.
At high energies, inelastic lepton-hadron or hadron-hadron scattering could then be described in terms of incoherent elastic scattering with the hadron's quark constituents. This necessitates the knowledge of how the momentum of a hadron is shared among the quarks. To this end so-called parton distribution functions (PDF) were introduced, which represent the probability to find inside a hadron a parton with a certain identity (flavour) and a certain fraction of the hadron's momentum. They are obtained from fits to experimental data.
This picture described hadron spectroscopy rather well, but led to a problem when considering baryons like the Ω^-. This spin-$\frac{3}{2}$-particle had a fully symmetric wavefunction, which was in contradiction to the Fermi-Dirac statistics it obeyed to. The solution of this problem consisted in introducing a new 'colour' quantum number carried by the quarks and represented by the three charges 'red', 'green' and 'blue'. The requirement of fully antisymmetric wavefunctions for the hadrons then translates as the colour wavefunction behaving as a singlet under $SU(3)$ transformations. This new colour symmetry is not to be confused with the $SU(3)$ flavour symmetry. The colour symmetry of the quarks implies that they cannot be observed as single particles and rather remain confined inside the hadrons. Nevertheless, over the time indirect experimental evidence gave strong support to this new model. The observation of scaling in proton-electron deep inelastic scattering (DIS) data hinted towards the hypothesis of nucleon substructure. The Callan-Gross relation holding experimentally between proton structure functions confirmed the fermionic nature of the quarks and their fractional charges successfully described the observed ratio

$$R = \frac{\sigma(e^+e^- \to \text{hadrons})}{\sigma(e^+e^- \to \mu^+\mu^-)}, \tag{2.1}$$

in electron-positron annihilation. This also confirmed the presence of a new degree of freedom which can take three values. Further experimental results were to confirm these observations. On the other hand it turned out that the $SU(3)$ flavour symmetry is not an exact symmetry of the theory. Six quark flavours are now known: up-, charm- and top quarks have a charge of $+\frac{2}{3}$, while down-, strange- and bottom quarks are $-\frac{1}{3}$-charged. Still, the up- down- and strange quarks are very light in comparison to the other three, such that their mass is often neglected. In this limit, flavour $SU(3)$ can be considered as an approximative symmetry of the Lagrangian. These experimental results motivated a field theoretical formulation of this model. Taking the colour quantum numbers of the quarks seriously as the charges of a colour field, one can work out the Lagrangian of QCD [60, 61],

$$\mathcal{L}_{QCD} = \mathcal{L}_{\text{quarks}} + \mathcal{L}_{\text{gauge}} + \mathcal{L}_{\text{gauge fix}} + \mathcal{L}_{\text{ghost}}. \tag{2.2}$$

The quark and gauge parts are ($\not{p} = p^\mu\gamma_\mu$) :

$$\mathcal{L}_{\text{quarks}} = \overline{q}_i(x)\big(i\not{D}_{ij} - m\delta_{ij}\big)q_j(x), \qquad (2.3) \qquad \mathcal{L}_{\text{gauge}} = -\frac{1}{4}F^a_{\mu\nu}F^{a,\mu\nu}, \qquad (2.5)$$

$$D^\mu_{ij} = \partial^\mu\delta_{ij} + ig_s A^\mu_a T^a_{ij}, \qquad (2.4) \qquad F^a_{\mu\nu} = \partial_\mu A^a_\nu - \partial_\nu A^a_\mu - g_s f^{abc}A^b_\mu A^c_\nu, \qquad (2.6)$$

where indices appearing pairwise are being summed over. For the sake of generality the number of colours is kept as N_C. The Lagrangian $\mathcal{L}_{QCD}$ is then invariant under a $SU(N_C)$ transformation, which is characterised by the generators T^a_{ij} and the structure constants f^{abc}, defined through the relation $[T^a, T^b]_{ij} = if^{abc}T^c_{ij}$. The indices i, j run over the N_C dimensions of the fundamental representation, to which the quark and antiquark fields $q_i, \overline{q}_i$ belong, while the colour gauge fields A^a_μ live in the $(N_C^2 - 1)$-dimensional adjoint representation and are labeled by the corresponding indices a, b, c. The covariant derivative D^μ_{ij} in $\mathcal{L}_{\text{quarks}}$ guarantees that it is invariant not only under a global but also under a local gauge transformation $\exp(\theta(x)_a T^a)$. The dynamics of the gauge field, represented by a new massless coloured particle called gluon, is encapsulated in the field strength tensor $F^a_{\mu\nu}$. The strength of the interaction is given by the strong coupling constant α_s respectively the gauge coupling $g_s = \sqrt{4\pi\alpha_s}$.
It turns out that $\mathcal{L}_{\text{gauge}}$ is ill-defined, since the gauge field exists in an infinite number of configurations which are equivalent under gauge transformations. In order to remove this degeneracy, one introduces two further contributions

$$\mathcal{L}_{\text{gauge fix}} = -\frac{1}{2\xi}f(A)^a f(A)^a, \qquad (2.7)$$

$$\mathcal{L}_{\text{ghost}} = \partial_\mu\eta^{a,\dagger}\big(\partial^\mu\delta^{ab} + g_s f_{abc}A^{c,\mu}\big)\eta^b. \qquad (2.8)$$

In $\mathcal{L}_{\text{gauge fix}}$, the function $f(A)^a$ implements a condition which fixes the gauge via $f(A)^a = 0$. Popular gauges are the covariant gauges $f(A)^a = \partial_\mu A^{a,\mu}$ and the axial gauges $f(A)^a = n \cdot A^a$. The gauge fixing condition still leaves some gauging freedom which is parametrised by the variable ξ. The procedure which leads to $\mathcal{L}_{\text{gauge fix}}$ requires the introduction of a further unphysical 'ghost' field [62]. These are Lorentz scalars but obey to Fermi-Dirac statistics, and are represented by Grassmannian numbers η^a. They don't appear as external particles but only inside loops, where they cancel unphysical polarisations of the gluons.
The complete Lagrangian $\mathcal{L}_{QCD}$ then describes a gauge-invariant theory of strong interactions and allows for perturbative predictions of QCD processes. This is done as already mentioned with Feynman rules derived from the Lagrangian.

2.2 Higgs mechanism

In contrast to QCD, the electroweak Lagrangian implements a $SU(2)_L \otimes U(1)_Y$ symmetry [63]. The gauge part is given by

$$\begin{aligned}\mathcal{L}_{\text{gauge}} &= -\frac{1}{4}W^{\alpha,\mu\nu}W^\alpha_{\mu\nu} - \frac{1}{4}B^{\mu\nu}B_{\mu\nu},\\ W^\alpha_{\mu\nu} &= \partial_\mu W^\alpha_\nu - \partial_\nu W^\alpha_\mu - g_W\epsilon^{\alpha\beta\gamma}W^\beta_\mu W^\gamma_\nu,\\ B_{\mu\nu} &= \partial_\mu B_\nu - \partial_\nu B_\mu,\end{aligned} \qquad (2.9)$$

with the massless $SU(2)_L$ gauge field triplet $W^{\alpha,\mu}$, $SU(2)_L$ gauge coupling g_W and $U(1)_Y$ gauge field B_μ. The interaction with matter is implemented in a similar way than in eq. (2.3) via the $SU(2)$ field doublet and the covariant derivative

$$\psi^l_{i,L} = \begin{pmatrix}\nu_l\\ l\end{pmatrix}_L = \left(\frac{1-\gamma_5}{2}\right)\begin{pmatrix}\nu_l\\ l\end{pmatrix} \quad , \quad D^\mu_{ij} = \delta_{ij}\partial^\mu + ig_W(T\cdot W^\mu)_{ij} + iY\delta_{ij}g'_W B^\mu, \qquad (2.10)$$

where g'_W is the $U(1)_Y$ gauge coupling, Y the weak hypercharge and T^α_{ij} are a representation of the $SU(2)_L$ weak isospin algebra.
The Higgs mechanism [7] addresses the problem that a mass term for the gauge bosons $\propto m^2W^2$ would violate gauge symmetry. The solution is to keep the symmetry at the Lagrangian level, while working with an effective theory with a lower degree of symmetry. The symmetry is broken by the ground state of the theory, while expanding around it yields the effective theory. This is done with the mechanism of spontaneous symmetry breaking. A new piece is added to the Lagrangian:

$$\phi_i = \begin{pmatrix} \phi^+ \\ \phi^0 \end{pmatrix} \quad , \qquad \mathcal{L}_{\text{Higgs}} = \big(iD^\mu \cdot \phi\big)^\dagger \big(iD_\mu \cdot \phi\big) - \mathcal{V}\big(\phi^\dagger\phi\big), \tag{2.11}$$

$$\mathcal{V}\big(\phi^\dagger\phi\big) = \mu^2\phi^\dagger\phi + \lambda\big(\phi^\dagger\phi\big)^2, \tag{2.12}$$

where in the most simple formulation ϕ_i is a complex scalar doublet. The potential $\mathcal{V}$ is symmetric under $SU(2)_L \otimes U(1)_Y$, however for the choice of parameters $\mu^2 < 0$, $\lambda > 0$, its minimum is not at $\phi_i = 0$. Rather one has a subset of degenerate minima given by

$$|\phi| = \sqrt{\frac{\mu^2}{2\lambda}} = \frac{v}{\sqrt{2}}. \tag{2.13}$$

The choice of a particular vacuum state among this subset spontaneously breaks the original symmetry. It can be chosen as

$$\langle\phi\rangle = \frac{1}{\sqrt{2}} \begin{pmatrix} 0 \\ v \end{pmatrix}. \tag{2.14}$$

This choice of vacuum breaks the $SU(2)_L \otimes U(1)_Y$ symmetry but preserves a $U(1)_Q$ subgroup, where $Q = T_3 + \frac{Y}{2}$ is the electric charge. This ensures that the photon remains massless. One can then parametrise quantum fluctuations around this vacuum as

$$\phi_i = \exp\big(-iT\cdot\xi\big)_{ij} \begin{pmatrix} 0 \\ \frac{\big(H(x)+v\big)}{\sqrt{(2)}} \end{pmatrix}. \tag{2.15}$$

In particular, the three Goldstone bosons ξ^a correspond to the three degrees of freedom of the broken symmetry subgroup. Inserting this into eq. (2.11), one obtains a Lagrangian where the W^1 and W^2 components of the weak isospin gauge field triplet obtain a mass $M_W = \frac{1}{2}vg_W$ from the absorbtion of the Goldstone bosons into an additional longitudinal degree of freedom. They are recombined as

$$W^{\pm,\mu} = \frac{1}{\sqrt{2}}\big(W^{1,\mu} \mp iW^{2,\mu}\big), \tag{2.16}$$

such that in the covariant derivative, eq. (2.10), the $T\cdot W^\mu$ term becomes

$$W^{3,\mu}T_3 + \frac{1}{\sqrt{2}}W^{+,\mu}T^+ + \frac{1}{\sqrt{2}}W^{-,\mu}T^-, \tag{2.17}$$

and $T^\pm = T^1 \pm iT^2$ are the raising and lowering operators acting on the weak isospin doublets. The new Lagrangian also features a combination of the $W^{3,\mu}$ and B^μ acquiring a mass:

$$Z^\mu = -B^\mu\sin(\theta_W) + W^{3,\mu}\cos(\theta_W) \tag{2.18}$$

with the Weinberg mixing angle θ_W and $M_Z = \frac{1}{2}v\sqrt{g_W^2 + g_W'^2}$. The combination orthogonal to it,

$$A^\mu = B^\mu\cos(\theta_W) + W^{3,\mu}\sin(\theta_W) \tag{2.19}$$

remains massless and is associated with the photon. In addition, the Lagrangian now features a Higgs boson $H(x)$ with a mass $m_H = v\sqrt{2\lambda}$.
Mass terms for the fermions can be obtained through interactions of the form:

$$g^l\overline{\psi_L^l}\phi l \qquad , \qquad g^d\overline{\psi_L^{ud}}\phi d_R \qquad , \qquad \psi_L^{ud} = \begin{pmatrix} u \\ d \end{pmatrix}_L , \tag{2.20}$$

where ψ_L^l is as in eq. (2.10), and g^l, g^d are the Yukawa couplings of the lepton and the down-quark. Performing again the expansion around the vacuum state in terms of v and $H(x)$, this yields mass terms

$$\frac{g^l v}{\sqrt{2}}\bar{l}l = m^l\bar{l}l \qquad , \qquad \frac{g^d v}{\sqrt{2}}\bar{d}d = m^d\bar{d}d, \tag{2.21}$$

as well as interaction terms

$$\frac{g^l}{\sqrt{2}}h\bar{l}l = \frac{m^l}{v}h\bar{l}l \qquad , \qquad \frac{g^d}{\sqrt{2}}h\bar{d}d = \frac{m^d}{v}h\bar{d}d, \tag{2.22}$$

where the interaction strength is proportional to the mass of the fermion. The neutrino ν_l and the up-quark do not receive a mass through this terms. The up quark can be given a mass by adding a further term involving the charge conjugate doublet ϕ^c:

$$g^u\overline{\psi^{ud}}\phi^c u_R \qquad , \qquad \phi^c = i\sigma_2\phi, \tag{2.23}$$

where σ_2 is the usual Pauli matrix. The remaining quarks can be given a mass with similar terms.

2.3 Higgs effective field theory

Effective theories are a widely used tool to describe phenomena which take place at scales where they are not sensitive to the structure of a more fundamental theory defined at much higher scales. This is the case for the interaction between the Higgs boson and gluons, which is mediated by a quark loop, where the dominant contribution comes from the top quark [17] since the coupling between the Higgs boson and fermions is proportional to the mass of the latter. A scale is thus set by the mass m_t of the top quark, at which the internal structure of the top quark loop is resolved. At much lower scales, this is not the case anymore and the interaction can be seen as a point-like vertex. The effective theory is then described in terms of the Lagrangian [18]

$$\mathcal{L}_\mathrm{eff} = -\frac{H}{v}\sum_i C_i\mathcal{O}_i, \tag{2.24}$$

where the terms $\mathcal{O}_i$ depend only on the light degrees of freedom. The operator $\mathcal{O}_g = F^a_{\mu\nu}F^{a,\mu\nu}$ is of particular interest, since the corresponding term in $\mathcal{L}_\mathrm{eff}$ describes the effective interaction between the Higgs boson and gluons. The coefficients C_i can be found by matching Greens functions evaluated once in the full and once in the effective theory. This yields for C_g [64]

$$\begin{aligned} C_g = -\frac{1}{12}\frac{\alpha_s^{(6)}(\mu)}{\pi}\Bigg\{1 + \left(\frac{\alpha_s^{(6)}(\mu)}{2\pi}\right)\left[\frac{11}{2} - \frac{1}{3}\log\left(\frac{\mu_R^2}{M_\mathrm{T}^2}\right)\right] + \left(\frac{\alpha_s^{(6)}(\mu)}{2\pi}\right)^2\Bigg[\frac{2693}{72} \\ - \frac{25}{12}\log\left(\frac{\mu_R^2}{M_\mathrm{T}^2}\right) + \frac{1}{9}\log^2\left(\frac{\mu_R^2}{M_\mathrm{T}^2}\right) + n_l\Bigg(-\frac{67}{24} + \frac{4}{3}\log\left(\frac{\mu_R^2}{M_\mathrm{T}^2}\right)\Bigg)\Bigg] + \mathcal{O}(\alpha_s^3)\Bigg\}, \end{aligned} \tag{2.25}$$

where n_l is the number of light quarks, M_T is the top quark pole mass and the evolution of the strong coupling constant α_s (see sec. 2.7) involves all quark flavours. With a similar matching procedure, this can be related to the strong coupling of the effective theory whose running is determined only through the light quark flavours:

$$\alpha_s^{(5)}(\mu) = \alpha_s^{(6)}(\mu)\Bigg\{1 - \frac{\alpha_s^{(6)}(\mu)}{2\pi}\frac{1}{3}\log\left(\frac{\mu_R^2}{M_\mathrm{T}^2}\right) + \left(\frac{\alpha_s^{(6)}(\mu)}{2\pi}\right)^2\left[-\frac{7}{6} - \frac{19}{6}\log\left(\frac{\mu_R^2}{M_\mathrm{T}^2}\right) + \frac{1}{9}\log^2\left(\frac{\mu_R^2}{M_\mathrm{T}^2}\right)\right]\Bigg\}. \tag{2.26}$$

Using this relation gives the coefficient

$$C_g = -\frac{1}{12}\frac{\alpha_s^{(5)}(\mu)}{\pi}\Bigg\{1 + \left(\frac{\alpha_s^{(5)}(\mu)}{2\pi}\right)\frac{11}{2} + \left(\frac{\alpha_s^{(5)}(\mu)}{2\pi}\right)^2\left[\frac{2777}{72} + \frac{19}{4}\log\left(\frac{\mu_R^2}{M_\mathrm{T}^2}\right) + n_l\left(-\frac{67}{24} + \frac{4}{3}\log\left(\frac{\mu_R^2}{M_\mathrm{T}^2}\right)\right)\right] + \mathcal{O}(\alpha_s^3)\Bigg\}. \tag{2.27}$$

It should be noted that the effective operators $\mathcal{O}_i$ have an anomalous dimension and therefore standard RGE evolution (see secs. 2.7, 5.1.6) does not apply. The contributions proportional to $\log\left(\frac{\mu_R^2}{M_\mathrm{T}^2}\right)$ should rather be considered separately from the remaining terms when evolving an observable to a different scale, and be plainly evaluated at that scale.
This effective Lagrangian gives rise to new Feynman rules. The coupling strength between the Higgs boson and gluons is given by

$$\lambda = \frac{\alpha_s}{3\pi v} = 2^{\frac{1}{4}}\sqrt{G_F}\frac{\alpha_s}{3\pi}, \tag{2.28}$$

with the Fermi constant G_F. It should be emphasised that the running (see sec. 2.7) of λ differs at two loops from the running of α_s. The resulting renormalisation scale dependence will be discussed in sec. 3.4.

2.4 Experimental setup

Due to the nature of quantum field theory, particle physics is a fundamentally statistical science. From the theory point of view, the predictions are made in terms of probabilities for a certain process to happen. Likewise, the objects of these predictions, elementary and composite particles, cannot be manipulated and observed individually in an experiment. The experimental apparatus of particle physics are therefore statistical machines, carrying out an 'experiment' (rather, an event) a large number of times, with results in terms of total probabilities and probability distributions.

2.4.1 Colliders

Colliders are facilities where two particle beams are accelerated in opposite directions and made to cross each other at a certain interaction point. With an energy E_B of the beams, the center-of-mass (c.o.m.) energy available in a collision is $2 \cdot E_B$, in contrast to experiments where a beam hits a fixed target and where the c.o.m. energy grows like the square root of the incoming beam energy. Via the De-Broglie relation

$$\lambda = \frac{h}{|\vec{p}|}, \tag{2.29}$$

where h is Plancks constant and $\vec{p}$ and λ are the momentum and wavelength of a wavepacket, it follows that at high energies shorter wavelengths and thus a better resolution power is obtained for the probing particles.
There are two common types of colliders, which both use electric potential differences to accelerate charged particles. In a linear collider, the particle beams are crossed once after an initial acceleration in a straight beam pipe. A circular collider consists of a storage ring, in which the beams circulate and may cross each other several times. A circular collider allows for acceleration to higher energies, and provides higher luminosities, however they are limited by synchrotron radiation and represent a huge technical challenge. The particles are maintained on their trajectory by magnets, while other magnets focus the beam such as to maximise the particle density. At the LHC, for instance, the necessary magnetic fields of up to ~ 8 Tesla require superconducting magnets to be used, which need to be cooled down to ~ 2°K with liquid helium. Furthermore an ultra-high vacuum must be kept in the beam pipe to reduce unwanted scattering with air molecules.
The main characteristics of a collider are the beam energy and the luminosity. The luminosity L can be understood as a measure of the intensity of the beam and is defined as

$$R = L\sigma, \tag{2.30}$$

where σ is the cross section and R the number of interactions per second. Assuming two beams with N particles, revolution frequency f and a gaussian profile of the region of overlap between the beams with dimensions s_x and s_y, the luminosity is given as

$$L = \frac{fN^2}{4\pi s_x s_y} \tag{2.31}$$

The integral of the luminosity over time is a measure of the data provided by the collider.
One distinguishes furthermore between hadron and lepton colliders. Hadrons are composite particles made of partons, where at high enough energies elastic scattering takes not anymore place between the hadrons but rather involves individual partons. Since their momentum is only constrained to sum up to the parent hadron's momentum, but otherwise is distributed randomly, the effective partonic c.o.m. energy can take any value between 0 and $2 \cdot E_B$. Hadron colliders thus scan an energy range and are good discovery machines, but with the drawback of a huge hadronic background. Leptons on the other hand are (to current knowledge) elementary particles. Lepton-lepton collisions thus always take place at a c.o.m. energy of $2 \cdot E_B$ and suffer from much less background. Lepton colliders are thus clean precision study machines.
This work treats phenomena taking place at the LHC, a proton-proton collider with a circumference of ~ 27 km. It is designed for a c.o.m. energy of 14 TeV and a luminosity of $\sim 10^{34}$ cm^{-2}s^{-1}. It has up to present day been operated at a c.o.m. energy of up to 8 TeV. The LHC can alternatively also accelerate lead ions to study quark-gluon plasmas.

2.4.2 Detectors and kinematic variables

Detectors collect the data from scattering events in terms of the trajectories and energies of final state particles, and in some cases their identities. There are four main detectors at the LHC. While CMS and ATLAS are general-purpose detectors, ALICE is specialised towards final states of heavy-ion collisions and LHCb towards physics involving bottom- and charm quarks. CMS and ATLAS both have a cylindrical onion geometry around the interaction point. This geometry concentrates the resolution power in the regions which are transverse to the beam where the interesting high energy physics takes place. The inner detector layers consist of trackers which record the particle trajectories. This region is usually subjected to a magnetic field to allow

momentum measurements on charged particle tracks. The next layers are made of the electric and hadronic calorimeter cells which measure the energy of the corresponding particle species. The final layer is made of the muon detectors. Two endcap regions are dedicated to particles emitted close to the beam.
The particle collisions happen at relativistic energies. Furthermore, since the partons usually carry different fractions of the parent hadron's momentum, the c.o.m. frame is related to the laboratory frame by a Lorentz boost along the beam direction (which from now on is taken as the z-direction). The measurement is thus made in terms of variables which are invariant under such a boost. These are usually the transverse momenta p_{T} and the azimuthal (around the z-axis) angle ϕ of the final state particles. Furthermore the rapidity is defined as

$$y = \frac{1}{2}\log\left(\frac{E+p_z}{E-p_z}\right). \tag{2.32}$$

This variable is not Lorentz-invariant, however differences in rapidity are. In particular, the final state phase-space expressed in terms of these variables is Lorentz-invariant. For massless particles, the rapidity converges to the pseudorapidity.

$$\eta = \log\left(\cot\left(\frac{\theta}{2}\right)\right), \tag{2.33}$$

which can be related to the polar angle θ. Since the Higgs boson is massive, however, for consistency the rapidity y is used throughout this work.

2.5 Collider observables

Following the previous sections all the necessary ingredients are there to write down the quantity of interest. At leading order, the total cross section σ_{LO} for the scattering of hadrons H_1 and H_2 is

$$\sigma_{LO}(H_1,H_2) = \sum_{i,j}\int \frac{\mathrm{d}\xi_1}{\xi_1}\frac{\mathrm{d}\xi_2}{\xi_2} f_i(\xi_1,\mu^2) f_j(\xi_2,\mu^2)\mathrm{d}\hat{\sigma}_{ij,LO}(\xi_1 H_1,\xi_2 H_2). \tag{2.34}$$

It is written as a sum over all possible contributions from the scattering of partons i inside hadron H_1 and j inside hadron H_2, who carry a fraction ξ_1 and ξ_2 of the momentum of their parent hadron. The respective partonic contributions are weighted by the PDF's $f_i(\xi_1,\mu^2)$ and $f_j(\xi_2,\mu^2)$ giving the probabilities to find partons with such identity and momentum assignements in the hadrons H_1 and H_2 and then integrated over the momentum fractions, since these are not specified by kinematics. The probability for the scattering with the partons specified above to happen is given by the partonic differential cross section

$$\mathrm{d}\hat{\sigma}_{ij,LO}(\xi_1 H_1,\xi_2 H_2) = \int_{\mathrm{d}\Phi_n} \mathrm{d}\hat{\sigma}^B_{ij,LO}(\xi_1 H_1,\xi_2 H_2;p_3,\ldots,p_{n+2}) J^{(n)}_m(p_3,\ldots,p_{n+2}). \tag{2.35}$$

Here $\mathrm{d}\hat{\sigma}^B_{ij,LO}$ is the born-level differential cross section for the $ij\to n$-partons scattering. The jet function J implements the definition of the observable under investigation in a certain experiment, typically by selecting out of the n partons a number m of jets satisfying certain kinematical conditions. At leading order, one has $n=m$. The final state n-particle phase-space subjected to the jet function is then integrated over to select all kinematical configurations contributing to the observable.

2.5.1 Partial amplitudes and colour ordering

The born differential cross section can be itself written as

$$\mathrm{d}\hat{\sigma}^B_{ij,LO}(p_1,p_2;p_3,\ldots,p_n+2)=\mathcal{N}^B_{LO}\sum_n \mathrm{d}\Phi_n\frac{1}{S_n}|\mathcal{M}^{(0)}_{n+2}(p_1,p_2;p_3,\ldots,p_{n+2})|^2, \tag{2.36}$$

where $\mathcal{N}^B_{LO}$ includes all non-QCD factors. The sum is over all configurations with n partons in the final state, and S_n is the symmetry factor accounting for identical partons in a particular configuration. The n-parton phase-space $\mathrm{d}\Phi_n$ is

$$\mathrm{d}\Phi_n(p_1,p_2;p_3,\ldots,p_{n+2})=\frac{\mathrm{d}^{d-1}p_3}{2E_3(2\pi)^{d-1}}\cdots\frac{\mathrm{d}^{d-1}p_{n+2}}{2E_{n+2}(2\pi)^{d-1}}(2\pi)^d\delta^d(p_1+p_2-p_3-\ldots-p_{n+2}). \tag{2.37}$$

At tree-level, the amplitude for the n-gluons process with fixed helicities can be written as [65, 66]:

$$\mathcal{M}^{(0)}_n(\{k_i,\lambda_i,a_i\})=g_s^{n-2}\sum_{\sigma\in\frac{S_n}{Z_n}}\mathrm{Tr}(T^{a_{\sigma(1)}}\cdots T^{a_{\sigma(n)}})M^{(0)}_n(\sigma(1^{\lambda_1}),\ldots,\sigma(n^{\lambda_n})), \tag{2.38}$$

where k_i, λ_i and a_i are the gluon momenta, helicities and colour charges. $g_s=\sqrt{4\pi\alpha_s}$ is the gauge coupling and the sum is over all non-cyclic permutations of the gluon indices. The 'partial amplitudes' M^{tree}_n do not carry colour information, which is itself encapsulated in the trace over colour matrices T^{a_i}. The partial amplitudes are separately gauge invariant and colour ordered, in the sense that they receive only contributions from Feynman diagrams with a cyclic ordering of the external gluons as in the colour trace. Gluons which are represented by colour matrices inside the same colour trace are called colour-connected. If the colour matrices are adjacent, the gluons are called colour-neighbouring.

Consider the n-particle scattering process involving m $q\bar{q}$ pairs of different flavour and $n-2m=l$ gluons, where i_k and j_k label a quark respectively an antiquark connected by an internal fermion line ($k\in 1,\ldots,m$). Let $\{n_1,\ldots,n_{m-1}\}$ be a partition of the l gluon indices. The amplitude for the process is then [67, 68]

$$\begin{aligned}\mathcal{M}^{(0)}_{m,l}=&\,g_s^{n-2}\sum_{\sigma\in\frac{S_l}{Z_l}}\sum_{\{n_i\}}\sum_{\rho}\frac{(-1)^p}{N^p}\\ &\times(T^{\sigma(a_{2m+1})}\ldots T^{\sigma(a_{n_1})})_{i_1\rho(j_1)}(T^{\sigma(a_{n_1+1})}\ldots T^{\sigma(a_{n_2})})_{i_2\rho(j_2)}\ldots(T^{\sigma(a_{n_{m-1}+1})}\ldots T^{\sigma(a_n)})_{i_m\rho(j_m)}\\ &\times M^{(0)}_{m,l}(1^{\lambda_1}_q,2^{\lambda_2}_{\bar{q}},3^{\lambda_3}_Q,4^{\lambda_4}_{\bar{Q}},\ldots;\sigma((2m+1)^{\lambda_{2m+1}}),\ldots,\sigma(n^{\lambda_n}))\end{aligned} \tag{2.39}$$

The rightmost sum is over the permutations ρ of the antiquark label, where p is the signature of the permutation ρ. The middle sum is over all ways of partitioning the l gluons $\sigma(2m+1)\ldots\sigma(n)$ amongst the m quark strings defined by $i_k\rho(j_k)$. A quark string without colour matrix between the quark and antiquark indices is a kronecker delta $\delta_{i_k\rho(j_k)}$. The leftmost sum is over the non-cyclic permutation of the l gluons. The colour stripped partial amplitudes $M^{tree}_{m,l}$ are again separately gauge invariant and colour ordered. A similar picture in terms of traces of colour matrices and quark strings multiplying colour-stripped partial amplitudes can be drawn for one-loop diagrams.

In order to write eq. (2.36) one needs to square either of eqs. (2.38) or (2.39), sum over the helicities and carry out the colour algebra. The technicalities involved in these steps are the subject of many textbooks, and this knowledge is assumed here. One then obtains in general a sum of interferences between various partial amplitudes times some colour factors, according to

which it is customary to order the sum. In the leading colour approximation, only the highest power of the number of colours N_C is retained and terms $\mathcal{O}(\frac{1}{N_C^2})$ neglected. One property of the partial amplitudes is incoherence at leading colour, such that the squared matrix element is just a sum of squares of partial amplitudes. At subleading colour this is not the case anymore, however for low multiplicities one can still write the squared matrix element as a sum of squared amplitudes where one or more gluons behave in an abelian way [65, 68, 69]. Abelian gluons are not colour connected to the other gluons inside a quark string, but only to the quark and antiquark at the ends of the string.
It should be noted here that the leading order does not necessarily correspond to tree-level diagrams. The interaction between certain types of particles can only take place if it is mediated by an internal loop, in which case the leading order contribution, eq. (2.34), would consist of one-loop Feynman diagrams. The leading order is usually denoted as 'born level', while 'tree level' labels diagrams without internal loops.

2.5.2 Jet selection

In order to study the behaviour of QCD many observables with sensitivity to different topological and kinematical properties of the collision have been devised. The sometimes rather involved definition of these observables is implemented in theoretical calculations in terms of a jet function. This reflects the fact that the observed outcome of a collision involving final state partons tends to form collimated sprays of hadrons, called jets. The jet function consists of some procedure to cluster partons in the final state of a perturbative computation, respectively the hadrons as registered in a detector, into jets. Thanks to the factorising nature of QCD, the 'theoretical' jets can be related to the experimentally measured ones up to non-perturbative corrections which can be expected not to change the picture too much [70]. The jet function may also implement selection criteria as applied in an experiment to single out the jets, namely restrictions on kinematical variables such as transverse momentum p_{T}, rapidity y, azimuthal angle ϕ of the jets as well as isolation criteria.
One central requirement on the jet clustering algorithm motivated from theory is that of IR safety (see section 2.8). This states that the outcome of the application of the jet algorithm on a set of partons should not depend of radiation of further partons, if the radiation does not change the distribution of energy inside the detector. There exist several jet algorithms, amongst which sequential recombination algorithms are often used [71]. Such algorithms base on an iterative chain of steps during which partons are merged into jets according to some distance measure. In general one evaluates for each particle a particle-beam distance d_{iB} and a particle-particle distance d_{ij} for each pair of particles according to

$$\begin{aligned} \Delta R_{ij}^2 &= (y_i - y_j)^2 + (\phi_i - \phi_j)^2, \\ d_{ij} &= \min(p_{\mathrm{T},i}^{2p}, p_{\mathrm{T},j}^{2p}) \frac{\Delta R_{ij}^2}{R^2} \\ d_{iB} &= p_{\mathrm{T},i}^{2p}, \end{aligned} \tag{2.40}$$

where p is either of $\{-1, 0, 1\}$ and R is a parameter. One then finds which of the d_{iB} and d_{ij} is smallest. If it is a d_{ij}, the corresponding particles i and j are being recombined into a new particle (sometimes called 'protojet') according to some prescription, where typically the momenta p_i and p_j are just being added. If the smallest of all distances is a d_{iB}, the corresponding particle is declared a jet and taken out of the list of particles to be considered in the next iteration. These steps are then repeated until the list of particles has been exhausted. Different values of p correspond to different jet algorithms. The $p = 1$ one is called 'inclusive

k_T' algorithm [72]. When $p = 0$ one obtains the 'Cambridge/Aachen' (C/A) algorithm [73]. This is being appreciated for leading to clustering sequences which are hierarchical in the angle between the particles being clustered. This allows a correspondence to the angular ordering of parton branching as motivated by QCD and used in the simulation of non-perturbative effects through showering of the partons. Finally setting $p = -1$ gives the 'anti-k_T' algorithm [74]. Unlike the k_T and C/A algorithms, which produce jets with jagged boundaries, the anti-k_T algorithm yields geometrically clean cone-like jets. However, its clustering history cannot be related to the branching behaviour of QCD.

2.6 Higher orders

Often the leading order prediction, eq. (2.34), does not provide a sufficiently satisfying description of the experimental data. In particular, processes which contribute substantially to the cross section may rely on additional internal loops in the Feynman diagrams to mediate the corresponding interaction. Furthermore, the leading order processes correspond to the minimal number of particles necessary in the final state to satisfy the requirement on the number of jets from the jet function, which results in a one-to-one correspondence between hard partons and jets. This gives a poor description of jets which can be improved by considering interactions with additional particles in the final state. Since diagrams with more loops and legs are accompanied with higher powers of the QCD coupling due to its presence in the three- and four-parton interaction vertices, such contributions will appear as higher orders in the expansion w.r.t. the coupling constant.
The next-to-leading order (NLO) contribution to the process described by eqs. (2.34) and (2.35) is given by

$$\mathrm{d}\hat{\sigma}_{ij,NLO} = \int_{\mathrm{d}\Phi_n} \mathrm{d}\hat{\sigma}^V_{ij,NLO} J^{(n)}_n + \int_{\mathrm{d}\Phi_{n+1}} \mathrm{d}\hat{\sigma}^R_{ij,NLO} J^{(n+1)}_n, \tag{2.41}$$

where the dependence on the external momenta is understood. The virtual contribution

$$\mathrm{d}\hat{\sigma}^V_{ij,NLO} = \mathcal{N}^V_{NLO} \sum_n \mathrm{d}\Phi_n \frac{1}{S_n} |\mathcal{M}^{(1)}_{n+2} \mathcal{M}^{(0)\dagger}_{n+2} + \mathcal{M}^{(0)}_{n+2} \mathcal{M}^{(1)\dagger}_{n+2}|, \tag{2.42}$$

contains interferences between tree-level and one-loop partial amplitudes. The real radiation contribution on the other hand contains only squares of partial amplitudes for the scattering of $n + 3$ partons.
The NNLO order contribution reads

$$\mathrm{d}\hat{\sigma}_{ij,NNLO} = \int_{\mathrm{d}\Phi_n} \mathrm{d}\hat{\sigma}^{VV}_{ij,NNLO} J^{(n)}_n + \int_{\mathrm{d}\Phi_{n+1}} \mathrm{d}\hat{\sigma}^{RV}_{ij,NNLO} J^{(n+1)}_n + \int_{\mathrm{d}\Phi_{n+2}} \mathrm{d}\hat{\sigma}^{RR}_{ij,NNLO} J^{(n+2)}_n, \tag{2.43}$$

where the double-virtual contribution features interferences between two-loop and tree-level partial amplitudes as well as squares of one-loop partial amplitudes for $2 \to n$ scattering, while the real-virtual contribution consists of interferences between tree-level and one-loop partial amplitudes for $2 \to (n + 1)$ scattering,

$$\mathrm{d}\hat{\sigma}^{VV}_{ij,NNLO} = \mathcal{N}^{VV}_{NNLO} \sum_n \mathrm{d}\Phi_n \frac{1}{S_n} |\mathcal{M}^{(2)}_{n+2} \mathcal{M}^{(0)\dagger}_{n+2} + \mathcal{M}^{(1)}_{n+2} \mathcal{M}^{(1)\dagger}_{n+2} + \mathcal{M}^{(0)}_{n+2} \mathcal{M}^{(2)\dagger}_{n+2}|, \tag{2.44}$$

$$\mathrm{d}\hat{\sigma}^{RV}_{ij,NNLO} = \mathcal{N}^{RV}_{NNLO} \sum_{n+1} \mathrm{d}\Phi_{n+1} \frac{1}{S_{n+1}} |\mathcal{M}^{(1)}_{n+3} \mathcal{M}^{(0)\dagger}_{n+3} + \mathcal{M}^{(0)}_{n+3} \mathcal{M}^{(1)\dagger}_{n+3}|. \tag{2.45}$$

The double-real contribution contains squares of tree-level partial amplitudes for $2 \to (n+2)$ scattering. The full NNLO partonic differential cross section is then

$$\mathrm{d}\hat{\sigma}_{ij}^{NNLO} = \mathrm{d}\hat{\sigma}_{ij,LO} + \mathrm{d}\hat{\sigma}_{ij,NLO} + \mathrm{d}\hat{\sigma}_{ij,NNLO}, \tag{2.46}$$

and replaces $\mathrm{d}\hat{\sigma}_{ij,LO}$ in eq. (2.34). The running of the couplings and the PDF's (see secs. 2.7 and 2.9) is carried out at NNLO for all three terms.

2.7 Renormalisation

When computing virtual contributions one has to evaluate diagrams like fig. 2.1. Since the momentum k flowing through the loop is not kinematically constrained, it needs to be integrated over. The most important features are briefly recalled here. The integration over the loop momentum yields divergences, which originate from probing the process at very short distances respectively at high momentum $|k|$, and are thus labeled ultraviolet (UV) divergences. Making these divergences explicit necessitates a regulation procedure. Dimensional regularisation is a procedure where the number of dimensions is continued to a real number $D = 4 - 2\epsilon$. This yields the divergences in terms of poles in ϵ and has the advantage of preserving gauge and Lorentz invariance.

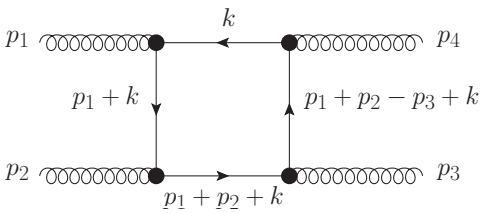

Figure 2.1: A one-loop Feynman diagram

The idea of renormalisation is to absorb these divergences in a redefinition of the couplings, field strengths and masses of the theory. One distinguishes then between the original 'bare' parameters, whose use in a calculation leads to UV divergences, and the renormalised parameters which include the short-distance effects and are the ones measured by experiments.

Technically the renormalisation is carried out by inclusion of new Feynman rules constructed such as to subtract the UV poles coming from the high-$|k|$ region [75]. These 'counterterm' rules are determined by studying self-energy and vertex correction diagrams at the required perturbative order. There is a certain arbitrariness concerning the absorbtion of finite terms besides the $\frac{1}{\epsilon}$ poles into the redefined parameters. This gives rise to different subtraction schemes, of which the $\overline{\mathrm{MS}}$ scheme [76] is the one used here.

One important issue is to define what is to be considered a short-distance effect and absorbed into the renormalised parameters. This is specified by introducing a new renormalisation scale μ_R, which corresponds to the typical scale at which the process takes place. Interactions which occur at much higher scales than μ_R cannot be resolved by the experiment and should be included in the redefined parameters. This induces a μ_R-dependence of the couplings, field strenghts and masses as well as of the amplitudes evaluated using the renormalised Lagrangian. Observable quantities however should be independent on μ_R, which is merely an auxilliary parameter with arbitrary value. This requirement leads to the so-called renormalisation group equations (RGE) [77], which control the μ_R-dependence of the masses and couplings such as to guarantee that bare quantities do not depend on the renormalisation scale. For the QCD coupling in particular one obtains

$$\mu_R^2 \frac{\mathrm{d}\alpha_s(\mu_R)}{\mathrm{d}\mu_R^2} = -\alpha_s(\mu_R)\left[\beta_0\Big(\frac{\alpha_s(\mu_R)}{2\pi}\Big) + \beta_1\Big(\frac{\alpha_s(\mu_R)}{2\pi}\Big)^2 + \beta_2\Big(\frac{\alpha_s(\mu_R)}{2\pi}\Big)^3 + \mathcal{O}(\alpha_s^4)\right], \tag{2.47}$$

with the coefficients (in the $\overline{\mathrm{MS}}$ scheme)

$$\beta_0 = \frac{11C_A - 4T_R N_F}{6},$$

$$\beta_1 = \frac{17C_A^2 - 10C_A T_R N_F - 6C_F T_R N_F}{6},$$
$$\beta_2 = \frac{1}{432}\Big(2857C_A^3 + 108C_F^2 T_R N_F - 1230C_F C_A T_R N_F - 2830C_A^2 T_R N_F + 264C_F T_R^2 N_F^2 + 316C_A T_R^2 N_F^2\Big), \tag{2.48}$$

where $C_A = N_C$ and $C_F = T_R \frac{N_C^2 - 1}{N_C}$ are the eigenvalues of the quadratic Casimir operator for the adjoint and fundamental representation of $SU(3)$ and the Dynkin index T_R is $\frac{1}{2}$. N_F is the number of quark flavours. Solving this equation allows to express the coupling at some scale μ_1 in terms of the coupling at another scale μ_2 as

$$\alpha_s(\mu_1) = \alpha_s(\mu_2)\left[1 + \beta_0 L_{12}\frac{\alpha_s(\mu_2)}{2\pi} + \Big(\beta_0^2 L_{12}^2 + \beta_1 L_{12}\Big)\Big(\frac{\alpha_s(\mu_R)}{2\pi}\Big)^2 + \mathcal{O}(\alpha_s^3)\right], \tag{2.49}$$

with $L_{12} = \log\left(\frac{\mu_2^2}{\mu_1^2}\right)$. By inserting eq. (2.49) in the expression for an observable which has been renormalised at the scale μ_1, one obtains the corresponding expression at the scale μ_2. In doing so, the boundary between resolved effects and effects absorbed into the renormalised Lagrangian has been shifted, and the corresponding change of the UV counterterms taken into account. In particular, replacing the bare coupling with the running coupling in an unrenormalised expression yields the renormalised expression. A similar running also applies to the effective coupling between the Higgs boson and gluons. It should be noted that in the same way as the UV poles are absorbed in the renormalised Lagrangian order-by-order in perturbation theory, so do the running couplings and masses control the scale (in)dependence of observables only up to corrections of higher perturbative order.
The running of the strong coupling α_s has some very deep consequences on the use and validity of perturbation theory in QCD. It turns out that at large scales α_s decreases, while at small scales it increases and ultimately diverges at a finite scale Λ_{QCD}. This can be explained in terms of vacuum fluctuations of the colour field, which tend to enhance the effect of the coupling because of the self-interacting nature of gluons. At high scales, these effects are resolved and explicitly present in the description of the interaction, while at small scales they are absorbed in α_s. This behaviour explains the confinement of partons inside the hadrons. At smaller, hadronic scales, the coupling is large and prevents any parton from escaping. At large scales on the other hand the partons can be considered essentially free, and the use of perturbation theory is justified [61, 78]. The scale Λ_{QCD} demarcates the boundary between these two regimes, at which perturbation theory breaks down. Its value is roughly 200 MeV, which corresponds to the inverse size of a proton. A further consequence concerns the PDF's. These describe the dynamics of the partons inside the hadrons at times far before the scattering. The PDF's thus describe phenomena taking place at low scales and cannot be described perturbatively.

2.8 Infrared divergences of colour ordered QCD matrix elements

After having their UV singularities removed by the renormalisation procedure, amplitudes involving charged particles still display a different kind of singular behaviour. These infrared divergences arise when the virtuality q^2 of an internal particle becomes small, and are therefore associated with the long-distance behaviour of the amplitudes, respectively with interactions happening long before or after the high virtuality part of the scattering. This interpretation leads to a 'factorised' picture of the process in terms of a factor describing the long-distance

physics times a 'hard' short-distance component, which involves only large scales and is insensitive to the IR behaviour.
This factorisation property can be observed on one hand in kinematical configurations where a parton becomes 'unresolved', that is, when the jet selection algorithm does not recognise it as an individual jet. Loop diagrams on the other hand also feature IR-like divergences since the integration over the loop momentum involves regions where the momentum of one of the particles in the loop vanishes. These diagrams also display a factorisation of their singularities.

2.8.1 Infrared behaviour in unresolved phase-space regions

In a Feynman diagram where two external particles with momenta p_1 and p_2 are connected to a third internal particle with momentum p_3 (for instance a quark and a gluon are connected to an internal quark), the propagator of the internal particle shows the following behaviour:

$$\frac{1}{(p_1+p_2)^2+m_3^2} = \frac{1}{2E_1E_2(1-\beta\cos(\theta_{12}))} \qquad , \qquad \beta = \sqrt{1-\frac{m_3^2}{E_3^2}}, \tag{2.50}$$

where E_i and m_i are the energies and masses of the corresponding particles and θ_{12} is the angle between the two external partons. Two different types of divergences may be discerned here, where the regions of phase-space where these occur may overlap. The propagator diverges when the energy of one of the external particles becomes small, which is labeled a soft divergence. On the other hand, when the mass m_3 of the internal particle is small, the denominator of the propagator vanishes in the limit where $\theta_{12} \to 0$, i.e. in configurations where the two external particles become collinear.
At tree level, the following factorisation patterns then hold for the single unresolved configurations [79]. In limites where a gluon b becomes soft, the squared colour ordered amplitude behaves as

$$|M_{n+1}^{(0)}(1,\dots,a,b,c,\dots,n+1)|^2 \overset{p_b\to 0}{\longrightarrow} \mathcal{S}_{abc}|M_n^{(0)}(1,\dots,a,c,\dots,n+1)|^2, \tag{2.51}$$

where the soft divergence is described by the eikonal factor

$$\mathcal{S}_{abc} = \frac{2s_{ac}}{s_{ab}s_{bc}}. \tag{2.52}$$

It should be noted that due to fermion number conservation, there are no single unresolved singularities associated with quarks becoming soft. This formula does not hold for the full matrix element squared because of interferences with the colour factors. In limites where two colour neighbouring partons a and b become collinear to form a parton c the squared colour ordered amplitude behaves as

$$|M_{n+1}^{(0)}(1,\dots,a,b,\dots,n+1)|^2 \overset{p_a\| p_b}{\longrightarrow} \frac{1}{s_{ab}} P_{ab\to c}^{\mu\nu}(z)|M_n^{(0)}(1,\dots,c,\dots,n+1)|_{\mu\nu}^2, \tag{2.53}$$

where $P_{ab\to c}$ describes the splitting of parton c into partons a and b and depends on the momentum fraction z of one of the two daughter partons. $|\mathcal{M}_n^{(0)}(1,\dots,c,\dots,n+1)|_{\mu\nu}^2$ is obtained by performing the average over all polarisations except the ones of partons a and b. If the parent parton c is a quark, then $P_{ab\to c}^{\mu\nu}(z)$ is the identity in colour space and one has complete factorisation. Collinear limites of partons which are not colour neighbouring do not lead to divergences. There are four splitting functions at NLO which after average over the spins read [80]:

$$P_{gg\to g}^{(0)}(z) = 2C_A\Big(\frac{z}{(1-z)_+} + \frac{(1-z)}{z} + z(1-z)\Big) + \frac{(11C_A - 4N_FT_F)}{6}\delta(1-z),$$

$$
\begin{aligned}
P^{(0)}_{q\bar{q}\to g}(z) &= T_F(z^2+(1-z)^2),\\
P^{(0)}_{qg\to q}(z) &= C_F\Big(\frac{1+z^2}{1-z}\Big)_+,\\
P^{(0)}_{gq\to q}(z) &= C_F\frac{1+(1-z)^2}{z},
\end{aligned}
\tag{2.54}
$$

where z is the momentum fraction carried away by one of the partons after the splitting and the plus distribution is defined as

$$
F(z)_+ = F(z) - \delta(1-z)\int_0^1 \mathrm{d}y F(y). \tag{2.55}
$$

For the splitting functions the notation $P^{(n)}_{ij} = P^{(n)}_{jX\to i}$, is used, where X is arbitrary and should be summed over the allowed parton identities.
If the jet function allows for two partons to become unresolved, which is the case when NNLO corrections are considered, two cases need to be distinguished. If the two unresolved particles are not colour neighbouring, then the factorisation pattern is described by a product of single unresolved factors. If the unresolved particles are colour neighbouring, new double unresolved limites appear. These are [81–84]:

Double soft	The energies of two colour connected partons simultaneously vanish.
Soft collinear	A pair of colour connected partons become collinear and the energy of a parton colour connected to one of the collinear partons vanishes.
Triple collinear	Three colour connected partons become simultaneously collinear.

Each of these limites is adequately described by a corresponding double unresolved factor times the squared matrix element containing only the resolved partons.
The single unresolved behaviour of one-loop diagrams has also been studied [85–87]. At the amplitude level, the pattern which emerges is that of a one-loop unresolved factor times a tree-level amplitude plus a tree-level unresolved factor times a one-loop amplitude. In terms of helicity amplitudes, in collinear limites one has

$$
\begin{aligned}
&M^{(1)}_{n+1}(1^{\lambda_1},\dots,a^{\lambda_a},b^{\lambda_b},\dots,(n+1)^{\lambda_{n+1}})\\
&\qquad\xrightarrow{p_a\| p_b}\sum_{\lambda=\pm}\Big[\mathrm{split}^{(0)}_{-\lambda}(a^{\lambda_a},b^{\lambda_b})M^{(1)}_n(1^{\lambda_1},\dots,K^{\lambda},\dots,(n+1)^{\lambda_{n+1}})\\
&\qquad\qquad+\mathrm{split}^{(1)}_{-\lambda}(a^{\lambda_a},b^{\lambda_b})M^{(0)}_n(1^{\lambda_1},\dots,K^{\lambda},\dots,(n+1)^{\lambda_{n+1}}\Big],
\end{aligned}
\tag{2.56}
$$

with $p_K = p_a + p_b$ and splitting amplitudes which can be considered as 'square roots' of the splitting functions. This formula can be generalised to higher loop orders provided the number of partons considered is small enough, which is used in sec. 3.5 to derive the two-loop splitting amplitudes. In soft limites, one has

$$
\begin{aligned}
M^{(1)}_{n+1}(1,\dots,a,b^{\lambda_b},c,\dots,n+1)\xrightarrow{p_b\to 0}&\ \mathrm{soft}^{(1)}(a,b^{\lambda_b},c)M^{(0)}_n(1,\dots,a,c,\dots,n+1)\\
&+\mathrm{soft}^{(0)}(a,b^{\lambda_b},c)M^{(1)}_n(1,\dots,a,c,\dots,n+1).
\end{aligned}
\tag{2.57}
$$

The same behaviour can be recovered for the interference of the tree- and one-loop amplitudes relevant for NNLO real-virtual corrections.

2.8.2 Infrared behaviour in loop diagrams

After renormalisation, loop amplitudes still contain divergences. These originate from regions of the loop integration where the loop momentum becomes unresolved w.r.t. the external momenta, much in the same way as in the previous section. After the integration, these divergences appear as explicit poles in the analytical expression of the amplitude. Catani [88] has shown how to organise the IR pole structure of the one- and two-loop contributions renormalised in the $\overline{\text{MS}}$ scheme in terms of the tree and renormalised one-loop amplitudes. This formula for the pole structure is proven [89] from the structure of soft and collinear radiation in perturbation theory and can be generalised to higher loop order.
The IR behaviour of a colour ordered one-loop amplitude is given by,

$$\mathcal{M}^{(1)} \quad = \quad \boldsymbol{I}^{(1)}_{\mathcal{M}}(\epsilon)\mathcal{M}^{(0)} + \mathcal{M}^{(1),\text{finite}}. \tag{2.58}$$

The IR singularity operators $\boldsymbol{I}^{(1)}_{\mathcal{M}}(\epsilon)$ are in general matrices in the colour space which act on the colour vector $\mathcal{M}$ and are given by,

$$\boldsymbol{I}^{(1)}_{\mathcal{M}}(\epsilon) = \frac{e^{\epsilon\gamma}}{2\Gamma(1-\epsilon)} \sum_i \frac{1}{\mathbf{T}_i^2} \mathcal{V}_i^{sing}(\epsilon) \sum_{j\neq i} \mathbf{T}_i \cdot \mathbf{T}_j \mathtt{S}_{ij}, \tag{2.59}$$

where

$$\mathtt{S}_{ij} = \left(\frac{\mu^2 e^{-i\lambda_{ij}\pi}}{2p_i \cdot p_j}\right)^{\epsilon}, \tag{2.60}$$

and $\lambda_{ij} = 1$ if both of i and j are incoming or outgoing and $\lambda_{ij} = 0$ otherwise. The singular function $\mathcal{V}_{ij}^{sing}$ depends on the identity of the partons and is given by

$$\begin{aligned} \mathcal{V}_i^{sing}(\epsilon) &= \mathbf{T}_i^2 \frac{1}{\epsilon^2} + \gamma_i \frac{1}{\epsilon}, \\ \mathbf{T}_q^2 = \mathbf{T}_{\overline{q}}^2 = C_F \quad &, \quad \mathbf{T}_g^2 = C_A, \\ \gamma_q = \gamma_{\overline{q}} = \frac{3}{2} C_F \quad &, \quad \gamma_g = \frac{11}{6} C_A - \frac{3}{2} T_R N_F. \end{aligned} \tag{2.61}$$

Using colour conservation, $\sum_{j\neq i} \mathbf{T}_j = -\mathbf{T}_i$, it can be showed that the $\frac{1}{\epsilon^2}$ pole factorise completely in colour space, whereas colour correlations between individual partons remain for the $\frac{1}{\epsilon}$ poles. A complete factorisation is possible for three-parton and four-gluon amplitudes. The $\boldsymbol{I}^{(1)}_{\mathcal{M}}$-operator then takes a very simple form in terms of a sum of contributions over all pairs of colour-neighbouring partons. The two-loop singularity structure is,

$$\begin{aligned} \mathcal{M}^{(2)} = \boldsymbol{I}^{(1)}_{\mathcal{M}}(\epsilon) &\left(\mathcal{M}^{(1)} - \frac{\beta_0}{\epsilon} \boldsymbol{I}^{(1)}_{\mathcal{M}}(\epsilon)\right) \mathcal{M}^{(0)} \\ &- \frac{1}{2} \boldsymbol{I}^{(1)}_{\mathcal{M}}(\epsilon) \boldsymbol{I}^{(1)}_{\mathcal{M}}(\epsilon) \mathcal{M}^{(0)} \\ &+ \left(e^{-\epsilon\gamma} \frac{\Gamma(1-2\epsilon)}{\Gamma(1-\epsilon)} \left(\frac{\beta_0}{\epsilon} + K\right) \boldsymbol{I}^{(1)}_{\mathcal{M}}(2\epsilon) + \boldsymbol{H}^{(2)}_{\mathcal{M}}(\epsilon)\right) \mathcal{M}^{(0)} + \mathcal{M}^{(2),\text{finite}} \end{aligned} \tag{2.62}$$

where the constant K is,

$$K = \left(\frac{67}{18} - \frac{\pi^2}{6}\right) C_A - \frac{10}{9} T_R N_F. \tag{2.63}$$

The origin of the various terms in eq. (2.60) is straightforward. Each parton pair ij in the event forms a radiating antenna of scale s_{ij}. Terms proportional to $\mathtt{S}_{ij}$ are canceled by real radiation

emitted from leg i and absorbed by leg j. The soft singularities $\mathcal{O}(1/\epsilon^2)$ are independent of the identity of the participating partons and are universal. However, the collinear singularities depend on the identities of the participating partons. For each quark one finds a contribution of $3/(4\epsilon)$ and for each gluon one finds a contribution of $\beta_0/(2\epsilon)$ coming from the integral over the collinear splitting function.
Finally, the last term of eq. (2.62) that involves $\boldsymbol{H}^{(2)}(\epsilon)$ produces only a single pole in ϵ and is given by,

$$\boldsymbol{H}^{(2)}_{\mathcal{M}}(\epsilon) = \frac{e^{\epsilon\gamma}}{4\,\epsilon\,\Gamma(1-\epsilon)} H^{(2)}_{\mathcal{M}} \,, \tag{2.64}$$

where the constant $H^{(2)}_{\mathcal{M}}$ is renormalisation scheme dependent. For less than five partons, the process-dependent $H^{(2)}_{\mathcal{M}}$ can be constructed by counting the number of radiating partons present in the event as with the single pole parts of $\boldsymbol{I}^{(1)}_{\mathcal{M}}(\epsilon)$. In the $\overline{\text{MS}}$ scheme,

$$\begin{aligned} H_q^{(2)} &= \left(\frac{7}{4}\zeta_3 + \frac{409}{864} - \frac{11\pi^2}{96}\right) N^2 + \left(-\frac{1}{4}\zeta_3 - \frac{41}{108} - \frac{\pi^2}{96}\right) + \left(-\frac{3}{2}\zeta_3 - \frac{3}{32} + \frac{\pi^2}{8}\right) \frac{1}{N^2} \\ &\quad + \left(\frac{\pi^2}{48} - \frac{25}{216}\right) \frac{(N^2-1)N_F}{N} \,, \end{aligned} \tag{2.65}$$

$$H_g^{(2)} = \left(\frac{1}{2}\zeta_3 + \frac{5}{12} + \frac{11\pi^2}{144}\right) N^2 + \frac{5}{27}\, N_F^2 + \left(-\frac{\pi^2}{72} - \frac{89}{108}\right) N N_F - \frac{N_F}{4N}. \tag{2.66}$$

2.8.3 Infrared cancellation

Despite their seemingly different nature, the IR divergences appearing in unresolved phase-space regions can be related to the ones of loop amplitudes. The relation bases on the optical theorem, which is itself a consequence of the unitarity of the S-matrix. In loop diagrams, the IR singularities come from regions of the integrals where the loop momenta become on-shell. In this regions, the loop integrals can be viewed as integrals over the on-shell phase-space of the loop momenta. This insight, which is quantified by the optical theorem, implies that both types of IR singularities in fact have the same origin. This has been used to prove the KLN theorem [90], which states that once the phase-space integral in eq. (2.41) is performed, the IR singularities of the real and virtual contributions cancel. In particular, the integral of a squared amplitude over the region of phase-space where a parton becomes unresolved yields poles in ϵ related to the antenna formed by the hard partons between which it was radiated. These poles have the same coefficients than the corresponding poles of the virtual contributions, but with a negative sign.
This cancellation however relies on the full phase-space integral to be performed. Often the integral in eq. (2.41) is constrained due to the presence of the jet function, which results in an incomplete cancellation of the IR singularities. This typically results in large logarithms of the scale at which the phase-space is cut, which may spoil the convergence of the perturbative series and need to be resummed. The cancellation also requires the jet function to be insensitive to unresolved radiation, that is, the reconstruction of jets out of partons should be independent on whether one of this partons has undergone a collinear splitting or radiated a soft particle. The k_{T}-algorithms belong to the class of IR-safe algorithms satisfying this condition.

2.9 Mass factorisation

In lepton-hadron and hadron-hadron colliders, final state partons can also become collinear with initial state ones. These unresolved limites yield the same singularities than in eq. (2.53),

however, since the initial state momenta are not part of the phase-space being integrated over, such collinear limites are not the object of a cancellation described in the previous section. The initial state collinear limites correspond to interactions taking place at times and distances far before the hard interaction. It appears thus natural to associate them with the PDF's which precisely describe the internal structure of the hadrons prior to the collision. The proper treatment is then to absorb the initial state collinear limites into a redefinition of the PDF's in the frame of a procedure which follows the same lines as the renormalisation of UV divergent quantities as described in section 2.7:

$$\begin{aligned} f_a(\xi,\mu_F^2) &= \tilde{f}_a(\xi) + \frac{\alpha_s(\mu_R)}{2\pi}\log\left(\frac{\mu_F^2}{\kappa^2}\right) P_{ab}^{(0)} \otimes \tilde{f}_b + \mathcal{O}(\alpha_s^2), \\ P_{ab}^{(0)} \otimes \tilde{f}_b &= \int_\xi^1 \frac{\mathrm{d}z}{z} P_{ab}^{(0)}(z)\tilde{f}_b\Big(\frac{\xi}{z}\Big), \end{aligned} \tag{2.67}$$

where $\tilde{f}$ are the bare PDF's and there is an implicit sum over all partons b which might split into parton a. κ^2 is a lower cutoff on the transverse momentum of the emitted parton which, similarly to ϵ, regulates the phase-space integration. In particular, a new, internal, factorisation scale μ_F is being introduced to separate the long-distance effects from the hard interaction. The requirement of independence of bare quantities of the factorisation scale leads to the DGLAP equations [80, 91] which describe the evolution of the PDF's along a change of scale. The effect of changing the factorisation scale from μ_1 to μ_2 can be implemented by substituting

$$\begin{aligned} f_a(\xi,\mu_1^2) = f_a(\xi,\mu_2^2) &- \frac{\alpha_s(\mu_R)}{2\pi} P_{ab}^{(0)} \otimes f_b(\xi,\mu_2^2) L_{12} \\ &- \left(\frac{\alpha_s(\mu_R)}{2\pi}\right)^2 \Bigg[P_{ab}^{(1)} \otimes f_b(\xi,\mu_2^2) L_{12} - \frac{1}{2} P_{ab}^{(0)} \otimes P_{bc}^{(0)} \otimes f_c(\xi,\mu_2^2) L_{12}^2 \\ &\qquad + P_{ab}^{(0)} \otimes f_b(\xi,\mu_2^2)\beta_0 L_{12}\Big(l + \frac{1}{2}L_{12}\Big)\Bigg], \end{aligned} \tag{2.68}$$

where $L_{12} = \log\left(\frac{\mu_2^2}{\mu_1^2}\right)$, $l = \log\left(\frac{\mu_R^2}{\mu_2^2}\right)$ and $P_{ab}^{(1)}$ is the one-loop splitting function.
eq. (2.67) can be inverted, which leads to a description of the cross section in terms of the physical PDF's instead of the bare ones together with a new mass factorisation counterterm which implements the absorbtion of the initial state singularities into the PDF's:

$$\mathrm{d}\hat{\sigma}_{ij,LO}(\xi_1 H_1, \xi_2 H_2) = \mathrm{d}\tilde{\sigma}_{ij,LO}(\xi_1 H_1, \xi_2 H_2), \tag{2.69}$$

$$\mathrm{d}\hat{\sigma}_{ij,NLO}(\xi_1 H_1, \xi_2 H_2) = \mathrm{d}\tilde{\sigma}_{ij,NLO}(\xi_1 H_1, \xi_2 H_2) + \mathrm{d}\hat{\sigma}^{MF}_{ij,NLO}(\xi_1 H_1, \xi_2 H_2), \tag{2.70}$$

$$\mathrm{d}\hat{\sigma}_{ij,NNLO}(\xi_1 H_1, \xi_2 H_2) = \mathrm{d}\tilde{\sigma}_{ij,NNLO}(\xi_1 H_1, \xi_2 H_2) + \mathrm{d}\hat{\sigma}^{MF}_{ij,NNLO}(\xi_1 H_1, \xi_2 H_2), \tag{2.71}$$

where

$$\begin{aligned} \mathrm{d}\hat{\sigma}^{MF}_{ij,NLO}(\xi_1 H_1, \xi_2 H_2) = &- \int \frac{\mathrm{d}z_1}{z_1}\Gamma^{(1)}_{ki}(z_1)\mathrm{d}\hat{\sigma}_{kj,LO}(z_1\xi_1 H_1, \xi_2 H_2) \\ &- \int \frac{\mathrm{d}z_2}{z_2}\Gamma^{(1)}_{lj}(z_2)\mathrm{d}\hat{\sigma}_{il,LO}(\xi_1 H_1, z_2\xi_2 H_2), \end{aligned} \tag{2.72}$$

$$\begin{aligned} \mathrm{d}\hat{\sigma}^{MF}_{ij,NNLO}(\xi_1 H_1, \xi_2 H_2) = &- \int \frac{\mathrm{d}z_1}{z_1}\Gamma^{(2)}_{ki}(z_1)\mathrm{d}\hat{\sigma}_{kj,LO}(z_1\xi_1 H_1, \xi_2 H_2) \\ &- \int \frac{\mathrm{d}z_1}{z_1}\Gamma^{(1)}_{ki}(z_1)\mathrm{d}\hat{\sigma}_{kj,NLO}(z_1\xi_1 H_1, \xi_2 H_2) \\ &- \int \frac{\mathrm{d}z_2}{z_2}\Gamma^{(2)}_{lj}(z_2)\mathrm{d}\hat{\sigma}_{il,LO}(\xi_1 H_1, z_2\xi_2 H_2) \end{aligned}$$

$$- \int \frac{\mathrm{d}z_2}{z_2} \Gamma^{(1)}_{lj}(z_2) \mathrm{d}\hat{\sigma}_{il,NLO}(\xi_1 H_1, z_2 \xi_2 H_2)$$
$$- \int \frac{\mathrm{d}z_1}{z_1} \int \frac{\mathrm{d}z_2}{z_2} \Gamma^{(1)}_{ki}(z_1) \Gamma^{(1)}_{lj}(z_2) \mathrm{d}\hat{\sigma}_{kl,LO}(z_1 \xi_1 H_1, z_2 \xi_2 H_2). \quad (2.73)$$

In the above expressions, there is again an implicit sum over the partons k and l. In dimensional regularisation the mass factorisation kernels read as

$$\Gamma^1_{ba}(z) = -\frac{1}{\epsilon} P^{(0)}_{ab}(z) \quad (2.74)$$
$$\Gamma^2_{ba}(z) = \frac{1}{2\epsilon^2} \left[\sum_c [P^{(0)}_{ac} \otimes P^{(0)}_{cb}](z) + 2\beta_0 P^{(0)}_{ab}(z) \right] - \frac{1}{2\epsilon} P^{(1)}_{ab}(z), \quad (2.75)$$

with the one-loop splitting functions $P^{(1)}_{ab}(z)$ [92].
It is a remarkable fact that altough PDF's themselves cannot be described perturbatively, their evolution as given by the mass factorisation kernels can be computed using perturbation theory.

2.10 Subtraction terms

In practical calculations, the cancellation described in section 2.8.3 is not realisable by analytical means, since the jet function substantially complicates the phase-space integration. An alternative consists in performing the integration numerically in the frame of a Monte-Carlo integration (see next section). This tries to estimate the integral by evaluating the integrand at a sample of random phase-space points. The integration boundaries can then easily and flexibly be implemented by applying an acceptance-rejection test on the phase-space points, basing on the jet function criteria. The integration can however develop numerical instabilities in phase-space regions where partons become unresolved and the integrand diverges. These divergences must therefore be removed *prior* to the integration. To this intent, a new contribution is introduced, which satisfies following requirements:

- It approximates the real radiation contributions in all their unresolved limites.
- It is sufficiently simple for the integration over the phase-space of the unresolved parton to be performed analytically.

A contribution which fulfils these conditions can be subtracted from the real contribution such as to remove its divergences locally for every phase-space point and obtain a function which is well-defined and integrable over the whole integration domain. Furthermore, once the integral over its unresolved phase-space has been carried out, the divergences become explicit in terms of poles in ϵ. This integrated subtraction term can be added back to the virtual contribution, where together with the mass factorisation counterterms it will cancel its pole structure analytically.
At NLO, the real contribution features $n+1$ partons whereas the jet function constrains only n to be resolved. Thus one parton may become unresolved, which leads to singularities as described in section 2.8.1. On the other hand, the virtual contribution contains loop diagrams which display a pole structure as in section 2.8.2. Following the previous discussion, subtraction terms are constructed such that in

$$\mathrm{d}\hat{\sigma}_{ij,NLO} = \int_{\mathrm{d}\Phi_{n+1}} [\mathrm{d}\hat{\sigma}^R_{ij,NLO} - \mathrm{d}\hat{\sigma}^S_{ij,NLO}] J^{(n+1)}_n$$
$$+ \int_{\mathrm{d}\Phi_n} [\mathrm{d}\hat{\sigma}^V_{ij,NLO} - \mathrm{d}\hat{\sigma}^T_{ij,NLO}] J^{(n)}_n, \quad (2.76)$$

$$\mathrm{d}\hat{\sigma}^{T}_{ij,NLO} = -\int_{1_{unresolved}} \mathrm{d}\hat{\sigma}^{S}_{ij,NLO} - \mathrm{d}\hat{\sigma}^{MF}_{ij,NLO}, \tag{2.77}$$

the content of the square brackets is well-defined and can be integrated over numerically.
At NNLO, three new contributions appear. The integration over the phase-space of the double-real contribution includes regions where up to two partons become unresolved. Again, subtraction terms need to be introduced to remove this complex singularity structure. The real-virtual contribution has simultaneously single unresolved limites (see eqs. (2.56) and (2.57)), as well as up to $\frac{1}{\epsilon^2}$ poles. A part of the double-real subtraction terms can be integrated over their single unresolved region such as to obtain integrated subtraction terms which in combination with the mass factorisation counterterms cancel the poles of the real-virtual matrix elements. At the same time, new subtraction terms need to be constructed in order to remove the single unresolved limites of the real-virtual matrix element. The double-virtual contribution finally displays poles up to $\frac{1}{\epsilon^4}$. These can be canceled by integrating the remaining double-real subtraction terms over their double unresolved regions as well as the real-virtual subtraction terms over their single unresolved regions, such as to cancel the double-virtual pole structure together with the mass factorisation counterterms. The picture which emerges at NNLO is thus the following:

$$\begin{aligned}\mathrm{d}\hat{\sigma}_{ij,NNLO} = &\int_{\mathrm{d}\Phi_{n+2}} [\mathrm{d}\hat{\sigma}^{RR}_{ij,NNLO} - \mathrm{d}\hat{\sigma}^{S}_{ij,NNLO}] J_n^{(n+2)} \\ &+ \int_{\mathrm{d}\Phi_{n+1}} [\mathrm{d}\hat{\sigma}^{RV}_{ij,NNLO} - \mathrm{d}\hat{\sigma}^{T}_{ij,NNLO}] J_n^{(n+1)} \\ &+ \int_{\mathrm{d}\Phi_{n}} [\mathrm{d}\hat{\sigma}^{VV}_{ij,NNLO} - \mathrm{d}\hat{\sigma}^{U}_{ij,NNLO}] J_n^{(n)},\end{aligned} \tag{2.78}$$

$$\mathrm{d}\hat{\sigma}^{T}_{ij,NNLO} = \mathrm{d}\hat{\sigma}^{VS}_{ij,NNLO} - \int_{1_{unresolved}} \mathrm{d}\hat{\sigma}^{S_1}_{ij,NNLO} - \mathrm{d}\hat{\sigma}^{MF_1}_{ij,NNLO}, \tag{2.79}$$

$$\mathrm{d}\hat{\sigma}^{U}_{ij,NNLO} = -\int_{1_{unresolved}} \mathrm{d}\hat{\sigma}^{VS}_{ij,NNLO} - \int_{2_{unresolved}} \mathrm{d}\hat{\sigma}^{S_2}_{ij,NNLO} - \mathrm{d}\hat{\sigma}^{MF_2}_{ij,NNLO}. \tag{2.80}$$

There are different subtraction formalisms available, following the different ways of approximating the real contributions. In this work the antenna subtraction formalism is being applied [49–52].

2.11 Monte-Carlo integration

In order to obtain the cross section, eq. (2.34), the integral over the phase-space needs to be performed. Due to its high dimensionality and the complicated integration boundaries which result from the jet function, classical Newton-type numerical integration is not suited. Monte-Carlo (MC) integration offers an appealing alternative, since it is very flexible and the error on the integration does not depend on the dimension. This is however at the cost of slow convergence towards the true result, and various strategies exist to improve the efficiency of the integration.
The basic idea of MC integration is to sample the integrand with randomly generated points. Using N random phase-space points $\vec{x}_i$, the integral can be evaluated as

$$E_N = \frac{1}{N}\sum_{n=1}^{N} f(\vec{x}_n), \tag{2.81}$$

$$\lim_{N\to\infty} E_N = I, \tag{2.82}$$

$$I = \int \mathrm{d}^D\vec{x} f(\vec{x}_i), \tag{2.83}$$

where D is the dimensionality of the integration volume, f is the integrand and the second equation holds due to the law of large numbers. The error on the integration is given by $\frac{S_N}{\sqrt{N}}$ where

$$S_N^2 = \frac{1}{N}\sum_{n=1}^{N} f(x_n)^2 - E_N^2, \tag{2.84}$$

which for large N converges towards the variance $\sigma^2(f)$. The error thus scales as $\frac{1}{\sqrt{N}}$.
A technique to improve the convergence of the integration is importance sampling. Obviously MC integration gives the best results when the integrand f is almost constant. The idea then is to 'flatten out' the integrand by performing the variable transformation

$$\int \mathrm{d}^D\vec{x} f(\vec{x}) = \int \mathrm{d}P(\vec{x}) \frac{f(\vec{x})}{p(\vec{x})}, \tag{2.85}$$

where

$$p(\vec{x}) = \frac{\partial^D}{\partial x_1 \ldots \partial x_D} P(\vec{x}) \qquad , \qquad \int \mathrm{d}^D\vec{x} p(\vec{x}) = 1. \tag{2.86}$$

This can be understood as generating the phase-space points according to the probability distribution $p(\vec{x})$. It turns out that the variance S^2 can be reduced by choosing $p(\vec{x})$ to be close to $f(\vec{x})$. This however requires a priori knowledge of the integrand.
VEGAS [37] is an adaptive MC algorithm which tackles this problem by iterating integrations, during which it gains information on the integrand which it uses to optimise the next integration. VEGAS uses a unit hypercube $[0,1]^D$ as integration volume . It starts by partitioning it into a rectangular grid and then performs the integration in each individual D-dimensional box. The result of this run is then used to adjust the grid such that more points are generated in phase-space regions where the magnitude of the integrand is large. VEGAS thus obtains knowledge of the integrand in terms of a step function, according to which it distributes the phase-space points. The rescaling of the grid is done independently for each integration variable x_i, which amounts in using a separable probability distribution

$$p(\vec{x}) = p_1(x_1) \cdot p_2(x_2) \cdot \ldots \cdot p_D(x_D). \tag{2.87}$$

This avoids keeping track of K^D boxes, where K is the number of grid points in one dimension. This approximation is efficient if the peaks of the integrand can be located from its projection on the x_i axis.
The integrations can be iterated until the grid provides a satisfactory description of the integrand. This is being done in a 'warmup' phase with typically less phase-space points. The optimised grid is then 'frozen' and a series of high-statistics production runs can be performed. For each run a central value, a variance and a χ^2 per degree of freedom is given, as well as a total average and variance over all production runs.

Chapter 3

Two-loop helicity amplitudes for H $\rightarrow$ 3 partons

In this chapter the computation of the two-loop helicity amplitudes for H $\rightarrow$ 3 partons [36], which are relevant for the double-virtual contribution to $pp \rightarrow H + 1J$, is described. Helicity amplitudes are in general interesting for several reasons:

- They are of use in processes where information about the polarisation state of external particles is needed, i.e. for observables at colliders with polarised beams, in oriented event shape variables and in decays of vector particles, when the direction of the decay products is considered.

- Helicity amplitudes, when expressed in the four-dimensional spinor helicity formalism, yield very compact expressions [69]. This greatly simplifies the study of formal aspects of scattering amplitudes, which has already led to many interesting developments like recursive formulae for multi-gluon processes [93].

- Furthermore, such amplitudes implement collinear factorisation in a more natural way as in helicity averaged squared matrix elements [69]. This gives them the advantage of better numerical stability.

The computation of the helicity amplitudes can be done by studying the Lorentz-invariant tensor structure of the full amplitude [94]. After enforcing gauge symmetry by applying the ward identities, one obtains its gauge invariant decomposition in terms of independent Lorentz tensors. The coefficients of this decomposition can be obtained out of a Feynman diagram calculation by projecting the amplitude onto the individual tensor structures using projection operators. The coefficients and projectors are defined in an arbitrary number D of dimensions. In particular, this allows to perform a fully D-dimensional computation of the Feynman diagrams.
The helicity amplitudes can be expressed in terms of the tensor coefficients, where this relation is valid at all orders in perturbation theory. Since the helicity amplitudes are defined in $D = 4$ dimensions, in doing this one needs to set the dimensionality of the Lorentz tensors to four. The mismatch induced by this procedure is of order ϵ when using dimensional regularisation with $D = 4 - 2\epsilon$.
In the following, some aspects of this calculation are detailed. Throughout this chapter the following conventions are used. One considers the decay of the Higgs boson to three gluons,

$$H(p_4) \longrightarrow g_1(p_1) + g_2(p_2) + g_3(p_3) \,, \tag{3.1}$$

or into a quark-antiquark pair and a gluon,

$$H(p_4) \longrightarrow q(p_1) + \bar{q}(p_2) + g_(p_3) \; . \tag{3.2}$$

It is convenient to define the invariants,

$$s_{12} = (p_1 + p_2)^2 \; , \qquad s_{13} = (p_1 + p_3)^2 \; , \qquad s_{23} = (p_2 + p_3)^2 \; , \tag{3.3}$$

which fulfill

$$p_4^2 = s_{12} + s_{13} + s_{23} \equiv s_{123} \equiv M_H^2 \; , \tag{3.4}$$

as well as the dimensionless invariants,

$$x = s_{12}/s_{123} \; , \qquad y = s_{13}/s_{123} \; , \qquad z = s_{23}/s_{123} \; , \tag{3.5}$$

which satisfy $x + y + z = 1$.

3.1 Tensor structures, helicity amplitudes and projectors

The amplitudes $|\mathcal{M}\rangle$ can be written as,

$$\begin{aligned} |\mathcal{M}_{ggg}\rangle &= S_{\mu\nu\rho}(g_1;g_2;g_3)\epsilon_1^\mu \epsilon_2^\nu \epsilon_3^\rho \, , \\ |\mathcal{M}_{q\bar{q}g}\rangle &= T_\rho(q,\bar{q};g)\epsilon^\rho \, , \end{aligned} \tag{3.6}$$

while the partonic currents may be perturbatively decomposed as,

$$\begin{aligned} S_{\mu\nu\rho}(g_1;g_2;g_3) &= \lambda\sqrt{4\pi\alpha_s} f^{a_1a_2a_3}\Big[S^{(0)}_{\mu\nu\rho}(g_1;g_2;g_3) + \left(\frac{\alpha_s}{2\pi}\right) S^{(1)}_{\mu\nu\rho}(g_1;g_2;g_3) \\ &\quad + \left(\frac{\alpha_s}{2\pi}\right)^2 S^{(2)}_{\mu\nu\rho}(g_1;g_2;g_3) + \mathcal{O}(\alpha_s^3)\Big], \end{aligned} \tag{3.7}$$

$$\begin{aligned} T_\rho(q;\bar{q};g) &= \lambda\sqrt{4\pi\alpha_s} T^a_{ij}\Big[T^{(0)}_\rho(q;\bar{q};g) + \left(\frac{\alpha_s}{2\pi}\right) T^{(1)}_\rho(q;\bar{q};g) \\ &\quad + \left(\frac{\alpha_s}{2\pi}\right)^2 T^{(2)}_\rho(q;\bar{q};g) + \mathcal{O}(\alpha_s^3)\Big], \end{aligned} \tag{3.8}$$

where $S^{(i)}_{\mu\nu\rho}$ and $T^{(i)}_\rho$ are the i-loop contributions to the amplitude. The SU(3) generators are normalised as $tr(T^a T^b) = \delta^{ab}/2$.

3.1.1 The general tensor for $H \to ggg$

The most general tensor structure for the partonic current $\mathcal{S}_{\mu\nu\rho}(g_1;g_2;g_3)$ is given by,

$$\begin{aligned} S_{\mu\nu\rho}(g_1;g_2;g_3)\epsilon_1^\mu\epsilon_2^\nu\epsilon_3^\rho &= \sum_{i,j,k=1}^{3} A_{i\,j\,k}\, p_i{\cdot}\epsilon_1\, p_j{\cdot}\epsilon_2\, p_k{\cdot}\epsilon_3 + \sum_{i=1}^{3} B_i\, p_i{\cdot}\epsilon_1\, \epsilon_2{\cdot}\epsilon_3 \\ &+ \sum_{i=1}^{3} C_i\, p_i{\cdot}\epsilon_2\, \epsilon_1{\cdot}\epsilon_3 + \sum_{i=1}^{3} D_i\, p_i{\cdot}\epsilon_3\, \epsilon_1{\cdot}\epsilon_2 \\ &= A_{211}\, p_2{\cdot}\epsilon_1\, p_1{\cdot}\epsilon_2\, p_1{\cdot}\epsilon_3 + A_{212}\, p_2{\cdot}\epsilon_1\, p_1{\cdot}\epsilon_2\, p_2{\cdot}\epsilon_3 + A_{231}\, p_2{\cdot}\epsilon_1\, p_3{\cdot}\epsilon_2\, p_1{\cdot}\epsilon_3 \\ &+ A_{232}\, p_2{\cdot}\epsilon_1\, p_3{\cdot}\epsilon_2\, p_2{\cdot}\epsilon_3 + A_{311}\, p_3{\cdot}\epsilon_1\, p_1{\cdot}\epsilon_2\, p_1{\cdot}\epsilon_3 + A_{312}\, p_3{\cdot}\epsilon_1\, p_1{\cdot}\epsilon_2\, p_2{\cdot}\epsilon_3 \\ &+ A_{331}\, p_3{\cdot}\epsilon_1\, p_3{\cdot}\epsilon_2\, p_1{\cdot}\epsilon_3 + A_{332}\, p_3{\cdot}\epsilon_1\, p_3{\cdot}\epsilon_2\, p_2{\cdot}\epsilon_3 \\ &+ B_2\, \epsilon_2{\cdot}\epsilon_3\, p_2{\cdot}\epsilon_1 + B_3\, \epsilon_2{\cdot}\epsilon_3\, p_3{\cdot}\epsilon_1 \\ &+ C_1\, \epsilon_1{\cdot}\epsilon_3\, p_1{\cdot}\epsilon_2 + C_3\, \epsilon_1{\cdot}\epsilon_3\, p_3{\cdot}\epsilon_2 \end{aligned}$$

$$+ \quad D_1\,\epsilon_1{\cdot}\epsilon_2\,p_1{\cdot}\epsilon_3 + D_2\,\epsilon_1{\cdot}\epsilon_2\,p_2{\cdot}\epsilon_3\,, \tag{3.9}$$

where the constraints $p_1 \cdot \epsilon_1 = 0$, $p_2 \cdot \epsilon_2 = 0$ and $p_3 \cdot \epsilon_3 = 0$ have been applied. The tensor must satisfy the QCD Ward identity when the gluon polarisation vectors ϵ_1, ϵ_2 and ϵ_3 are replaced with the respective gluon momentum,

$$\begin{aligned}
(\epsilon_1 \to p_1) \to S_{\mu\nu\rho}(g_1;g_2;g_3)p_1^\mu\epsilon_2^\nu\epsilon_3^\rho &= 0\,,\\
(\epsilon_2 \to p_2) \to S_{\mu\nu\rho}(g_1;g_2;g_3)\epsilon_1^\mu p_2^\nu\epsilon_3^\rho &= 0\,,\\
(\epsilon_3 \to p_3) \to S_{\mu\nu\rho}(g_1;g_2;g_3)\epsilon_1^\mu\epsilon_2^\nu p_3^\rho &= 0\,.
\end{aligned} \tag{3.10}$$

These constraints yield relations amongst the 14 distinct tensor structures and applying these identities give the gauge invariant form of the tensor,

$$S_{\mu\nu\rho}(g_1;g_2;g_3)\epsilon_1^\mu\epsilon_2^\nu\epsilon_3^\rho = A_{211}T_{211} + A_{311}T_{311} + A_{232}T_{232} + A_{312}T_{312}\,, \tag{3.11}$$

where A_{ijk} are gauge independent functions and the tensor structures T_{ijk} are given by,

$$\begin{aligned}
T_{232} &= p_2{\cdot}\epsilon_1\,p_3{\cdot}\epsilon_2\,p_2{\cdot}\epsilon_3 - \frac{1}{2}\,\epsilon_2{\cdot}\epsilon_3\,p_2{\cdot}\epsilon_1\,s_{23} - \frac{p_3{\cdot}\epsilon_1\,p_3{\cdot}\epsilon_2\,p_2{\cdot}\epsilon_3\,s_{12}}{s_{13}} + \frac{1}{2}\,\frac{\epsilon_2{\cdot}\epsilon_3\,p_3{\cdot}\epsilon_1\,s_{23}\,s_{12}}{s_{13}}\,,\\
T_{211} &= p_2{\cdot}\epsilon_1\,p_1{\cdot}\epsilon_2\,p_1{\cdot}\epsilon_3 - \frac{1}{2}\,\epsilon_1{\cdot}\epsilon_2\,p_1{\cdot}\epsilon_3\,s_{12} - \frac{p_2{\cdot}\epsilon_1\,p_1{\cdot}\epsilon_2\,p_2{\cdot}\epsilon_3\,s_{13}}{s_{23}} + \frac{1}{2}\,\frac{\epsilon_1{\cdot}\epsilon_2\,p_2{\cdot}\epsilon_3\,s_{13}\,s_{12}}{s_{23}}\,,\\
T_{311} &= p_3{\cdot}\epsilon_1\,p_1{\cdot}\epsilon_2\,p_1{\cdot}\epsilon_3 - \frac{1}{2}\,\epsilon_1{\cdot}\epsilon_3\,p_1{\cdot}\epsilon_2\,s_{13} - \frac{p_3{\cdot}\epsilon_1\,p_3{\cdot}\epsilon_2\,p_1{\cdot}\epsilon_3\,s_{12}}{s_{23}} + \frac{1}{2}\,\frac{\epsilon_1{\cdot}\epsilon_3\,p_3{\cdot}\epsilon_2\,s_{13}\,s_{12}}{s_{23}}\,,\\
T_{312} &= p_3{\cdot}\epsilon_1\,p_1{\cdot}\epsilon_2\,p_2{\cdot}\epsilon_3 - p_2{\cdot}\epsilon_1\,p_3{\cdot}\epsilon_2\,p_1{\cdot}\epsilon_3 + \frac{1}{2}\,\epsilon_1{\cdot}\epsilon_3\,p_3{\cdot}\epsilon_2\,s_{12} + \frac{1}{2}\,\epsilon_1{\cdot}\epsilon_2\,p_1{\cdot}\epsilon_3\,s_{23}\\
&\quad - \frac{1}{2}\,\epsilon_1{\cdot}\epsilon_3\,p_1{\cdot}\epsilon_2\,s_{23} + \frac{1}{2}\,\epsilon_2{\cdot}\epsilon_3\,p_2{\cdot}\epsilon_1\,s_{13} - \frac{1}{2}\,\epsilon_1{\cdot}\epsilon_2\,p_2{\cdot}\epsilon_3\,s_{13} - \frac{1}{2}\,\epsilon_2{\cdot}\epsilon_3\,p_3{\cdot}\epsilon_1\,s_{12}\,.
\end{aligned} \tag{3.12}$$

The coefficients are functions of the invariants s_{12}, s_{23} and s_{13} and are further related by symmetry under the interchange of the three gluons,

$$\begin{aligned}
A_{211}(s_{12},s_{13},s_{23}) &= -A_{311}(s_{13},s_{12},s_{23})\,,\\
A_{232}(s_{12},s_{13},s_{23}) &= -A_{311}(s_{12},s_{23},s_{13})\,.
\end{aligned} \tag{3.13}$$

The coefficients A_{ijk} may be easily extracted from a Feynman diagram calculation using projectors such that,

$$\sum_{\text{spins}} \mathcal{P}(A_{ijk})\,S_{\mu\nu\rho}(g_1;g_2;g_3)\epsilon_1^\mu\epsilon_2^\nu\epsilon_3^\rho = A_{ijk}\,, \tag{3.14}$$

where the four projectors are given by,

$$\begin{aligned}
\mathcal{P}(A_{311}) &= -\frac{(D-4)}{s_{12}\,s_{23}\,s_{13}\,(D-3)}T^\dagger_{232} - \frac{s_{23}\,(D-4)}{{s_{13}}^2 s_{12}^2\,(D-3)}T^\dagger_{211}\\
&\quad + \frac{s_{23}\,D}{s_{12}\,{s_{13}}^3\,(D-3)}T^\dagger_{311} - \frac{(D-2)}{{s_{13}}^2 s_{12}\,(D-3)}T^\dagger_{312},\\
\mathcal{P}(A_{232}) &= \frac{s_{13}\,D}{s_{12}\,{s_{23}}^3\,(D-3)}T^\dagger_{232} + \frac{(D-4)}{s_{23}\,s_{12}^2\,(D-3)}T^\dagger_{211}\\
&\quad - \frac{(D-4)}{s_{12}\,s_{23}\,s_{13}\,(D-3)}T^\dagger_{311} + \frac{(D-2)}{{s_{23}}^2 s_{12}\,(D-3)}T^\dagger_{312},\\
\mathcal{P}(A_{312}) &= \frac{(D-2)}{{s_{23}}^2 s_{12}\,(D-3)}T^\dagger_{232} + \frac{(D-2)}{s_{13}\,s_{12}^2\,(D-3)}T^\dagger_{211}
\end{aligned}$$

$$
\begin{aligned}
\mathcal{P}(A_{211}) &= -\frac{(D-2)}{{s_{13}}^2 s_{12}\,(D-3)}T^\dagger_{311} + \frac{D}{s_{12}\,s_{23}\,s_{13}\,(D-3)}T^\dagger_{312}, \\
&\quad \frac{(D-4)}{s_{23}\,{s_{12}}^2\,(D-3)}T^\dagger_{232} + \frac{s_{23}\,D}{s_{13}\,{s_{12}}^3\,(D-3)}T^\dagger_{211} \\
&\quad -\frac{s_{23}\,(D-4)}{{s_{13}}^2{s_{12}}^2\,(D-3)}T^\dagger_{311} + \frac{(D-2)}{s_{13}\,{s_{12}}^2\,(D-3)}T^\dagger_{312}.
\end{aligned}
\tag{3.15}
$$

Each of the tensor coefficients A_{ijk} has a perturbative expansion of the form,

$$
A_{ijk} = \lambda\sqrt{4\pi\alpha_s}\left[A^{(0)}_{ijk} + \left(\frac{\alpha_s}{2\pi}\right)A^{(1)}_{ijk} + \left(\frac{\alpha_s}{2\pi}\right)^2 A^{(2)}_{ijk} + \mathcal{O}\left((\alpha_s)^3\right)\right], \tag{3.16}
$$

while the tree-level values are,

$$
\begin{aligned}
A^{(0)}_{211} &= \frac{2}{s_{13}}, \\
A^{(0)}_{311} &= -\frac{2}{s_{12}}, \\
A^{(0)}_{232} &= \frac{2}{s_{12}}, \\
A^{(0)}_{312} &= -\frac{2}{s_{12}} - \frac{2}{s_{23}} - \frac{2}{s_{13}}.
\end{aligned}
\tag{3.17}
$$

3.1.2 The general tensor for $H \to q\bar{q}g$

The most general tensor structure for the partonic current $T_\rho(q;\bar{q};g)$ is given by,

$$
T_\rho(q;\bar{q};g)\epsilon^\rho_3 = A_1\bar{u}(p_1)\not{p}_3 v(p_2)p_1\cdot\epsilon_3 + A_2\bar{u}(p_1)\not{p}_3 v(p_2)p_2\cdot\epsilon_3 + A_3\bar{u}(p_1)\not{\epsilon}_3 v(p_2), \tag{3.18}
$$

where $p_3\cdot\epsilon_3 = 0$ has been applied. The QCD Ward identity yields,

$$
A_3 = -p_1\cdot p_3 A_1 - p_2\cdot p_3 A_2,
$$

such that the amplitude can be written as,

$$
\begin{aligned}
T_\rho(q;\bar{q};g)\epsilon^\rho_3 &= A_1\left(\bar{u}(p_1)\not{p}_3 v(p_2)p_2\cdot\epsilon_3 - \bar{u}(p_1)\not{\epsilon}_3 v(p_2)p_2\cdot p_3\right) \\
&\quad + A_2\left(\bar{u}(p_1)\not{p}_3 v(p_2)p_1\cdot\epsilon_3 - \bar{u}(p_1)\not{\epsilon}_3 v(p_2)p_1\cdot p_3\right) \qquad (3.19) \\
&\equiv A_1 T_1 + A_2 T_2\,. \qquad (3.20)
\end{aligned}
$$

The coefficients A_i can be extracted from a Feynman diagram calculation by using projectors such that,

$$
\sum_{\text{spins}} \mathcal{P}(A_i)T_\rho(q;\bar{q};g)\epsilon^\rho_3 = A_i\,, \tag{3.21}
$$

where the projectors are given by,

$$
\begin{aligned}
\mathcal{P}(A_1) &= \frac{(D-2)}{2(D-3)s_{12}s^2_{13}}T^\dagger_1 - \frac{(D-4)}{2(D-3)s_{12}s_{13}s_{23}}T^\dagger_2\,, \qquad (3.22) \\
\mathcal{P}(A_2) &= -\frac{(D-4)}{2(D-3)s_{12}s_{13}s_{23}}T^\dagger_1 + \frac{(D-2)}{2(D-3)s_{12}s^2_{23}}T^\dagger_2\,. \qquad (3.23)
\end{aligned}
$$

Each of the coefficients A_i has a perturbative expansion of the form,

$$A_i \;=\; \lambda\sqrt{4\pi\alpha_s}\left[A_i^{(0)} + \left(\frac{\alpha_s}{2\pi}\right)A_i^{(1)} + \left(\frac{\alpha_s}{2\pi}\right)^2 A_i^{(2)} + \mathcal{O}\left((\alpha_s)^3\right)\right] , \tag{3.24}$$

while the tree-level values are simply,

$$A_1^{(0)} = A_2^{(0)} = \frac{1}{s_{12}} . \tag{3.25}$$

3.1.3 Helicity amplitudes

The general form of the renormalised helicity amplitude $|\mathcal{M}_{ggg}^{\lambda_1\lambda_2\lambda_3}\rangle$ for the decay, $H(p_4) \to g_1(p_1,\lambda_1) + g_2(p_2,\lambda_2) + g_3(p_3,\lambda_3)$ can be written as,

$$|\mathcal{M}_{ggg}^{\lambda_1\lambda_2\lambda_3}\rangle = S_{\mu\nu\rho}(g_1;g_2;g_3)\epsilon_{1,\lambda_1}^{\mu}(p_1)\epsilon_{2,\lambda_2}^{\nu}(p_2)\epsilon_{3,\lambda_3}^{\rho}(p_3) , \tag{3.26}$$

where the $\lambda_i = \pm$ denote helicity. Similarly, the amplitude for the decay $|\mathcal{M}_{q\bar{q}g}^{\lambda_1\lambda_2\lambda_3}\rangle$ for the decay, $H(p_4) \to q(p_1,\lambda_1) + \bar{q}(p_2,\lambda_2) + g(p_3,\lambda_3)$ can be written as,

$$|\mathcal{M}_{q\bar{q}g}^{\lambda_1\lambda_2\lambda_3}\rangle = T_{\rho}(q^{\lambda_1};\bar{q}^{\lambda_2};g)\epsilon_{3,\lambda_3}^{\rho}(p_3) . \tag{3.27}$$

The helicity amplitudes can be obtained from the general D-dimensional tensors of eqs. (3.9) and (3.18) by setting the dimensionality of the Lorentz matrices to be four and using standard four-dimensional helicity techniques [69,95,96]. This corresponds to working in the 't Hooft-Veltman scheme. The standard convention of denoting the two helicity states of a four-dimensional light-like spinor $\psi(p)$ by,

$$\psi_{\pm}(p) = \frac{1}{2}(1 \pm \gamma_5)\psi(p), \tag{3.28}$$

is being used with the further notation,

$$|p\pm\rangle = \psi_{\pm}(p), \qquad\qquad \langle p\pm| = \overline{\psi}_{\pm}(p). \tag{3.29}$$

Particles may thus be crossed to the initial state by reversing the sign of the helicity. The basic quantity is the spinor product,

$$\langle pq\rangle = \langle p-|q+\rangle, \qquad\qquad [pq] = [p+|q-], \tag{3.30}$$

such that

$$\langle pq\rangle[qp] = 2p\cdot q. \tag{3.31}$$

The polarisation vector of an outgoing light-like particle with momentum p can then be written as

$$\epsilon_{\pm}^{\mu}(p;q) = \pm\frac{\langle q\mp|\gamma^{\mu}|p\mp\rangle}{\sqrt{2}\langle q\mp|p\pm\rangle} \tag{3.32}$$

where q is a light-like reference momentum that satisfies $q\cdot p \neq 0$ but which otherwise can be chosen freely. Important identities relating spinorial objects are the Fierz rearrangement,

$$\langle p+|\gamma^{\mu}|q+\rangle\langle r+|\gamma^{\mu}|s+\rangle = 2[pr]\langle sq\rangle \tag{3.33}$$

and charge conjugation,

$$\langle p+|\gamma^{\mu}|q+\rangle = \langle q-|\gamma^{\mu}|p-\rangle. \tag{3.34}$$

Contractions with gamma matrices can be expressed in terms of projection operators,

$$\not{k}_i = \Big[\frac{1}{2}(1+\gamma_5) + \frac{1}{2}(1-\gamma_5)\Big]\not{k}_i = |i^+\rangle\langle i^+| + |i^-\rangle\langle i^-|. \tag{3.35}$$

Substituting eq. (3.12) into eq. (3.11), one can express the helicity amplitudes for $H \to ggg$ directly in terms of spinor products. It turns out that the only two independent helicity amplitudes are $|\mathcal{M}^{+++}_{ggg}\rangle$ and $|\mathcal{M}^{++-}_{ggg}\rangle$. The other helicity amplitudes are obtained from $|\mathcal{M}^{+++}_{ggg}\rangle$ and $\mathcal{M}^{++-}_{ggg}\rangle$ by the usual parity relation and by exploiting the symmetry of the gluons. Explicitly, choosing p_{i+1} as reference momentum for ϵ_{i,λ_i} one finds,

$$\begin{aligned} |\mathcal{M}^{+++}_{ggg}\rangle &= \alpha\,\frac{1}{\sqrt{2}}\frac{M_H^4}{\langle p_1p_2\rangle\langle p_2p_3\rangle\langle p_3p_1\rangle}, \\ |\mathcal{M}^{++-}_{ggg}\rangle &= \beta\,\frac{1}{\sqrt{2}}\frac{[p_1p_2]^3}{[p_2p_3][p_1p_3]}, \end{aligned} \tag{3.36}$$

where the coefficients α and β multiply the tree-level helicity amplitudes and are written in terms of the tensor coefficients,

$$\begin{aligned} \alpha &= \frac{s_{12}s_{13}s_{23}}{2M_H^4}\left(\frac{s_{12}}{s_{23}}A_{211} + \frac{s_{23}}{s_{13}}A_{232} - \frac{s_{13}}{s_{23}}A_{311} - 2A_{312}\right), \\ \beta &= \frac{s_{13}}{2}A_{211}. \end{aligned} \tag{3.37}$$

Likewise (3.19) yields the helicity amplitudes for $H \to q\bar{q}g$ in terms of spinor products. There is only one independent helicity amplitude $|\mathcal{M}^{-++}_{q\bar{q}g}\rangle$ and all other amplitudes can be obtained from $|\mathcal{M}^{-++}_{q\bar{q}g}\rangle$ using the usual parity and charge conjugation relations. By choosing p_1 as reference momentum for ϵ_{3,λ_3}, one obtains,

$$|\mathcal{M}^{-++}_{q\bar{q}g}\rangle = \gamma\,\frac{1}{\sqrt{2}}\frac{[p_2p_3]^2}{[p_1p_2]}\,. \tag{3.38}$$

The helicity coefficient γ is obtained from the tensor coefficients as,

$$\gamma = s_{12}\,A_1\,. \tag{3.39}$$

As with the tensor coefficients, the helicity amplitude coefficients α, β and γ are vectors in colour space and have perturbative expansions,

$$\Omega = \lambda\sqrt{4\pi\alpha_s}T_\Omega\left[\Omega^{(0)} + \left(\frac{\alpha_s}{2\pi}\right)\Omega^{(1)} + \left(\frac{\alpha_s}{2\pi}\right)^2\Omega^{(2)} + \mathcal{O}(\alpha_s^3)\right]\,,$$

for $\Omega = \alpha, \beta, \gamma$. The colour factor is $T_\alpha = T_\beta = f^{a_1a_2a_3}$ and $T_\gamma = T^{a_3}_{i_1j_2}$.

3.2 REDUZE and master integrals

The rich tensorial structure of the gluon self-couplings results in a large number of two-loop integrals to be computed. These can be expressed by introducing a basis of propagator momenta, called an auxilliary topology, such that all scalar products involving loop momenta which appear in a given Feynman diagram can be written as linear combinations of these propagators. The loop integrals can then be expressed in terms of powers of these propagators, either in the denominator or in the numerator of the integrand:

$$\mathbf{I}_{t,r,s}(k_1,\ldots,k_l,p_1,\ldots,p_n) = \int \mathrm{d}^D k_1 \ldots \int \mathrm{d}^D k_l \frac{P_{j_{t+1}}^{s_1}\cdots P_{j_n}^{s_{n-t}}}{P_{j_1}^{r_1}\cdots P_{j_t}^{r_t}}, \tag{3.40}$$

where $r = \sum_i r_i$ and $s = \sum_i s_i$ and the integral is completely specified by the r_i's and s_i's. The subset of t propagators needed to describe the integrals of a given Feynman diagram is called a topology and subsets of a topology where one or more propagators have been removed are called subtopologies.
The number of independent integrals can be reduced by using integration-by-parts (IBP) identities [32, 33]. These follow from the fact that in dimensional regularisation, the integral over a total derivative vanishes. By carrying out derivatives of the type

$$\int \mathrm{d}^D k_i \frac{\partial}{\partial k_i} [q^\mu \mathbf{I}_{t,r,s}(k_1, \ldots, k_l, p_1, \ldots, p_n)] = 0, \tag{3.41}$$

where q is a loop or external momentum, one obtains relations between different integrals. Obviously a great number of these identities can be derived in this way, and not all of them are linearly independent. Such identities can be used to set up a homogeneous system of equations which can be solved for a small set of integrals, called master integrals, in terms of which all other integrals can be expressed. This procedure has been automatised and implemented in the program REDUZE [97] using the Laporta algorithm [98], which is based on a lexicographic ordering of the integrals. REDUZE also offers the optional use of Lorentz invariance (LI) [99] identities, which are not linearly independent to the IBP identities but can speed up the calculation.
The master integrals relevant for this calculation are two-loop four-point functions with one leg off-shell. These functions were all computed in [34, 35] in dimensional regularisation using the method of differential equations [99] which is sketched in the following:
For a given t-propagator topology, one first needs to choose the master integral. One typically takes $\mathbf{I}_{t,t,0}$, the integral where all propagators in the denominator are raised to unit power and no further propagator in the numerator. Certain topologies depend on two master integrals and thus require a further choice. Differentiating the master integral with respect to one of the Lorentz invariants it depends on yields a combination of integrals, among which are integrals with one of the propagators in the denominator raised to power two and potentially a propagator in the numerator, as well as the master integral and integrals appearing in subtopologies:

$$\begin{aligned} s_{ij} \frac{\partial}{\partial s_{ij}} \mathbf{I}_{t,t,0}(s_{ij}, s_{jk}, s_{ki}) \sim \mathbf{I}_{t,t+1,1}(s_{ij}, s_{jk}, s_{ki}) + \mathbf{I}_{t,t+1,0}(s_{ij}, s_{jk}, s_{ki}). \\ + \mathbf{I}_{t,t,0}(s_{ij}, s_{jk}, s_{ki}) + \mathbf{I}_{t-1,r,s}(s_{ij}, s_{jk}, s_{ki}). \end{aligned} \tag{3.42}$$

By application of IBP identities the first two integrals can again be mapped to a linear combination of the master integral and integrals contained in subtopologies, such as to yield following differential equation:

$$\begin{aligned} s_{ij} \frac{\partial}{\partial s_{ij}} \mathbf{I}_{t,t,0}(s_{ij}, s_{jk}, s_{ki}) = A(s_{ij}, s_{jk}, s_{ki}) \mathbf{I}_{t,t,0}(s_{ij}, s_{jk}, s_{ki}) \\ + F(s_{ij}, s_{jk}, s_{ki}, \mathbf{I}_{t-1,r,s}(s_{ij}, s_{jk}, s_{ki})). \end{aligned} \tag{3.43}$$

These equations can be solved in a bottom-up approach, where one first solves the differential equations for the topologies with the smallest number t of propagators, such that integrals contained in this topology are known in terms of the corresponding master integrals when they appear as the inhomogeneous term in differential equations for topologies with more propagators in the denominator. Boundary conditions can be obtained from the analyticity of the master integral at $y = 0$ and $z = 0$. A special treatment is required for topologies depending on two master integrals, especially in the case of non-planar topologies [35].
The results of [34, 35] take the form of a Laurent series in ϵ, starting at ϵ^{-4}, with coefficients

containing one- and two-dimensional harmonic polylogarithms (HPLs [100] and 2dHPLs [34]), which are a generalisation of Nielsen's polylogarithms [101]. Several numerical implementations of HPLs and 2dHPLs are available [102, 103].

3.3 Feynman diagrammatic calculation

The calculation of the two-loop Feynman amplitudes contributing to $H \to ggg$ and $H \to q\bar{q}g$ follows closely the calculation of the two-loop helicity amplitudes for $\gamma^* \to q\bar{q}g$ [104], which contribute to the NNLO corrections to $e^+e^- \to 3j$ and related event shapes [105, 106], and of the two-loop helicity amplitudes for $q\bar{q} \to V\gamma$ [107]. Two completely independent calculations of the amplitudes have been performed, which provides a strong internal cross-check of the results.

The Feynman diagrams contributing to the i-loop amplitude $|\mathcal{M}^{(i)}\rangle$ $(i = 0, 1, 2)$ were all generated using QGRAF [108]. For $H \to ggg$, there are four diagrams at tree-level, 60 diagrams at one loop and 1306 diagrams at two loops, while for $H \to q\bar{q}g$, there is one diagram at tree-level, 15 diagrams at one loop and 328 diagrams at two loops. Computer algebra methods implemented in FORM [112] have been used to perform the evaluation of the Feynman rules, as well as the summation over colours and spins after application of the D-dimensional projectors given in eqs. (3.15) and (3.23). When summing over the polarisations of the external gluons in the projectors, the axial gauge with a D-dimensional metric has been used. Internal gluons were kept in Feynman gauge, resulting in internal ghost contributions to the loop amplitudes. The integrals appearing in the individual two-loop diagrams contain up to seven propagators in the denominator, and up to five irreducible scalar products in the numerator (i.e. scalar products which can not be expressed as linear combinations of the occurring propagators). Since the loop momenta as assigned by QGRAF do not in general match the momenta of the auxilliary topology, an iterated shifting and matching algorithm for the momenta has been implemented in FORM. It furthermore might require a permutation of the external momenta, which is undone after insertion of the master integrals. The planar resp. nonplanar topologies are

Planar topology	Non-planar topology
$q_1 = k_1$	$q_1 = k_1$
$q_2 = k_2$	$q_2 = k_2$
$q_3 = k_1 - k_2$	$q_3 = k_1 - k_2$
$q_4 = k_1 - p_1$	$q_4 = k_1 - k_2 - p_3$
$q_5 = k_2 - p_1$	$q_5 = k_2 - p_1$
$q_6 = k_1 - p_1 - p_2$	$q_6 = k_1 - p_1 - p_3$
$q_7 = k_2 - p_1 - p_2$	$q_7 = k_2 - p_1 - p_2$
$q_8 = k_1 - p_1 - p_2 - p_3$	$q_8 = k_1 - p_1 - p_2 - p_3$
$q_9 = k_2 - p_1 - p_2 - p_3$	$q_9 = k_2 - p_1 - p_2 - p_3$

Expressing the diagrams in terms of the topologies and performing the reduction yields very large expressions $\mathcal{O}$(MByte). This partly originates in the fact that FORM performs operations only term by term and thus is unable to cancel expressions of the form

$$\left(1 - \frac{a}{a+b} - \frac{b}{a+b}\right) \cdot \text{large expression}, \tag{3.44}$$

where a and b represent two Lorentz invariants. This problem has been solved by performing a partial fractioning at strategic places in the computation. In the case above for instance, the

replacement

$$\frac{a}{a+b} \to 1 - \frac{b}{a+b}, \tag{3.45}$$

implements the cancellation of the 'hidden zero'. In fact, repeated application of the above replacement and

$$\frac{1}{a(a+b)} \to \frac{1}{ab} - \frac{1}{b(a+b)}, \tag{3.46}$$

achieves the cancellation of all hidden zeroes where the denominator and the numerator can be factorised into products of linear combinations of the s_{ij}'s. To achieve this the partial fractioning has to be hierarchical in the invariants, that is, it is first performed with $a = s_{12}$ in the above formulae, then with $a = s_{13}$ in cases where b does not contain any s_{12}'s. The dimension $D = 4 - 2\epsilon$ has also been included in this procedure.
Inserting the master integrals into the amplitudes and truncating the Laurent series to the required order, the unrenormalised one-loop and two-loop helicity coefficients are obtained. Their Laurent expansion contains HPLs and 2dHPLs up to weight 4.
The expressions for the master integrals derived in [34] apply to the kinematical situation of a $1 \to 3$ decay, while the $H + 1J$ production corresponds to a $2 \to 2$ scattering process. The helicity amplitudes must therefore be crossed to the appropriate kinematical configuration. Their definitions in terms of momentum spinors eqs. (3.36),(3.38) remain unchanged by the crossing, such that only the helicity coefficients α, β, γ are to be continued to the appropriate kinematical region. This requires the analytic continuation of the polylogarithmic functions, which is described in detail in [107, 113]. For Higgs boson production plus one jet, the helicity coefficients have to be continued to three kinematical regions, depending on which of s_{12}, s_{13}, s_{23} is the s-channel variable. In the case of the $q\bar{q}g$ amplitudes:

$$\begin{aligned}
&\text{region } \mathbf{2}: \quad && q(p_1) + \bar{q}(p_2) \to H(p_4) + g(-p_3), \\
&\text{region } \mathbf{3}: \quad && q(p_1) + g(p_3) \to H(p_4) + q(-p_2), \\
&\text{region } \mathbf{4}: \quad && \bar{q}(p_2) + g(p_3) \to H(p_4) + \bar{q}(-p_1).
\end{aligned}$$

Since the helicity coefficient α corresponds to the $|\mathcal{M}^{+++}_{ggg}\rangle$ helicity amplitude, due to the symmetry between gluons $\alpha_2 = \alpha_3 = \alpha_4$ holds. The β coefficient corresponds to the $|\mathcal{M}^{++-}_{ggg}\rangle$ helicity amplitude, such that $\beta_3 = \beta_4$ and only the crossings into regions **2** and **4** are needed. That this holds represents an additional check of the computation. For the $q\bar{q}g$ amplitudes on the other hand the helicity coefficient γ is different in all three crossings.

3.4 Results

Renormalisation of UV divergences is performed in the $\overline{\text{MS}}$ scheme. Denoting unrenormalised quantities with a superscript U, it is carried out by replacing the bare coupling α^U with the renormalised coupling $\alpha_s \equiv \alpha_s(\mu^2)$, evaluated at the renormalisation scale μ^2,

$$\alpha^U \mu_0^{2\epsilon} S_\epsilon = \alpha_s \mu^{2\epsilon} \left[1 - \frac{\beta_0}{\epsilon} \left(\frac{\alpha_s}{2\pi} \right) + \left(\frac{\beta_0^2}{\epsilon^2} - \frac{\beta_1}{2\epsilon} \right) \left(\frac{\alpha_s}{2\pi} \right)^2 + \mathcal{O}(\alpha_s^3) \right] , \tag{3.47}$$

where

$$S_\epsilon = (4\pi)^\epsilon e^{-\epsilon\gamma} \qquad \text{with Euler constant } \gamma = 0.5772\ldots$$

and μ_0^2 is the mass parameter introduced in dimensional regularisation [109–111] to maintain a dimensionless coupling in the bare QCD Lagrangian density; β_0 and β_1 are the first two

coefficients of the QCD β-function, see section 2.7. The renormalisation relation for the effective coupling λ is given in [114] as,

$$\lambda^U = \lambda \left[1 - \frac{\beta_0}{\epsilon}\left(\frac{\alpha_s}{2\pi}\right) + \left(\frac{\beta_0^2}{\epsilon^2} - \frac{\beta_1}{\epsilon}\right)\left(\frac{\alpha_s}{2\pi}\right)^2 + \mathcal{O}(\alpha_s^3)\right] , \tag{3.48}$$

The i-loop contribution to the unrenormalised coefficients is denoted by $\Omega^{(i),\mathrm{U}}$, using the same normalisation as for the decomposition of the renormalised amplitude (3.40). The renormalised coefficients are then obtained as,

$$\begin{aligned}
\Omega^{(0)} &= \Omega^{(0),\mathrm{U}}, \\
\Omega^{(1)} &= S_\epsilon^{-1}\Omega^{(1),\mathrm{U}} - \frac{3\beta_0}{2\epsilon}\Omega^{(0),\mathrm{U}}, \\
\Omega^{(2)} &= S_\epsilon^{-2}\Omega^{(2),\mathrm{U}} - \frac{5\beta_0}{2\epsilon}S_\epsilon^{-1}\Omega^{(1),\mathrm{U}} - \left(\frac{5\beta_1}{4\epsilon} - \frac{15\beta_0^2}{8\epsilon^2}\right)\Omega^{(0),\mathrm{U}}.
\end{aligned} \tag{3.49}$$

For the remainder of this chapter the renormalisation scale is set to $\mu^2 = M_H^2 = s_{123}$. The full renormalisation scale dependence of the helicity coefficients is:

$$\begin{aligned}
\Omega &= \lambda\sqrt{4\pi\alpha_s(\mu^2)}T_\Omega\Bigg\{\Omega^{(0)} + \left(\frac{\alpha_s(\mu^2)}{2\pi}\right)\left[\Omega^{(1)} + \frac{3}{2}\beta_0\Omega^{(0)}\ln\left(\frac{\mu^2}{s_{123}}\right)\right] \\
&\quad + \left(\frac{\alpha_s(\mu^2)}{2\pi}\right)^2\left[\Omega^{(2)} + \left(\frac{5}{2}\beta_0\Omega^{(1)} + \frac{5}{2}\beta_1\Omega^{(0)}\right)\ln\left(\frac{\mu^2}{s_{123}}\right) + \frac{15}{8}\beta_0^2\Omega^{(0)}\ln^2\left(\frac{\mu^2}{s_{123}}\right)\right] \\
&\quad + \mathcal{O}(\alpha_s^3)\Bigg\}.
\end{aligned} \tag{3.50}$$

The renormalisation scale dependence of a pure QCD process is described in sec. 5.1.6. Differences with the above formula start at two-loops with the β_1 coefficient, as can also be seen by comparing eqs. (3.47) and (3.48).

3.4.1 Infrared factorisation

Following the discussion in section 2.8.2, the IR singularity operators $\boldsymbol{I}_\Omega^{(1)}(\epsilon)$ can be written as

$$\boldsymbol{I}_\alpha^{(1)}(\epsilon) = -\frac{e^{\epsilon\gamma}}{2\Gamma(1-\epsilon)}\left[N\left(\frac{1}{\epsilon^2} + \frac{\beta_0}{N\epsilon}\right)(\mathtt{S}_{12} + \mathtt{S}_{13} + \mathtt{S}_{23})\right] , \tag{3.51}$$

$$= \boldsymbol{I}_\beta^{(1)}(\epsilon), \tag{3.52}$$

$$\boldsymbol{I}_\gamma^{(1)}(\epsilon) = -\frac{e^{\epsilon\gamma}}{2\Gamma(1-\epsilon)}\left[N\left(\frac{1}{\epsilon^2} + \frac{3}{4\epsilon} + \frac{\beta_0}{2N\epsilon}\right)(\mathtt{S}_{13} + \mathtt{S}_{23}) - \frac{1}{N}\left(\frac{1}{\epsilon^2} + \frac{3}{2\epsilon}\right)\mathtt{S}_{12}\right] , \tag{3.53}$$

where, since $\mu^2 = s_{123}$ holds,

$$\mathtt{S}_{ij} = \left(-\frac{s_{123}}{s_{ij}}\right)^\epsilon . \tag{3.54}$$

Note that on expanding $\mathtt{S}_{ij}$, imaginary parts are generated, the sign of which is fixed by the small imaginary part $+i0$ of s_{ij}.

The constant $H_\Omega^{(2)}$ of eq. (2.62) can be constructed by counting the number of radiating partons present in the event. In this case,

$$H_\alpha^{(2)} = H_\beta^{(2)} = 3H_g^{(2)},$$

$$H_\gamma^{(2)} \;=\; 2H_q^{(2)} + H_g^{(2)}. \tag{3.55}$$

At leading order, one can insert the values of the tensorial coefficients given in eqs. (3.17) and (3.25), into eqs. (3.37) and (3.39) respectively to find,

$$\alpha^{(0)} = \beta^{(0)} = \gamma^{(0)} = 1\,. \tag{3.56}$$

The renormalised NLO helicity amplitude coefficients can be straightforwardly obtained to all orders in ϵ from the helicity coefficients $\Omega^{(1)}$. For practical purposes they are needed through to $\mathcal{O}(\epsilon^2)$ in evaluating the one-loop self-interference and the IR divergent one-loop contribution to the two-loop amplitude, while only the finite piece is needed for the one-loop self-interference. They can be decomposed according to their colour structure as follows,

$$\Omega^{(1),finite} \;=\; \left(N_C\; A_\Omega^{(1)} + \frac{1}{N_C}\; B_\Omega^{(1)} + N_F C_\Omega^{(1)} \right). \tag{3.57}$$

This makes sense in view of applying a subtraction scheme since different channels of the real corrections integrate down to different colour structures of the virtual contributions. Such a decomposition thus helps to implement the subtraction terms in a modular way. Furthermore, for some subleading orders in N_C the subtraction terms take very simple forms.
The finite two-loop remainder is obtained by subtracting the predicted IR structure (expanded through to $\mathcal{O}(\epsilon^0)$) from the renormalised helicity coefficient. The finite remainder can be decomposed according to the colour Casimirs as follows,

$$\Omega^{(2),finite} \;=\; \left(N_C^2 A_\Omega^{(2)} + N_C^0 B_\Omega^{(2)} + \frac{1}{N_C^2} C_\Omega^{(2)} + \frac{N_F}{N_C} D_\Omega^{(2)} + N_C N_F E_\Omega^{(2)} + N_F^2 F_\Omega^{(2)} \right), \tag{3.58}$$

where the functions $A_\Omega^{(2)}$-$F_\Omega^{(2)}$ contain HPL's and 2dHPL's up to weight four which depend on dimensionless ratios of the invariants.

3.5 Application to two-loop splitting amplitudes

The computation described above can be upgraded to allow for the calculation of the two-loop splitting amplitudes. These are necessary to describe the collinear behaviour of two-loop matrix elements in single collinear limites. In the course of a subtraction procedure, the splitting functions are integrated over the phase-space of the unresolved parton. Since this yields single poles in ϵ, the splitting functions need to be known up to $\mathcal{O}(\epsilon)$, since this results in finite terms which need to be accounted for. The splitting amplitudes can be extracted using the l-loop generalisation of eq. (2.56):

$$\begin{aligned}
|\mathcal{M}^{(0)}_{H\to ggg}\mathcal{M}^{(l)\dagger}_{H\to ggg}| &\simeq \frac{8\pi\alpha_0}{s_{13}} \sum_{k=0}^{l} \left(\frac{\alpha_0 S_\epsilon}{2\pi}\right)^k \left(\frac{s_{13}}{\mu^2}\right)^{-k\epsilon} P_{gg}^{(k)}(z) |\mathcal{M}^{(0)}_{H\to gg}\mathcal{M}^{(l-k)\dagger}_{H\to gg}|, \\
|\mathcal{M}^{(0)}_{H\to q\bar{q}g}\mathcal{M}^{(l)\dagger}_{H\to q\bar{q}g}| &\simeq \frac{8\pi\alpha_0}{s_{12}} \sum_{k=0}^{l} \left(\frac{\alpha_0 S_\epsilon}{2\pi}\right)^k \left(\frac{s_{12}}{\mu^2}\right)^{-k\epsilon} P_{q\bar{q}}^{(k)}(z) |\mathcal{M}^{(0)}_{H\to gg}\mathcal{M}^{(l-k)\dagger}_{H\to gg}|, \\
|\mathcal{M}^{(0)}_{\gamma^*\to q\bar{q}g}\mathcal{M}^{(l)\dagger}_{\gamma^*\to q\bar{q}g}| &\simeq \frac{8\pi\alpha_0}{s_{13}} \sum_{k=0}^{l} \left(\frac{\alpha_0 S_\epsilon}{2\pi}\right)^k \left(\frac{s_{13}}{\mu^2}\right)^{-k\epsilon} P_{gq}^{(k)}(z) |\mathcal{M}^{(0)}_{H\to q\bar{q}}\mathcal{M}^{(l-k)\dagger}_{H\to q\bar{q}}|,
\end{aligned} \tag{3.59}$$

where α_0 is the bare coupling, $P_{ij}^{(k)}(z)$ is the k-loop splitting function and the hard matrix elements $|\mathcal{M}^{(0)}_{H\to ij}\mathcal{M}^{(l-k)\dagger}_{H\to ij}|$ and $|\mathcal{M}^{(0)}_{\gamma^*\to ij}\mathcal{M}^{(l-k)\dagger}_{\gamma^*\to ij}|$ are given in terms of the corresponding form

factors, which are known up to three loops in QCD [115]. The '$\simeq$' means equality up to terms which are power-supressed in the limit. This means that if the two-loop interferences on the left hand side of the above equations are known up to $\mathcal{O}(\epsilon)$, the splitting functions at the same loop and ϵ order can be solved for. To this end, the master integrals of [34, 35] have been recomputed [116] up to transcendental weight five using the method of differential equations described in this chapter in a canonical basis [117] where the master integrals have uniform transcendental weight. The boundary conditions have been obtained from the expansion of the master integrals around the soft limit [118]. This yields the splitting functions in terms of a Laurent series in ϵ with coefficients which are combinations of 2dHPL's.
As an application, the double-virtual-real contribution to the N^{3}LO Higgs boson production has been considered [116]. These are the two-loop three parton $p_1p_2 \to Hp_3$ interferences, where one parton is allowed to become unresolved. With the two-loop splitting functions, subtraction terms have been constructed which remove the corresponding divergences. Using a suitable phase-space parametrisation, the integration over the single unresolved phase-space of the splitting functions is performed. For $q\overline{q}$ initial states there is no collinear limit and the integration can be easily performed order-by-order in ϵ using the recursive definition of the 2dHPL's. For the qg initial state a collinear limit between the initial and final quarks is successfully subtracted using the $P^{(k)}_{q\overline{q}}$ splitting function. The residue of the subtraction is then finite and can be integrated in the same way as for the $q\overline{q}$ initial state. The treatment of the gg initial state is similar up to a soft limit which needs to be subtracted beforehand. This necessitates the two-loop soft current [118]. The collinear limites are then canceled with subtraction terms based on the $P^{(k)}_{gg}$ splitting functions, where also here the soft limit has been removed.
Analytic expressions are given for the integrated double-virtual-real subtraction terms. Together with the other contributions (triple-real, triple-virtual, double-real-virtual and real-virtual squared), once available, the total cross section for Higgs boson production at N^{3}LO can be calculated.

Chapter 4

Antenna subtraction

Antenna subtraction is an implementation of the idea of subtraction as described in section 2.10. It has been successfully applied both at NLO and at NNLO, in particular with the calculation of the NNLO corrections to e^+e^--production [53, 54], to the all gluons contribution to dijet production [55] as well as to the production of heavy particles [119].
The insight that the soft and collinear radiation described in section 2.8 can be consistently integrated into the notion of radiation between a pair of hard 'radiators' [120] is at the basis of antenna subtraction. According to this, the factorisation of tree-level amplitudes can be described in terms of an antenna function, $X(p_a, p_1, \ldots, p_n, p_b)$, which describes faithfully the radiation of partons with momenta $p_1, \ldots, p_n$ off their colour-neighbouring hard partons with momenta p_a and p_b in all their unresolved limites. This generality is reflected in a momentum map $(p_a, p_1, \ldots, p_n, p_b) \to (p_A, p_B)$, which maps to the set of resolved momenta prior to the radiation and interpolates between all unresolved limites. Using these functions, subtraction terms can be written which reproduce and subtract away the IR divergent behaviour of matrix elements with unresolved coloured particles.
This can also be performed at the level of squared colour ordered amplitudes. The factorisation properties are then encapsulated in the spin-summed squared antenna functions. They can readily be obtained from normalised matrix elements of suitable decay processes, which however goes along with the drawback of involved colour logistics when squaring amplitudes with large parton multiplicities. In the following, the term 'antenna function' will always denominate the squared antenna functions.
Since they are functions of low multiplicity, the integral over the phase-space of the potentially unresolved momenta $p_1, \ldots, p_n$ can be performed analytically using the factorisation of phase-space. This yields the integrated antenna functions $\mathcal{X}(p_A, p_B)$, which depend only on the mapped momenta p_A and p_B. As expected, using dimensional regularisation these feature a structure of explicit $\frac{1}{\epsilon}$ poles. These cancel analytically the pole structure of loop matrix elements when added back as described in section 2.10.

4.1 Antenna functions

There are different classes of antenna functions depending on the identity of the hard radiator partons: gluon-gluon, (anti)quark-gluon and quark-antiquark antennae. This fixes a basic two-parton antenna X_2^0 which is just the squared amplitude for a process involving the hard radiators only. For the gluon-gluon antennae one considers the $H \to 2g$ decay, for the quark-gluon antennae one uses the decay $\tilde{X} \to \tilde{g}g$ of a heavy neutralino to a massless gluino and a gluon, and for quark-antiquark antennae the decay of an off-shell photon $\gamma^\star \to q\overline{q}$ is used. These X_2^0 antennae are normalised to one. The n-parton l-loop antenna function X_n^l is then

obtained as the squared amplitude for the real radiation correction of appropriate multiplicity and loop order to the underlying 2-parton process normalised to the corresponding X_2^0 antenna. It therefore naturally contains all IR singularities of unresolved partons radiated off the two hard radiators specified by the antenna kind.
As already mentioned the antenna functions are obtained from spin-summed squared amplitudes. Since according to eq. (2.53) the IR behaviour of squared amplitudes in collinear limites is given in terms of a tensorial splitting function, this means that angular terms are left over if antenna functions are used to subtract such divergences. These angular terms average to zero after performing the phase-space integral. One alternative solution is to average over phase-space points which are related by a rotation by an angle $\frac{\pi}{2}$ around the axis of the collinear limit under consideration. The angular terms then cancel out and a pointwise subtraction is maintained.
Depending on the identity of the partons in the antenna, including the radiated ones, different letters are used to label the antenna. Pure gluonic antennae are named $F_n^l(\ldots)$. Since an $F_n^0(1,\ldots,n)$ antenna is proportional to a $|M_{H\to ng}(1,\ldots,n)|^2$ squared amplitude, any of the n partons can become unresolved. The momentum maps, on the other hand, require two partons to be assigned as hard radiators. In order to avoid one of the hard radiators to become soft, partial fractioning is used to decompose the antennae into sub-antennae whose singularity structure corresponds to a single phase-space mapping. These are identified with a small letter, for instance $f_n^0(\ldots)$ for a gluons-only subantenna. Clearly different decompositions of the antennae are necessary depending on the kinematics, since an initial state parton is constrained to be resolved due to the convolution with a PDF, and thus can be unambigously labeled as a hard radiator.

4.2 Real subtraction term

The construction of the real subtraction terms is guided by the colour-connected nature of unresolved singularities in colour-ordered amplitudes. At NLO, the singularities appearing due to a parton j which is colour connected to the hard partons i and k are encapsulated in the three-parton tree-level antenna function $X_3^0(i,j,k)$ associated with a mapping $(i,j,k)\to(I,K)$. The antenna multiplies a 'reduced' matrix element which depends only on the hard mapped momenta, thus reflecting the factorising nature of IR singularities. The antenna and mapping are such that in limites where j becomes unresolved, they collapse to the correct unresolved factor as in section 2.8.1, times the reduced matrix element where the momenta I and K have been adequately reconstructed out of i, j and k. For a squared colour ordered amplitude $|M_{n+3}^{(0)}(1,2;3,\ldots,n{+}3)|^2$, the following subtraction terms remove all single unresolved singularities:

$$\begin{aligned}\mathrm{d}\hat{\sigma}_{NLO}^R = \mathcal{N}_{NLO}^R \sum_j \mathrm{d}\Phi_{n+1}\frac{1}{S_{n+1}} \\ \times X_3^0(i,j,k)|M_{n+2}^{(0)}(\ldots,I,K,\ldots)|^2 J_n^{(n)}(p_3,\ldots,p_I,p_K,\ldots,p_{n+3}),\end{aligned} \tag{4.1}$$

where the sum is over all partons in the final state, and the order of the momenta in the antennae and reduced squared amplitudes follow the colour ordering of the squared amplitude they subtract the singularities from. This means in particular that either of partons i or k may be in the initial state. Depending on this the mappings take different forms which are detailed in the following sections, together with the antennae they are associated to. In general the mappings are required to conserve momentum and keep the mapped momenta on-shell.
The previous discussion shows that colour ordering is a useful guide for the construction of the

subtraction terms. It is therefore convenient to work with squared colour ordered amplitudes instead of the full squared matrix element. The matrix element can then be obtained by summing over the different colour orderings. In the remainder of this chapter, this sum will be left implicit and the term 'squared amplitude' will refer to squared colour ordered amplitudes respectively interferences of colour ordered amplitudes of different loop orders.

4.2.1 Final-final kinematics

When both partons are in the final state, the $i, j, k \to I, K$ mapping is given by [120, 121]:

$$\begin{aligned} p_I^\mu &= p_{\widetilde{(ij)}}^\mu = x p_i^\mu + r p_j^\mu + z p_K^\mu \\ p_K^\mu &= p_{\widetilde{(jk)}}^\mu = (1-x) p_i^\mu + (1-r) p_j^\mu + (1-z) p_K^\mu, \end{aligned} \tag{4.2}$$

where

$$\begin{aligned} x &= \frac{1}{2(s_{ij}+s_{ik})}\Big[(1+\rho)s_{ijk} - 2r s_{jk}\Big], & \rho^2 &= 1 + \frac{4r(1-r)s_{ij}s_{jk}}{s_{ijk}s_{ik}}, \\ z &= \frac{1}{2(s_{jk}+s_{ik})}\Big[(1-\rho)s_{ijk} - 2r s_{ij}\Big], & r &= \frac{s_{jk}}{s_{ij}+s_{jk}}. \end{aligned} \tag{4.3}$$

It has the following properties in unresolved limites of the parton j:

$p_j \to 0$	$p_I \to p_i$	$p_K \to p_k$
$p_j \| p_i$	$p_I \to p_i + p_j$	$p_K \to p_k$
$p_j \| p_k$	$p_I \to p_i$	$p_K \to p_j + p_k$.

Thus at NLO the real subtraction contribution $\mathrm{d}\sigma^S$ typically contains terms of the following kind:

$$X_3^0(i,j,k)|M_{n+2}^0(1,\ldots,I,K,\ldots,n+3)|^2 J_n^{(n)}(p_3,\ldots,p_I,p_K,\ldots,p_{n+3}), \tag{4.4}$$

where the reduced squared amplitude M and the jet function J_n depend on the mapped momenta. Taking advantage of the factorisation of phase-space

$$\begin{aligned} \mathrm{d}\Phi_{n+1}(p_{\hat{1}}, p_{\hat{2}}; p_3, \ldots, p_i, p_j, p_k, \ldots, p_{n+3}) = \mathrm{d}\Phi_n(p_{\hat{1}}, p_{\hat{2}}; p_3, \ldots, p_I, p_K, \ldots, p_{n+3}) \\ \cdot \mathrm{d}\Phi_{X_{ijk}}(p_i, p_j, p_k; p_I + p_K), \end{aligned} \tag{4.5}$$

where hatted momenta are in the initial state and the antenna phase-space $\mathrm{d}\Phi_{X_{ijk}}$ is proportional to the $1 \to 3$ decay phase-space, one can perform the integration

$$\frac{1}{C(\epsilon)} \int \mathrm{d}\Phi_{X_{ijk}} X_3^0(i,j,k) = \mathcal{X}(I,K), \tag{4.6}$$

where the normalisation factor $C(\epsilon)$ is

$$C(\epsilon) = (4\pi)^\epsilon \frac{e^{-\epsilon\gamma_E}}{8\pi^2}. \tag{4.7}$$

This yields the integrated antenna function $\mathcal{X}(I,K)$, which depends only on the scale $s_{IK} = s_{ijk}$. At NNLO one also needs three-parton one-loop antenna functions $X_3^1(i,j,k)$ to reproduce the single unresolved divergences of one-loop matrix elements as well as four-parton tree-level antenna functions $X_4^0(i,j,k,l)$ to reproduce the double unresolved behaviour of tree-level matrix elements. While the same mapping can be used for the X_3^1 as for the X_3^0 antennae, a new

mapping $(i,j,k,l) \to (I,L)$ is needed to interpolate between the double unresolved limites of the $X_4^0(i,j,k,l)$ antenna. It also implements momentum conservation, yields on-shell mapped momenta and is given by [122]:

$$
\begin{aligned}
p_I^\mu &= p^\mu_{\widetilde{(ijk)}} = x p_i^\mu + r_1 p_j^\mu + r_2 p_k^\mu + z p_l^\mu, \\
p_K^\mu &= p^\mu_{\widetilde{(jkl)}} = (1-x) p_i^\mu + (1-r_1) p_j^\mu + (1-r_2) p_k^\mu + (1-z) p_l^\mu, \\
r_1 &= \frac{s_{jk}+s_{jl}}{s_{ij}+s_{jk}+s_{jl}}, \\
r_2 &= \frac{s_{kl}}{s_{ik}+s_{jk}+s_{kl}}, \\
x &= \frac{1}{2(s_{ij}+s_{ik}+s_{il})}\Big[(1+\rho)s_{ijkl} - r_1(s_{jk}+2s_{jl}) - r_2(s_{jk}+2s_{kl}) \\
&\qquad + (r_1-r_2)\frac{s_{ij}s_{kl}-s_{ik}s_{jl}}{s_{il}}\Big], \\
z &= \frac{1}{2(s_{il}+s_{jl}+s_{kl})}\Big[(1-\rho)s_{ijkl} - r_1(s_{jk}+2s_{ij}) - r_2(s_{jk}+2s_{ik}) \\
&\qquad - (r_1-r_2)\frac{s_{ij}s_{kl}-s_{ik}s_{jl}}{s_{il}}\Big], \\
\rho^2 &= 1 + \frac{(r_1-r_2)^2}{s_{il}^2 s_{ijkl}^2}\lambda(s_{ij}s_{kl}, s_{il}s_{jk}, s_{ik}s_{jl}) \\
&\qquad + \frac{1}{s_{il}s_{ijkl}}\Big[2(r_1(1-r_2)+r_2(1-r_1))(s_{ij}s_{kl}+s_{ik}s_{jl}-s_{jk}s_{il}) \\
&\qquad + 4r_1(1-r_1)s_{ij}s_{jl} + 4r_2(1-r_2)s_{ik}s_{kl}\Big], \\
\lambda(u,v,w) &= u^2+v^2+w^2-2(uv+uw+vw).
\end{aligned}
\tag{4.8}
$$

In the various double unresolved limites it fulfills:

$p_j \ , \ p_k \to 0$	$p_I \to p_i$	$p_L \to p_l$,
$p_i \vert\vert p_j \vert\vert p_k$	$p_I \to p_i + p_j + p_k$	$p_L \to p_l$,
$p_j \vert\vert p_k \vert\vert p_l$	$p_I \to p_i$	$p_L \to p_j + p_k + p_l$,
$p_j \to 0 \ , \ p_k \vert\vert p_l$	$p_I \to p_i$	$p_L \to p_k + p_l$,
$p_k \to 0 \ , \ p_i \vert\vert p_j$	$p_I \to p_i + p_j$	$p_L \to p_l$,
$p_i \vert\vert p_j \ , \ p_k \vert\vert p_l$	$p_I \to p_i + p_j$	$p_L \to p_k + p_l$.

In colour ordered limites of the F_4^0 antenna where only one of the partons j and k becomes unresolved, this mapping collapses to a NLO final-final mapping. This allows the subtraction of single unresolved limites from the four-parton antenna function with products of tree-parton antennae as described in section 4.5.1. These antennae and mappings are sufficient to construct all subtraction terms for observables at e^+e^- colliders.

4.2.2 Initial-final kinematics

In electron-hadron scattering experiments, one parton is in the initial state. Collinear emission off these partons takes place prior to the scattering and the associated singularities need to be absorbed into the PDF's. The extraction of these divergences requires the analytic continuation of the antenna function to kinematics where one of the hard radiators is in the initial state as

well as an initial-final mapping $(\hat{i},j,k) \to (\hat{I},K) = (\hat{\tilde{i}},K)$, where the initial state parton is merely being rescaled as denoted by the bar notation [50]:

$$\begin{aligned} p_I^\mu &= p_{\hat{\tilde{i}}}^\mu = x_i p_i^\mu, \\ p_K^\mu &= p_{\widetilde{(jk)}}^\mu = p_j^\mu + p_k^\mu - (1-x_i)p_i^\mu, \end{aligned} \tag{4.9}$$

where

$$x_i = \frac{s_{ij}+s_{ik}+s_{jk}}{s_{ij}+s_{ik}}. \tag{4.10}$$

When j becomes unresolved it fulfills:

$$\begin{array}{l|lll} p_j \to 0 & p_{\hat{\tilde{i}}} \to p_{\hat{i}} & p_K \to p_k \\ p_j || p_{\hat{i}} & p_{\hat{\tilde{i}}} \to z_i p_{\hat{i}} & p_K \to p_k \\ p_j || p_k & p_{\hat{\tilde{i}}} \to p_{\hat{i}} & p_K \to p_j + p_k, \end{array}$$

where $(1-z)$ is the momentum fraction carried away by the collinear parton j. The new NLO subtraction term corresponding to this configuration is

$$X_3^0(\hat{i},j,k)|M_{n+2}^0(1,\ldots,\hat{\tilde{i}},K,\ldots,n+3)|^2 J_n^{(n)}(p_3,\ldots,p_K,\ldots,p_{n+3}). \tag{4.11}$$

In the initial-final case, the factorisation of phase-space reads as a convolution of a n-particle phase-space with a two-particle phase-space:

$$\begin{aligned} \mathrm{d}\Phi_{n+1}(p_{\hat{1}},p_{\hat{2}};p_3,\ldots,p_j,p_k,\ldots,p_{n+3}) = \mathrm{d}\Phi_n(p_{\hat{1}},x_2 p_{\hat{2}};p_3,\ldots,p_K,\ldots,p_{n+3}) \\ \cdot \frac{Q^2}{2\pi}\mathrm{d}\Phi_2(p_j,p_k;p_{\hat{2}},q)\frac{\mathrm{d}x_2}{x_2}, \end{aligned} \tag{4.12}$$

$$q = p_j + p_k - p_2, \tag{4.13}$$

$$Q^2 = -q^2, \tag{4.14}$$

and similarly for subtraction terms involving p_a. Performing the integration over the antenna phase-space yields

$$\frac{1}{C(\epsilon)}\int \mathrm{d}\Phi_2 \frac{Q^2}{2\pi} X_3^0(\hat{i},j,k) = \mathcal{X}(\hat{\tilde{i}},K,z_i), \tag{4.15}$$

where $C(\epsilon)$ is given as in eq. (4.7). There remains a dependence on the momentum fraction z_i of the initial state parton after collinear emission prior to the scattering. The momentum fraction is not kinematically fixed (altough its boundaries are) and has to be integrated over. This integration formally corresponds to the convolution in eq. (2.67) resp. in the mass factorisation counterterms, and is therefore combined with it. The NLO initial-final mapping holds also for the $X_3^1(\hat{i},j,k)$ appearing at NNLO. In a similar way as for the final-final kinematics, a new mapping $(\hat{i},j,k,l) \to (\hat{\tilde{i}},L)$ is required to implement the double unresolved behaviour of the four-parton tree-level antennae $X_4^0(\hat{i},j,k,l)$ [121]:

$$\begin{aligned} p_I^\mu &= p_{\hat{\tilde{i}}}^\mu = x p_i^\mu, \\ p_K^\mu &= p_{\widetilde{(jkl)}}^\mu = p_j^\mu + p_k^\mu + p_l^\mu - (1-x)p_i^\mu, \end{aligned} \tag{4.16}$$

where

$$x_i = \frac{s_{ij}+s_{ik}+s_{il}+s_{jk}+s_{jl}+s_{kl}}{s_{ij}+s_{ik}+s_{il}}. \tag{4.17}$$

In the double unresolved colour ordered limites of the partons j and k it satisfies the appropriate limites:

$p_j \ , \ p_k \to 0$	$p_{\hat{\tilde{i}}} \to p_{\hat{i}}$	$p_L \to p_l,$
$p_{\hat{i}} \| p_j \| p_k$	$p_{\hat{\tilde{i}}} \to z p_{\hat{i}}$	$p_L \to p_l,$
$p_j \| p_k \| p_l$	$p_{\hat{\tilde{i}}} \to p_{\hat{i}}$	$p_L \to p_j + p_k + p_l,$
$p_j \to 0 \ , \ p_k \| p_l$	$p_{\hat{\tilde{i}}} \to p_{\hat{i}}$	$p_L \to p_k + p_l,$
$p_k \to 0 \ , \ p_{\hat{i}} \| p_j$	$p_{\hat{\tilde{i}}} \to z p_{\hat{i}}$	$p_L \to p_l,$
$\hat{p}_i \| p_j \ , \ p_k \| p_l$	$p_{\hat{\tilde{i}}} \to z p_{\hat{i}}$	$p_L \to p_k + p_l,$

where z is again the momentum fraction of $p_{\hat{\tilde{i}}}$ left after the collinear splittings. This mapping collapses to a NLO initial-final mapping in single unresolved limites of the four-parton antenna.

4.2.3 Initial-initial kinematics

In hadron-hadron scattering, up to two partons present in the antenna function may be in the initial state. This requires antennae where both radiators are in the initial state and a further mapping $(3, \dots, \hat{i}, j, \hat{k}, \dots, n+3) \to (\tilde{3}, \dots, \hat{\tilde{i}}, \hat{\tilde{k}}, \dots, \widetilde{n+3})$. Since the momenta $\hat{i}$ and $\hat{k}$ are again only rescaled there is no way to balance the transverse momentum of the parton j with the mapped momenta. A Lorentz boost $p_l \to p_{\tilde{l}}$ thus needs to be performed on the partons outside the antenna in order to maintain momentum conservation. The mapping is given by [50]:

$$\begin{aligned} p_I^\mu &= p_{\hat{\tilde{i}}}^\mu = x_i p_{\hat{i}}^\mu \\ p_K^\mu &= p_{\hat{\tilde{k}}}^\mu = x_k p_{\hat{k}}^\mu \\ p_{\tilde{l}}^\mu &= p_l^\mu - \frac{2p_l \cdot (q+\tilde{q})}{(q+\tilde{q})^2}(q^\mu + \tilde{q}^\mu) + \frac{2p_l \cdot q}{q^2}\tilde{q}^\mu, \end{aligned} \tag{4.18}$$

where the momenta p_l are the final state momenta not involved in the antenna, and

$$\begin{aligned} x_i &= \sqrt{\frac{s_{ik}+s_{jk}}{s_{ik}+s_{ij}}}\sqrt{\frac{s_{ik}+s_{ij}+s_{jk}}{s_{ik}}}, \\ x_k &= \sqrt{\frac{s_{ik}+s_{ij}}{s_{ik}+s_{jk}}}\sqrt{\frac{s_{ik}+s_{jk}+s_{ij}}{s_{ik}}}, \end{aligned} \qquad \begin{aligned} q^\mu &= p_i^\mu + p_k^\mu - p_j^\mu, \\ \tilde{q}^\mu &= p_{\hat{\tilde{i}}}^\mu + p_{\hat{\tilde{k}}}^\mu. \end{aligned} \tag{4.19}$$

The mapping satisfies:

$p_j \to 0$	$p_{\hat{\tilde{i}}} \to p_{\hat{i}}$	$p_{\hat{\tilde{k}}} \to p_{\hat{k}}$
$p_j \| p_{\hat{i}}$	$p_{\hat{\tilde{i}}} \to z_i p_{\hat{i}}$	$p_{\hat{\tilde{k}}} \to p_{\hat{k}}$
$p_j \| p_k$	$p_{\hat{\tilde{i}}} \to p_{\hat{i}}$	$p_{\hat{\tilde{k}}} \to z_k p_{\hat{k}},$

where again $(1-z)$ is the momentum fraction carried away by the collinear parton j. This gives rise to a further subtraction term

$$X_3^0(\hat{i}, j, \hat{k}) |M_{n+2}^0(\tilde{1}, \dots, \hat{\tilde{i}}, \hat{\tilde{k}}, \dots, \widetilde{n+3})|^2 J_n^{(n)}(p_{\tilde{3}}, \dots, p_{\widetilde{n+3}}). \tag{4.20}$$

The factorisation of phase-space reads as the convolution of a n-particle phase-space and the phase-space of parton j:

$$\begin{aligned} \mathrm{d}\Phi_{n+1}(p_{\hat{1}}, p_{\hat{2}}; p_1, \dots, p_j, \dots, p_{n+1}) = \mathrm{d}\Phi_n(x_1 p_{\hat{1}}, x_2 p_{\hat{2}}; p_{\tilde{1}}, \dots, p_{\widetilde{n+1}}) \\ \cdot \delta(x_1 - \hat{x}_1)\delta(x_2 - \hat{x}_2)[\mathrm{d}p_j]\mathrm{d}x_1\mathrm{d}x_2 \end{aligned} \tag{4.21}$$

$$[\mathrm{d}p_j] = \frac{\mathrm{d}^{d-1}p_j}{2E_j(2\pi)^{d-1}}, \tag{4.22}$$

and integration over the phase-space of parton j gives:

$$\frac{1}{C(\epsilon)}\int [\mathrm{d}p_j] x_i x_k \delta(x_i - \hat{x}_i)\delta(x_k - \hat{x}_k) X_3^0(\hat{i}, j, \hat{k}) = \mathcal{X}(\hat{\tilde{i}}, \hat{\tilde{k}}, z_i, z_k), \tag{4.23}$$

where $C(\epsilon)$ is given as in eq. (4.7). The integrated antenna depends on the momentum fraction of both initial state partons after initial collinear emission and is subjected to a double convolution over x_i and x_k. As before the NLO initial-final mapping holds also for the $X_3^1(\hat{i}, j, \hat{k})$ which appear at NNLO, together with a four-parton initial-initial antenna $X_4^0(\hat{i}, j, k, \hat{l})$. The initial-initial mapping $(3, \ldots, \hat{i}, j, k, \hat{l}, \ldots, n+4) \to (\tilde{3}, \ldots, \hat{\tilde{i}}, \hat{\tilde{l}}, \ldots, \widetilde{n+4})$ comes with a Lorentz boost applied to the remaining partons not present in the antenna to maintain momentum conservation, and reads [121]:

$$\begin{aligned}
p_I^\mu &= p_{\hat{\tilde{i}}}^\mu = x_i p_i^\mu \\
p_L^\mu &= p_{\hat{\tilde{l}}}^\mu = x_l p_l^\mu \\
p_{\tilde{m}}^\mu &= p_m^\mu - \frac{2p_m\cdot(q+\tilde{q})}{(q+\tilde{q})^2}(q^\mu + \tilde{q}^\mu) + \frac{2p_m\cdot q}{q^2}\tilde{q}^\mu, \\
q^\mu &= p_i^\mu + p_l^\mu - p_j^\mu - p_k^\mu, \\
\tilde{q}^\mu &= p_{\hat{\tilde{i}}}^\mu + p_{\hat{\tilde{l}}}^\mu, \\
x_i &= \sqrt{\frac{s_{il}+s_{jl}+s_{kl}}{s_{il}+s_{ij}+s_{kl}}}\sqrt{\frac{s_{ij}+s_{ik}+s_{il}+s_{jk}+s_{jl}+s_{kl}}{s_{il}}}, \\
x_l &= \sqrt{\frac{s_{il}+s_{ij}+s_{ik}}{s_{il}+s_{jl}+s_{kl}}}\sqrt{\frac{s_{ij}+s_{ik}+s_{il}+s_{jk}+s_{jl}+s_{kl}}{s_{il}}}.
\end{aligned} \tag{4.24}$$

In double unresolved colour ordered limites of p_j and p_k its properties are:

$p_j\ ,\ p_k \to 0$	$p_{\hat{\tilde{i}}} \to p_{\hat{i}}$	$p_{\hat{\tilde{l}}} \to p_{\hat{l}}$,
$p_{\hat{i}} \| p_j \| p_k$	$p_{\hat{\tilde{i}}} \to z_i p_{\hat{i}}$	$p_{\hat{\tilde{l}}} \to p_{\hat{l}}$,
$p_j \| p_k \| p_{\hat{l}}$	$p_{\hat{\tilde{i}}} \to p_{\hat{i}}$	$p_{\hat{\tilde{l}}} \to z_l p_{\hat{l}}$,
$p_j \to 0\ ,\ p_k \| p_{\hat{l}}$	$p_{\hat{\tilde{i}}} \to p_{\hat{i}}$	$p_{\hat{\tilde{l}}} \to z_l p_{\hat{l}}$,
$p_k \to 0\ ,\ p_{\hat{i}} \| p_j$	$p_{\hat{\tilde{i}}} \to z_i p_{\hat{i}}$	$p_{\hat{\tilde{l}}} \to p_{\hat{l}}$,
$\hat{p}_i \| p_j\ ,\ p_k \| p_{\hat{l}}$	$p_{\hat{\tilde{i}}} \to z_i p_{\hat{i}}$	$p_{\hat{\tilde{l}}} \to z_l p_{\hat{l}}$,

where z_i and z_l are the momentum fractions of $p_{\hat{\tilde{i}}}$ and $p_{\hat{\tilde{l}}}$ after the collinear splitting. This mapping collapses to a NLO initial-initial mapping in single unresolved limites of the four-parton antenna.
The construction of subtraction terms using X_3^1 and X_4^0 antennae is depicted in 4.5. Their integration is described in [123].

4.3 Integrated subtraction terms and mass factorisation

As seen in the previous section, the subtraction terms involving initial-final or initial-initial antennae subtract amongst others collinear limites between initial and final state partons. Following the discussion in section 2.9, these need to be absorbed into the renormalised PDF's. To this end the mass factorisation counterterms, which arise from the renormalisation of the PDF's, are added to the integrated antennae such as to remove the corresponding poles. Both

the mass factorisation counterterms and the integrated antennae with at least one hard momentum in the initial state come with an integration over the momentum fraction of the initial state parton left after collinear radiation prior to the scattering. It is appealing to combine these into integrated dipoles $\mathbf{J}_2$ which encapsulate all poles in ϵ associated with real radiation off an initial-final or initial-initial antenna configuration. The poles in ϵ originating in real radiation off a final-final antenna configuration on the other hand are fully contained in the integrated final-final antenna, which can thus directly be translated into the corresponding $\mathbf{J}_2$ operators. The general prescription on how to combine the mass factorisation counterterms and integrated antennae into the integrated dipoles is listed in [124]. The gluons-only case will be illustrated in the next section with the example of NLO $H + 1J$.
The integrated dipoles have the same pole structure at NLO and at NNLO as the IR singularity operators $\mathbf{I}_2(I, J; \epsilon)$, such that the integrated subtraction terms $\mathrm{d}\hat{\sigma}^T_{NLO}$ together with $\mathrm{d}\hat{\sigma}^{MF}_{NLO}$ can always be rearranged to reproduce the known universal IR behaviour of loop matrix elements. In close correspondence to the way the real subtraction terms have been constructed, the integrated subtraction terms are given at NLO by a sum over all pairs of colour neighbouring partons in the squared amplitude:

$$\begin{aligned}\mathrm{d}\hat{\sigma}^T_{NLO} = -\mathcal{N}^R_{NLO} \int \frac{\mathrm{d}z_1}{z_1}\frac{\mathrm{d}z_2}{z_2}\mathrm{d}\Phi_n(z_1p_1, z_2p_2; p_3, \ldots, p_{n+2})\frac{1}{S_n} \\ \times \sum_{I,K} \mathbf{J}^{(1)}_2(I, K; \epsilon)|M^{(0)}_{n+2}(\ldots, I, K, \ldots)|J^{(n)}_n(p_3, \ldots, p_I, p_K, \ldots, p_{n+2}),\end{aligned} \tag{4.25}$$

where all integrated subtraction terms have been placed under an integral over the momentum fractions z_1 and z_2, if necessary by multiplying with appropriate delta distributions $\delta(1 - z_i)$, in order to ease the handling of the various convolutions appearing in the integrated antennae and mass factorisation counterterms.

4.4 NLO subtraction for N_F=0 $H + 1J$

In order to obtain the NLO cross section for gluons-only $H + 1J$, a combination of subtraction terms $\mathrm{d}\hat{\sigma}^S_{gg,NLO}$ must be found such that in

$$\begin{aligned}\mathrm{d}\hat{\sigma}_{gg,NLO} = &\int_{\mathrm{d}\Phi_{n+1}} [\mathrm{d}\hat{\sigma}^R_{gg,NLO} - \mathrm{d}\hat{\sigma}^S_{gg,NLO}]J^{(n+1)}_n \\ &+ \int_{\mathrm{d}\Phi_n} [\mathrm{d}\hat{\sigma}^V_{gg,NLO} - \mathrm{d}\hat{\sigma}^T_{gg,NLO}]J^{(n)}_n,\end{aligned} \tag{4.26}$$

$$\mathrm{d}\hat{\sigma}^T_{gg,NLO} = -\int_{1_{unresolved}} \mathrm{d}\hat{\sigma}^S_{gg,NLO} - \mathrm{d}\hat{\sigma}^{MF}_{gg,NLO}, \tag{4.27}$$

The content of the square brackets is free of IR divergences. The subtraction of the IR limites of the real contribution for purely gluonic $H + 1J$ production requires initial-final and initial-initial phase-space mappings and the corresponding all-gluons (sub)antennae. The final-final subantennae are also presented here since at NNLO there will be enough final state partons in the double-real contribution to allow for their appearance. In the final-final case, one decomposes the three-gluon tree-level antenna as [49]:

$$F^0_3(i, j, k) = f^0_3(i, k, j) + f^0_3(k, j, i) + f^0_3(j, i, k), \tag{4.28}$$

where in the subantenna

$$f^0_3(i, j, k) = \frac{1}{s^2_{ijk}}\left(2\frac{s^2_{ijk}s_{ik}}{s_{ij}s_{jk}} + \frac{s_{ik}s_{ij}}{s_{jk}} + \frac{s_{ik}s_{jk}}{s_{ij}} + \frac{8}{3}s_{ijk} + \mathcal{O}(\epsilon)\right), \tag{4.29}$$

the gluons i and k are identified as the hard radiators. It contains the full $p_j \to 0$ soft limit and parts of the $p_i||p_j$ and $p_j||p_k$ collinear limites. In the initial-final case the initial state gluon is one of the hard radiators. Since the initial-final mapping is symmetric w.r.t. the other two gluons and all limites factor down to gluons as well, any of the two final state gluons could be the hard radiator and thus no decomposition in subantennae is needed. Nevertheless, since at NNLO initial-final antennae are needed to subtract single unresolved limites from the four-gluon antennae, which are colour ordered, it is still convenient to decompose the antenna as

$$F_3^0(\hat{1}, j, k) = f_3^0(\hat{1}, j, k) + f_3^0(\hat{1}, k, j), \tag{4.30}$$

where the subantenna $f_3^0(\hat{1}, j, k)$ contains the full $p_j \to 0$ soft limit, the full $p_{\hat{1}}||p_j$ collinear limit and part of the $p_j||p_k$ limit. It reads

$$\begin{aligned} f_3^0(\hat{1}, j, k) = \frac{1}{2s_{1jk}^2}\Bigg(&\frac{8s_{1k}^2}{s_{1j}} + \frac{8s_{jk}^2}{s_{1j}} + \frac{12s_{jk}s_{1k}}{s_{1j}} + \frac{4s_{1k}^3}{s_{jk}s_{1j}} + \frac{4s_{jk}}{s_{1j}(s_{1j}+s_{1k})} \\ &+ \frac{8s_{1k}^2}{s_{jk}} + \frac{6s_{1j}s_{1k}}{s_{jk}} + 12s_{jk} + 12s_{1j} + 12s_{1k} + \mathcal{O}(\epsilon)\Bigg), \end{aligned} \tag{4.31}$$

where the Lorentz invariants have been appropriately crossed to the initial-final kinematics. In the initial-initial case both hard radiators are fixed and no decomposition is needed. The full three-gluon tree-level antenna is

$$\begin{aligned} F_3^0(\hat{1}, i, \hat{2}) = \frac{1}{2s_{1i2}^2}\Bigg(&\frac{8s_{1i}^2}{s_{2i}} + \frac{8s_{1i}^2}{s_{12}} + \frac{8s_{2i}^2}{s_{1i}} + \frac{8s_{2i}^2}{s_{12}} + \frac{8s_{12}^2}{s_{1i}} + \frac{8s_{12}^2}{s_{2i}} \\ &+ \frac{12s_{1i}s_{2i}}{s_{12}} + \frac{12s_{12}s_{2i}}{s_{1i}} + \frac{12s_{1i}s_{12}}{s_{2i}} + \frac{4s_{1i}^3}{s_{12}s_{2i}} + \frac{4s_{2i}^3}{s_{12}s_{1i}} + \frac{4s_{12}^3}{s_{1i}s_{2i}} \\ &+ 24s_{12} + 24s_{1i} + 24s_{2i} + \mathcal{O}(\epsilon)\Bigg), \end{aligned} \tag{4.32}$$

where the invariants are crossed to the final-final kinematics.
The real contribution to the NLO purely-gluonic $H + 1J$ process is the four-gluon tree-level matrix element. It involves three colour orderings:

$$|\mathcal{M}_4^{(0)}(\hat{1}, \hat{2}, 3, 4)|^2 = \mathcal{N}_{NLO}^R\Big[|M_4^{(0)}(\hat{1}, \hat{2}, 3, 4)|^2 + |M_4^{(0)}(\hat{1}, \hat{2}, 4, 3)|^2 + |M_4^{(0)}(\hat{1}, 3, \hat{2}, 4)|^2\Big], \tag{4.33}$$

where $|M_4^{(0)}|^2$ are the helicity-summed partial amplitudes squared. The following expression is then free of unresolved IR singularities:

$$\begin{aligned} \mathrm{d}\hat{\sigma}_{NLO}^R + \mathrm{d}\hat{\sigma}_{NLO}^S = \mathcal{N}_{NLO}^R\Bigg[&|M_4^{(0)}(\hat{1}, \hat{2}, 3, 4)|^2 J_1^{(2)}(p_3, p_4) - f_3^0(\hat{2}, 3, 4)|M_3^{(0)}(\hat{1}, \hat{\hat{2}}, \widetilde{(34)})|^2 J_1^{(1)}(p_{\widetilde{(34)}}) \\ &- f_3^0(\hat{1}, 4, 3)|M_3^{(0)}(\hat{\hat{1}}, \hat{2}, \widetilde{(34)})|^2 J_1^{(1)}(p_{\widetilde{(34)}}) \\ &+ |M_4^{(0)}(\hat{1}, \hat{2}, 4, 3)|^2 J_1^{(2)}(p_3, p_4) - f_3^0(\hat{2}, 4, 3)|M_3^{(0)}(\hat{1}, \hat{\hat{2}}, \widetilde{(34)})|^2 J_1^{(1)}(p_{\widetilde{(34)}}) \\ &- f_3^0(\hat{1}, 3, 4)|M_3^{(0)}(\hat{\hat{1}}, \hat{2}, \widetilde{(34)})|^2 J_1^{(1)}(p_{\widetilde{(34)}}) \\ &+ |M_4^{(0)}(\hat{1}, 3, \hat{2}, 4)|^2 J_1^{(2)}(p_3, p_4) - F_3^0(\hat{1}, 3, \hat{2})|M_3^{(0)}(\hat{\hat{1}}, \hat{\hat{2}}, \tilde{4})|^2 J_1^{(1)}(p_{\tilde{4}}) \\ &- F_3^0(\hat{1}, 4, \hat{2})|M_3^{(0)}(\hat{\hat{1}}, \hat{\hat{2}}, \tilde{3})|^2 J_1^{(1)}(p_{\tilde{3}})\Bigg], \end{aligned} \tag{4.34}$$

where the IR divergences of each of the squared partial amplitudes have been removed by a combination of two subtraction terms contained in $\mathrm{d}\hat{\sigma}^S_{NLO}$, respectively. The virtual contribution is the tree-level one-loop interference of three-parton amplitudes and has only one colour ordering:

$$|2\mathcal{M}_3^{(1)}(\hat{1},\hat{2},3)\mathcal{M}_3^{(0)\dagger}(\hat{1},\hat{2},3)| = \mathcal{N}^V_{NLO}|2M_3^{(1)}(\hat{1},\hat{2},3)M_3^{(0)\dagger}(\hat{1},\hat{2},3)|. \tag{4.35}$$

Integrating $\mathrm{d}\hat{\sigma}^S_{NLO}$ over the phase-space of the unresolved parton in the antennae and relabeling the mapped momenta $\{\widetilde{(34)},\tilde{3},\tilde{4}\} \to 3$ one obtains a set of integrated antennae:

$$\begin{aligned}\int_{1_{unresolved}} \mathrm{d}\hat{\sigma}^S_{NLO} = \mathcal{N}^R_{NLO}\Bigg[& \\ & \int \frac{\mathrm{d}z_2}{z_2}\frac{1}{2}\mathcal{F}_3^0(s_{23},z_2)|M_3^{(0)}(\hat{1},\hat{\tilde{2}},3)|^2 + \int \frac{\mathrm{d}z_1}{z_1}\frac{1}{2}\mathcal{F}_3^0(s_{13},z_1)|M_3^{(0)}(\hat{\tilde{1}},\hat{2},3)|^2 \\ & + \int \frac{\mathrm{d}z_2}{z_2}\frac{1}{2}\mathcal{F}_3^0(s_{23},z_2)|M_3^{(0)}(\hat{1},\hat{\tilde{2}},3)|^2 + \int \frac{\mathrm{d}z_1}{z_1}\frac{1}{2}\mathcal{F}_3^0(s_{13},z_1)|M_3^{(0)}(\hat{\tilde{1}},\hat{2},3)|^2 \\ & + \int \frac{\mathrm{d}z_1}{z_2}\frac{\mathrm{d}z_2}{z_2}\Big\{\mathcal{F}_3^0(s_{12},z_1,z_2)|M_3^{(0)}(\hat{\tilde{1}},\hat{\tilde{2}},3)|^2 + \mathcal{F}_3^0(s_{12},z_1,z_2)|M_3^{(0)}(\hat{\tilde{1}},\hat{\tilde{2}},3)|^2\Big\}\Bigg] J_1^{(1)}(p_3),\end{aligned} \tag{4.36}$$

to which the mass factorisation counterterms are added:

$$\begin{aligned}\mathrm{d}\hat{\sigma}^{MF}_{NLO} = -\mathcal{N}^R_{NLO}\Bigg[& \int \frac{\mathrm{d}z_1}{z_1}\Gamma_{gg}^{(1)}(z_1)|M_3^{(0)}(\hat{\tilde{1}},\hat{2},3)|^2 J_1^{(1)}(p_3) \\ & + \int \frac{\mathrm{d}z_2}{z_2}\Gamma_{gg}^{(1)}(z_2)|M_3^{(0)}(\hat{1},\hat{\tilde{2}},3)|^2 J_1^{(1)}(p_3)\Bigg],\end{aligned} \tag{4.37}$$

where $p_{\hat{\tilde{1}}} = z_1 p_{\hat{1}}$ and $p_{\hat{\tilde{2}}} = z_2 p_{\hat{2}}$. The two contributions $\mathrm{d}\hat{\sigma}^T_{NLO}$ and $\mathrm{d}\hat{\sigma}^{MF}_{NLO}$ can be combined into integrated dipoles according to the following prescription [124]:

$$\begin{aligned}\mathbf{J}_2^{(1,FF)}(I,J) &= \frac{1}{3}\mathcal{F}_3^0(s_{IJ}) \\ \mathbf{J}_2^{(1,IF)}(\hat{1},J,z_1) &= \frac{1}{2}\mathcal{F}_3^0(s_{1J},z_1) - \frac{1}{2}\Gamma_{gg}^{(1)}(z_1) \\ \mathbf{J}_2^{(1,II)}(\hat{1},\hat{2},z_1,z_2) &= \mathcal{F}_3^0(s_{12},z_1,z_2) - \frac{1}{2}\Gamma_{gg}^{(1)}(z_1)\delta(1-z_2) - \frac{1}{2}\Gamma_{gg}^{(1)}(z_2)\delta(1-z_1),\end{aligned} \tag{4.38}$$

where

$$\mathbf{J}_2^{(1,..)}(I,J) = \boldsymbol{I}^{(1)}(s_{IJ},\epsilon) + \text{finite pieces}. \tag{4.39}$$

The integrated subtraction terms and mass factorisation counterterms can then be rephrased as:

$$\begin{aligned}\mathrm{d}\hat{\sigma}^T_{NLO} = -\mathcal{N}^R_{NLO}\int \frac{\mathrm{d}z_1}{z_1}\int \frac{\mathrm{d}z_2}{z_2}\Big[& \mathbf{J}_2^{(1,IF)}(\hat{1},3,z_1)\delta(1-z_2) + \mathbf{J}_2^{(1,IF)}(\hat{2},3,z_2)\delta(1-z_1) \\ & + \mathbf{J}_2^{(1,II)}(\hat{1},\hat{2},z_1,z_2)\Big]\cdot 2|M_3^{(0)}(\hat{\tilde{1}},\hat{\tilde{2}},3)|^2 J_1^{(1)}(p_3)\end{aligned} \tag{4.40}$$

which faithfully reproduces the pole structure of the virtual contribution according to sec. 2.8.2 and therefore removes its poles in ϵ. The convolution may be rearranged such as to involve $|M_3^{(0)}(\hat{1},\hat{2},3)|^2$ instead of $|M_3^{(0)}(\hat{\tilde{1}},\hat{\tilde{2}},3)|^2$ in the upper formula. This changes the convolution with the PDF's and will be discussed in sec. 5.1.5.

4.5 NNLO subtraction

In this section the construction of the subtraction terms which remove the various IR divergences at NNLO is described. It is broken up in three main parts following the outline in eq. (2.78),

$$\begin{aligned}
\mathrm{d}\hat{\sigma}_{ij,NNLO} = &\int_{\mathrm{d}\Phi_{n+2}} [\mathrm{d}\hat{\sigma}^{RR}_{ij,NNLO} - \mathrm{d}\hat{\sigma}^{S}_{ij,NNLO}] J_n^{(n+2)} \\
&+ \int_{\mathrm{d}\Phi_{n+1}} [\mathrm{d}\hat{\sigma}^{RV}_{ij,NNLO} - \mathrm{d}\hat{\sigma}^{T}_{ij,NNLO}] J_n^{(n+1)} \\
&+ \int_{\mathrm{d}\Phi_{n}} [\mathrm{d}\hat{\sigma}^{VV}_{ij,NNLO} - \mathrm{d}\hat{\sigma}^{U}_{ij,NNLO}] J_n^{(n)}. \qquad (4.41)
\end{aligned}$$

The individual subtraction terms are further broken up in contributions which dedicately remove certain types of divergences:

$$\mathrm{d}\hat{\sigma}^{S}_{ij,NNLO} = \mathrm{d}\hat{\sigma}^{S,a}_{ij,NNLO} + \mathrm{d}\hat{\sigma}^{S,b_1}_{ij,NNLO} + \mathrm{d}\hat{\sigma}^{S,b_2}_{ij,NNLO} + \mathrm{d}\hat{\sigma}^{S,c}_{ij,NNLO} + \mathrm{d}\hat{\sigma}^{S,d}_{ij,NNLO} \qquad (4.42)$$

$$\begin{aligned}
\mathrm{d}\hat{\sigma}^{T}_{ij,NNLO} &= \mathrm{d}\hat{\sigma}^{VS}_{ij,NNLO} - \int_{1_{unresolved}} \mathrm{d}\hat{\sigma}^{S_1}_{ij,NNLO} - \mathrm{d}\hat{\sigma}^{MF_1}_{ij,NNLO}, \\
&= \mathrm{d}\hat{\sigma}^{T,a}_{ij,NNLO} + \mathrm{d}\hat{\sigma}^{T,b_1}_{ij,NNLO} + \mathrm{d}\hat{\sigma}^{T,b_2}_{ij,NNLO} + \mathrm{d}\hat{\sigma}^{T,b_3}_{ij,NNLO} + \mathrm{d}\hat{\sigma}^{T,c}_{ij,NNLO} \qquad (4.43)
\end{aligned}$$

$$\mathrm{d}\hat{\sigma}^{U}_{ij,NNLO} = -\int_{1_{unresolved}} \mathrm{d}\hat{\sigma}^{VS}_{ij,NNLO} - \int_{2_{unresolved}} \mathrm{d}\hat{\sigma}^{S_2}_{ij,NNLO} - \mathrm{d}\hat{\sigma}^{MF_2}_{ij,NNLO}. \qquad (4.44)$$

A part $\mathrm{d}\hat{\sigma}^{S_1}_{ij,NNLO}$ of the double-real subtraction terms is integrated over its single unresolved phase-space and combined with the mass factorisation counterterms $\mathrm{d}\hat{\sigma}^{MF_1}_{ij,NNLO}$ to form integrated dipoles in a similar way as in the NLO case. These subtract either the poles in ϵ of the actual real-virtual matrix element or of the one-loop antennae and one-loop reduced matrix elements which appear in the subtraction terms in $\mathrm{d}\hat{\sigma}^{VS}_{ij,NNLO}$. This is then itself integrated over its single unresolved phase-space and added back to the double-virtual contribution. Together with the integral over the double unresolved phase-space of the remaining double-real subtraction terms $\mathrm{d}\hat{\sigma}^{S_2}_{ij,NNLO}$ and the mass factorisation counterterms $\mathrm{d}\hat{\sigma}^{MF_2}_{ij,NNLO}$ it removes the pole structure of the two-loop matrix element.
In the following, the different contributions are explained and exemplified with parts of the NNLO subtraction terms for $H + 1J$. Full generality is maintained concerning whether the hard radiator momenta of an antenna correspond to initial- or final-state partons. All cases have been treated in the previous section and can readily be applied.
The mass factorisation counterterms at NNLO read

$$\begin{aligned}
\mathrm{d}\hat{\sigma}^{MF,1}_{ij,NNLO}(\xi_1 H_1, \xi_2 H_2) = &-\int \frac{\mathrm{d}z_1}{z_1}\frac{\mathrm{d}z_2}{z_2} \\
&\times \Gamma^{(1)}_{ij;kl}(z_1, z_2) \Big[\mathrm{d}\hat{\sigma}^{R}_{kl,NLO} - \mathrm{d}\hat{\sigma}^{S}_{kl,NLO}\Big](z_1\xi_1 H_1, z_2\xi_2 H_2) \qquad (4.45)
\end{aligned}$$

$$\begin{aligned}
\mathrm{d}\hat{\sigma}^{MF,2}_{ij,NNLO}(\xi_1 H_1, \xi_2 H_2) = &-\int \frac{\mathrm{d}z_1}{z_1}\frac{\mathrm{d}z_2}{z_2} \Bigg\{ \Gamma^{(2)}_{ij;kl}(z_1, z_2) \mathrm{d}\hat{\sigma}^{B}_{kl,LO}(z_1\xi_1 H_1, z_2\xi_2 H_2) \\
&+ \Gamma^{(1)}_{ij;kl}(z_1, z_2) \Big[\mathrm{d}\hat{\sigma}^{V}_{kl,NLO} - \mathrm{d}\hat{\sigma}^{T}_{kl,NLO}\Big](z_1\xi_1 H_1, z_2\xi_2 H_2) \Bigg\}, \qquad (4.46)
\end{aligned}$$

where the mass factorisation kernels are given in eq. (2.72) and the content of the square brackets are the subtracted NLO real and virtual contributions respectively.

4.5.1 Double-real contribution

The double-real contribution contains single- as well as double unresolved limites. In order to remove the single-unresolved limites, a combination of NLO-like subtraction terms $\mathrm{d}\hat{\sigma}^{S,a}_{NNLO}$ is used. Its construction follows closely the lines of the real subtraction terms at NLO, up to the reduced squared amplitude and the jet function which feature an external parton more. It contains terms of the form:

$$\begin{aligned}\mathrm{d}\hat{\sigma}^{S,a}_{NNLO} = \mathcal{N}^{RR}_{NNLO} \sum_j \mathrm{d}\Phi_{n+2} \frac{1}{S_{n+2}} \\ \times X^0_3(i,j,k) |M^0_{n+3}(1,\ldots,I,K,\ldots,n+4)|^2 J^{(n+1)}_n(p_3,\ldots,p_I,p_K,\ldots,p_{n+4}). \quad (4.47)\end{aligned}$$

In contrast to the real subtraction term, not all momenta in the reduced squared amplitude are constrained to be resolved by the jet function. It may therefore itself develop single unresolved singularities in double unresolved configurations of the unmapped momenta. These factorise in terms of products of single unresolved factors and do not correspond to divergences of the double-real squared amplitude. They will be removed with an additional subtraction term.
The double unresolved limites of the double-real squared amplitude can be subtracted with terms of the form

$$\begin{aligned}\mathrm{d}\hat{\sigma}^{S,b_1}_{NNLO} = \mathcal{N}^{RR}_{NNLO} \sum_{j,k} \mathrm{d}\Phi_{n+2} \frac{1}{S_{n+2}} \\ \times X^0_4(i,j,k,l) |M^{(0)}_{n+2}(\ldots,I,L,\ldots)|^2 J^{(n)}_n(p_3,\ldots,p_I,p_L,\ldots,p_{n+4}), \quad (4.48)\end{aligned}$$

where the sum is over all colour ordered pairs of partons in the double-real squared amplitude. This term introduces additional spurious singularities in single unresolved limites of the four-parton antenna. Since these correspond themselves to squared amplitudes, IR factorisation applies and the singularities can be subtracted by NLO-like subtraction terms for the X^0_4. This is made possible due to the $4 \to 2$ NNLO mapping collapsing to a $3 \to 2$ NLO mapping in single unresolved limites. The subtraction terms for a $X^0_4(i,j,k,l)$ antenna thus consist of a sum of two iterated three-parton antennae, where the arguments of the primary antenna are dictated by the colour ordering of the four-parton antenna and the secondary one is the reduced antenna function which depends on a $3 \to 2$ mapping:

$$\begin{aligned}\mathrm{d}\hat{\sigma}^{S,b_2}_{NNLO} = \mathcal{N}^{RR}_{NNLO} \sum_j \mathrm{d}\Phi_{n+2} \frac{1}{S_{n+2}} \\ \times X^0_3(i,j,k) X^0_3(I,K,l) |M^{(0)}_{n+2}(\ldots,\mathcal{I},L,\ldots)|^2 J^{(n)}_n(p_3,\ldots,p_\mathcal{I},p_L,\ldots,p_{n+4}), \quad (4.49)\end{aligned}$$

where the sum is over all partons of the four-parton antenna which may become unresolved, and the proper reduced squared amplitude depends on two iterated $3 \to 2$ mappings. These subtraction terms contain in turn singularities in double unresolved limites where also the secondary antenna has a single unresolved limit. These do as well not correspond to physical limites of the double-real squared amplitude and are subtracted together with the double unresolved singularities of $\mathrm{d}\hat{\sigma}^{S,a}_{NNLO}$ by a new contribution $\mathrm{d}\hat{\sigma}^{S,c}_{NNLO}$ constructed in the following way:
For every four-parton antenna $X^0_4(i,j,k,l)$ one considers the ordering of the hard radiators with their colour neighbours which do not participate in the antenna, and where the potentially unresolved partons j and k have been removed for now: $(\ldots,a,i,l,b,\ldots)$. This becomes possible only for processes with at least five partons, where the ordering becomes (a,i,l,a). This ordering now defines three regions which the unresolved partons are radiated from: The region (I) between the genuine hard radiators i and l, and region (II) and (III) between one of them

and its colour neighbour a resp. b. The unresolved partons are now successively radiated. The primary radiation can take place in any of the three regions, with a relative minus sign if the parton is radiated from region (II) or (III) and where the momenta of the ordering are subjected to an adequate $3 \to 2$ NLO mapping. The second unresolved parton is always radiated from the mapped momenta of region (I), which are then accordingly remapped. For a $(\ldots, a, i, l, b, \ldots)$ ordering this gives rise to the following structure:

$$\begin{aligned}
&+\frac{1}{2} X_3^0(i,j,l) X_3^0(\widetilde{(ij)}, k, \widetilde{(jl)}) M_{n+2}^{(0)}(\ldots, a, \widetilde{((ij)k)}, \widetilde{(k(jl))}, b, \ldots) \\
&-\frac{1}{2} X_3^0(a,j,i) X_3^0(\widetilde{(ij)}, k, l) M_{n+2}^{(0)}(\ldots, \widetilde{(aj)}, \widetilde{((ij)k)}, \widetilde{(kl)}, b, \ldots) \\
&-\frac{1}{2} X_3^0(l,j,b) X_3^0(i, k, \widetilde{(jl)}) M_{n+2}^{(0)}(\ldots, a, \widetilde{(ik)}, \widetilde{(k(jl))}, \widetilde{(jb)}, \ldots),
\end{aligned} \tag{4.50}$$

where the jet function has been omitted for readability. A similar group of terms is generated where the rôles of j and k are interchanged. Such blocks of terms cancel the remaining double unresolved limites of $\mathrm{d}\hat{\sigma}_{NNLO}^{S,a}$ and $\mathrm{d}\hat{\sigma}_{NNLO}^{S,b_2}$. This leaves divergences which are associated with large angle soft emission. These need to be canceled with a structure whose construction follows the same line than described above. Two soft partons are successively radiated from the underlying ordering $(\ldots, a, i, l, b, \ldots)$ in the same pattern as in eq. (4.50). Since in soft limites all mappings become identical, however, the primary mapping needs not to be fixed by the region in which the first radiation has occured, in contrast to the previous case. It can be arbitrarily chosen, where if possible a final-final mapping is opted for. This is the case for processes involving at least six partons. In five-parton processes an initial-final mapping needs to be taken, whereas in four-parton processes such limites do not appear. Since the primary mapping is fixed for emission off all three regions of the ordering, the corresponding secondary antennae and reduced squared amplitudes are identical for all terms and can be factored out.
For the emission of a soft parton j followed by a parton k, the momenta of the underlying ordering are considered after the primary mapping and after the secondary one. The subtraction terms receive contributions from large angle soft antennae for primary radiation off both sets of momenta, with a relative minus sign for radiation off the set of momenta after the secondary mapping. Letting the primary radiation take place off each of the three regions thus leads to a group of six terms, which, assuming a $(i,j,l) \to (\widetilde{(ij)}, \widetilde{(jl)})$ final-final primary mapping takes the following form:

$$\begin{aligned}
-\frac{1}{2}\Big[&\big(S_{\widetilde{(ij)},j,\widetilde{(jl)}} - S_{\widetilde{((ij)k)},j,\widetilde{(k(jl))}}\big) \\
&-\big(S_{a,j,\widetilde{(ij)}} - S_{a,j,\widetilde{((ij)k)}}\big) \\
&-\big(S_{\widetilde{(jl)},j,b} - S_{\widetilde{(k(jl))},j,b}\big)\Big] X_3^0(\widetilde{(ij)}, k, \widetilde{(jl)}) \\
&\times M_{n+2}^{(0)}(\ldots, a, \widetilde{((ij)k)}, \widetilde{(k(jl))}, b, \ldots) J_n^{(n)}(p_3, \ldots, p_a, p_{\widetilde{((ij)k)}}, p_{\widetilde{(k(jl))}}, p_b, \ldots, p_{n+4}),
\end{aligned} \tag{4.51}$$

where the soft antennae S are eikonal factors as given in eq. (2.52).
The picture which emerges so far is to let the colour ordering of the double-real squared amplitude guide the construction of the single unresolved terms $\mathrm{d}\hat{\sigma}_{NNLO}^{S,a}$ and the double unresolved terms $\mathrm{d}\hat{\sigma}_{NNLO}^{S,b_1}$. Each of the four-parton antennae then leads to further blocks of terms in $\mathrm{d}\hat{\sigma}_{NNLO}^{S,b_2}$ and $\mathrm{d}\hat{\sigma}_{NNLO}^{S,c}$ whose construction are dictated by the colour ordering of the four-parton antennae and their colour neighbours in the double-real squared amplitude. In purely gluonic $H + 1J$ production, $\mathrm{d}\hat{\sigma}_{NNLO}^{S,c}$ receives contributions from initial-final F_4^0 antennae and

initial-initial ones where the initial state partons are not adjacent.
If one considers for instance a $F_4^0(\hat{2},i,k,j)$ antenna, which appears in the double-real subtraction terms for the $\{\hat{1},\hat{2},i,k,j\}$ colour ordering of the five-gluon matrix element, and omits the potentially unresolved partons i and k one obtains the underlying ordering $\{\hat{1},\hat{2},j,\hat{1}\}$. The partons i and k are then successively radiated in the pattern described above. This yields the following block of antennae in $\mathrm{d}\hat{\sigma}^{S,c}_{NNLO}$:

$$\begin{aligned}
\frac{1}{2}\Bigg(& f_3^0(\hat{2},i,j)f_3^0(\hat{\tilde{2}},k,\widetilde{(ij)})|M_3^{(0)}(\hat{1},\hat{\tilde{2}},\widetilde{((ij)k)})|^2 J_1^{(1)}(p_{\widetilde{((ij)k)}}) \\
& -F_3^0(\hat{1},i,\hat{2})f_3^0(\hat{\tilde{2}},\tilde{k},\tilde{j})|M_3^{(0)}(\hat{\tilde{1}},\hat{\tilde{2}},\widetilde{(\tilde{j}\tilde{k})})|^2 J_1^{(1)}(p_{\widetilde{(\tilde{j}\tilde{k})}}) \\
& -f_3^0(\hat{1},i,j)f_3^0(\hat{2},k,\widetilde{(ij)})|M_3^{(0)}(\hat{\tilde{1}},\hat{\tilde{2}},\widetilde{((ij)k)})|^2 J_1^{(1)}(p_{\widetilde{((ij)k)}}) \quad + (i\leftrightarrow k)\Bigg).
\end{aligned} \tag{4.52}$$

For the large angle soft terms, the primary mapping is chosen as $(\hat{1},i,j)\to(\hat{\tilde{1}},\widetilde{(ij)})$. The underlying ordering thus becomes $\{\hat{\tilde{1}},\hat{2},\widetilde{(ij)},\hat{\tilde{1}}\}$. The secondary mapping is then $(\hat{2},k,\widetilde{(ij)})\to(\hat{\tilde{2}},\widetilde{((ij)k)})$, after which the ordering is $\{\hat{\tilde{1}},\hat{\tilde{2}},\widetilde{((ij)k)},\hat{\tilde{1}}\}$. The large angle soft block is then

$$\begin{aligned}
& \left[\left(S_{\hat{\tilde{2}}i\widetilde{((ij)k)}}-S_{\hat{2}i\widetilde{(ij)}}\right)-\left(S_{\hat{\tilde{1}}i\widetilde{((ij)k)}}-S_{\hat{\tilde{1}}i\widetilde{(ij)}}\right)-\left(S_{\hat{\tilde{1}}i\hat{\tilde{2}}}-S_{\hat{\tilde{1}}i\hat{2}}\right)\right] \\
& \times f_3^0(\hat{2},k,\widetilde{(ij)})|M_3^{(0)}(\hat{\tilde{1}},\hat{\tilde{2}},\widetilde{((ij)k)})|^2 J_1^{(1)}(p_{\widetilde{((ij)k)}}) \quad + (i\leftrightarrow k).
\end{aligned} \tag{4.53}$$

Finally, in order to subtract single unresolved limites of the four-parton antenna, a contribution to $\mathrm{d}\hat{\sigma}^{S,b_2}_{NNLO}$ is introduced, which reads

$$\begin{aligned}
& f_3^0(\hat{2},i,k)F_3^0(\hat{\tilde{2}},\widetilde{(ik)},j)|M_3^{(0)}(\hat{1},\hat{\tilde{2}},\widetilde{((ik)j)})|^2 J_1^{(1)}(p_{\widetilde{((ik)j)}}) \\
& +f_3^0(i,k,j)F_3^0(\hat{2},\widetilde{(ik)},\widetilde{(jk)})|M_3^{(0)}(\hat{1},\hat{\tilde{2}},\widetilde{(\widetilde{(ik)}(jk))})|^2 J_1^{(1)}(p_{\widetilde{(\widetilde{(ik)}(jk))}}) \\
& +f_3^0(\hat{2},j,k)F_3^0(\hat{\tilde{2}},i,\widetilde{(jk)})|M_3^{(0)}(\hat{1},\hat{\tilde{2}},\widetilde{(i(jk))})|^2 J_1^{(1)}(p_{\widetilde{(i(jk))}}).
\end{aligned} \tag{4.54}$$

All other F_4^0 antennae lead to analogous contributions to $\mathrm{d}\hat{\sigma}^{S,b_2}_{NNLO}$ and, if they are not initial-initial antennae with adjacent initial partons, to $\mathrm{d}\hat{\sigma}^{S,c}_{NNLO}$. The full double-real subtraction terms are written in appendices A.1, A.2, A.3 and A.4.
In processes with at least six partons, double unresolved limites appear where the unresolved partons do not share a common radiator. These colour-unconnected singularities are double counted in $\mathrm{d}\hat{\sigma}^{S,a}_{NNLO}$, which requires further subtraction terms $\mathrm{d}\hat{\sigma}^{S,d}_{NNLO}$ constructed as

$$\begin{aligned}
\mathrm{d}\hat{\sigma}^{S,d}_{NNLO} = & -\mathcal{N}^{RR}_{NNLO}\sum_{j,m}\mathrm{d}\Phi_{n+2}\frac{1}{S_{n+2}}X_3^0(i,j,k)X_3^0(l,m,n) \\
& \times|M^{(0)}_{n+2}(\ldots,I,K,\ldots,L,N,\ldots)|^2 J_n^{(n)}(p_3,\ldots,p_I,p_K,\ldots,p_L,p_N,\ldots,p_{n+4}),
\end{aligned} \tag{4.55}$$

where the sum is over all partons which are separated by more than one parton in the colour ordering of the double-real squared amplitude. Such subtraction terms are however not needed for NNLO $H+1J$ production.

4.5.2 Real-virtual contribution

The real-virtual contribution contains both poles up to $\frac{1}{\epsilon^2}$ and single unresolved limites obeying the factorisation behaviour described in eqs. (2.56) and (2.57). Both these divergences need to

be removed with dedicated subtraction terms. These are constructed partly from the double-real counterterms integrated over their single-unresolved phase-space, and partly from new subtraction terms which will need to be integrated over their own single-unresolved phase-space and added back to the double-virtual contribution.
In order to reconstruct the correct integrated dipole factors out of the integrated antennae and the real-virtual mass factorisation counterterms $\mathrm{d}\hat{\sigma}^{MF,1}_{ij,NNLO}$, the latter must be appropriately decomposed:

$$\begin{aligned}
\mathrm{d}\hat{\sigma}^{MF,1}_{ij,NNLO} &= \mathrm{d}\hat{\sigma}^{MF,1,a}_{ij,NNLO} + \mathrm{d}\hat{\sigma}^{MF,1,b_1}_{ij,NNLO} + \mathrm{d}\hat{\sigma}^{MF,1,b_2}_{ij,NNLO} + \mathrm{d}\hat{\sigma}^{MF,1,b_3}_{ij,NNLO},\\
\mathrm{d}\hat{\sigma}^{MF,1,a}_{ij,NNLO}(\xi_1 H_1, \xi_2 H_2) &= -\int \frac{\mathrm{d}z_1}{z_1}\frac{\mathrm{d}z_2}{z_2}\Gamma^{(1)}_{ij;kl}(z_1,z_2)\mathrm{d}\hat{\sigma}^{R}_{kl,NLO}(z_1\xi_1 H_1, z_2\xi_2 H_2),\\
\mathrm{d}\hat{\sigma}^{MF,1,b_1}_{ij,NNLO}(\xi_1 H_1, \xi_2 H_2) &= \int \frac{\mathrm{d}z_1}{z_1}\frac{\mathrm{d}z_2}{z_2}\Gamma^{(1)}_{ab;ab}(z_1,z_2)\mathrm{d}\hat{\sigma}^{S}_{kl,NLO}(z_1\xi_1 H_1, z_2\xi_2 H_2),\\
\mathrm{d}\hat{\sigma}^{MF,1,b_2}_{ij,NNLO}(\xi_1 H_1, \xi_2 H_2) &= \int \frac{\mathrm{d}z_1}{z_1}\frac{\mathrm{d}z_2}{z_2}\Gamma^{(1)}_{ij;kl}(z_1,z_2)\mathrm{d}\hat{\sigma}^{S}_{kl,NLO}(z_1\xi_1 H_1, z_2\xi_2 H_2),\\
\mathrm{d}\hat{\sigma}^{MF,1,b_3}_{ij,NNLO}(\xi_1 H_1, \xi_2 H_2) &= -\mathrm{d}\hat{\sigma}^{MF,1,b_1}_{ij,NNLO}(\xi_1 H_1, \xi_2 H_2),
\end{aligned} \tag{4.56}$$

where a and b are the species of the initial state partons in the reduced squared amplitudes in $\mathrm{d}\hat{\sigma}^{S}_{kl,NLO}$. The components of $\mathrm{d}\hat{\sigma}^{MF,1}_{ij,NNLO}$ above are assigned to the different real-virtual subtraction terms such as to complete the assembly of the $\mathbf{J}_2$ operators in the same spirit as for the NLO integrated subtraction terms. In the case of N_F=0 $H+1J$ production, where only gluons are involved, this decomposition becomes trivial. As in the NLO case the whole real-virtual counterterm is written as a convolution in the momentum fraction variables z_1 and z_2, where the z_i-independent parts are multiplied by adequate delta distributions.
Removing the explicit pole structure of the real-virtual squared amplitude requires the same kind of string of $\mathbf{J}_2$ operators as in the NLO virtual counterterms, but with a parton more. It appears therefore natural to integrate the single unresolved counterterm $\mathrm{d}\hat{\sigma}^{S,a}_{NNLO}$, which has the same structure than the NLO real counterterm but with one parton more, over its unresolved phase-space and combine it with $\mathrm{d}\hat{\sigma}^{MF,1,a}_{ij,NNLO}$ to form the term

$$\begin{aligned}
\mathrm{d}\hat{\sigma}^{T,a}_{NNLO} = -\mathcal{N}^{RV}_{NNLO}\sum_{i,j}\int \frac{\mathrm{d}z_1}{z_1}\frac{\mathrm{d}z_2}{z_2}\mathrm{d}\Phi_{n+1}(z_1 p_1, z_2 p_2, p_3, \ldots, n+3)\frac{1}{S_{n+1}}\\
\times \mathbf{J}^{(1)}_2(i,j;\epsilon)|M^{(0)}_{n+3}(1,\ldots,n+3)|^2 J^{(n+1)}_n(p_3,\ldots,p_{n+3}).
\end{aligned} \tag{4.57}$$

In addition to the explicit pole structure the real-virtual contribution also has 'tree × loop' and 'loop × tree' single unresolved divergences. The former is subtracted by means of tree-level three-parton antennae times one-loop reduced squared amplitudes. The one-loop interference introduces new poles in ϵ, which need to be removed. To this end new integrated antennae are introduced and combined with $\mathrm{d}\hat{\sigma}^{MF,1,b_1}_{ij,NNLO}$ to form the appropriate $\mathbf{J}_2$-operators:

$$\begin{aligned}
\mathrm{d}\hat{\sigma}^{T,b_1}_{NNLO} = \mathcal{N}^{RV}_{NNLO}\int \frac{\mathrm{d}z_1}{z_1}\frac{\mathrm{d}z_2}{z_2}\mathrm{d}\Phi_{n+1}(z_1 p_1, z_2 p_2, p_3, \ldots, n+3)\frac{1}{S_{n+1}}\\
\times\sum_j X^0_3(i,j,k)\Big[\delta(1-z_1)\delta(1-z_2)|\{2M^{(1)}_{n+2}M^{(0)\dagger}_{n+2}\}(1,\ldots,I,K,\ldots,n+2)|\\
+ c_J\sum_{m,n}\mathbf{J}^{(1)}_2(m,n;\epsilon)|M^{(0)}_{n+2}(1,\ldots,I,K,\ldots,n+3)|^2\Big]J^{(n)}_n(p_3,\ldots,p_I,p_K,\ldots,p_{n+3}),
\end{aligned} \tag{4.58}$$

where the sum over j is over all potentially unresolved partons of the real-virtual squared amplitude. The sum over m,n runs over all colour-neighbouring partons in the one-loop reduced

interference. The constant c_J is equal to one unless $n = 0$ and all partons are gluons, in which case c_J is two. The $\mathrm{d}\hat{\sigma}^{T,b_1}_{NNLO}$ contribution is new and has to be added back to the double-virtual contribution.
The 'loop $\times$ tree' part of the IR factorisation of the real-virtual squared amplitude requires another subtraction term made up of a one-loop three-parton antenna times a tree-level reduced squared amplitude:

$$\begin{aligned}\mathrm{d}\hat{\sigma}^{T,b_2}_{NNLO} = \mathcal{N}^{RV}_{NNLO} \int \frac{\mathrm{d}z_1}{z_1}\frac{\mathrm{d}z_2}{z_2}\mathrm{d}\Phi_{n+1}(z_1p_1, z_2p_2, p_3, \ldots, n+3)\frac{1}{S_{n+1}} \\ \times \sum_j \Bigg[X^1_3(i,j,k)\delta(1-z_1)\delta(1-z_2) + \sum_{m,n} \mathbf{J}^{(1)}_2(m,n;\epsilon) X^0_3(i,j,k) \\ - M_X X^0_3(i,j,k)\mathbf{J}^{(1)}_2(I,K;\epsilon)\Bigg] \\ \times |M^{(0)}_{n+2}(1,\ldots,I,K,\ldots,n+3)|^2 J^{(n)}_n(p_3,\ldots,p_I,p_K,\ldots,p_{n+3}),\end{aligned} \tag{4.59}$$

where as usual the j sum runs over all unresolved partons. Since the one-loop antenna is derived from a one-loop matrix element, it features explicit poles up to $\frac{1}{\epsilon^2}$ which must be subtracted with appropriate $\mathbf{J}_2$ operators. In the second line the $\mathbf{J}_2$ operators are assembled from the integral of $\mathrm{d}\hat{\sigma}^{S,b_2}_{NNLO}$ together with $\mathrm{d}\hat{\sigma}^{MF,1,b_2}_{ij,NNLO}$ and the sum over m and n runs over all colour-neighbouring partons in the one-loop antenna. The $\mathbf{J}_2$ operator in the third line is built from introducing new integrated antennae and combining them with $\mathrm{d}\hat{\sigma}^{MF,1,b_3}_{ij,NNLO}$. The constant M_X depends on the identity of the partons in the antenna and its values are tabulated in [124]. For purely gluonic antennae it is $M_X = 2$. The whole contribution except the integrated antennae in the second line have to be added back to the double-virtual contribution.
One issue with the previous terms is that the one-loop antenna $X^1_3(i,j,k)$ is renormalised at the scale s_{ijk}, whereas the real-virtual squared amplitude and remaining subtraction terms are renormalised at the generic scale μ^2. In order to be consistent with this the one-loop antenna needs to be evolved to the scale μ^2 with the following term:

$$\begin{aligned}\mathrm{d}\hat{\sigma}^{T,b_3}_{NNLO} = \mathcal{N}^{RV}_{NNLO} \int \frac{\mathrm{d}z_1}{z_1}\frac{\mathrm{d}z_2}{z_2}\mathrm{d}\Phi_{n+1}(z_1p_1, z_2p_2, p_3, \ldots, n+3)\frac{1}{S_{n+1}} \\ \times \sum_j \beta_0 \log\left(\frac{\mu^2}{|s_{ijk}|}\right) X^0_3(i,j,k)\delta(1-z_1)\delta(1-z_2) \\ \times |M^{(0)}_{n+2}(1,\ldots,I,K,\ldots,n+3)|^2 J^{(n)}_n(p_3,\ldots,p_I,p_K,\ldots,p_{n+3}).\end{aligned} \tag{4.60}$$

with the usual sum over unresolved partons.
The last group of terms consists mainly of the integral of $\mathrm{d}\hat{\sigma}^{S,c}_{NNLO}$ over its unresolved phase-space. It reads

$$\begin{aligned}\mathrm{d}\hat{\sigma}^{T,c}_{NNLO} = \mathcal{N}^{RV}_{NNLO} \int \frac{\mathrm{d}z_1}{z_1}\frac{\mathrm{d}z_2}{z_2}\mathrm{d}\Phi_{n+1}(z_1p_1, z_2p_2, p_3, \ldots, n+3)\frac{1}{S_{n+1}} \Bigg\{ \\ \frac{1}{2}\sum_j \Bigg[\Bigg(\quad \big(\mathcal{X}^0_3(s_{ik}) - \mathcal{X}^0_3(s_{(ij)(ik)})\big) \\ - \big(\mathcal{X}^0_3(s_{ai}) - \mathcal{X}^0_3(s_{a(ij)})\big) - \big(\mathcal{X}^0_3(s_{kb}) - \mathcal{X}^0_3(s_{(kj)b})\big)\Bigg) \\ - \Bigg(\quad \big(\mathcal{S}(s_{ik}, s_{ik}, 1) - \mathcal{S}(s_{(ij)(jk)}, s_{ik}, x_{(ij)(jk),ik})\big)\end{aligned}$$

$$
\begin{aligned}
&-\big(\mathcal{S}(s_{ai},s_{ik},x_{ai,ik})-\mathcal{S}(s_{a(ij)},s_{ik},x_{a(ij),ik})\big)\\
&-\big(\mathcal{S}(s_{kb},s_{ik},x_{kb,ik})-\mathcal{S}(s_{(jk)b},s_{ik},x_{(jk)b,ik})\big)\Big)\delta(1-z_1)\delta(1-z_2)\Big]\Big\}\\
&\times X_3^0(i,j,k)|M^{(0)}_{n+2}(1,\dots,I,K,\dots,n+3)|^2 J_n^{(n)}(p_3,\dots,p_I,p_K,\dots,p_{n+3}),
\end{aligned}
\tag{4.61}
$$

where j sums over the unresolved partons and $\mathcal{S}$ are the integrated soft functions. The definition for the initial-final ones, which are relevant for this work, can be found in appendix B. The integrated antennae $\mathcal{X}_3^0(s_{(ij)(ik)})$, $\mathcal{X}_3^0(s_{a(ij)})$ and $\mathcal{X}_3^0(s_{(kj)b})$ have been added in order to cancel the poles of the integrated antennae from the double-real subtraction term. The corresponding terms need to be integrated and added back to the double-virtual contribution.
Considering again the case of $H+1J$ production, the real-virtual matrix element has the same colour orderings as the real one, eq. (4.33). The subtraction of its single unresolved singularities has the same structure as in eq. (4.34), where the individual subtraction terms are replaced by corresponding blocks of $\mathrm{d}\hat{\sigma}^{T,b}_{NNLO}$ and $\mathrm{d}\hat{\sigma}^{T,c}_{NNLO}$. For instance, the real subtraction term

$$
f_3^0(\hat{2},3,4)|M_3^{(0)}(\hat{1},\hat{\hat{2}},\widetilde{(34)})|^2 J_1^{(1)}(p_{\widetilde{(34)}}),
\tag{4.62}
$$

can be translated to the real-virtual subtraction terms

$$
\begin{aligned}
\mathrm{d}\hat{\sigma}^{T,\{234\}}_{NNLO} &= f_3^0(\hat{2},3,4)|2M_3^{(1)}(\hat{1},\hat{\hat{2}},\widetilde{(34)})M_3^{(0)\dagger}(\hat{1},\hat{\hat{2}},\widetilde{(34)})|\delta(1-z_1)\delta(1-z_2)J_1^{(1)}(p_{\widetilde{(34)}})\\
&\quad+\Big[\mathbf{J}_2^{(1,II)}(\hat{1},\hat{\hat{2}};z_1,z_2)+\mathbf{J}_2^{(1,IF)}(\hat{\hat{2}},\widetilde{(34)};z_2)\delta(1-z_1)\\
&\quad+\ \mathbf{J}_2^{(1,IF)}(\widetilde{(34)},\hat{1};z_1)\delta(1-z_2)\Big]|M_3^{(0)}(\hat{1},\hat{\hat{2}},\widetilde{(34)})|^2 J_1^{(1)}(p_{\widetilde{(34)}})\\
&\quad+\Big(f_3^1(\hat{2},3,4,\sqrt{s_{234}})\delta(1-z_1)\delta(1-z_2)\\
&\qquad+\Big[\mathbf{J}_2^{(1,IF)}(\hat{2},3;z_2)\delta(1-z_1)+\mathbf{J}_2^{(1,FF)}(3,4)\delta(1-z_1)\delta(1-z_2)\\
&\qquad+\mathbf{J}_2^{(1,IF)}(\hat{2},4;z_2)\delta(1-z_1)-2\mathbf{J}_2^{(1,IF)}(\hat{\hat{2}},\widetilde{(34)};z_2)\delta(1-z_1)\Big]f_3^0(\hat{2},3,4)\Big)\\
&\qquad\times|M_3^{(0)}(\hat{1},\hat{\hat{2}},\widetilde{(34)})|^2 J_1^{(1)}(p_{\widetilde{(34)}})\\
&\quad+\frac{11}{6}f_3^0(\hat{2},3,4)\log(\frac{\mu^2}{\sqrt{s_{234}}})|M_3^{(0)}(\hat{1},\hat{\hat{2}},\widetilde{(34)})|^2\delta(1-z_1)\delta(1-z_2)J_1^{(1)}(p_{\widetilde{(34)}})\\
&\quad+\frac{1}{2}\Big(\Big(\mathcal{F}_3^0(s_{\hat{\hat{2}},\widetilde{(34)}})-\mathcal{S}(s_{\hat{\hat{2}},\widetilde{(34)}},s_{(\hat{2},4)})\Big)-\Big(\mathcal{F}_3^0(s_{(\hat{2},4)})-\mathcal{S}(s_{(\hat{2},4)},s_{(\hat{2},4)})\Big)\\
&\qquad-\Big(\mathcal{F}_3^0(s_{\hat{1},\widetilde{(34)}})-\mathcal{S}(s_{\hat{1},\widetilde{(34)}},s_{(\hat{2},4)})\Big)+\Big(\mathcal{F}_3^0(s_{\hat{1},4})-\mathcal{S}(s_{\hat{1},4},s_{(\hat{2},4)})\Big)\\
&\qquad-\Big(\mathcal{F}_3^0(s_{\hat{1},\hat{\hat{2}}})-\mathcal{S}(s_{\hat{1},\hat{\hat{2}}},s_{(\hat{2},4)})\Big)+\Big(\mathcal{F}_3^0(s_{\hat{1},\hat{2}})-\mathcal{S}(s_{\hat{1},\hat{2}},s_{(\hat{2},4)})\Big)\Big)\\
&\qquad\times f_3^0(\hat{2},3,4)|M_3^{(0)}(\hat{1},\hat{\hat{2}},\widetilde{(34)})|^2 J_1^{(1)}(p_{\widetilde{(34)}}),
\end{aligned}
\tag{4.63}
$$

where in the one-loop antenna the scale it has been renormalised at has been specified. The remaining real-virtual subtraction terms except $\mathrm{d}\hat{\sigma}^{T,a}_{NNLO}$ can be contructed in this way and are listed in appendices A.5 and A.6.

4.5.3 Double-virtual contribution

The two-loop double-virtual squared amplitude has no further unresolved limites but contains poles up to $\frac{1}{\epsilon^4}$. In order to remove them, the remaining double-real subtraction terms are

integrated over their double unresolved phase-space regions and the real-virtual subtraction terms are integrated over their single unresolved phase-space. Together with the double-virtual mass factorisation counterterm $\mathrm{d}\hat{\sigma}^{MF,2}_{ij,NNLO}$ they can be cast into a form which matches the pole structure as predicted in eq. (2.62). Also here the integrated counterterms are written as a convolution over z_1 and z_2. The integrated counterterm is

$$\begin{aligned}
\mathrm{d}\hat{\sigma}^{U}_{NNLO} = -\mathcal{N}^{VV}_{NNLO} \int \frac{\mathrm{d}z_1}{z_1}\frac{\mathrm{d}z_2}{z_2}\mathrm{d}\Phi_n(z_1p_1, z_2p_2, p_3, \ldots, n+2)\frac{1}{S_n}\Bigg\{ \\
\sum_{i,j}\mathbf{J}^{(1)}_2(i,j;\epsilon)\Bigg(|\{2M^{(1)}_{n+2}M^{(0)\dagger}_{n+2}\}(1,\ldots,n+2)| - \frac{\beta_0}{\epsilon}|M^{(0)}_{n+2}(1,\ldots,n+2)|^2\Bigg) \\
+\frac{1}{2}\Big[\Big\{\sum_{m,n}\mathbf{J}^{(1)}_2(m,n;\epsilon)\Big\}\otimes\Big\{\sum_{m',n'}\mathbf{J}^{(1)}_2(m',n';\epsilon)\Big\}\Big](z_1,z_2)|M^{(0)}_{n+2}(1,\ldots,n+2)|^2 \\
+\sum_{i,j}\mathbf{J}^{(2)}_2(i,j;\epsilon)M^{(0)}_{n+2}(1,\ldots,n+2)|^2\Bigg\}J^{(n)}_n(p_3,\ldots,p_{n+2}),
\end{aligned} \tag{4.64}$$

where the respective sums are over the colour-neighbouring pairs of partons in the double-virtual squared amplitude. The form of the two-loop integrated dipoles $\mathbf{J}^{(2)}_2$ depends on the kinematics and can be found in [124]. The first line of this equation contains the same $\frac{1}{\epsilon^4}$ and $\frac{1}{\epsilon^3}$ poles as the first line of eq. (2.62). The difference in $\frac{1}{\epsilon^2}$ comes from the fact that the $\mathbf{J}_2$ and the $\mathbf{I}^{(1)}$ operators differ in their finite pieces. For the same reason, the first two lines of eqs. (4.64) and (2.62) agree up to $\frac{1}{\epsilon}$ pieces. The full equations agree up to finite pieces. The reconstruction of the double unresolved $\mathbf{J}^{(2)}_2$ operators and the convolutions of $\mathbf{J}^{(1)}_2$ operators is described in appendix A.7.

4.6 Subtraction terms for $H + 1J$

There are 12 distinct colour orderings contributing to the double-real $H + 5g$ matrix element. These are classified into two topologies depending on whether the two initial state momenta are adjacent (IIFFF topology) or not (IFIFF topology). Since the structure of the subtraction terms depends only on the colour ordering, for squared amplitudes of the same topology they are identical up to cyclic permutation of the momenta. The double-real subtraction terms need therefore only to be written for a specific colour ordering for each topology and can then be called with permutated momenta in the arguments of the corresponding numerical routines for different squared amplitudes.

A very convenient feature of antenna subtraction is that the individual subtraction terms do not depend on the partons which are outside the radiating antenna. Therefore, the subtraction terms for an amplitude with a certain set of partons are contained in the subtraction terms for the amplitudes with the same set plus an additional parton. The double-real subtraction terms for pure-QCD $5g$ scattering can thus be obtained from the purely gluonic double-real subtraction terms for NNLO dijet production [125]. Since the Higgs boson is colour-neutral and thus is not involved in any singularity, these are the same as for $H + 5g$ scattering. It has been checked that the double-real subtraction terms obtained in this way fulfil the structure described in sec. 4.5.1.

By symmetrising the subtraction terms over the initial state partons $\hat{1}$ and $\hat{2}$, the number of colour orderings reduces to six. These are

IIFFF	IFIFF
$\{\hat{1},\hat{2},3,4,5\}$	$\{\hat{1},3,\hat{2},4,5\}$
$\{\hat{1},\hat{2},4,5,3\}$	$\{\hat{1},4,\hat{2},5,3\}$
$\{\hat{1},\hat{2},5,3,4\}$	$\{\hat{1},5,\hat{2},3,4\}$.

For the IIFFF topology the $\mathrm{d}\hat{\sigma}^{S,a}_{NNLO}$ contribution is

$$\begin{aligned}
\mathrm{d}\hat{\sigma}^{S,a}_{NNLO}(\hat{1},\hat{2},i,j,k) =& f_3^0(\hat{2},i,j)|M_4^{(0)}(\hat{1},\hat{\tilde{2}},\widetilde{(ij)},k)|^2 J_1^{(2)}(\widetilde{p_{ij}},p_k)\\
&+f_3^0(i,j,k)|M_4^{(0)}(\hat{1},\hat{2},\widetilde{(ij)},\widetilde{(jk)})|^2 J_1^{(2)}(\widetilde{p_{ij}},\widetilde{p_{jk}})\\
&+f_3^0(\hat{1},k,j)|M_4^{(0)}(\hat{\tilde{1}},(\hat{2}),i,\widetilde{(kj)})|^2 J_1^{(2)}(p_i,\widetilde{p_{kj}})\\
&+f_3^0(\hat{2},k,j)|M_4^{(0)}(\hat{1},\hat{\tilde{2}},\widetilde{(jk)},i)|^2 J_1^{(2)}(p_i,\widetilde{p_{kj}})\\
&+f_3^0(k,j,i)|M_4^{(0)}(\hat{1},\hat{2},\widetilde{(jk)},\widetilde{(ij)})|^2 J_1^{(2)}(\widetilde{p_{ij}},\widetilde{p_{jk}})\\
&+f_3^0(\hat{1},i,j)|M_4^{(0)}(\hat{\tilde{1}},\hat{2},k,\widetilde{(ij)})|^2 J_1^{(2)}(\widetilde{p_{ij}},p_k),
\end{aligned} \tag{4.65}$$

while the $\mathrm{d}\hat{\sigma}^{S,b_1}_{NNLO}$ contribution is

$$\begin{aligned}
\mathrm{d}\hat{\sigma}^{S,b_1}_{NNLO}(\hat{1},\hat{2},i,j,k) =& F_4^0(\hat{2},i,j,k)|M_3^{(0)}(\hat{1},\hat{\tilde{2}},\widetilde{(ijk)})|^2 J_1^{(1)}(\widetilde{p_{ijk}})\\
&+F_4^0(i,j,k,\hat{1})|M_3^{(0)}(\hat{\tilde{1}},\hat{2},\widetilde{(ijk)})|^2 J_1^{(1)}(\widetilde{p_{ijk}})\\
&-F_4^0(\hat{1},i,\hat{2},k)|M_3^{(0)}(\hat{\tilde{1}},\hat{\tilde{2}},\tilde{j})|^2 J_1^{(1)}(\widetilde{p_j}).
\end{aligned} \tag{4.66}$$

The remaining contributions follow from the colour ordering of the F_0^4 as described in sec. 4.5.1. For the IFIFF topology the $\mathrm{d}\hat{\sigma}^{S,a}_{NNLO}$ contribution is

$$\begin{aligned}
\mathrm{d}\hat{\sigma}^{S,a}_{NNLO}(\hat{1},i,\hat{2},j,k) =& F_3^0(\hat{1},i,\hat{2})|M_4^{(0)}(\hat{\tilde{1}},\hat{\tilde{2}},\tilde{j},\tilde{k})|^2 J_1^{(2)}(\widetilde{p_j},\widetilde{p_k})\\
&+f_3^0(\hat{2},j,k)|M_4^{(0)}(\hat{1},i,\hat{\tilde{2}},\widetilde{(jk)})|^2 J_1^{(2)}(p_i,\widetilde{p_{jk}})\\
&+f_3^0(\hat{1},k,j)|M_4^{(0)}(\hat{\tilde{1}},i,\hat{2},\widetilde{(jk)})|^2 J_1^{(2)}(p_i,\widetilde{p_{jk}})\\
&+F_3^0(\hat{1},i,\hat{2})|M_4^{(0)}(\hat{\tilde{1}},\hat{\tilde{2}},\tilde{k},\tilde{j})|^2 J_1^{(2)}(\widetilde{p_k},\widetilde{p_j})\\
&+f_3^0(\hat{2},k,j)|M_4^{(0)}(\hat{1},i,\hat{\tilde{2}},\widetilde{(jk)})|^2 J_1^{(2)}(p_i,\widetilde{p_{jk}})\\
&+f_3^0(\hat{1},j,k)|M_4^{(0)}(\hat{\tilde{1}},i,\hat{2},\widetilde{(jk)})|^2 J_1^{(2)}(p_i,\widetilde{p_{jk}}),
\end{aligned} \tag{4.67}$$

and the $\mathrm{d}\hat{\sigma}^{S,b_1}_{NNLO}$ contribution is

$$\begin{aligned}
\mathrm{d}\hat{\sigma}^{S,b_1}_{NNLO}(\hat{1},\hat{2},i,j,k) =& F_4^0(\hat{2},j,k,\hat{1})|M_3^{(0)}(\hat{\tilde{1}},\tilde{i},\hat{\tilde{2}})|^2 J_1^{(1)}(\widetilde{p_i})\\
&+F_4^0(\hat{2},k,j,\hat{1})|M_3^{(0)}(\hat{\tilde{1}},\tilde{i},\hat{\tilde{2}})|^2 J_1^{(1)}(\widetilde{p_i})\\
&+F_4^0(\hat{1},i,\hat{2},j)|M_3^{(0)}(\hat{\tilde{1}},\hat{\tilde{2}},\tilde{k})|^2 J_1^{(1)}(\widetilde{p_k})\\
&+F_4^0(\hat{1},i,\hat{2},k)|M_3^{(0)}(\hat{\tilde{1}},\hat{\tilde{2}},\tilde{j})|^2 J_1^{(1)}(\widetilde{p_j}),
\end{aligned} \tag{4.68}$$

and again the colour ordering of the double unresolved antennae guide the construction of the remaining pieces. Since the double-real contribution involves only 5 partons, there are no colour unconnected subtraction terms $\mathrm{d}\hat{\sigma}^{S,d}_{NNLO}$. Furthermore, there are not enough partons to use a final-final mapping for the large angle soft terms. An initial-final mapping has therefore been used. For a colour ordering $(\hat{1},\hat{2},i,j,k)$, the initial-final primary mappings are $(\hat{1},k,j)\to\hat{\tilde{1}},\widetilde{(kj)}$

and $(\hat{2}, i, j) \to \hat{\tilde{2}}, \widetilde{(ij)}$. These lead to eikonals of the form $S_{\hat{2},k,\widetilde{(jk)}}$ in the $\mathrm{d}\hat{\sigma}^{S,c}_{NNLO}$ blocks originating from initial-initial F_4^0's, which in j soft limites lead to numerical instabilities. In order to avoid this, the freedom to use arbitrary primary mappings for the LAS terms has been used to choose mappings $(\hat{1}, i, k) \to \hat{\tilde{1}}, \widetilde{(ik)}$ and $(\hat{1}, k, i) \to \hat{\tilde{1}}, \widetilde{(ki)}$ for these blocks, which do not follow the colour ordering of the actual double-real squared amplitude.
The individual contributions to the double-real subtraction terms have been tabulated versus all possible single, double single and triple collinear limites. It has been checked that spurious divergences in $\mathrm{d}\hat{\sigma}^{S,a}_{NNLO}$ and $\mathrm{d}\hat{\sigma}^{S,b_2}_{NNLO}$ are indeed cancelled by the $\mathrm{d}\hat{\sigma}^{S,c}_{NNLO}$ pieces and that the remaining ones indeed match the physical singularities of the squared amplitudes for a fixed colour ordering. In single soft limites, the remaining divergences from the antenna functions have been collected and found to agree with the expected structure of the large-angle soft terms.
The real-virtual matrix element receives contributions from 3 colour orderings. These are again classified into a topology where the initial state momenta are adjacent (IIFF topology) and one where they are not (IFIF topology). The corresponding subtraction terms have been constructed following the guidelines in section 4.5.2. It has then been checked that the double-real subtraction terms integrated over the single-unresolved phase-space yield the same structure. The integrated LAS terms have been modified to be consistent with the change of primary mapping mentioned above.
The double-virtual matrix element features only one colour ordering (see chapter 3). The double-virtual subtraction terms have been constructed according to section 4.5.2 resp. [124]. Since only three partons are involved, the complete factorisation mentioned in section 2.8.2 and observed in section 3.4.1 applies and the subtraction terms could be organised according to the three different pairs of partons.

Chapter 5

Implementation

The following chapter describes the implementation of a program which carries out the computation of $H + 1J$ at NNLO using the antenna subtraction formalism discussed in the previous chapter. Of course a comprehensive description at the technical level would be beyond the scope of this text. Rather, an understanding is given of the main ideas and concepts which have been elaborated to solve some of the issues appearing in such computations.
The program evaluates the dominant gluons-only ($N_F = 0$) contribution to $H + 1J$ at an 8 TeV LHC. The remaining contributions are included in the larger framework NNLOJET.

5.1 Code

The central program is called HJET and carries out the phase-space integration as in eq. (2.43) using VEGAS. The program is written in FORTRAN90, except for some external routines

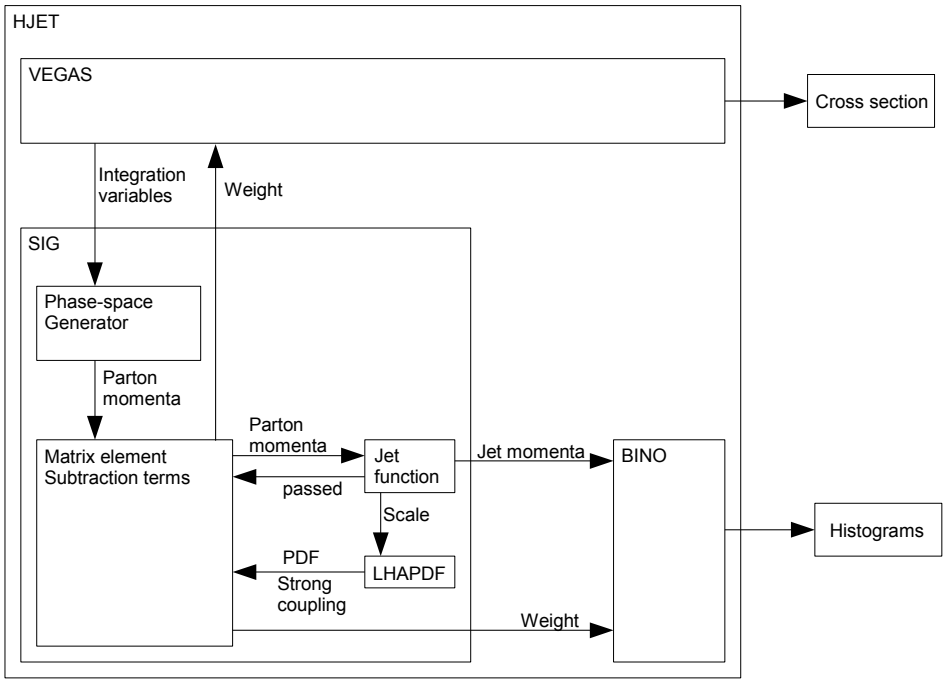

Figure 5.1: Flowchart of the program

written in F77 which have been integrated by means of interfaces. The REAL and COMPLEX variables are declared at arbitrary precision, where double precision is set as a default. The inner working of the program is sketched in fig. 5.1. VEGAS calls a function SIG, to which it gives its integration variables as input and which returns the weight of the function to be integrated. The VEGAS variables are points in an unit hypercube of appropriate dimension. The possibility to integrate simultaneously over phase-spaces of different multiplicities in a single HJET call is implemented. To this end the program features actually four identical (up to the dimensionality of the integration volume) VEGAS routines. The implemented multiplicities are three-parton, four-parton and two complementary five-parton phase-spaces (see section 5.1.1). The computation is set up by a run card in which the relevant flags and variables are stored. In the following, details of the main components will be explained.

5.1.1 Phase-space generator

The phase-space generator takes the VEGAS integration variables, the masses of the involved particles and the center-of-mass energy of the collision as input and converts it into points in the phase-spaces of the required multiplicities. These are the n-partons plus two photon phase-spaces, where $n \in \{3, 4, 5\}$. The momenta are generated on-shell and obey momentum conservation. The two photons are such that $p_{\gamma_1} + p_{\gamma_2} = p_H$.
The momenta are generated starting from a $2 \to 2$ scattering. The initial state momenta p_1 and p_2 lie along the z-axis and are fully determined from the center-of-mass energy and the masses of the initial state partons. The final state momenta are back-to-back and correspond to the diphoton and partonic subsystems. The mass of the diphoton subsystem is determined with a VEGAS variable according to a Breit-Wigner distribution which takes the Higgs boson mass and width as additional input. Alternatively a delta function can be used which amounts to set the diphoton mass to the parametric Higgs boson mass. The momenta of the partonic and diphoton subsystems are determined from their masses and by converting a second VEGAS variable into a polar angle. The momenta of the individual photons are assigned by converting two VEGAS variables into an azimuthal and a polar angle. Using these, the photon momenta are computed back-to-back in the rest frame of the diphoton system and subsequently boosted into the center-of-mass frame. If there are more than one parton in the final state, their momenta are determined in a similar way by means of iterated $1 \to 2$ branchings. Three additional VEGAS variables are used for each extra parton, one to fix an invariant mass of the partonic subsystem and the two others to obtain an azimuthal and a polar angle. The two daughter momenta are computed in their own center-of-mass frame using the angles and then boosted into the center-of-mass frame of the collision. Thus a point in the three-parton phase-space needs four integration variables to be computed, while points in the four- and five-parton phase-spaces need seven respectively ten integration variables. Except for the diphoton invariant mass all angles and invariant masses are chosen linearly from the VEGAS variables. The generator also computes a weight, basing on the Jacobian factors for reconstructing the phase-space variables from the VEGAS variables and the weight of the $2 \to 2$ and $1 \to 2$ phase-spaces.
One particular issue the phase-space generator has to address is the cancellation of angular terms in collinear limites (see section 4.1), which is done by averaging over phase-space points which are rotated by $\frac{\pi}{2}$ around the collinear axis. In the four-parton phase-space, where single collinear limites need to be accounted for, the momenta of the final state partons p_3 and p_4 are rotated around the initial momentum p_1 in their center-of-mass frame. The additional set of rotated momenta obtained in this way allows to average out the angular terms corresponding to $p_3||p_4$, $p_3||p_1$ and $p_4||p_1$ collinear limites. The $p_3||p_2$ and $p_4||p_2$ limites can however not be dealt with in this way. The strategy then is to divide the phase-space into a region which contains the

initial state collinear limites involving p_1, together with an additional set of momenta rotated around p_1. This is done by requiring either of s_{13} or s_{14} to be the smallest invariant. With $z \to -z$ momenta are generated in a second region where p_3 and p_4 can only become collinear with p_2, together with a set of momenta rotated around p_2. One thus obtains four sets of momenta, where summing over the unrotated momenta of both regions gives full phase-space coverage, while averaging with the angular partner sets allows to get rid of the angular terms.
In the five parton phase-space relevant for the double-real $p_1 + p_2 \to p_3 + p_4 + p_5 + p_{\gamma_1} + p_{\gamma_2}$ contribution, the angular terms corresponding to double single collinear limites as well as triple collinear limites must be canceled. This is done by averaging over the original momenta and three sets of rotated momenta. One set is obtained by rotating the (345) system around p_1, a second one by rotating the (45) system around p_3. The third rotated set is obtained by performing the (345) rotation followed by the (45) one. The phase-space is decomposed in six regions involving triple collinear limites, which from now on will be denoted by (5A), and six double single collinear regions denoted by (5B). They are obtained through the following conditions and permutations thereof, where s_1 and s_2 are the smallest and second smallest Lorentz invariants:

$$\begin{aligned}
&(\{s_1, s_2\} \in \{s_{34}, s_{13}\}) \text{ or} \\
&(\{s_1, s_2\} \in \{s_{35}, s_{13}\}) \text{ or} \\
&(s_1 = s_{45} \text{ and } s_2 = \min(s_{34}, s_{35}) \text{ and } s_{14} + s_{15} < s_{24} + s_{25}) \text{ or} \\
&(s_1 = s_{13} \text{ and } s_2 = \min s_{14}, s_{15}),
\end{aligned} \tag{5.1}$$

for the triple collinear sector (5A) and

$$\begin{aligned}
&(s_1 = s_{13} \text{ and } s_2 = \min(s_{23}, s_{24}, s_{25})) \\
&(\{s_1, s_2\} \in \{s_{13}, s_{45}\}),
\end{aligned} \tag{5.2}$$

for the double single collinear sector (5B). Together with the rotated sets one therefore obtains 24 (5A) sets and 24 (5B) sets. The symmetry of the squared amplitudes under permutations of the gluons allows one however to use only one of the six regions for each rotated set, such that only four (5A) and four (5B) phase-space points need to be evaluated for each event.
The phase-space generator only produces initial state momenta with energy equal to the half of the hadronic c.o.m. energy. When PDF's are used, the partonic c.o.m. energy is given as an input, and a Lorentz boost in z-direction is performed on all generated momenta to obtain kinematics consistent with the momentum fractions ξ_1 and ξ_2.
Of course the numerical precision of the computation is limited and for phase-space configurations where the amplitude becomes singular enough the subtraction breaks down. A phase-space cutoff c is therefore implemented which rejects points corresponding to Lorentz invariants which are too small, $s_{ij} > c \cdot s_{\mathrm{p}}$, where $s_{\mathrm{p}} = \xi_1 \xi_2 s$ is the partonic and s the hadronic c.o.m. energy. For debugging and testing purposes the phase-space has been sampled with $c = 10^{-9}$, where the onset of numerical instabilities has been observed. For production $c = 10^{-6}$ is set.
It may accidentally happen that momenta involved in an antenna are mapped such that $s_{IJ} < c \cdot s_{\mathrm{p}}$, leading to potential instabilities. A secondary cutoff on the mapped momenta has been experimented with, but has been rejected since this spoils the intricate cancellation pattern between spurious divergences in the subtraction terms.

5.1.2 Matrix elements

Depending on the multiplicity and loop order the matrix elements required for $N_F = 0$ are implemented and evaluated in different ways.

All tree level processes have been coded up in HJET in terms of helicity amplitudes taken from the literature. The spinors for a momentum k are evaluated with following procedure: [69].

$$u_+(k) = v_-(k) = \frac{1}{\sqrt{2}} \begin{bmatrix} \sqrt{k^+} \\ \sqrt{k^-} e^{i\phi_k} \\ \sqrt{k^+} \\ \sqrt{k^-} e^{i\phi_k} \end{bmatrix}, \quad u_-(k) = v_+(k) = \frac{1}{\sqrt{2}} \begin{bmatrix} \sqrt{k^-} e^{-i\phi_k} \\ -\sqrt{k^+} \\ -\sqrt{k^-} e^{-i\phi_k} \\ \sqrt{k^+} \end{bmatrix}, \tag{5.3}$$

where

$$e^{\pm i\phi_k} = \frac{k^1 \pm ik^2}{\sqrt{(k^1)^2 + (k^2)^2}}, \quad k^\pm = k^0 \pm k^3. \tag{5.4}$$

The case where k is an initial-state momentum ($k^1 = k^2 = 0$, $k^0 = \pm k^3$) is treated separately; the phase $e^{\pm i\phi_k}$ is then (-1). For a certain momentum assignement for the amplitude the spinor products and Lorentz invariants are computed once and for all and stored inside a matrix to prevent redundant evaluation of the spinors. The analytical continuation of the spinor products with one resp. two momenta in the initial state is performed by multiplying it with **i** resp. (-1) [126]. The helicity amplitudes are then evaluated by calling the elements of the storage matrix. Certain amplitudes also involve the Higgs mass, where the offshell mass of the diphoton system has to be used in order to preserve momentum conservation. Usually, not all helicity amplitudes are given but only some minimal set which allows to reconstruct the remaining ones using their symmetries. Parity conjugation allows to flip all helicities and is easily performed by taking the complex conjugate and multiplying with a minus sign. Together with cyclicity and reflection [93]

$$M_n(1, 2, \ldots, n-1, n) = M_n(n, 1, 2, \ldots, n-1), \tag{5.5}$$

$$M_n(1, 2, \ldots, n) = (-1)^n M_n(n, \ldots, 2, 1), \tag{5.6}$$

this is enough to reconstruct all helicity amplitudes for $H + 3g$ out of the '$+++$' and '$++-$' amplitudes. For tree-level Higgs plus four [127] and five gluons [28], where the amplitudes with zero, one and two adjacent gluons of negative helicity are given, the dual Ward identity [93] is needed in order to reconstruct amplitudes with alternating helicities:

$$M(1, 2, 3, \ldots, n) + M(2, 1, 3, \ldots, n) + \ldots + M(2, 3, \ldots, 1, n) = 0. \tag{5.7}$$

Using this identity may lead to helicity amplitudes being called more than once with the same indices when the sum over colour orderings is performed. This redundancy leads to speed loss in particular in the evaluation of the $H + 5g$ matrix element. A cache system has therefore been implemented which stores the amplitudes once evaluated with a certain permutation of indices and retrieves them if this particular permutation is again requested. In a sample run where the number of required jets has been set to three in order to prevent the evaluation of the subtraction terms this results in reducing the runtime by a factor of ~ 0.6. After their evaluation, the helicity amplitudes are squared and summed over the helicities to obtaine the colour ordered amplitude squared relevant for the various subtraction terms. The matrix elements are obtained by further summing over the colour orderings. While the three-gluon matrix element has only one colour ordering, the four-gluon matrix element has three orderings and can be written as

$$|\mathcal{M}_4^{(0)}(1, 2, 3, 4)|^2 = \frac{\lambda^2 g_s^4 N_C^3 C_F}{2} \sum_{\text{Hel}} \Big[|M_4^{(0)}(1, 2, 3, 4)|^2 + |M_4^{(0)}(1, 2, 4, 3)|^2 + |M_4^{(0)}(1, 3, 2, 4)|^2 \Big], \tag{5.8}$$

where the effective coupling λ is given in eq. (2.28). The five gluon matrix element can not anymore be expressed in terms of squares of partial amplitudes. It can be written as [28]:

$$|\mathcal{M}_5^{(0)}(1,2,3,4,5)|^2 = \frac{\lambda^2 g_s^6 N_C^4 C_F}{2} \sum_{\text{Hel}} \sum_{i,j=1}^{6} C_{ij} m_i (m_j)^*, \tag{5.9}$$

where

$$C_{ij} = \begin{pmatrix} 4 & 2 & 2 & 1 & 1 & 0 \\ 2 & 4 & 1 & 0 & 2 & 1 \\ 2 & 1 & 4 & 2 & 0 & 1 \\ 1 & 0 & 2 & 4 & 1 & 2 \\ 1 & 2 & 0 & 1 & 4 & 2 \\ 0 & 1 & 1 & 2 & 2 & 4 \end{pmatrix} \quad , \quad m_i = \begin{pmatrix} M_5^{(0)}(1,2,3,4,5) \\ M_5^{(0)}(1,2,4,3,5) \\ M_5^{(0)}(1,3,2,4,5) \\ M_5^{(0)}(1,3,4,2,5) \\ M_5^{(0)}(1,4,2,3,5) \\ M_5^{(0)}(1,4,3,2,5) \end{pmatrix}. \tag{5.10}$$

The one-loop $H + 4g$ interference has been extracted from MCFM [136] and is also given in terms of helicity amplitudes [30]. In order to account for differences in the renormalisation scheme they are multiplied with a factor of $\frac{S_\epsilon}{c_\Gamma}$, where

$$S_\epsilon = (4\pi)^\epsilon e^{-\epsilon\gamma} \quad , \quad c_\Gamma = (4\pi)^\epsilon \frac{\Gamma(1+\epsilon)\Gamma(1-\epsilon)^2}{\Gamma(1-2\epsilon)}. \tag{5.11}$$

For one-loop n-gluon amplitudes this amounts to add a term $\frac{n\pi^2}{12}|\mathcal{M}_n^{(0)}|^2$. The amplitudes contain poles in ϵ with coefficients which can be targeted with an 'ϵ_{order}' index. For $\epsilon_{\text{order}} = 2, 1, 0$, the routines return the coefficient of the $\frac{1}{\epsilon^2}$ and $\frac{1}{\epsilon}$ poles or the finite pieces, respectively.
The one-loop $H + 3g$ interference relevant for the virtual contribution and real-virtual subtraction terms is coded up and evaluated numerically in terms of helicity amplitudes and the NLO helicity coefficients whose evaluation is depicted in 3.1.3. In order to evaluate the amplitudes for all helicities, the two helicity amplitudes need to be available in all permutations of the external momenta. The continuation to the different kinematical regions of the scattering is described at the end of section 3.3. For the all-plus helicity amplitude the coefficient $\alpha = \alpha_2$ is the same in all three regions, while for the two-plus minus amplitude the helicity coefficients β_2 and β_4 are needed. In order to obtain all six permutations each of the three regions is evaluated twice, where in the dimensionless arguments of the coefficients a $1 \leftrightarrow 2$ permutation is done. With $u_{13} = -\frac{s_{13}}{s_{12}}$, $u_{23} = -\frac{s_{23}}{s_{12}}$ and $v = \frac{s_{123}}{s_{12}}$, the correct helicity coefficients at l loops is, respectively,

permutation	$+++$	$++-$
$12 \to 3H$	$\alpha^{(l)}(u_{13}, v)$	$\beta_2^{(l)}(u_{13}, v)$
$21 \to 3H$	$\alpha^{(l)}(u_{23}, v)$	$\beta_2^{(l)}(u_{23}, v)$
$13 \to 2H$	$\alpha^{(l)}(u_{23}, v)$	$\beta_4^{(l)}(u_{23}, v)$
$23 \to 1H$	$\alpha^{(l)}(u_{13}, v)$	$\beta_4^{(l)}(u_{13}, v)$
$31 \to 2H$	$\alpha^{(l)}(u_{23}, v)$	$\beta_4^{(l)}(u_{23}, v)$
$32 \to 1H$	$\alpha^{(l)}(u_{13}, v)$	$\beta_4^{(l)}(u_{13}, v)$.

The spinor products in the helicity amplitude on the other hand can just be called with permutated indices. The two-dimensional harmonic polylogarithms are evaluated using the program TDHPL [102]. The two-loop $H + 3g$ amplitudes can also be evaluated in this way, which is being used as a cross-check. In order to check numerically the ϵ pole cancellation between the

real-virtual interferences and subtraction terms, the pole coefficients of the three-gluon one-loop interferences are also needed, since they appear in $\mathrm{d}\hat{\sigma}^{T,b_1}_{NNLO}$. These have been evaluated in FORM, translated to FORTRAN and can be targeted depending on the ϵ_{order} index.
The two-loop $H + 3g$ interference has been evaluated analytically in FORM using the helicity amplitudes and the two-loop helicity coefficients, together with the double-virtual subtraction term. This allows for a faster numerical evaluation since the 2dHPL's need only to be evaluated once, after which they are stored and called upon request. The analytical computation also allows to check the cancellation of $\frac{1}{\epsilon}$ poles between the interference and the integrated subtraction terms. The FORM output, which depends only on the 3 Lorentz invariants s_{12}, s_{13} and s_{23} is converted to a FORTRAN routine which is called by the main program.
In the above matrix elements the Higgs boson is on-shell. Finite width effects are included with a Breit-Wigner factor. The decay of the Higgs boson is mediated through top-quark and W-boson loops [128], and is approximated as a constant since the Higgs width is relatively small compared to its mass.

5.1.3 Antennae

The antenna functions are implemented as described in [49]. In particular, the poles of the one-loop antennae are implemented in terms of $\boldsymbol{I}^{(1)}(\epsilon)$ operators. They can be accessed with the ϵ_{order} index, as well as the pole coefficients of the integrated antennae and soft factors. The integrated soft factors are quoted in [124,129]. Using them in the initial-final configuration with a primary mapping as described in section 4.6, it turns out that a number of large logarithmic terms vanish in blocks like in eq. (4.61). This cancellation is therefore performed analytically and the block of integrated soft terms is implemented as a whole in FORTRAN.

5.1.4 Jet function, coupling and PDF's

The jet function is an essential part of the computation. It takes as argument a number of jets and a list of parton momenta which it clusters into jet momenta according to the algorithm described in section 2.5.2, where one can switch between the k_{T}- or anti-k_{T} algorithm by means of a flag in the run card. The transverse momenta and rapidities of the jets are then evaluated and possibly subjected to cut criteria dictated by the experiment one wants to compare to. The number of jets which passed through the cuts is then counted and compared to the input number of jets. If the number of passed jets is less than the input one, the function returns FALSE. It can be set in the run card whether the jets are counted exclusively or inclusively (which is the default). The jet function accordingly returns TRUE only if the number of passed jets is exactly equal to the input number or if it is that number or more, respectively. All cut parameters can be controlled in the run card.
Based on the jet momenta, further derived kinematical variables can be calculated for histogramming purposes. These are the cosine of the angle of the Higgs boson decay products in the Collins-Soper frame and the azimuthal angle between the two jets with highest transverse momentum, if any. These are stored with the jet momenta into a module to which the binning program has access to. Furthermore, a dynamical scale is calculated. This scale is returned as an output of the jet function to be used as renormalisation/factorisation scale for the evaluation of the PDF's and the coupling constant.
The couplings and PDF's are obtained through the LHAPDF [130] library to which the program is linked. In order to perform the convolution with the PDF's, two additional VEGAS variables are used and converted into the momentum fractions ξ_1 and ξ_2 which yields a further jacobian factor. These then work as an input to the LHAPDF routines, together with the factorisation scale obtained from the jet function. Their output is an array with 13 components, these are

6 quark and 6 antiquark PDF's and a gluon PDF. The strong coupling constant, associated with the respective PDF set and evaluated at the renormalisation scale, is also obtained from LHAPDF. Both the PDF's and the coupling constant are evaluated at the correct order of their respective running, which is set during the initialisation of LHAPDF. There are different sets of PDF's at choice, where by now the MSTW08 [131] and NNPDF23 [132] sets have been implemented.
Since the antenna mappings alter the final state of an event, the jet function needs to be applied not only to the actual matrix element but also to every single subtraction term, that is every time a reduced squared amplitude is called. Furthermore, the mapped momenta may yield different dynamical scales upon application of the jet function. For this reason, the PDF's and the coupling constant must be reevaluated for each subtraction term. This is very costly, in particular because of the PDF evaluation. A good use of the jet function is therefore crucial to keep the running time of the program as low as possible. Since the PDF's need only to be evaluated if the respective subtraction term passes the jet function, it is natural for every subtraction term first to compute the mapped momenta and then place the evaluation of the subtraction term with its coupling and PDF's inside an IF-block whose execution is decided by the jet function.

5.1.5 Convolutions

When evaluating the integrated subtraction terms various convolutions over the momentum fractions z_1 and z_2 after initial collinear splittings need to be performed. One particular issue is the emergence of distributions. These are either delta distributions $\delta(1-z_i)$ or plus distributions

$$\mathcal{D}_n(z_i) = \left(\frac{\ln^n(1-z_i)}{1-z_i}\right)_+ . \tag{5.12}$$

Integrating over a delta distribution, one has

$$\int_0^1 \mathrm{d}x\ A(x)\delta(1-x) = \int_z^1 \mathrm{d}x\ A(x)\delta(1-x) = A(1) = \frac{A(1)}{1-z}\int_z^1 \mathrm{d}x. \tag{5.13}$$

Thus the coefficient of $\delta(1-z_i)$ can be consistently kept under a z_i integration by evaluating it at $z_i = 1$ and correcting for the lower boundary. For the plus distributions, in general one has

$$\left(\frac{f(x)}{1-x}\right)_+ =: \frac{f(x)}{1-x} - \delta(1-x)\int_0^1 \mathrm{d}y \frac{f(y)}{1-y}, \tag{5.14}$$

$$\int_z^1 \mathrm{d}x\ g(x)\left(\frac{f(x)}{1-x}\right)_+ = \int_z^1 \mathrm{d}x\big[g(x)-g(1)\big]\frac{f(x)}{1-x} - \int_0^z \mathrm{d}x\ g(1)\frac{f(x)}{1-x}. \tag{5.15}$$

Eq. (5.14) suggests that the handling of the plus distribution can be reduced to that of the delta distributions plus some regular term. Note that the second term in eq. (5.14) removes an integration but replaces it with a new one. Thus, even if in the second and third term of eq. (5.15) all x-dependent terms of the original integral, encapsulated in the function g, have been evaluated at $x = 1$, there is still an x-dependence in those terms. Furthermore, if $f(x) = 1$, the last term in eq. (5.15) can be rewritten as

$$-\int_0^z \mathrm{d}x\ g(1)\frac{1}{1-x} = g(1)\ln(1-z) = \int_z^1 \mathrm{d}x\ g(1)\frac{\ln(1-z)}{1-z}, \tag{5.16}$$

such as to have the same integration boundaries as the other two terms (more generally such a trick can be done if the primitive of $\frac{f(x)}{1-x}$ can be found).

The real-virtual and double-virtual subtraction terms can be written in the following form:

$$\begin{aligned}\mathrm{d}\sigma = \int_0^1\int_0^1 \frac{\mathrm{d}\xi_1}{\xi_1}\frac{\mathrm{d}\xi_2}{\xi_2} a(\xi_1,\mu^2)a(\xi_2,\mu^2) \int_0^1\int_0^1 \frac{\mathrm{d}x_1}{x_1}\frac{\mathrm{d}x_2}{x_2} \\ \times M(x_1,x_2,\{x_1x_2\xi_1\xi_2 p\},\mu^2) J(\{x_1x_2\xi_1\xi_2 p\})\mathrm{d}PS(\{x_1x_2\xi_1\xi_2 p\}),\end{aligned} \tag{5.17}$$

where the a's are the PDF's. The matrix element inherits an explicit dependence on the x_i's through the integrated antennae and mass factorisation counterterms, as well as an implicit dependence through the rescaled momenta $\{x_1x_2\xi_1\xi_2 p\}$. This dependence also enters the jet function and thus, ultimately, the renormalisation scale. Following the above discussion, the matrix element can be decomposed in four components depending on the presence of delta distributions in x_1 and x_2:

$$\begin{aligned}M(x_1,x_2,\{x_1x_2\xi_1\xi_2 p\},\mu^2) = \Big(&A(x_1,x_2)\delta(1-x_1)\delta(1-x_2) + B(x_1,x_2)\delta(1-x_1) \\ &+ C(x_1,x_2)\delta(1-x_2) + D(x_1,x_2)\Big) m(\{x_1x_2\xi_1\xi_2 p\},\mu^2),\end{aligned} \tag{5.18}$$

where the reduced matrix element m depends only implicitly on the x_i through the rescaled momenta. Clearly when the integration over x_i is carried out this dependence will be altered. The matrix element and the jet function would be required to be evaluated at four different phase-space points. An alternative is to insert ones in form of $\int \mathrm{d}z_i\delta(z_i-\xi_i x_i)$ and reshuffle the integrals such as to remove the implicit x-dependence from the matrix elements and jet functions:

$$\int_0^1 \frac{\mathrm{d}\xi_i}{\xi_i} a(\xi_i,\mu^2)\int_0^1 \frac{\mathrm{d}x_i}{x_i} M(x_i,\{x_i\xi_i p\},\mu^2) = \int_0^1 \frac{\mathrm{d}z_i}{z_i}\int_{z_i}^1 \frac{\mathrm{d}x_i}{x_i} a\Big(\frac{z_i}{x_i},\mu^2\Big) M(x_i,\{z_i p\},\mu^2). \tag{5.19}$$

The four components of the matrix element and their respective weight can now be considered in turn. A pair of indices (i_1,i_2) is used to determine which component is targeted. The index i_i is set to one if a $\delta(1-x_i)$ is present and zero else.
The region $(0,0)$ contains the $D(x_1,x_2)$ coefficient. The weight is

$$\omega_{0,0} = a\Big(\frac{z_1}{x_1},\mu^2\Big)a\Big(\frac{z_2}{x_2},\mu^2\Big) \times \frac{1}{z_1z_2x_1x_2} \times \mathcal{J}(1-z_1)(1-z_2). \tag{5.20}$$

The first two factors can be directly read off the right-hand side of eq. (5.19), since no delta function alters the x dependence. $\mathcal{J}$ is the Jacobian factor for choosing z_1 and z_2, whereas $(1-z_1)(1-z_2)$ are the Jacobians for the linear picking of x_1 and x_2.
The $(1,0)$ region contains the $B(x_1,x_2)$ coefficient and a $\delta(1-x_1)$ distribution. The weight therefore is

$$\omega_{1,0} = a(z_1,\mu^2)a\Big(\frac{z_2}{x_2},\mu^2\Big) \times \frac{1}{z_1z_2x_2} \times \mathcal{J}(1-z_2), \tag{5.21}$$

where x_1 has been set to one. Furthermore, following the discussion after eq. (5.13), a factor $(1-z_1)$ has been divided out. The treatment of region $(0,1)$ is totally analogous.
Finally, the weight of region $(1,1)$ is

$$\omega_{1,1} = a(z_1,\mu^2)a(z_2,\mu^2) \times \frac{1}{z_1z_2} \times \mathcal{J}. \tag{5.22}$$

Eq. (5.17) can then be rewritten as

$$\mathrm{d}\sigma = \int_0^1\int_0^1 \mathrm{d}z_1\mathrm{d}z_2 \int_{z_1}^1\int_{z_2}^1 \mathrm{d}x_1\mathrm{d}x_2$$

$$\times \Big[\omega_{1,1}A(x_1,x_2)+\omega_{1,0}B(x_1,x_2)+\omega_{0,1}C(x_1,x_2)+\omega_{0,0}D(x_1,x_2)\Big]$$
$$\times m(\{z_1z_2p\},\mu^2)J(\{z_1z_2p\})\mathrm{d}PS(\{z_1z_2p\}), \tag{5.23}$$

where the matrix element and jet function need only to be evaluated at one phase-space point but the PDF's need to be evaluated four times each. Note that without the presence of plus distributions the dependence of the coefficients in the square brackets would be $A(x_1,x_2) = A(1,1)$, $B(x_1,x_2) = B(1,x_2)$, and $C(x_1,x_2) = C(x_1,1)$. In general however x_1 and x_2 still need to be sampled over for all four components.
It turns out that the plus distributions $\mathcal{D}_n(x_i)$ do not multiply further x_i-dependent terms in the integrated antennae (which amounts to setting $g(x) = 1$ in eq. (5.15)), which allows for a slightly different treatment. For $\mathcal{D}_0(x)$, $f(x) = 1$ in eq. (5.15), which becomes

$$\int_z^1 \mathrm{d}x\ \mathcal{D}_0(x) = \int_z^1 \mathrm{d}x\ \left(\frac{1}{1-x}\right)_+ = \int_z^1 \mathrm{d}x\big[1_x - 1_1\big]\frac{1}{1-x} - \int_z^1 \mathrm{d}x\ 1_1\frac{\ln(1-z)}{1-z}, \tag{5.24}$$

where 1_1 represents the fact that a delta distribution has set all other occurrences of x, in particular in the PDF's, to one, whereas the 1_x represents a term multiplied by PDF's which are still x-dependent. A single weight for $\mathcal{D}_n(x_i)$ terms can therefore be constructed. The range of indices for the distribution regions is accordingly extended, where the index i_i corresponds to $\mathcal{D}_{i_i-2}(x_i)$ distributions. The region $(2,0)$ for instance contains $\mathcal{D}_0(x_1)$ distributions and x_2 dependent regular terms. According to eq. (5.24), the corresponding weight is

$$\omega_{2,0} = \frac{\omega_{0,0}}{1-x_1} - \frac{(1-z_1)\omega_{1,0}}{1-x_1} + \ln(1-z_1)\omega_{1,0}. \tag{5.25}$$

As already mentioned, the $\omega_{1,0}$ weight come with a relative $\frac{1}{1-z_1}$ factor to account for the 'empty' x integral in the right-hand side of eq. (5.13). In eq. (5.24) however, the second and third term reintroduce an actual integration over x. Therefore the second and third term of eq. (5.25) come with a $(1-x_1)$ factor to compensate for this. The other weights can be assembled in a similar way and are listed in appendix C.
In order to perform the convolutions, two additional VEGAS variables are used. The total number of integration variables, including phase-space generation, convolution with the PDF's and convolution with the splitting functions and integrated antennae, is therefore 8 (4+2+2) for the double-virtual, 11 (7+2+2) for the real-virtual and 12 (10+2) for the double-real.
At NNLO distributions up to $\mathcal{D}_1(x)$ appear in the virtual and real-virtual counterterms and up to $\mathcal{D}_3(x)$ in the double-virtual ones, thus the distribution indices range up to $i_i = 5$. In the program HJET the integrated subtraction terms are arranged in terms of a double loop over the corresponding range of distribution indices i_1,i_2. For each combination of indices the correct weight is evaluated in the PDF routines depending on the $\{\xi_1,\xi_2,z_1,z_2\}$ set. The integrated antennae and mass factorisation counterterms are combined inside routines which return the integrated dipoles as in eq. (4.25). These routines are arranged as a case-by-case structure which evaluates the coefficient of a distribution corresponding to a certain (i_1,i_2) pair.

5.1.6 Scale variation

As elaborated in section 2.7, the renormalised coupling and PDF's make sure that bare quantities are independent of the renormalisation and factorisation scales. Due to the truncation of the perturbative series, however, a residual dependence on these scales remains in theory predictions. Since including corrections of higher order is supposed to attenuate this dependence, the study of the sensitivity of a theory prediction on variations of μ_R and μ_F can give an estimate of the

effect of missing higher orders. It has become customary to take a common scale $\mu_R = \mu_F = \mu$, vary it by factors of 2 and $\frac{1}{2}$ and quoting the theory error as the change of the prediction under those variations.
Since in the computation of the two-loop $H + 3g$ helicity amplitudes (chapter 3) a fix scale choice $\mu_R = m_H$ has been made, the double-virtual contribution can not be directly evaluated at different scales. Instead, the running coupling and PDF's are being used as described by eqs. (2.49) and (2.68) to evolve the different contributions to the required scales. The cross section as evaluated at the scale $\mu_F = \mu_R = \mu_0 = m_H$ is

$$\begin{aligned}\sigma(\mu_0, \mu_0, \alpha_s(\mu_0)) &= \left(\frac{\alpha_s(\mu_0)}{2\pi}\right)^n \hat{\sigma}_{ij}^{(0)} \otimes f_i(\mu_0) \otimes f_j(\mu_0) \\ &\quad + \left(\frac{\alpha_s(\mu_0)}{2\pi}\right)^{n+1} \hat{\sigma}_{ij}^{(1)} \otimes f_i(\mu_0) \otimes f_j(\mu_0) \\ &\quad + \left(\frac{\alpha_s(\mu_0)}{2\pi}\right)^{n+2} \hat{\sigma}_{ij}^{(2)} \otimes f_i(\mu_0) \otimes f_j(\mu_0) + \mathcal{O}(\alpha_s^{n+3}) \,, \end{aligned} \tag{5.26}$$

with an implicit sum over parton indices appearing twice. Inserting eqs. (2.49) and (2.68), the cross section at arbitrary scales μ_R and μ_F is

$$\begin{aligned}&\sigma(\mu_R,\mu_F, \alpha_s(\mu_R), L_R, L_F) = \\ &\quad \left(\frac{\alpha_s(\mu_R)}{2\pi}\right)^n \hat{\sigma}_{ij}^{(0)} \otimes f_i(\mu_F) \otimes f_j(\mu_F) \\ &\quad + \left(\frac{\alpha_s(\mu_R)}{2\pi}\right)^{n+1} \hat{\sigma}_{ij}^{(1)} \otimes f_i(\mu_F) \otimes f_j(\mu_F) \\ &\qquad + L_R \left(\frac{\alpha_s(\mu_R)}{2\pi}\right)^{n+1} n\,\beta_0\,\hat{\sigma}_{ij}^{(0)} \otimes f_i(\mu_F) \otimes f_j(\mu_F) && \text{(a)} \\ &\qquad + L_F \left(\frac{\alpha_s(\mu_R)}{2\pi}\right)^{n+1} \Big[- \hat{\sigma}_{ij}^{(0)} \otimes f_i(\mu_F) \otimes \Big(P_{jk}^{(0)} \otimes f_k(\mu_F)\Big) && \text{(b)} \\ &\qquad\qquad - \hat{\sigma}_{ij}^{(0)} \otimes \Big(P_{ik}^{(0)} \otimes f_k(\mu_F)\Big) \otimes f_j(\mu_F)\Big] && \text{(c)} \\ &\quad + \left(\frac{\alpha_s(\mu_R)}{2\pi}\right)^{n+2} \hat{\sigma}_{ij}^{(2)} \otimes f_i(\mu_F) \otimes f_j(\mu_F) \\ &\qquad + L_R \left(\frac{\alpha_s(\mu_R)}{2\pi}\right)^{n+2} \Big((n+1)\,\beta_0\,\hat{\sigma}_{ij}^{(1)} + n\,\beta_1\,\hat{\sigma}_{ij}^{(0)}\Big) \otimes f_i(\mu_F) \otimes f_j(\mu_F) && \text{(d)} \\ &\qquad + L_R^2 \left(\frac{\alpha_s(\mu_R)}{2\pi}\right)^{n+2} \frac{n(n+1)}{2}\,\beta_0^2\,\hat{\sigma}_{ij}^{(0)} \otimes f_i(\mu_F) \otimes f_j(\mu_F) \\ &\qquad + L_F \left(\frac{\alpha_s(\mu_R)}{2\pi}\right)^{n+2} \Big[- \hat{\sigma}_{ij}^{(1)} \otimes f_i(\mu_F) \otimes \Big(P_{jk}^{(0)} \otimes f_k(\mu_F)\Big) && \text{(e)} \\ &\qquad\qquad - \hat{\sigma}_{ij}^{(1)} \otimes \Big(P_{ik}^{(0)} \otimes f_k(\mu_F)\Big) \otimes f_j(\mu_F) && \text{(f)} \\ &\qquad\qquad - \hat{\sigma}_{ij}^{(0)} \otimes f_i(\mu_F) \otimes \Big(P_{jk}^{(1)} \otimes f_k(\mu_F)\Big) \\ &\qquad\qquad - \hat{\sigma}_{ij}^{(0)} \otimes \Big(P_{ik}^{(1)} \otimes f_k(\mu_F)\Big) \otimes f_j(\mu_F)\Big] \\ &\qquad + L_F^2 \left(\frac{\alpha_s(\mu_R)}{2\pi}\right)^{n+2} \Big[\hat{\sigma}_{ij}^{(0)} \otimes \Big(P_{ik}^{(0)} \otimes f_k(\mu_F)\Big) \otimes \Big(P_{jl}^{(0)} \otimes f_l(\mu_F)\Big) \\ &\qquad\qquad + \frac{1}{2}\hat{\sigma}_{ij}^{(0)} \otimes f_i(\mu_F) \otimes \Big(P_{jk}^{(0)} \otimes P_{kl}^{(0)} \otimes f_l(\mu_F)\Big)\end{aligned}$$

$$
\begin{aligned}
&+ \frac{1}{2}\hat{\sigma}_{ij}^{(0)} \otimes \left(P_{ik}^{(0)} \otimes P_{kl}^{(0)} \otimes f_l(\mu_F)\right) \otimes f_j(\mu_F) \\
&+ \frac{1}{2}\beta_0\, \hat{\sigma}_{ij}^{(0)} \otimes f_i(\mu_F) \otimes \left(P_{jk}^{(0)} \otimes f_k(\mu_F)\right) \\
&+ \frac{1}{2}\beta_0\, \hat{\sigma}_{ij}^{(0)} \otimes \left(P_{ik}^{(0)} \otimes f_k(\mu_F)\right) \otimes f_j(\mu_F)\Big] \\
+ L_F L_R \left(\frac{\alpha_s(\mu_R)}{2\pi}\right)^{n+2} &\Big[- (n+1)\,\beta_0\, \hat{\sigma}_{ij}^{(0)} \otimes f_i(\mu_F) \otimes \left(P_{jk}^{(0)} \otimes f_k(\mu_F)\right) \\
&- (n+1)\,\beta_0\, \hat{\sigma}_{ij}^{(0)} \otimes \left(P_{ik}^{(0)} \otimes f_k(\mu_F)\right) \otimes f_j(\mu_F)\Big] \\
+ \mathcal{O}(\alpha_s^{n+3})\,, &
\end{aligned}
\tag{5.27}
$$

where $L_R = \frac{\mu_R^2}{\mu_0^2}$ and $L_F = \frac{\mu_F^2}{\mu_0^2}$. The terms responsible for the scale variation of the real and virtual contribution, lines (a)-(c), have been added to the routines which evaluate the integrated real counterterm. In particular, this allows to use the infrastructure for the convolutions with the mass factorisation counterterms to perform the convolutions in lines (b) and (c). To this end, the splitting functions have also been implemented with two distribution indices as additional arguments. It should be noted that $\hat{\sigma}_{ij}^{(0)}$, $\hat{\sigma}_{ij}^{(1)}$ and $\hat{\sigma}_{ij}^{(2)}$ in the above formula represent the full LO, NLO and NNLO cross sections. In particular, $\hat{\sigma}_{ij}^{(1)}$ in lines (d)-(f) includes the real and virtual contribution together with the corresponding subtraction terms. The convolution of the real contribution with its subtraction terms has been implemented in the routines which evaluate the real-virtual subtraction term, again to use the already implemented convolution. The terms where L_R and L_F multiply the real matrix element have been added as a correction to $\mathrm{d}\hat{\sigma}_{NNLO}^{T,a}$ (eq. (4.57)), which contains the appropriate squared amplitude, while the corresponding terms involving the real counterterms have been added to the part of $\mathrm{d}\hat{\sigma}_{NNLO}^{T,b_1}$ (eq. (4.58)) which multiplies the tree-level squared amplitude. All remaining scale variation terms involve three-parton kinematics, either through the tree-level or one loop $H+3g$ matrix element. These have been added in the FORM computation of the double-virtual contribution where all required matrix elements and convolutions are available analytically. The special treatment of the Higgs effective vertex corrections (eq. (2.27)) due to its anomalous dimension is recalled here. With this the NNLO cross section can be evaluated at arbitrary renormalisation and factorisation scales.

5.1.7 Binning

The binning of the events into histograms is performed with the external routine BINO.f, which provides bookkeeping of multiple histograms with variable bin numbers and widths. The squared amplitudes and every distinct subtraction term (i.e. every line in the subtraction terms which calls the jet function) are binned individually. The call for binning is associated with passing the jet function and takes as arguments the weight to be binned. This weight also includes a VEGAS weight which accounts for the number of events in a VEGAS run. This is already included internally by VEGAS for the total cross section and thus only has to be passed to BINO without including it into the weight handed back to VEGAS. The kinematical information needed by BINO is stored inside a module which gets updated every time the jet function accepts a set of momenta.
After the run the output of BINO is a file containing three coloumns, the central value of the bins, the weight stored in the respective bin as well as an error associated with each bin.

5.2 Experimental setup and runs

This section details how the HJET program is being run. It performs 10 warmup and 10 production runs as a default, however these numbers can be modified in the run card. Most of the contributions for NNLO $H + 1J$ can be integrated with satisfactory precision on a single core with runtimes ranging from few minutes to few hours. The exceptions are the real-virtual contribution and the two double-real contributions integrated over the two phase-spaces (5A) and (5B). In order to deliver the necessary statistics to these contributions in a reasonable time several independent runs can be performed with different random seeds. The histograms obtained in this way are then combined into a final histogram with reduced statistical error. This trivial parallelisation has been used on a large scale with the supercomputer ZBOX.

5.2.1 Experimental parameters

The jet function has been implemented such as to allow comparisons with most common experimental setups. The jet algorithm has been implemented as in section 2.5.2 with p and R as parameters. The basic implemented cuts are in the transverse momentum p_{T} and rapidity y, which can be set independently for the jets and the photons from the Higgs boson decay. The possibility to apply stepped p_{T} cuts to the jets is implemented in terms of a 'cutstep' variable which fixes by which amount the p_{T} cut decreases for the next subleading jet. The distance on the $y - \phi$ plane $\Delta R = \sqrt{(\Delta y)^2 + (\Delta\phi)^2}$, where ϕ is the azimuthal angle, can also be subjected to cuts with independent cut values for the jet-jet, jet-photon and photon-photon distance. A window on the invariant mass of the diphoton system can also be set. All cut values and the jet radius can be set in a run card file, as well as the minimal required number of jets and whether they are selected inclusively or exclusively. Further tunable parameters are the Higgs boson mass and width as well as the masses of the top quark and W boson which enter the effective coupling and the Higgs boson decay. The dynamical scale, which determines the evolution of the strong coupling and the PDF's can be chosen to be the parametric Higgs boson mass m_H, the leading jet transverse momentum $p_{T,1}$, the combination $\sqrt{p_{T,1}^2 + m_H^2}$ or the scalar sum of the jet transverse momenta H_{T}.
Additional cuts can be implemented without further conceptual difficulty since the full kinematical information is available event-by-event.

5.2.2 Warmup runs

As mentioned above the production phase of VEGAS can be trivially parallelised by running many instances of the program with modest statistics on a supercomputer such as to achieve acceptable runtimes, and then combine the results of the individual runs. The warmup phase however cannot be parallelised with reasonable effort. Due to the large dimensionality of the double-real phase-space, the optimisation of the integration grid can take a huge amount of time. Since most supercomputers automatically abort a job after 24 hours of runtime, they are not suitable to perform the warmup. The grid optimisation has therefore been separated from the production phase by implementing a switch which makes HJET do only the warmup and then stores the grid in a file. The grid optimisation can therefore be carried out on a single core for an arbitrarily long time. Using the grid file, multiple production runs can then be launched on a supercomputer by using different random seeds. The grid files are stored in a separate directory and are identified by a name composed of the respective phase-space (A,B,C and D for the 3-, 4- (5A)- and (5B)-particle phase-space), the number of loops in the matrix

element being integrated, the number of jets required, the phase-space cutoff and an additional three-letter identifier.

5.2.3 Run parameters

These are the parameters which manage the individual runs. The most important set of parameters decides which contribution is integrated over. It consists of four logical variables which switch on and off the integration over the four phase-spaces, together with a parameter which decides the number of loops the matrix element involves. Since it makes no sense to fill histograms during the grid optimisation phase, the binning of the events can be deactivated with a suitable switch. The evolution from a central scale μ_C to a renormalisation scale $\mu_R = c_R \cdot \mu_C$ and factorisation scale $\mu_F = c_F \cdot \mu_C$ as described in section 5.1.6 is done by setting c_R and c_F. Various flags allow for a debugging of the program. This includes switching on or off the integration over the PDF's, the $H \to \gamma\gamma$ decay and the corrections to the Higgs effective vertex. A further switch lets the integrand be evaluated only for phase-space points more singular than the previously computed one, and writes the ratio of the squared amplitude to the corresponding real subtraction terms on the screen. This lets VEGAS adapt the grid towards deeply singular phase-space regions and allows for testing the convergence of the subtraction.
If HJET is run as a single instance it uses fixed random seeds. In this mode it outputs the intermediate results of the VEGAS iterations on the screen and writes the histogram files in the directory where it has been compiled. If multiple instances are to be run in parallel a shell script has been written in order to manage the calls to the program. The script has been written such as to comply to the syntax used to launch tasks on the ZBOX. The parameters of the script are the number of runs, an identifier for a directory where the program output is to be stored, the three-letter identifier of the grid to be used if the program is run only in the production mode, as well as a master seed. This master seed is used to produce the random seeds for the individual runs. The name of the directory where the output of HJET is stored is composed from the file identifier, the number of runs and the master seed. The output in parallel mode consists of a copy of the run card, a log file where the VEGAS output is written and the histogram files.

5.2.4 Post processing

After the completion of the runs, various FORTRAN programs have been written to process the results. Following tasks can be performed:

- The averaging of the total cross section, taken from the corresponding log files, over multiple runs.
- The averaging of the raw histograms of individual runs into combined histograms with reduced statistical error.
- The addition of histograms corresponding to the different contributions to a certain distribution evaluated at a certain scale. The errors are added in quadrature bin-by-bin.
- The combination of distributions into K-factor plots with corresponding bin-by-bin error from standard error propagation. This program also allows to set a range in the distribution variable where bins are combined into larger ones to improve potentially poor statistics.
- The integration of the histograms to perform consistency checks with the total cross section.

Chapter 6

Validation

In this chapter the validation of the matrix elements and subtraction terms is described.

6.1 Internal checks

Various internal consistency checks can be performed of the different ingredients of the computation. The reconstruction of the helicity amplitudes out of a minimal set of those has been checked by verifying the dual Ward identity for various assignements of helicity for the four- and five-gluons case. A further check of the helicity amplitudes is obtained by the invariance of the matrix element squared under permutations of the external momenta after the sum over the colour orderings has been performed.
The limiting behaviour of the real subtraction terms is checked by forcing VEGAS into a particular unresolved phase-space region by evaluating the integrand only at phase-space points where a certain Lorentz invariant or a combination thereof is smaller than the previously considered one, and setting it to zero otherwise. Since VEGAS concentrates its resolution power into regions where the integrand is largest, this yields a sequence of phase-space points which are increasingly unresolved. The convergence of the real subtraction terms to the squared

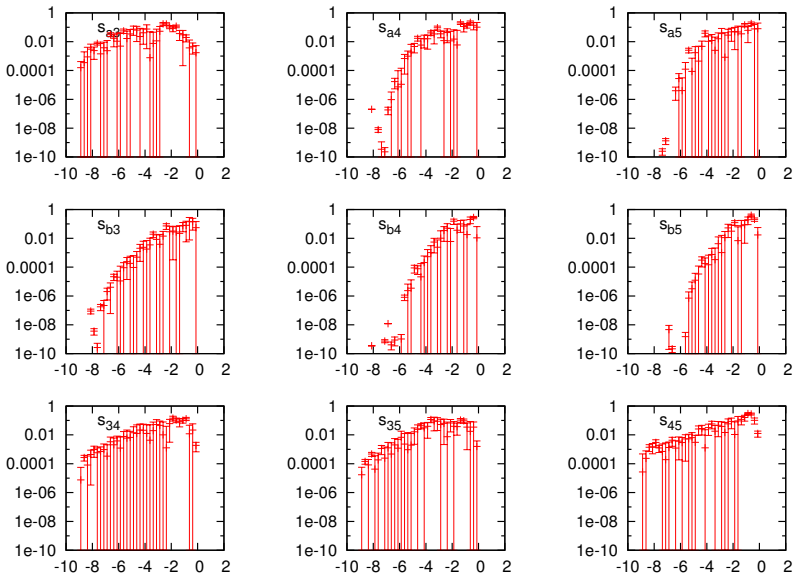

Figure 6.1: Distribution of subtracted double-real weight versus partonic phase-space variables

amplitude in that particular limit is observed, typically until numerical instabilities spoil the subtraction. This allows also to study the sometimes intricate cancellation pattern between spurious singularities of the real subtraction terms for an individual phase-space point. At the same time it has also been verified that the antennae converge towards the correct eikonal or splitting function. All double unresolved limites of the double real subtraction terms and single unresolved limites of the real-virtual subtraction terms have been extensively studied in this way.
A further check of the real subtraction can be performed by carrying out an integration run over the corresponding phase-space and histogramming the subtracted integrand w.r.t. the Lorentz invariants. Such a histogram is displayed in fig. 6.1, for an integration of the subtracted double-real contribution over the (5A) phase-space. The invariants are normalised to the partonic c.o.m. energy and are allowed to become as small as the phase-space cutoff $10^{-9}s_{\mathrm{p}}$, where it can be clearly seen that the weight is successfully supressed in the unresolved regions. Similar histograms were produced for the integration over the (5B) phase-space and the integration of the real-virtual contribution over the four-particle phase-space.
The integrated subtraction terms of the virtual and double-virtual contribution can be validated by checking analytically that their poles in ϵ indeed cancel the pole structure of the matrix element squared. This has been verified analytically with FORM. Since the 4-gluon one-loop amplitude squared has not been implemented in FORM, the cancellation of its pole structure has been checked numerically. To this end, the coefficients of the ϵ poles of the integrated double-real subtraction terms have been implemented numerically as described in the previous chapter and are compared with the coefficients of the squared amplitude as they have been implemented in MCFM. The $\epsilon_{\mathrm{order}}$ flag can be used to select whether an integrated antenna routine returns the $\frac{1}{\epsilon^2}$ coefficient, the $\frac{1}{\epsilon}$ one or the finite piece. The comparison has been performed and yields agreement at machine precision.

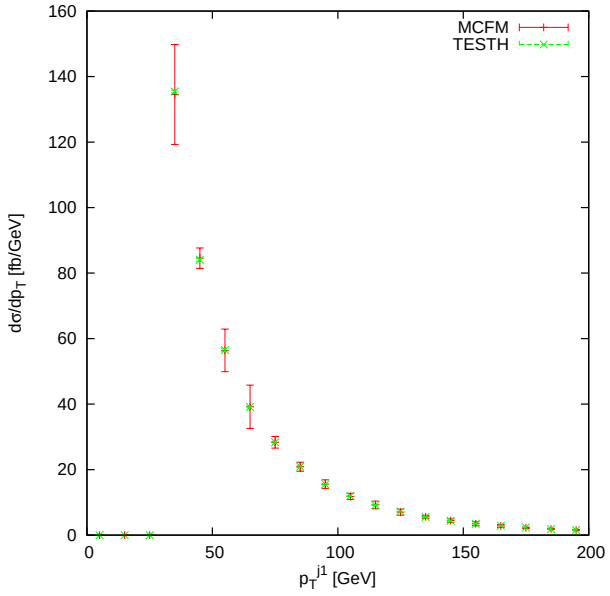

Figure 6.2: Comparison of the distribution of the leading jet p_{T} between HJET and MCFM

6.2 Comparison with Madgraph5/MCFM-6.6

The cross section obtained at different perturbative orders can be compared with the existing theoretical predictions. At tree-level, the $gg \to ngH$ with $n \in \{1, 2, 3\}$ have been compared with the MADGRAPH5 [137] prediction using its default settings and several center-of-mass energies, where excellent agreement has been obtained. At NLO, a comparison with the MCFM-6.6 prediction for $H + 1J$ has been carried out. In doing so, care had to be taken to correctly isolate the $N_F = 0$ contribution in the amplitudes and subtraction terms. The parameters have been chosen such as to reproduce the NLO result of [59]. The comparison yields excellent agreement both for the cross-section as well as for the distribution of kinematical variables (see fig. 6.2). When setting the minimal number of jets to two in the jet function, the $H + 2J$ prediction can be compared at NLO with MCFM. This tests the $H + 5g$ tree-level matrix element and the one-loop $H + 4g$ interference as well as the $\mathrm{d}\hat{\sigma}^{S,a}_{NNLO}$ and $\mathrm{d}\hat{\sigma}^{T,a}_{NNLO}$ parts of the respective subtraction terms. The cross sections have been compared and good agreement was obtained.

Chapter 7

Results

In this chapter, the results from the HJET runs are presented. A first run has been carried out with the same setup as for the computation in [59] to verify the consistency of the total cross sections. Since the other calculation has been performed using a different subtraction scheme, this represents a nontrivial check of the validity of the subtraction. Furthermore, distributions in p_{T} and y have been produced and their perturbative behaviour has been investigated.
A second run has been performed in order to compare the prediction for various distributions of kinematical variables with experimental measurements from ATLAS [6]. It is obvious that such a comparison can only be of limited significance since the prediction presented in this work includes only the $N_F = 0$ contribution to $H + 1J$. Nevertheless it is the dominant part and a comparison with ATLAS data still can give an order-of-magnitude estimate of the agreement of the prediction with measurements.

7.1 Total cross section

In order to compare with the gluons-only calculation of [59], the corresponding setup was implemented. The Higgs boson is kept onshell by dividing out the Breit-Wigner factor and omitting the $H \to \gamma\gamma$ decay matrix element. The relevant parameters of the jet function are

jet p_{T} cut	30 GeV
jet algorithm	inclusive k_{T} ($p = 1$ in eq. (2.40))
jet radius	0.5.

The Higgs mass and width were set as 125 GeV and 0.0036 GeV, respectively. The central scale was chosen to be the parametric Higgs mass. The total cross section obtained at different perturbative orders is

$$\begin{aligned} \sigma_{LO} &= 2.72^{+1.22}_{-0.78} \text{ pb}, \\ \sigma_{NLO} &= 4.38^{+0.76}_{-0.74} \text{ pb}, \\ \sigma_{NNLO} &= 6.34^{+0.28}_{-0.49} \text{ pb}, \end{aligned} \tag{7.1}$$

in very good agreement with [59]. The inclusion of the NNLO correction leads to a sizeable reduction of the scale uncertainty. The breakup of the NNLO total cross section in its individual components is illustrated in the following table:

contribution	cross section [pb]	approx. processor time
tree	1.942 ± 0.001	∼10min
virt	2.886 ± 0.001	∼40min
real	-0.572 ± 0.001	<4h
VV	3.103 ± 0.003	∼10min
RV	-1.162 ± 0.005	<350h
RRA	0.094 ± 0.024	<350h + ∼5 days warmup (1 core)
RRB	0.051 ± 0.016	<300h + ∼5 days warmup (1 core)

It is striking that both double-real contributions are very small, which means that the double-real subtraction terms are a good approximation of the actual matrix element also outside of the singular phase-space regions. On the other hand, their errors on the integration dominate over the other contributions in spite of a large amount of statistics.

7.1.1 Differential distributions

In the kinematical distributions and ratio plots, the error band describes the scale variation envelope as described above, where the denominator in the ratio plots is evaluated at fixed central scale, such that the band only reflects the variation of the numerator. Error bars on the distributions indicate the numerical integration errors on individual bins. In Figure 7.1, it can be observed that the Higgs boson transverse momentum distribution receives sizeable NNLO corrections throughout the whole range in p_{T}, which enhance the NLO cross section by a quasi constant factor of about 1.4, slightly decreasing towards higher p_{T}. The p_{T} distribution of the Higgs boson has a residual NNLO theory uncertainty ranging between 5% and 16%, where the same scale variation pattern as for the inclusive cross section above has been used. At high values of p_{T}, the effective theory approximation used for the coupling of the Higgs boson to gluons breaks down, since the large momentum transfer in the process starts resolving the top quark loop. Consequently, one expects top quark mass effects for $p_{\mathrm{T}} \gtrsim m_{\mathrm{t}}$ to be more important than the higher order corrections in the effective theory. The ratio plot, Figure 7.1(b), is extended to values well beyond $p_{\mathrm{T}} \gtrsim m_{\mathrm{t}}$ to illustrate the smooth behaviour and the qualitative tendency of the NNLO corrections in the effective theory.
At leading order $p_{T,H}$ is kinematically forced to be equal to the transverse momentum of the jet, and is consequently larger than the transverse momentum cut on the jet. At higher orders,

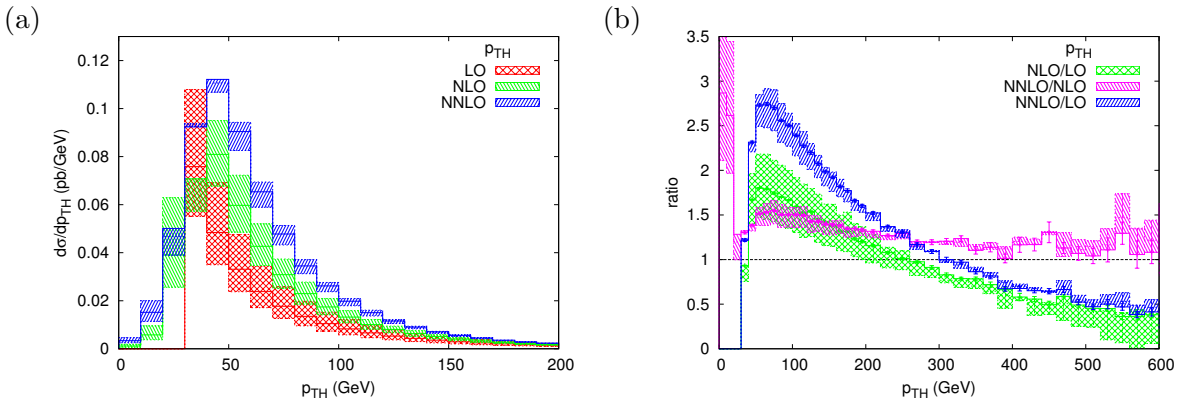

Figure 7.1: (a) Transverse momentum distribution of the Higgs boson in inclusive $H + 1j$ production in pp collisions with $\sqrt{s} = 8$ TeV at LO, NLO, NNLO and (b) Ratios of different perturbative orders, NLO/LO, NNLO/LO and NNLO/NLO.

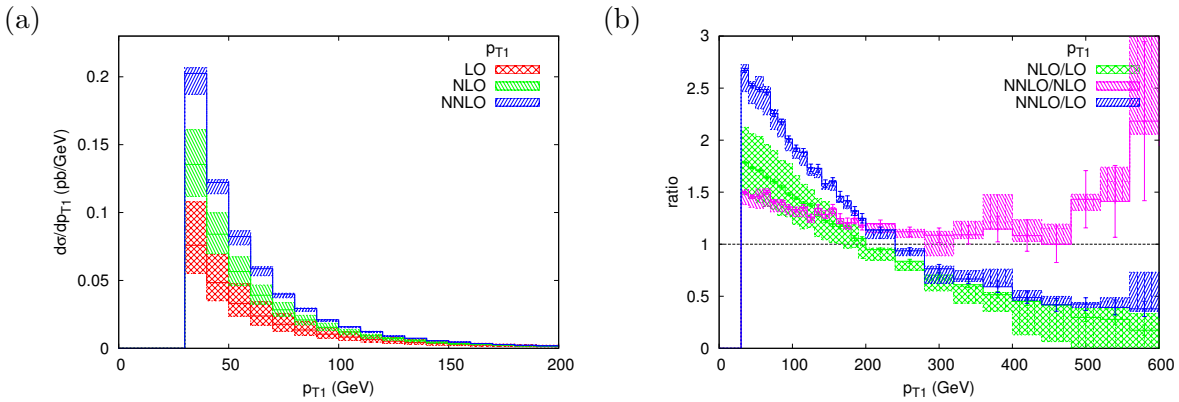

Figure 7.2: (a) Transverse momentum distribution of the leading jet in inclusive $H + 1J$ production in pp collisions with $\sqrt{s} = 8$ TeV at LO, NLO, NNLO and (b) Ratios of different perturbative orders, NLO/LO, NNLO/LO and NNLO/NLO.

higher multiplicity final states are allowed and this kinematical restriction no longer applies. These kinematical situations often lead to instabilities in the perturbative expansion, with large corrections at each order. This is manifestly not the case here: NNLO corrections to the Higgs boson p_{T} distribution in $H+1J$ events turn out to be moderate below the jet cut of $p_{\mathrm{T}} = 30$ GeV. A similar pattern to the Higgs p_{T} distribution, is also observed for the leading jet, Figure 7.2, which displays a slightly smaller scale uncertainty amounting up to 12%, and displays rising NNLO corrections for very large values of p_{T}, again likely beyond the applicability of the effective theory approximation.
The rapidity distributions of the Higgs boson and the leading jet are displayed in Figure 7.3 and 7.4 respectively. It can be observed that the NLO corrections are largest at central rapidity, while becoming moderate at larger rapidities, while the ratio NNLO/NLO remains rather constant throughout the rapidity range. The residual theory uncertainty at NNLO is quasi constant for both distributions, and amounts to 9%. Both the transverse momentum and rapidity distributions highlight the fact that the NNLO corrections to $H + 1J$ production in the gluon-only channel substantially enhance the normalisation of NLO predictions, while not modifying the NLO shape, except around the production threshold.

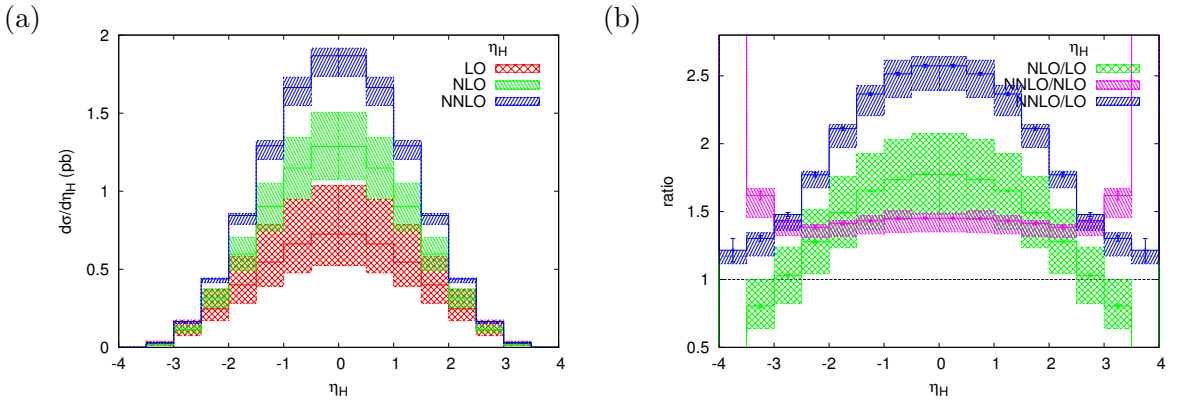

Figure 7.3: (a) Rapidity distribution of the Higgs boson in inclusive $H+1J$ production in pp collisions with $\sqrt{s} = 8$ TeV at LO, NLO, NNLO and (b) Ratios of different perturbative orders, NLO/LO, NNLO/LO and NNLO/NLO.

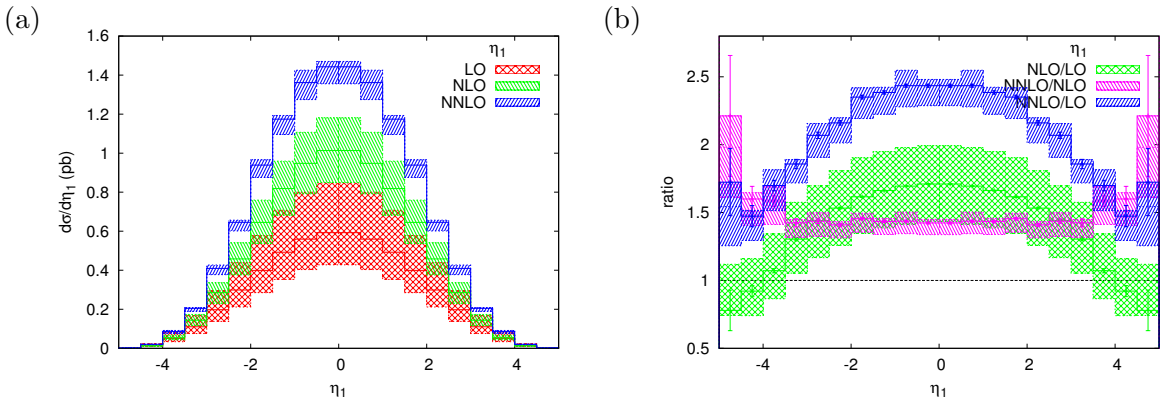

Figure 7.4: (a) Rapidity distribution of the leading jet in inclusive $H+1J$ production in pp collisions with $\sqrt{s} = 8$ TeV at LO, NLO, NNLO and (b) ratios of different perturbative orders, NLO/LO, NNLO/LO and NNLO/NLO.

7.2 Comparison with ATLAS

The data being compared with is from a measurement of Higgs boson production in the $H \to \gamma\gamma$ decay channel performed at the ATLAS detector [6]. The fiducial cross section is defined through

jet p_{T} cut	30 GeV
jet algorithm	anti-k_{T} ($p = -1$ in eq. (2.40))
jet radius	0.4
jet y cut	4.4
leading/subleading photon cut p_{T}	$0.35/0.25 \cdot m_{\gamma\gamma}$
photon y cut	2.37
photon-jet distance	$\Delta_{\gamma J} > 0.4$
diphoton mass window	105 GeV $< m_{\gamma\gamma} <$ 160 GeV,

where the jet function in HJET has been modified accordingly. The Higgs boson mass and width were set as 125 GeV and 0.0041 GeV, respectively. HJET has been run with a decaying Higgs boson as well as with an onshell Higgs. The $H \to \gamma\gamma$ branching fraction turns out to be slightly lower than the measured value of 0.228% by a factor of 1.19, which has been corrected for. An additional factor of 0.975 has been taken from [6] to account for the photon isolation criteria, and a further factor of 0.992 accounts for hadronisation and underlying event effects. Both have been estimated from Monte-Carlo simulations. The results for the run at the different perturbative orders are

$$\sigma_{LO} = 6.61^{+3.18}_{-1.99} \text{ fb}$$
$$\sigma_{NLO} = 8.43^{+0.26}_{-1.03} \text{ fb}$$
$$\sigma_{NNLO} = 10.51^{+0.55}_{-0.53} \text{ fb},$$

where the errors have been evaluated by scale variation using H_{T} as central scale. The upward reduction of the uncertainty when going from LO to NLO is dramatic and likely an underestimate due to an extremum in the scale dependence. To fully understand this effect, an assessment of the theory error using more than three points in the μ_R-μ_F plane is necessary. The statistics of the run are displayed in the following table:

channel	cross section [fb]	approx. processor time
tree	5.118 ± 0.003	1min
virt	5.755 ± 0.019	20min
real	-2.604 ± 0.008	3h
VV	4.251 ± 0.006	4min
RV	-3.153 ± 0.050	220h
RRA	0.887 ± 0.058	1500h + ∼4 days warmup (1 core)
RRB	0.269 ± 0.026	1400h + ∼4 days warmup (1 core).

It appears that the relative double-real contributions are substantially larger than in the first run. This might be due to the more exclusive phase-space, since in the vicinity of the cuts the mapped momenta of the real subtraction terms can be spread across the boundaries. A substantial part of the subtraction terms is then rejected by the jet function, which spoils the internal cancellations of spurious singularities and leads to a large integrand. It also leads to a less stable integration, in particular of the double-real contribution. It was observed in the aberrant behaviour of preliminary distribution plots, where the NNLO error bands grew significantly larger than the NLO ones, in contradiction to the total cross section results above. This could be traced back to the averaging procedure in BINO, where the bins are determined by unweighted average of the event weights, while VEGAS uses a weighting procedure to determine the total cross section which is more efficient in rejecting outliers. The VEGAS-HJET interface has been upgraded to allow the averaging weight to be communicated to BINO, such as to implement VEGAS's averaging procedure also for the binning of the kinematical variables. This results in satisfying histograms, which are displayed in the following. It should be noted that since the various contributions to the real subtraction terms may end up in different bins for a single event, it is not possible to reproduce VEGAS's treatment of the error on the average, since for this an a priori knowledge of the number of bin entries would be necessary.
In fig. 7.5 the transverse momentum distribution at NLO and NNLO is compared with data from ATLAS. The instabilities in the bins right at the jet p_T cut are manifest, whereas the other bins are well behaved. As can be seen in fig. 7.5 (b), the qualitative behaviour of the NNLO corrections away from the p_T cut is similar to the first run, with a change in the overall normalisation while not changing the shape of the distribution. The K-factors are however subjected to increased fluctuations and bigger bin errors as compared to fig. 7.1 (b). This points again at the instabilities mentioned earlier.

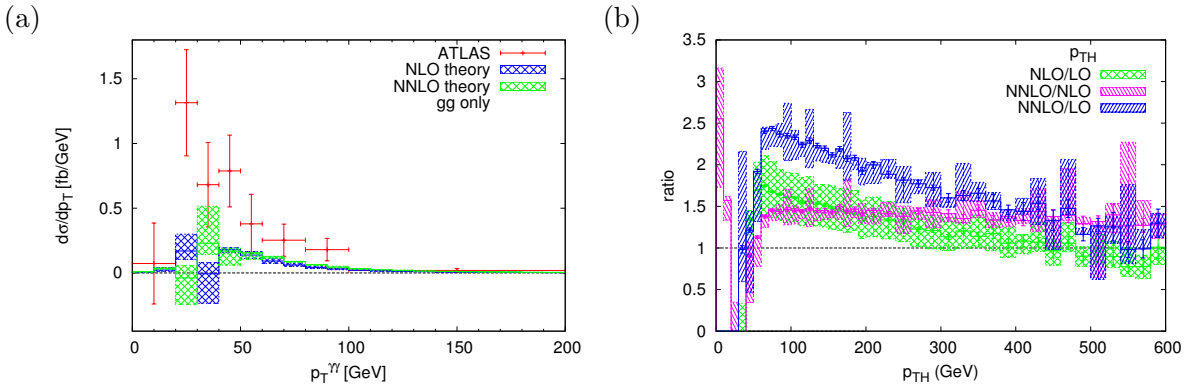

Figure 7.5: (a) Transverse momentum distribution of the Higgs boson in $H + 1J$ production in the fiducial region in pp collisions with $\sqrt{s} = 8$ TeV at NLO and NNLO compared to ATLAS data and (b) Ratios of different perturbative orders, NLO/LO, NNLO/LO and NNLO/NLO.

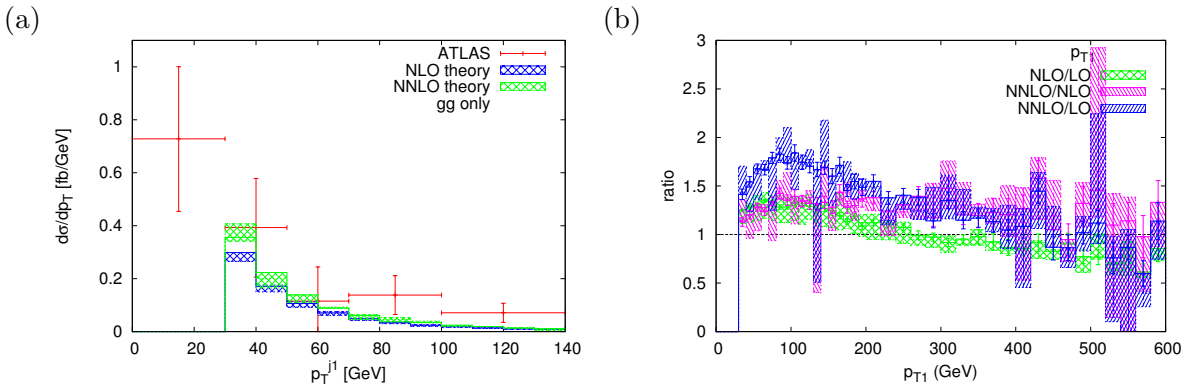

Figure 7.6: (a) Transverse momentum distribution of the leading jet in $H+1J$ production in the fiducial region in pp collisions with $\sqrt{s} = 8$ TeV at NLO and NNLO compared to ATLAS data and (b) Ratios of different perturbative orders, NLO/LO, NNLO/LO and NNLO/NLO. The data point in the first bin in (a) represents events with no jet above the p_{T} cut.

In gluon fusion, the gluons-only contribution to Higgs production is known to contribute roughly 60% to the total cross section, while the quark-gluon channel amounts to around 30%. Altough the prediction in fig. 7.5 (a) slightly underestimates the data, it appears that including the missing contributions will lead to a good description of the measurement. This can also be seen in the distributions of p_{T} and y of the leading jet, see figs. 7.6 and 7.7. The prediction undershoots the data in particular in regions of high p_{T} and small y. This is not surprising, since quark jets are known to yield a harder spectrum than gluon jets. One should however keep in mind that at very high p_{T} the infinite top mass approximation breaks down. The K-factors are again similar in shape to the ones of the first run, while being numerically smaller. This reflects the behaviour of the cross section, where the relative enhancement due to higher order corrections is smaller in the second run.
Fig. 7.8 displays the scalar sum of jet transverse momenta H_{T} and the $p_{\mathrm{T},2}$ distribution of the subleading jet. The H_{T} distribution shows very good agreement with data in the small and intermediate H_{T} range while undershooting the measured values at high H_{T}. The $p_{\mathrm{T},2}$ distribution on the other hand clearly underestimates the data over the whole transverse momentum range. This is due to two reasons: first, in a NNLO $H+1J$ calculation the subleading jet is effectively described at NLO accuracy, which is still quite sensitive to higher perturbative

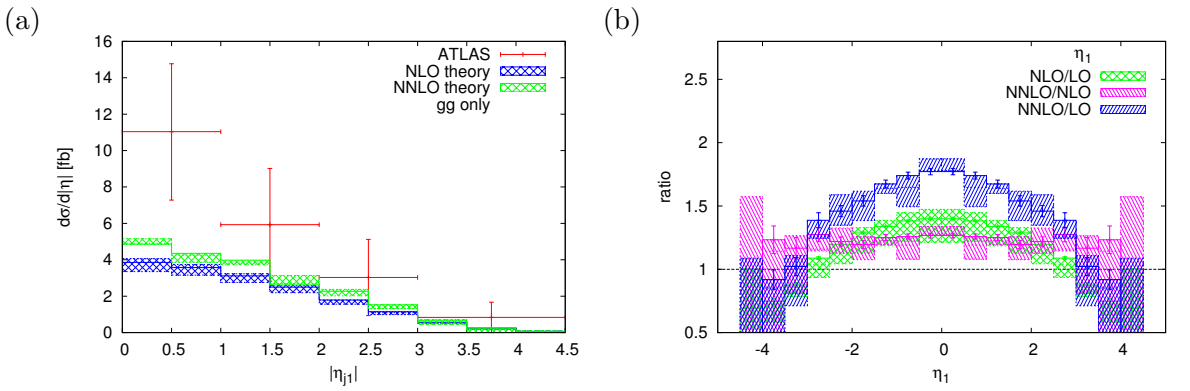

Figure 7.7: (a) Rapidity distribution of the Higgs boson in $H+1J$ production in the fiducial region in pp collisions with $\sqrt{s} = 8$ TeV at NLO and NNLO compared to ATLAS data and (b) Ratios of different perturbative orders, NLO/LO, NNLO/LO and NNLO/NLO.

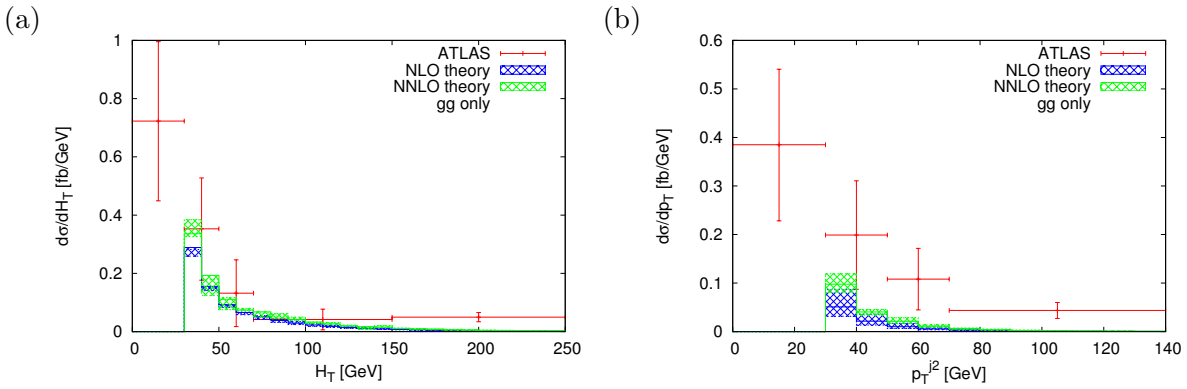

Figure 7.8: (a) Transverse momentum distribution of the subleading jet in $1H + J$ production in the fiducial region in pp collisions with $\sqrt{s} = 8$ TeV at NLO and NNLO compared to ATLAS data and (b) Distribution scalar sum of jet transverse momenta in inclusive $H + 1J$ production in pp collisions with $\sqrt{s} = 8$ TeV at NLO and NNLO compared to ATLAS data. In (a) the data point in the first bin represents events with no jet above the p_{T} cut, while in (b) it includes events with at most one resolved jet.

orders. Second, for the subleading jet the other Higgs boson production channels, in particular VBF, are not negligible anymore. One can therefore espect substantial corrections to the $p_{\mathrm{T},2}$ distribution.

Chapter 8

Conclusions and outlook

This work adressed the production of a Higgs boson via gluon fusion at the LHC together with a hadronic jet at NNLO in the strong coupling. The coupling of the Higgs boson to gluons is implemented in the infinite top mass approximation. The completion of this computation requires the two-loop helicity amplitudes for $H \to 3$ partons. These were computed in dimensional regularisation by projecting the amplitude onto the Lorentz invariant decomposition in tensor structures. The reduction to master integrals has been performed with the program REDUZE. The master integrals are known in terms of a Laurent series in ϵ, where the coefficients are HPL's and 2dHPL's which depend on dimensionless arguments. The one- and two-loop helicity amplitudes are expressed as a helicity coefficient times the tree-level helicity amplitude. The pole structure of the coefficients agrees with the predicted universal IR behaviour of loop amplitudes.
In order to obtain the cross section, the integration over the phase-spaces of the relevant matrix elements is performed. The manipulation of the various IR singularities is carried out using the antenna subtraction formalism. Subtraction terms have been derived for the double-real and real-virtual contributions. These have been found to correctly approximate the corresponding matrix elements in all their unresolved limites, such as to make the integration over the respective phase-spaces well-defined. The integrated subtraction terms have been constructed for the real-virtual and double-virtual contributions. It has been checked analytically for the double-virtual and numerically for the real-virtual that they fully cancel the ϵ pole structure of the loop matrix elements.
The phase-space integration and the convolution with the parton distribution functions is carried out numerically with a flexible parton-level event generator called HJET. The program is written in FORTRAN and bases on the adaptive Monte-Carlo integrator VEGAS. The computation is implemented in a fully exclusive way and allows for the configuration of experimental setups at will. The output of HJET are the total cross section and user-defined distributions in kinematical variables. The components of the computation have been subjected to several consistency checks and the predictions for the total cross section and distributions have been compared both at LO and NLO to the predictions of independent event generators.
Two proof-of-concept calculations have been carried out with HJET. The first one with an on-shell Higgs boson aims at a comparison with existing results for gluons-only $H + 1J$ production and the investigation of the perturbative behaviour of the distributions in a rather inclusive setup. For the total cross section excellent agreement is observed as well as a reduction of the scale uncertainty. The NNLO correction to the differential distributions amounts to a change in their overall normalisation, while leaving the shape unchanged. The scale uncertainty for the distributions is also reduced. The second computation implements the setup of the ATLAS experiment to allow a comparison with data. Due to the more exclusive phase-space, the inte-

gration of the double real contribution appears to be less stable. Still, the qualitative features of the distributions are conserved. Comparison with data shows reasonable agreement, in particular in the low and intermediate p_{T} regions. In the high p_{T} domain, the quark-gluon contribution is expected to improve the situation, while at very high p_{T} the infinite top-quark approximation breaks down and a computation with full top-mass dependence would be needed.
Future work comprises the implementation and testing of the quark-gluon and quark-antiquark contributions. The program HJET will then allow for a full phenomenological description of the $H + 1J$ process at NNLO.

Acknowledgements

I would like to thank Thomas Gehrmann for making this project possible, and for the invaluable support and advice he provided during these four years.
I would also like to thank Nigel Glover and Xuan Chen for the fruitful and pleasant collaboration, as well as for many interesting discussions.
I finally would like to thank all members of the physics institute of the University of Zürich for the good time I had there.

Appendix A

NNLO subtraction terms

Here the full double-real subtraction terms for $H+1J$ are listed. The large angle soft terms and their identification with integrated soft factors are listed separately.

A.1 The double-real IIFFF terms

These are the double-real subtraction terms for the IIFFF topology.

$$
\begin{aligned}
\mathrm{d}\hat{\sigma}^{S,a}_{NNLO}(\hat{1},\hat{2},i,j,k) =& f_3^0(\hat{2},i,j)|M_4^{(0)}(\hat{1},\hat{\tilde{2}},\widetilde{(ij)},k)|^2 J_1^{(2)}(p_{\widetilde{(ij)}},p_k) \\
&+f_3^0(i,j,k)|M_4^{(0)}(\hat{1},\hat{2},\widetilde{(ij)},\widetilde{(jk)})|^2 J_1^{(2)}(p_{\widetilde{(ij)}},p_{\widetilde{(jk)}}) \\
&+f_3^0(\hat{1},k,j)|M_4^{(0)}(\hat{\tilde{1}},(\hat{2}),i,\widetilde{(kj)})|^2 J_1^{(2)}(p_i,p_{\widetilde{(kj)}}) \\
&+f_3^0(\hat{2},k,j)|M_4^{(0)}(\hat{1},\hat{\tilde{2}},\widetilde{(jk)},i)|^2 J_1^{(2)}(p_i,p_{\widetilde{(kj)}}) \\
&+f_3^0(k,j,i)|M_4^{(0)}(\hat{1},\hat{2},\widetilde{(jk)},\widetilde{(ij)})|^2 J_1^{(2)}(p_{\widetilde{(ij)}},p_{\widetilde{(jk)}}) \\
&+f_3^0(\hat{1},i,j)|M_4^{(0)}(\hat{\tilde{1}},\hat{2},k,\widetilde{(ij)})|^2 J_1^{(2)}(p_{\widetilde{(ij)}},p_k), \qquad \text{(A.1)} \\
\mathrm{d}\hat{\sigma}^{S,B_{1,2}}_{NNLO}(\hat{1},\hat{2},i,j,k) =& F_4^0(\hat{2},i,j,k)|M_3^{(0)}(\hat{1},\hat{\tilde{\tilde{2}}},\widetilde{(ijk)})|^2 J_1^{(1)}(p_{\widetilde{(ijk)}}) \\
&- f_3^0(\hat{2},i,j)F_3^0(\hat{\tilde{2}},\widetilde{(ij)},k)|M_3^{(0)}(\hat{1},\hat{\tilde{\tilde{2}}},\widetilde{(\widetilde{(ij)}k)})|^2 J_1^{(1)}(p_{\widetilde{(\widetilde{(ij)}k)}}) \\
&- f_3^0(i,j,k)F_3^0(\hat{2},\widetilde{(ij)},\widetilde{(jk)})|M_3^{(0)}(\hat{1},\hat{\tilde{2}},\widetilde{(\widetilde{(ij)}(jk)}))|^2 J_1^{(1)}(p_{\widetilde{(\widetilde{(ij)}(jk))}}) \\
&- f_3^0(\hat{2},k,j)F_3^0(\hat{\tilde{2}},\widetilde{(jk)},i)|M_3^{(0)}(\hat{1},\hat{\tilde{\tilde{2}}},\widetilde{(i(jk))})|^2 J_1^{(1)}(p_{\widetilde{(i(jk))}}) \\
&+F_4^0(i,j,k,\hat{1})|M_3^{(0)}(\hat{\tilde{1}},\hat{2},\widetilde{(ijk)})|^2 J_1^{(1)}(p_{\widetilde{(ijk)}}) \\
&- f_3^0(\hat{1},i,j)F_3^0(\hat{\tilde{1}},\widetilde{(ij)},k)|M_3^{(0)}(\hat{\tilde{\tilde{1}}},\hat{2},\widetilde{(\widetilde{(ij)}k)})|^2 J_1^{(1)}(p_{\widetilde{(\widetilde{(ij)}k)}}) \\
&- f_3^0(i,j,k)F_3^0(\hat{1},\widetilde{(ij)},\widetilde{(jk)})|M_3^{(0)}(\hat{\tilde{1}},\hat{2},\widetilde{(\widetilde{(ij)}(jk)}))|^2 J_1^{(1)}(p_{\widetilde{(\widetilde{(ij)}(jk))}}) \\
&- f_3^0(\hat{1},k,j)F_3^0(\hat{\tilde{1}},\widetilde{(jk)},i)|M_3^{(0)}(\hat{\tilde{\tilde{1}}},\hat{2},\widetilde{(i(jk))})|^2 J_1^{(1)}(p_{\widetilde{(i(jk))}}) \\
&-F_4^0(\hat{1},i,\hat{2},k)|M_3^{(0)}(\hat{\tilde{1}},\hat{\tilde{2}},\tilde{j})|^2 J_1^{(1)}(p_{\tilde{j}}) \\
&+ F_3^0(\hat{1},i,\hat{2})F_3^0(\hat{\tilde{1}},\hat{\tilde{2}},\tilde{k})|M_3^{(0)}(\hat{\tilde{\tilde{1}}},\hat{\tilde{\tilde{2}}},\tilde{\tilde{j}})|^2 J_1^{(1)}(p_{\tilde{\tilde{j}}}) \\
&+ F_3^0(\hat{1},k,\hat{2})F_3^0(\hat{\tilde{1}},\hat{\tilde{2}},\tilde{i})|M_3^{(0)}(\hat{\tilde{\tilde{1}}},\hat{\tilde{\tilde{2}}},\tilde{\tilde{j}})|^2 J_1^{(1)}(p_{\tilde{\tilde{j}}}) \qquad \text{(A.2)}
\end{aligned}
$$

$$
\begin{aligned}
\mathrm{d}\hat{\sigma}^{S,C}_{NNLO}(\hat{1},\hat{2},i,j,k) = \frac{1}{2}\Bigg(& -f_3^0(\hat{2},i,j)f_3^0(\hat{1},k,\widetilde{(ij)})|M_3^{(0)}(\hat{\bar{1}},\hat{\bar{2}},\widetilde{((ij)k)})|^2 J_1^{(1)}(p_{\widetilde{((ij)k)}}) \\
& -f_3^0(\hat{2},k,j)f_3^0(\hat{1},i,\widetilde{(jk)})|M_3^{(0)}(\hat{\bar{1}},\hat{\bar{2}},\widetilde{(i(jk))})|^2 J_1^{(1)}(p_{\widetilde{(i(jk))}}) \\
& -f_3^0(\hat{1},k,j)f_3^0(\hat{2},i,\widetilde{(jk)})|M_3^{(0)}(\hat{\bar{1}},\hat{\bar{2}},\widetilde{(i(jk))})|^2 J_1^{(1)}(p_{\widetilde{(i(jk))}}) \\
& -f_3^0(\hat{1},i,j)f_3^0(\hat{2},k,\widetilde{(ij)})|M_3^{(0)}(\hat{\bar{1}},\hat{\bar{2}},\widetilde{((ij)k)})|^2 J_1^{(1)}(p_{\widetilde{((ij)k)}}) \\
& +f_3^0(\hat{2},i,j)f_3^0(\hat{\bar{2}},k,\widetilde{(ij)})|M_3^{(0)}(\hat{1},\hat{\bar{\bar{2}}},\widetilde{((ij)k)})|^2 J_1^{(1)}(p_{\widetilde{((ij)k)}}) \\
& +f_3^0(\hat{2},k,j)f_3^0(\hat{\bar{2}},i,\widetilde{(jk)})|M_3^{(0)}(\hat{1},\hat{\bar{\bar{2}}},\widetilde{(i(jk))})|^2 J_1^{(1)}(p_{\widetilde{(i(jk))}}) \\
& +f_3^0(\hat{1},k,j)f_3^0(\hat{\bar{1}},i,\widetilde{(jk)})|M_3^{(0)}(\hat{\bar{\bar{1}}},\hat{2},\widetilde{(i(jk))})|^2 J_1^{(1)}(p_{\widetilde{(i(jk))}}) \\
& +f_3^0(\hat{1},i,j)f_3^0(\hat{\bar{1}},k,\widetilde{(ij)})|M_3^{(0)}(\hat{\bar{\bar{1}}},\hat{2},\widetilde{((ij)k)})|^2 J_1^{(1)}(p_{\widetilde{((ij)k)}}) \\
& +f_3^0(\hat{2},k,j)F_3^0(\hat{1},\hat{\bar{2}},i)|M_3^{(0)}(\hat{1},\hat{\bar{\bar{2}}},\widetilde{(kj)})|^2 J_1^{(1)}(p_{\widetilde{(kj)}}) \\
& +f_3^0(\hat{2},i,j)F_3^0(\hat{1},\hat{\bar{2}},k)|M_3^{(0)}(\hat{1},\hat{\bar{\bar{2}}},\widetilde{(ij)})|^2 J_1^{(1)}(p_{\widetilde{(ij)}}) \\
& +f_3^0(\hat{1},k,j)F_3^0(\hat{\bar{1}},\hat{2},i)|M_3^{(0)}(\hat{\bar{\bar{1}}},\hat{2},\widetilde{(kj)})|^2 J_1^{(1)}(p_{\widetilde{(kj)}}) \\
& +f_3^0(\hat{1},i,j)F_3^0(\hat{\bar{1}},\hat{2},k)|M_3^{(0)}(\hat{\bar{\bar{1}}},\hat{2},\widetilde{(ij)})|^2 J_1^{(1)}(p_{\widetilde{(ij)}}) \\
& -F_3^0(\hat{1},\hat{2},i)f_3^0(\hat{\bar{2}},\tilde{k},\tilde{j})|M_3^{(0)}(\hat{1},\hat{\bar{\bar{2}}},\widetilde{(\tilde{k}\tilde{j})})|^2 J_1^{(1)}(p_{\widetilde{(\tilde{k}\tilde{j})}}) \\
& -F_3^0(\hat{1},\hat{2},k)f_3^0(\hat{\bar{2}},\tilde{i},\tilde{j})|M_3^{(0)}(\hat{1},\hat{\bar{\bar{2}}},\widetilde{(\tilde{i}\tilde{j})})|^2 J_1^{(1)}(p_{\widetilde{(\tilde{i}\tilde{j})}}) \\
& -F_3^0(\hat{1},\hat{2},i)f_3^0(\hat{\bar{1}},\tilde{k},\tilde{j})|M_3^{(0)}(\hat{\bar{\bar{1}}},\hat{2},\widetilde{(\tilde{k}\tilde{j})})|^2 J_1^{(1)}(p_{\widetilde{(\tilde{k}\tilde{j})}}) \\
& -F_3^0(\hat{1},\hat{2},k)f_3^0(\hat{\bar{1}},\tilde{i},\tilde{j})|M_3^{(0)}(\hat{\bar{\bar{1}}},\hat{2},\widetilde{(\tilde{i}\tilde{j})})|^2 J_1^{(1)}(p_{\widetilde{(\tilde{i}\tilde{j})}}) \\
& -F_3^0(\hat{1},k,\hat{2})F_3^0(\hat{\bar{1}},i,\hat{\bar{2}})|M_3^{(0)}(\hat{\bar{\bar{1}}},\hat{\bar{\bar{2}}},\tilde{\tilde{j}})|^2 J_1^{(1)}(p_{\tilde{\tilde{j}}}) \\
& -F_3^0(\hat{1},i,\hat{2})F_3^0(\hat{\bar{1}},k,\hat{\bar{2}})|M_3^{(0)}(\hat{\bar{\bar{2}}},\hat{\bar{\bar{2}}},\tilde{\tilde{j}})|^2 J_1^{(1)}(p_{\tilde{\tilde{j}}})\Bigg)
\end{aligned}
\tag{A.3}
$$

A.2 The double-real IFIFF terms

These are the double-real subtraction terms for the IFIFF topology.

$$
\begin{aligned}
\mathrm{d}\hat{\sigma}^{S,a}_{NNLO}(\hat{1},i,\hat{2},j,k) = & F_3^0(\hat{1},i,\hat{2})|M_4^{(0)}(\hat{\bar{1}},\hat{\bar{2}},\tilde{j},\tilde{k})|^2 J_1^{(2)}(p_{\tilde{j}},p_{\tilde{k}}) \\
& +f_3^0(\hat{2},j,k)|M_4^{(0)}(\hat{1},i,\hat{\bar{2}},\widetilde{(jk)})|^2 J_1^{(2)}(p_i,p_{\widetilde{(jk)}}) \\
& +f_3^0(\hat{1},k,j)|M_4^{(0)}(\hat{\bar{1}},i,\hat{2},\widetilde{(jk)})|^2 J_1^{(2)}(p_i,p_{\widetilde{(jk)}}) \\
& +F_3^0(\hat{1},i,\hat{2})|M_4^{(0)}(\hat{\bar{1}},\hat{\bar{2}},\tilde{k},\tilde{j})|^2 J_1^{(2)}(p_{\tilde{k}},p_{\tilde{j}}) \\
& +f_3^0(\hat{2},k,j)|M_4^{(0)}(\hat{1},i,\hat{\bar{2}},\widetilde{(jk)})|^2 J_1^{(2)}(p_i,p_{\widetilde{(jk)}}) \\
& +f_3^0(\hat{1},j,k)|M_4^{(0)}(\hat{\bar{1}},i,\hat{2},\widetilde{(jk)})|^2 J_1^{(2)}(p_i,p_{\widetilde{(jk)}}),
\end{aligned}
\tag{A.4}
$$

$$
\mathrm{d}\hat{\sigma}^{S,b_{1,2}}_{NNLO}(\hat{1},i,\hat{2},j,k) = F_4^0(\hat{2},j,k,\hat{1})|M_3^{(0)}(\hat{\bar{1}},\tilde{i},\hat{\bar{2}})|^2 J_1^{(1)}(p_{\tilde{i}})
$$

$$
\begin{aligned}
&- f_3^0(\hat{2},j,k)F_3^0(\hat{\tilde{2}},\widetilde{(jk)},\hat{1})|M_3^{(0)}(\hat{\tilde{1}},\hat{\tilde{\tilde{2}}},\tilde{i})|^2 J_1^{(1)}(p_{\tilde{i}}) \\
&- f_3^0(\hat{1},k,j)F_3^0(\hat{2},\widetilde{(jk)},\hat{\tilde{1}})|M_3^{(0)}(\hat{\tilde{\tilde{1}}},\hat{\tilde{2}},\tilde{i})|^2 J_1^{(1)}(p_{\tilde{i}}) \\
&+F_4^0(\hat{2},k,j,\hat{1})|M_3^{(0)}(\hat{\tilde{1}},\tilde{i},\hat{\tilde{2}})|^2 J_1^{(1)}(p_{\tilde{i}}) \\
&- f_3^0(\hat{2},k,j)F_3^0(\hat{\tilde{2}},\widetilde{(jk)},\hat{1})|M_3^{(0)}(\hat{\tilde{1}},\hat{\tilde{\tilde{2}}},\tilde{i})|^2 J_1^{(1)}(p_{\tilde{i}}) \\
&- f_3^0(\hat{1},j,k)F_3^0(\hat{2},\widetilde{(jk)},\hat{\tilde{1}})|M_3^{(0)}(\hat{\tilde{\tilde{1}}},\hat{\tilde{2}},\tilde{i})|^2 J_1^{(1)}(p_{\tilde{i}}) \\
&+F_4^0(\hat{1},i,\hat{2},j)|M_3^{(0)}(\hat{\tilde{1}},\hat{\tilde{2}},\tilde{k})|^2 J_1^{(1)}(p_{\tilde{k}}) \\
&- F_3^0(\hat{1},i,\hat{2})F_3^0(\hat{\tilde{1}},\hat{\tilde{2}},\tilde{j})|M_3^{(0)}(\hat{\tilde{\tilde{1}}},\hat{\tilde{\tilde{2}}},\tilde{\tilde{k}})|^2 J_1^{(1)}(p_{\tilde{\tilde{k}}}) \\
&- F_3^0(\hat{2},j,\hat{1})F_3^0(\hat{\tilde{1}},\tilde{i},\hat{\tilde{2}})|M_3^{(0)}(\hat{\tilde{\tilde{1}}},\hat{\tilde{\tilde{2}}},\tilde{\tilde{k}})|^2 J_1^{(1)}(p_{\tilde{\tilde{k}}}) \\
&+F_4^0(\hat{1},i,\hat{2},k)|M_3^{(0)}(\hat{\tilde{1}},\hat{\tilde{2}},\tilde{j})|^2 J_1^{(1)}(p_{\tilde{j}}) \\
&- F_3^0(\hat{1},i,\hat{2})F_3^0(\hat{\tilde{1}},\hat{\tilde{2}},\tilde{k})|M_3^{(0)}(\hat{\tilde{\tilde{1}}},\hat{\tilde{\tilde{2}}},\tilde{\tilde{j}})|^2 J_1^{(1)}(p_{\tilde{\tilde{j}}}) \\
&- F_3^0(\hat{2},k,\hat{1})F_3^0(\hat{\tilde{1}},\tilde{i},\hat{\tilde{2}})|M_3^{(0)}(\hat{\tilde{\tilde{1}}},\hat{\tilde{\tilde{2}}},\tilde{\tilde{j}})|^2 J_1^{(1)}(p_{\tilde{\tilde{j}}})
\end{aligned} \tag{A.5}
$$

$$
\begin{aligned}
\mathrm{d}\hat{\sigma}^{S,c}_{NNLO}(\hat{1},i,\hat{2},j,k) = &-f_3^0(\hat{2},j,k)F_3^0(\hat{1},i,\hat{\tilde{2}})|M_3^{(0)}(\hat{\tilde{1}},\hat{\tilde{\tilde{2}}},\widetilde{\widetilde{(jk)}})|^2 J_1^{(1)}(p_{\widetilde{\widetilde{(jk)}}}) \\
&-f_3^0(\hat{2},k,j)F_3^0(\hat{1},i,\hat{\tilde{2}})|M_3^{(0)}(\hat{\tilde{1}},\hat{\tilde{\tilde{2}}},\widetilde{\widetilde{(jk)}})|^2 J_1^{(1)}(p_{\widetilde{\widetilde{(jk)}}}) \\
&-f_3^0(\hat{1},k,j)F_3^0(\hat{\tilde{1}},i,\hat{2})|M_3^{(0)}(\hat{\tilde{\tilde{1}}},\hat{2},\widetilde{\widetilde{(jk)}})|^2 J_1^{(1)}(p_{\widetilde{\widetilde{(jk)}}}) \\
&-f_3^0(\hat{1},j,k)F_3^0(\hat{\tilde{1}},i,\hat{2})|M_3^{(0)}(\hat{\tilde{\tilde{1}}},\hat{\tilde{2}},\widetilde{\widetilde{(jk)}})|^2 J_1^{(1)}(p_{\widetilde{\widetilde{(jk)}}}) \\
&+F_3^0(\hat{1},j,\hat{2})F_3^0(\hat{\tilde{1}},\tilde{i},\hat{\tilde{2}}|M_3^{(0)}(\hat{\tilde{\tilde{1}}},\hat{\tilde{\tilde{2}}},\tilde{\tilde{k}})|^2 J_1^{(1)}(p_{\tilde{\tilde{k}}}) \\
&+F_3^0(\hat{1},k,\hat{2})F_3^0(\hat{\tilde{1}},\tilde{i},\hat{2}|M_3^{(0)}(\hat{\tilde{\tilde{1}}},\hat{\tilde{\tilde{2}}},\tilde{\tilde{j}})|^2 J_1^{(1)}(p_{\tilde{\tilde{j}}})
\end{aligned} \tag{A.6}
$$

A.3 The IIFFF large angle soft terms

The large angle soft terms for the IIFFF topology. For the fifth and sixth block an alternative primary mapping has been applied.

unintegrated	integrated
$+S_{\hat{\bar{1}}i(\widetilde{(ij)k})}$	$+\mathcal{S}_{(\hat{\bar{1}}(\widetilde{IJ})),(\hat{2}J)}$
$-S_{\hat{1}i\widetilde{(ij)}}$	$-\mathcal{S}_{(\hat{1}J),(\hat{2}J)}$
$-S_{\hat{\bar{2}}i(\widetilde{(ij)k})}$	$-\mathcal{S}_{(\hat{2}(\widetilde{IJ})),(\hat{2}J)}$
$+S_{\hat{\bar{2}}i\widetilde{(ij)}}$	$+\mathcal{S}_{(\hat{2}J),(\hat{2}J)}$
$-S_{\hat{\bar{2}}i\hat{1}}$	$-\mathcal{S}_{(\hat{\bar{1}}\hat{2}),(\hat{2}J)}$
$+S_{\hat{\bar{2}}i\hat{1}}$	$+\mathcal{S}_{(\hat{1}\hat{2}),(\hat{2}J)}$
$\times f_3^0(\hat{1},k,\widetilde{(ij)})\vert M_3^{(0)}(\hat{\bar{1}},\widetilde{((ij)k)},\hat{\bar{2}})\vert^2$	
primary mapping: $(\hat{2}ij)$	$\hat{\bar{2}}\to\hat{2},\widetilde{(ij)}\to J,\hat{1}\to\hat{1},k\to I$
$+S_{\hat{\bar{1}}k(\widetilde{i(jk)})}$	$+\mathcal{S}_{(\hat{\bar{1}}(\widetilde{IJ})),(\hat{2}J)}$
$-S_{\hat{1}k\widetilde{(jk)}}$	$-\mathcal{S}_{(\hat{1}J),(\hat{2}J)}$
$-S_{\hat{\bar{2}}k(\widetilde{i(jk)})}$	$-\mathcal{S}_{(\hat{2}(\widetilde{IJ})),(\hat{2}J)}$
$+S_{\hat{\bar{2}}k\widetilde{(jk)}}$	$+\mathcal{S}_{(\hat{2}J),(\hat{2}J)}$
$-S_{\hat{\bar{2}}k\hat{1}}$	$-\mathcal{S}_{(\hat{\bar{1}}\hat{2}),(\hat{2}J)}$
$+S_{\hat{\bar{2}}k\hat{1}}$	$+\mathcal{S}_{(\hat{1}\hat{2}),(\hat{2}J)}$
$\times f_3^0(\hat{1},i,\widetilde{(jk)})\vert M_3^{(0)}(\hat{\bar{1}},\widetilde{i(jk)}),\hat{\bar{2}})\vert^2$	
primary mapping: $(\hat{2}kj)$	$\hat{\bar{2}}\to\hat{2},\widetilde{(jk)}\to J,\hat{1}\to\hat{1},i\to I$
$+S_{\hat{\bar{2}}i(\widetilde{(ij)k})}$	$+\mathcal{S}_{(\hat{\bar{2}}(\widetilde{IJ})),(\hat{1}J)}$
$-S_{\hat{2}i\widetilde{(ij)}}$	$-\mathcal{S}_{(\hat{2}J),(\hat{1}J)}$
$-S_{\hat{\bar{1}}i(\widetilde{(ij)k})}$	$-\mathcal{S}_{(\hat{1}(\widetilde{IJ})),(\hat{1}J)}$
$+S_{\hat{\bar{1}}i\widetilde{(ij)}}$	$+\mathcal{S}_{(\hat{1}J),(\hat{1}J)}$
$-S_{\hat{\bar{1}}i\hat{\bar{2}}}$	$-\mathcal{S}_{(\hat{1}\hat{\bar{2}}),(\hat{1}J)}$
$+S_{\hat{\bar{1}}i\hat{2}}$	$+\mathcal{S}_{(\hat{1}\hat{2}),(\hat{1}J)}$
$\times f_3^0(\hat{2},k,\widetilde{(ij)})\vert M_3^{(0)}(\hat{\bar{1}},\widetilde{((ij)k)},\hat{\bar{2}})\vert^2$	
primary mapping: $(\hat{1}ij)$	$\hat{\bar{1}}\to\hat{1},\widetilde{(ij)}\to J,\hat{2}\to\hat{2},k\to I$
$+S_{\hat{\bar{2}}k(\widetilde{i(jk)})}$	$+\mathcal{S}_{(\hat{\bar{2}}(\widetilde{IJ})),(\hat{1}J)}$
$-S_{\hat{2}k\widetilde{(jk)}}$	$-\mathcal{S}_{(\hat{2}J),(\hat{1}J)}$
$-S_{\hat{\bar{1}}k(\widetilde{i(jk)})}$	$-\mathcal{S}_{(\hat{1}(\widetilde{IJ})),(\hat{1}J)}$
$+S_{\hat{\bar{1}}k\widetilde{(jk)}}$	$+\mathcal{S}_{(\hat{1}J),(\hat{1}J)}$
$-S_{\hat{\bar{1}}k\hat{\bar{2}}}$	$-\mathcal{S}_{(\hat{1}\hat{\bar{2}}),(\hat{1}J)}$
$+S_{\hat{\bar{1}}k\hat{2}}$	$+\mathcal{S}_{(\hat{1}\hat{2}),(\hat{1}J)}$
$\times f_3^0(\hat{2},i,\widetilde{(jk)})\vert M_3^{(0)}(\hat{\bar{1}},\widetilde{i(jk)}),\hat{\bar{2}})\vert^2$	
primary mapping: $(\hat{1}kj)$	$\hat{\bar{1}}\to\hat{1},\widetilde{(jk)}\to J,\hat{2}\to\hat{2},i\to I$

$+S_{\hat{\bar{1}}\tilde{i}\hat{2}}$	$+\mathcal{S}_{(\hat{\underline{1}}\hat{2}),(\hat{1}I)} \to +\mathcal{S}_{(\hat{\underline{1}}\hat{2}),\widetilde{(\hat{1}I)}}$
$-S_{\hat{\bar{1}}\tilde{i}\tilde{j}}$	$-\mathcal{S}_{(\hat{\underline{1}}J),(\hat{1}I)} \to -\mathcal{S}_{(\hat{1}\tilde{J}),\widetilde{(\hat{1}I)}}$
$-S_{\hat{2}\tilde{i}\tilde{j}}$	$-\mathcal{S}_{(\hat{\underline{2}}J),(\hat{1}I)} \to -\mathcal{S}_{(\hat{2}\tilde{J}),\widetilde{(\hat{1}I)}}$
$+S_{\hat{1}ij}$	$+\mathcal{S}_{(\hat{1}J),(\hat{1}I)}$
$+S_{\hat{2}ij}$	$+\mathcal{S}_{(\hat{2}J),(\hat{1}I)}$
$-S_{\hat{1}i\hat{2}}$	$-\mathcal{S}_{(\hat{1}\hat{2}),(\hat{1}I)}$
$\times F_3^0(\hat{\bar{1}},\widetilde{(ik)},\hat{2})\vert M_3^{(0)}(\hat{\bar{\bar{1}}},\tilde{j},\hat{\bar{2}})\vert^2 \times 1/2 + (\hat{1} \leftrightarrow \hat{2})$	
primary mapping: $(\hat{1}ik)$	$\hat{\bar{1}} \to \hat{1}, \widetilde{(ik)} \to I, \hat{2} \to \hat{2}, j \to J$
$+S_{\hat{\bar{1}}\tilde{k}\hat{2}}$	$+\mathcal{S}_{(\hat{\underline{1}}\hat{2}),(\hat{1}I)} \to +\mathcal{S}_{(\hat{\underline{1}}\hat{2}),\widetilde{(\hat{1}I)}}$
$-S_{\hat{\bar{1}}\tilde{k}\tilde{j}}$	$-\mathcal{S}_{(\hat{\underline{1}}J),(\hat{1}I)} \to -\mathcal{S}_{(\hat{1}\tilde{J}),\widetilde{(\hat{1}I)}}$
$-S_{\hat{2}\tilde{k}\tilde{j}}$	$-\mathcal{S}_{(\hat{\underline{2}}J),(\hat{1}I)} \to -\mathcal{S}_{(\hat{2}\tilde{J}),\widetilde{(\hat{1}I)}}$
$+S_{\hat{1}kj}$	$+\mathcal{S}_{(\hat{1}J),(\hat{1}I)}$
$+S_{\hat{2}kj}$	$+\mathcal{S}_{(\hat{2}J),(\hat{1}I)}$
$-S_{\hat{1}k\hat{2}}$	$-\mathcal{S}_{(\hat{1}\hat{2}),(\hat{1}I)}$
$\times F_3^0(\hat{\bar{1}},\widetilde{(ik)},\hat{2})\vert M_3^{(0)}(\hat{\bar{\bar{1}}},\tilde{j},\hat{\bar{2}})\vert^2 \times 1/2 + (\hat{1} \leftrightarrow \hat{2})$	
primary mapping: $(\hat{1}ki)$	$\hat{\bar{1}} \to \hat{1}, \widetilde{(ik)} \to I, \hat{2} \to \hat{2}, j \to J$

A.4 The IFIFF large angle soft terms

The large angle soft terms for the IFIFF topology. Also here an alternative primary mapping has been applied.

$+S_{\hat{\bar{1}}\tilde{j}\hat{2}}$	$+\mathcal{S}_{(\hat{\underline{1}}\hat{2}),(\hat{1}I)} \to +\mathcal{S}_{(\hat{\underline{1}}\hat{2}),\widetilde{(\hat{1}I)}}$
$-S_{\hat{\bar{1}}\tilde{j}\tilde{k}}$	$-\mathcal{S}_{(\hat{\underline{1}}J),(\hat{1}I)} \to -\mathcal{S}_{(\hat{1}\tilde{J}),\widetilde{(\hat{1}I)}}$
$-S_{\hat{2}\tilde{j}\tilde{k}}$	$-\mathcal{S}_{(\hat{\underline{2}}J),(\hat{1}I)} \to -\mathcal{S}_{(\hat{2}\tilde{J}),\widetilde{(\hat{1}I)}}$
$+S_{\hat{1}jk}$	$+\mathcal{S}_{(\hat{1}J),(\hat{1}I)}$
$+S_{\hat{2}jk}$	$+\mathcal{S}_{(\hat{2}J),(\hat{1}I)}$
$-S_{\hat{1}j\hat{2}}$	$-\mathcal{S}_{(\hat{1}\hat{2}),(\hat{1}I)}$
$\times F_3^0(\hat{\bar{1}},\widetilde{(ij)},\hat{2})\vert M_3^{(0)}(\hat{\bar{\bar{1}}},\tilde{k},\hat{\bar{2}})\vert^2 \times 1/2 + (\hat{1} \leftrightarrow \hat{2})$	
primary mapping: $(\hat{1}ji)$	$\hat{\bar{1}} \to \hat{1}, \widetilde{(ij)} \to I, \hat{2} \to \hat{2}, k \to J$
$+S_{\hat{\bar{1}}\tilde{k}\hat{2}}$	$+\mathcal{S}_{(\hat{\underline{1}}\hat{2}),(\hat{1}I)} \to +\mathcal{S}_{(\hat{\underline{1}}\hat{2}),\widetilde{(\hat{1}I)}}$
$-S_{\hat{\bar{1}}\tilde{k}\tilde{j}}$	$-\mathcal{S}_{(\hat{\underline{1}}J),(\hat{1}I)} \to -\mathcal{S}_{(\hat{1}\tilde{J}),\widetilde{(\hat{1}I)}}$
$-S_{\hat{2}\tilde{k}\tilde{j}}$	$-\mathcal{S}_{(\hat{\underline{2}}J),(\hat{1}I)} \to -\mathcal{S}_{(\hat{2}\tilde{J}),\widetilde{(\hat{1}I)}}$
$+S_{\hat{1}kj}$	$+\mathcal{S}_{(\hat{1}J),(\hat{1}I)}$
$+S_{\hat{2}kj}$	$+\mathcal{S}_{(\hat{2}J),(\hat{1}I)}$
$-S_{\hat{1}k\hat{2}}$	$-\mathcal{S}_{(\hat{1}\hat{2}),(\hat{1}I)}$
$\times F_3^0(\hat{\bar{1}},\widetilde{(ik)},\hat{2})\vert M_3^{(0)}(\hat{\bar{\bar{1}}},\tilde{j},\hat{\bar{2}})\vert^2 \times 1/2 + (\hat{1} \leftrightarrow \hat{2})$	
primary mapping: $(\hat{1}ki)$	$\hat{\bar{1}} \to \hat{1}, \widetilde{(ik)} \to I, \hat{2} \to \hat{2}, j \to J$

A.5 The real-virtual IIFF subtraction terms

The real-virtual subtraction terms for the IIFF topology. The whole contribution depends only on two momentum mappings.

$$
\begin{aligned}
\mathrm{d}\hat{\sigma}^{S,a}_{NNLO}(\hat{1},\hat{2},i,j) = -\Bigg(& \mathbf{J}^{(1,II)}_2(\hat{1},\hat{2};z_1,z_2) \\
& +\mathbf{J}^{(1,IF)}_2(\hat{2},i;z_2)\delta(1-z_1) \\
& +\mathbf{J}^{(1,FF)}_2(i,j)\delta(1-z_1)\delta(1-z_2) \\
& +\mathbf{J}^{(1,IF)}_2(j,\hat{1};z_1)\delta(1-z_2)\Bigg)|M^{(0)}_4(\hat{1},\hat{2},i,j)|^2 J^{(2)}_1(p_i,p_j)
\end{aligned} \tag{A.7}
$$

$$
\begin{aligned}
\mathrm{d}\hat{\sigma}^{S,b_1}_{NNLO}(\hat{1},\hat{2},i,j) = & \Bigg(f^0_3(\hat{2},i,j)|2M^{(1)}_3(\hat{1},\hat{\tilde{2}},\widetilde{(ij)})M^{(0)\dagger}_3(\hat{1},\hat{\tilde{2}},\widetilde{(ij)})|\delta(1-z_1)\delta(1-z_2) \\
& +\Big(\mathbf{J}^{(1,II)}_2(\hat{1},\hat{\tilde{2}};z_1,z_2) \\
& \quad +\mathbf{J}^{(1,IF)}_2(\hat{\tilde{2}},\widetilde{(ij)};z_2)\delta(1-z_1) \\
& \quad +\mathbf{J}^{(1,IF)}_2(\widetilde{(ij)},\hat{1};z_1)\delta(1-z_2)\Big)|M^{(0)}_3(\hat{1},\hat{\tilde{2}},\widetilde{(ij)})|^2\Bigg) J^{(1)}_1(p_{\widetilde{(ij)}}) \\
& +\Bigg(f^0_3(\hat{1},j,i)|2M^{(1)}_3(\hat{\tilde{1}},\hat{2},\widetilde{(ij)})M^{(0)\dagger}_3(\hat{\tilde{1}},\hat{2},\widetilde{(ij)})|\delta(1-z_1)\delta(1-z_2) \\
& +\Big(\mathbf{J}^{(1,II)}_2(\hat{\tilde{1}},\hat{2};z_1,z_2) \\
& \quad +\mathbf{J}^{(1,IF)}_2(\hat{2},\widetilde{(ij)};z_2)\delta(1-z_1) \\
& \quad +\mathbf{J}^{(1,IF)}_2(\widetilde{(ij)},\hat{\tilde{1}};z_1)\delta(1-z_2)\Big)|M^{(0)}_3(\hat{\tilde{1}},\hat{2},\widetilde{(ij)})|^2\Bigg) J^{(1)}_1(p_{\widetilde{(ij)}})
\end{aligned} \tag{A.8}
$$

$$
\begin{aligned}
\mathrm{d}\hat{\sigma}^{S,b_2}_{NNLO}(\hat{1},\hat{2},i,j) = & \Bigg(f^1_3(\hat{2},i,j,\sqrt{s_{2ij}})\delta(1-z_1)\delta(1-z_2) \\
& +\Big(\mathbf{J}^{(1,IF)}_2(\hat{2},i;z_2)\delta(1-z_1) \\
& \quad +\mathbf{J}^{(1,FF)}_2(i,j)\delta(1-z_1)\delta(1-z_2) \\
& \quad +\mathbf{J}^{(1,IF)}_2(\hat{2},j;z_2)\delta(1-z_1) \\
& \quad -2\mathbf{J}^{(1,IF)}_2(\hat{\tilde{2}},\widetilde{(ij)};z_2)\delta(1-z_1)\Big) f^0_3(\hat{2},i,j)\Bigg)|M^{(0)}_3(\hat{1},\hat{\tilde{2}},\widetilde{(ij)})|^2 J^{(1)}_1(p_{\widetilde{(ij)}}) \\
& \Bigg(f^1_3(\hat{1},j,i,\sqrt{s_{1ji}})\delta(1-z_1)\delta(1-z_2) \\
& +\Big(\mathbf{J}^{(1,IF)}_2(\hat{1},j;z_1)\delta(1-z_2) \\
& \quad +\mathbf{J}^{(1,FF)}_2(i,j)\delta(1-z_1)\delta(1-z_2) \\
& \quad +\mathbf{J}^{(1,IF)}_2(\hat{1},i;z_1)\delta(1-z_2)
\end{aligned}
$$

$$-2\mathbf{J}_2^{(1,IF)}(\hat{\bar{1}},\widetilde{(ij)};z_1)\delta(1-z_2)\Big)f_3^0(\hat{1},j,i)\Bigg)|M_3^{(0)}(\hat{\bar{1}},\hat{2},\widetilde{(ij)})|^2J_1^{(1)}(p_{\widetilde{(ij)}}) \tag{A.9}$$

$$\begin{aligned}\mathrm{d}\hat{\sigma}^{S,b_3}_{NNLO}(\hat{1},\hat{2},i,j) = \frac{11}{6}\Bigg(& f_3^0(\hat{2},i,j)\log(\frac{m_H}{\sqrt{s_{2ij}}})|M_3^{(0)}(\hat{1},\hat{\bar{2}},\widetilde{(ij)})|^2J_1^{(1)}(p_{\widetilde{(ij)}}) \\ &+f_3^0(\hat{1},j,i)\log(\frac{m_H}{\sqrt{s_{1ji}}})|M_3^{(0)}(\hat{\bar{1}},\hat{2},\widetilde{(ij)})|^2J_1^{(1)}(p_{\widetilde{(ij)}})\Bigg)\delta(1-z_1)\delta(1-z_2)\end{aligned} \tag{A.10}$$

$$\begin{aligned}\mathrm{d}\hat{\sigma}^{S,c}_{NNLO}(\hat{1},\hat{2},i,j) = \frac{1}{2}\Bigg(& \Big(\mathcal{F}_3^0(s_{(\hat{\bar{2}},\widetilde{(ij)})}) - \mathcal{S}(s_{(\hat{\bar{2}},\widetilde{(ij)})},s_{(\hat{2},j)})\Big) \\ &-\Big(\mathcal{F}_3^0(s_{(\hat{2},j)}) - \mathcal{S}(s_{(\hat{2},j)},s_{(\hat{2},j)})\Big) \\ &-\Big(\mathcal{F}_3^0(s_{\hat{1},\widetilde{(ij)}}) - \mathcal{S}(s_{\hat{1},\widetilde{(ij)}},s_{(\hat{2},j)})\Big) \\ &+\Big(\mathcal{F}_3^0(s_{\hat{1},j}) - \mathcal{S}(s_{\hat{1},j},s_{(\hat{2},j)})\Big) \\ &-\Big(\mathcal{F}_3^0(s_{\hat{1},\hat{\bar{2}}}) - \mathcal{S}(s_{\hat{1},\hat{\bar{2}}},s_{(\hat{2},j)})\Big) \\ &+\Big(\mathcal{F}_3^0(s_{\hat{1},\hat{2}}) - \mathcal{S}(s_{\hat{1},\hat{2}},s_{(\hat{2},j)})\Big)\Bigg)f_3^0(\hat{2},i,j)|M_3^{(0)}(\hat{1},\hat{\bar{2}},\widetilde{(ij)})|^2J_1^{(1)}(p_{\widetilde{(ij)}}) \\ +\frac{1}{2}\Bigg(& \Big(\mathcal{F}_3^0(s_{\hat{\bar{1}},\widetilde{(ij)}}) - \mathcal{S}(s_{\hat{\bar{1}},\widetilde{(ij)}},s_{\hat{1},i})\Big) \\ &-\Big(\mathcal{F}_3^0(s_{\hat{1},i}) - \mathcal{S}(s_{\hat{1},i},s_{\hat{1},i})\Big) \\ &-\Big(\mathcal{F}_3^0(s_{\hat{2},\widetilde{(ij)}}) - \mathcal{S}(s_{\hat{2},\widetilde{(ij)}},s_{\hat{1},i})\Big) \\ &+\Big(\mathcal{F}_3^0(s_{\hat{2},i}) - \mathcal{S}(s_{\hat{2},i},s_{\hat{1},i})\Big) \\ &-\Big(\mathcal{F}_3^0(s_{\hat{2},\hat{\bar{1}}}) - \mathcal{S}(s_{\hat{2},\hat{\bar{1}}},s_{\hat{1},i})\Big) \\ &+\Big(\mathcal{F}_3^0(s_{\hat{2},\hat{1}}) - \mathcal{S}(s_{\hat{2},\hat{1}},s_{\hat{1},i})\Big)\Bigg)f_3^0(\hat{1},j,i)|M_3^{(0)}(\hat{\bar{1}},\hat{2},\widetilde{(ij)})|^2J_1^{(1)}(p_{\widetilde{(ij)}})\end{aligned} \tag{A.11}$$

A.6 The real-virtual IFIF subtraction terms

The real-virtual subtraction terms for the IFIF topology. Also here, only two mappings are required.

$$\begin{aligned}\mathrm{d}\hat{\sigma}^{S,a}_{NNLO}(\hat{1},i,\hat{2},j) = -\Bigg(& \mathbf{J}_2^{(1,IF)}(\hat{1},i;z_1)\delta(1-z_2) \\ &+\mathbf{J}_2^{(1,IF)}(\hat{2},i;z_2)\delta(1-z_1) \\ &+\mathbf{J}_2^{(1,IF)}(\hat{2},j;z_2)\delta(1-z_1)\end{aligned}$$

$$+\mathbf{J}_2^{(1,IF)}(\hat{1},j;z_1)\delta(1-z_2)\Big)|M_4^{(0)}(\hat{1},i,\hat{2},j)|^2 J_1^{(2)}(p_i,p_j) \tag{A.12}$$

$$\begin{aligned}
\mathrm{d}\hat{\sigma}^{S,b_1}_{NNLO}(\hat{1},i,\hat{2},j) = \Bigg(& F_3^0(\hat{1},i,\hat{2})|2M_3^{(1)}(\hat{\tilde{1}},\hat{\tilde{2}},\tilde{j})M_3^{(0)\dagger}(\hat{\tilde{1}},\hat{\tilde{2}},\tilde{j})|\delta(1-z_1)\delta(1-z_2) \\
& +\Big(\mathbf{J}_2^{(1,II)}(\hat{\tilde{1}},\hat{\tilde{2}};z_1,z_2) \\
& \quad +\mathbf{J}_2^{(1,IF)}(\hat{\tilde{1}},\tilde{j};z_1)\delta(1-z_2) \\
& \quad +\mathbf{J}_2^{(1,IF)}(\hat{\tilde{2}},\tilde{j};z_2)\delta(1-z_1)\Big)|M_3^{(0)}(\hat{\tilde{1}},\hat{\tilde{2}},\tilde{j})|^2\Bigg) J_1^{(1)}(p_{\tilde{j}}) \\
& +\Bigg(F_3^0(\hat{2},j,\hat{1})|2M_3^{(1)}(\hat{\tilde{1}},\hat{\tilde{2}},\tilde{i})M_3^{(0)\dagger}(\hat{\tilde{1}},\hat{\tilde{2}},\tilde{i})|\delta(1-z_1)\delta(1-z_2) \\
& +\Big(\mathbf{J}_2^{(1,II)}(\hat{\tilde{1}},\hat{\tilde{2}};z_1,z_2) \\
& \quad +\mathbf{J}_2^{(1,IF)}(\hat{\tilde{1}},\tilde{i};z_1)\delta(1-z_2) \\
& \quad +\mathbf{J}_2^{(1,IF)}(\hat{\tilde{2}},\tilde{i};z_2)\delta(1-z_1)\Big)|M_3^{(0)}(\hat{\tilde{1}},\hat{\tilde{2}},\tilde{i})|^2\Bigg) J_1^{(1)}(p_{\tilde{i}})
\end{aligned} \tag{A.13}$$

$$\begin{aligned}
\mathrm{d}\hat{\sigma}^{S,b_1}_{NNLO}(\hat{1},i,\hat{2},j) = \Bigg(& F_3^1(\hat{1},i,\hat{2},\sqrt{s_{1i2}})\delta(1-z_1)\delta(1-z_2) \\
& +\Big(\mathbf{J}_2^{(1,IF)}(\hat{1},i;z_1)\delta(1-z_2) \\
& \quad +\mathbf{J}_2^{(1,IF)}(\hat{2},i;z_2)\delta(1-z_1) \\
& \quad +\mathbf{J}_2^{(1,II)}(\hat{1},\hat{2};z_1,z_2) \\
& \quad -2\mathbf{J}_2^{(1,II)}(\hat{\tilde{1}},\hat{\tilde{2}};z_1,z_2)\Big)F_3^0(\hat{1},i,\hat{2})\Bigg)|M_3^{(0)}(\hat{\tilde{1}},\hat{\tilde{2}},\tilde{j})|^2 J_1^{(1)}(p_{\tilde{j}}) \\
& \Bigg(F_3^1(\hat{2},j,\hat{1},\sqrt{s_{2j1}})\delta(1-z_1)\delta(1-z_2) \\
& +\Big(\mathbf{J}_2^{(1,IF)}(\hat{2},j;z_2)\delta(1-z_1) \\
& \quad +\mathbf{J}_2^{(1,IF)}(\hat{1},j;z_1)\delta(1-z_2)) \\
& \quad +\mathbf{J}_2^{(1,II)}(\hat{1},\hat{2};z_1,z_2) \\
& \quad -2\mathbf{J}_2^{(1,II)}(\hat{\tilde{2}},\hat{\tilde{1}};z_1,z_2)\Big)F_3^0(\hat{2},j,\hat{1})\Bigg)|M_3^{(0)}(\hat{\tilde{1}},\hat{\tilde{2}},\tilde{i})|^2 J_1^{(1)}(p_{\tilde{i}})
\end{aligned} \tag{A.14}$$

$$\begin{aligned}
\mathrm{d}\hat{\sigma}^{S,b_3}_{NNLO}(\hat{1},i,\hat{2},j) = \frac{11}{6}\Bigg(& F_3^0(\hat{1},i,\hat{2})\log(\frac{m_H}{\sqrt{s_{1i2}}})|M_3^{(0)}(\hat{\tilde{1}},\hat{\tilde{2}},\tilde{j})|^2 J_1^{(1)}(p_{\tilde{j}}) \\
& +F_3^0(\hat{2},j,\hat{1})\log(\frac{m_H}{\sqrt{s-2j1}})|M_3^{(0)}(\hat{\tilde{1}},\hat{\tilde{2}},\tilde{i})|^2 J_1^{(1)}(p_{\tilde{i}})\Bigg)\delta(1-z_1)\delta(1-z_2)
\end{aligned} \tag{A.15}$$

$$
\begin{aligned}
\mathrm{d}\hat{\sigma}^{S,c}_{NNLO}(\hat{1},i,\hat{2},j) = \frac{1}{2}\Bigg(& \Big(\mathcal{F}_3^0(s_{\hat{\hat{1}},\hat{\hat{2}}}) - \mathcal{S}(s_{\hat{\hat{1}},\hat{\hat{2}}}, s_{\hat{1},i})\Big) \\
& -\Big(\mathcal{F}_3^0(s_{\hat{1},\hat{2}}) - \mathcal{S}(s_{\hat{1},\hat{2}}, s_{\hat{1},i})\Big) \\
& -\Big(\mathcal{F}_3^0(s_{\hat{\hat{1}},\tilde{j}}) - \mathcal{S}(s_{\hat{\hat{1}},\tilde{j}}, s_{\hat{1},i})\Big) \\
& +\Big(\mathcal{F}_3^0(s_{\hat{1},j}) - \mathcal{S}(s_{\hat{1},j}, s_{\hat{1},i})\Big) \\
& -\Big(\mathcal{F}_3^0(s_{\hat{\hat{2}},\tilde{j}}) - \mathcal{S}(s_{\hat{\hat{2}},\tilde{j}}, s_{\hat{1},i})\Big) \\
& +\Big(\mathcal{F}_3^0(s_{\hat{2},j}) - \mathcal{S}(s_{\hat{2},j}, s_{\hat{1},i})\Big)\Bigg) F_3^0(\hat{1},i,\hat{2})|M_3^{(0)}(\hat{\hat{1}},\hat{\hat{2}},\tilde{j})|^2 J_1^{(1)}(p_{\tilde{j}}) \\
& +\frac{1}{2}\Bigg(\Big(\mathcal{F}_3^0(s_{\hat{\hat{2}},\hat{\hat{1}}}) - \mathcal{S}(s_{\hat{\hat{2}},\hat{\hat{1}}}, s_{\hat{1},j})\Big) \\
& -\Big(\mathcal{F}_3^0(s_{\hat{2},\hat{1}}) - \mathcal{S}(s_{\hat{2},\hat{1}}, s_{\hat{1},j})\Big) \\
& -\Big(\mathcal{F}_3^0(s_{\hat{\hat{2}},\tilde{i}}) - \mathcal{S}(s_{\hat{\hat{2}},\tilde{i}}, s_{\hat{1},j})\Big) \\
& +\Big(\mathcal{F}_3^0(s_{\hat{2},i}) - \mathcal{S}(s_{\hat{2},i}, s_{\hat{1},j})\Big) \\
& -\Big(\mathcal{F}_3^0(s_{\hat{\hat{1}},\tilde{i}}) - \mathcal{S}(s_{\hat{\hat{1}},\tilde{i}}, s_{\hat{1},j})\Big) \\
& +\Big(\mathcal{F}_3^0(s_{\hat{1},i}) - \mathcal{S}(s_{\hat{1},i}, s_{\hat{1},j})\Big)\Bigg) F_3^0(\hat{2},j,\hat{1})|M_3^{(0)}(\hat{\hat{1}},\hat{\hat{2}},\tilde{i})|^2 J_1^{(1)}(p_{\tilde{i}}) \qquad \text{(A.16)}
\end{aligned}
$$

A.7 The double-virtual term

A.7.1 The full subtraction term

The double-virtual subtraction terms as coded up in form read

$$
\begin{aligned}
\mathrm{d}\sigma^U(\hat{1},\hat{2},3) = {} & \mathbf{J}_3^{(1)}(\hat{1},\hat{2},3,z_1,z_2)\Big(|2M_3^{(1)}(\hat{1},\hat{2},3)M_3^{(0)\dagger}(\hat{1},\hat{2},3)| - \frac{\beta_0}{\epsilon}|M_3^{(0)}(\hat{1},\hat{2},3)|^2\Big)J_1^{(1)}(p_3) \\
& + \frac{1}{2}\mathbf{J}_3^{(1)} \otimes \mathbf{J}_3^{(1)}(\hat{1},\hat{2},3,z_1,z_2)\cdot|M_3^{(0)}(\hat{1},\hat{2},3)|^2 J_1^{(1)}(p_3) \\
& + \mathbf{J}_3^{(2)}(\hat{1},\hat{2},3,z_1,z_2)\cdot|M_3^{(0)}(\hat{1},\hat{2},3)|^2 J_1^{(1)}(p_3). \qquad \text{(A.17)}
\end{aligned}
$$

A.7.2 The $\mathbf{J}_3^{(1)}$ term

The first term of the above equation is

$$
\mathbf{J}_3^{(1)}(\hat{1},\hat{2},3,z_1,z_2) = \mathbf{J}_2^{(1,II)}(\hat{1},\hat{2},z_1,z_2) + \mathbf{J}_2^{(1,IF)}(\hat{1},3,z_1,z_2) + \mathbf{J}_2^{(1,IF)}(\hat{2},3,z_1,z_2), \qquad \text{(A.18)}
$$

$$
\mathbf{J}_2^{(1,II)}(\hat{1},\hat{2},z_1,z_2) = \Big(\frac{s_{12}}{\mu^2}\Big)^{-\epsilon}\mathcal{F}_3^0(z_1,z_2) - \frac{1}{2}\Gamma_{gg}^1(z_1)\delta(1-z_2) - \frac{1}{2}\Gamma_{gg}^1(z_2)\delta(1-z_1), \qquad \text{(A.19)}
$$

$$
\mathbf{J}_2^{(1,IF)}(\hat{i},3,z_1,z_2) = \frac{1}{2}\Big(\Big(\frac{s_{i3}}{\mu^2}\Big)^{-\epsilon}\mathcal{F}_3^0(z_i) - \Gamma_{gg}^1(z_i)\Big)\delta(1-z_j), \qquad \text{(A.20)}
$$

where i represents an initial-state momentum and j is the other one. The dependence on the antenna scale has been extracted from the integrated antennae and made explicit.

A.7.3 The $\mathbf{J}_3^{(1)} \otimes \mathbf{J}_3^{(1)}$ term

This is the second line of eq. (A.17). The various convolutions can be found in [123].

$$
\begin{aligned}
\frac{1}{2}\mathbf{J}_3^{(1)} \otimes \mathbf{J}_3^{(1)}(\hat{1},\hat{2},3,z_1,z_2) = &\left(\frac{s_{12}}{\mu^2}\right)^{-2\epsilon}[\mathcal{F}_3^0 \otimes \mathcal{F}_3^0]^{II,II}(z_1,z_2) \\
&+ \frac{1}{4}\left(\frac{s_{13}}{\mu^2}\right)^{-2\epsilon}[\mathcal{F}_3^0 \otimes \mathcal{F}_3^0]^{IF,IF}(z_1,z_2) \\
&+ \frac{1}{4}\left(\frac{s_{23}}{\mu^2}\right)^{-2\epsilon}[\mathcal{F}_3^0 \otimes \mathcal{F}_3^0]^{IF,IF}(z_2,z_1) \\
&+ \left(\frac{s_{12}}{\mu^2}\right)^{-\epsilon}\left(\frac{s_{13}}{\mu^2}\right)^{-\epsilon}[\mathcal{F}_3^0 \otimes \mathcal{F}_3^0]^{II,IF}(z_1,z_2) \\
&+ \left(\frac{s_{12}}{\mu^2}\right)^{-\epsilon}\left(\frac{s_{23}}{\mu^2}\right)^{-\epsilon}[\mathcal{F}_3^0 \otimes \mathcal{F}_3^0]^{II,IF}(z_2,z_1) \\
&+ \frac{1}{2}\left(\frac{s_{13}}{\mu^2}\right)^{-\epsilon}\left(\frac{s_{23}}{\mu^2}\right)^{-\epsilon}[\mathcal{F}_3^0 \otimes \mathcal{F}_3^0]^{IF_1,IF_2}(z_1,z_2) \\
&- 2\left(\frac{s_{12}}{\mu^2}\right)^{-\epsilon}[\Gamma_{gg}^1 \otimes \mathcal{F}_3^0]^{II}(z_1,z_2) \\
&- 2\left(\frac{s_{12}}{\mu^2}\right)^{-\epsilon}[\Gamma_{gg}^1 \otimes \mathcal{F}_3^0]^{II}(z_2,z_1) \\
&- \left(\frac{s_{13}}{\mu^2}\right)^{-\epsilon}[\Gamma_{gg}^1 \otimes \mathcal{F}_3^0]^{IF_1}(z_1,z_2) \\
&- \left(\frac{s_{13}}{\mu^2}\right)^{-\epsilon}[\Gamma_{gg}^1 \otimes \mathcal{F}_3^0]^{IF_2}(z_1,z_2) \\
&- \left(\frac{s_{23}}{\mu^2}\right)^{-\epsilon}[\Gamma_{gg}^1 \otimes \mathcal{F}_3^0]^{IF_1}(z_2,z_1) \\
&- \left(\frac{s_{23}}{\mu^2}\right)^{-\epsilon}[\Gamma_{gg}^1 \otimes \mathcal{F}_3^0]^{IF_2}(z_2,z_1) \\
&+ [\Gamma_{gg}^1 \otimes \Gamma_{gg}^1](z_1,z_2) \\
&+ [\Gamma_{gg}^1 \otimes \Gamma_{gg}^1](z_2,z_1) \\
&+ 2\Gamma_{gg}^1(z_1)\Gamma_{gg}^1(z_2).
\end{aligned}
\tag{A.21}
$$

A.7.4 The $\mathbf{J}_3^{(2)}$ term

The last term in (A.17) is the double unresolved integrated dipole

$$\mathbf{J}_3^{(2)}(\hat{1},\hat{2},3,z_1,z_2) = \mathbf{J}_2^{(2,II)}(\hat{1},\hat{2},z_1,z_2) + \mathbf{J}_2^{(2,IF)}(\hat{1},3,z_1,z_2) + \mathbf{J}_2^{(2,IF)}(\hat{2},3,z_1,z_2) \tag{A.22}$$

$$\begin{aligned}
\mathbf{J}_2^{(2,II)}(\hat{1},\hat{2},z_1,z_2) = &\left(\frac{s_{12}}{\mu^2}\right)^{-2\epsilon}\mathcal{F}_4^0(z_1,z_2)\\
&+\frac{1}{2}\left(\frac{s_{12}}{\mu^2}\right)^{-2\epsilon}\tilde{\mathcal{F}}_4^0(z_1,z_2)\\
&+\left(\frac{s_{12}}{\mu^2}\right)^{-2\epsilon}\mathcal{F}_3^1(z_1,z_2)\\
&+\frac{\beta_0}{\epsilon}\left(\frac{s_{12}}{\mu^2}\right)^{-2\epsilon}\mathcal{F}_3^0(z_1,z_2)\\
&-\left(\frac{s_{12}}{\mu^2}\right)^{-2\epsilon}[\mathcal{F}_3^0\otimes\mathcal{F}_3^0]^{II,II}(z_1,z_2)\\
&-\frac{1}{2}\overline{\Gamma}_{gg}^2(z_1)\delta(1-z_2)\\
&-\frac{1}{2}\overline{\Gamma}_{gg}^2(z_2)\delta(1-z_1)
\end{aligned} \tag{A.23}$$

$$\begin{aligned}
\mathbf{J}_2^{(2,IF)}(\hat{i},\hat{3},z_i,z_j) = &\frac{1}{2}\left(\frac{s_{i3}}{\mu^2}\right)^{-2\epsilon}\mathcal{F}_4^0(z_i)\delta(1-z_j)\\
&+\frac{1}{2}\left(\frac{s_{i3}}{\mu^2}\right)^{-2\epsilon}\mathcal{F}_3^1(z_i)\delta(1-z_j)\\
&+\frac{\beta_0}{2\epsilon}\left(\frac{s_{i3}}{\mu^2}\right)^{-2\epsilon}\mathcal{F}_3^0(z_i)\delta(1-z_j)\\
&-\frac{1}{4}\left(\frac{s_{i3}}{\mu^2}\right)^{-2\epsilon}[\mathcal{F}_3^0\otimes\mathcal{F}_3^0]^{IF,IF}(z_1,z_2)\\
&-\frac{1}{2}\overline{\Gamma}_{gg}^2(z_i)\delta(1-z_j).
\end{aligned} \tag{A.24}$$

Appendix B

Integrated LAS

The integrated large angle soft terms for an initial-final mapping are defined through

$$\begin{aligned}\mathcal{S}^{IF}(s_{ac}, s_{IK}, y_{ac,iK}) =& \frac{1}{C(\epsilon)} \int \mathrm{d}\Phi_{\hat{i}jk} \frac{Q^2}{2\pi} S_{ajc}, \\ =& \left(\frac{|s_{IK}|}{\mu^2}\right)^{-\epsilon} \Bigg\{ \left[\frac{1}{\epsilon^2} - \frac{1}{\epsilon} \ln(y_{ac,iK}) \frac{1}{2} \ln^2(y_{ac,iK}) - \frac{\pi^2}{12} \right] \delta(1-x) \\ &+ \left[\frac{2}{\epsilon}(1 - \mathcal{D}_0(x)) + 4\mathcal{D}_1(x) + 2\ln\left(\frac{s_{ac}|s_{IK}|}{s_{aK}s_{cK}}\right) \right. \\ &- 4\ln(1-x) - \frac{4x}{(1-x)} \ln(x) + \frac{2x}{(1-x)} \ln(y_{ac,iK}) \\ &\left. - \frac{2}{(1-x)} \ln\left(\frac{s_{ac}|s_{IK}|}{s_{aK}s_{cK}}\right) \right] + \mathcal{O}(\epsilon) \Bigg\} \end{aligned} \tag{B.1}$$

where

$$S_{ajc} = \frac{2s_{ac}}{s_{aj}s_{jc}}, \tag{B.2}$$

and

$$y_{ac,iK} = \frac{s_{ac}|s_{IK}|}{(s_{aK} + (1-x)s_{ai})(s_{cK} + (1-x)s_{ci})}. \tag{B.3}$$

In the above formula, x is the momentum fraction of the initial leg after initial collinear radiation. If the unresolved momentum j is boosted following an initial-initial mapping, the following treatment is adopted. Since the eikonal in eq. (B.1) consists only of Lorentz invariants, the boost can be inverted, as labeled by an underline:

$$S_{a\tilde{j}c} = S_{\underline{a}j\underline{c}}. \tag{B.4}$$

Thus,

$$\frac{1}{C(\epsilon)} \int \mathrm{d}\Phi_{\hat{i}jk} \frac{Q^2}{2\pi} S_{a\tilde{j}c} = \tilde{\mathcal{S}}^{IF}(s_{ac}, s_{IK}, y_{ac,iK}) = \mathcal{S}^{IF}(s_{\underline{ac}}, s_{IK}, y_{\underline{ac},iK}). \tag{B.5}$$

Since the integrated eikonal also only depends on Lorentz invariants, the boost can again be applied, such that

$$\tilde{\mathcal{S}}^{IF}(s_{ac}, s_{IK}, y_{ac,iK}) = \mathcal{S}^{IF}(s_{ac}, s_{\tilde{I}\tilde{K}}, y_{ac,\tilde{i}\tilde{K}}). \tag{B.6}$$

This allows to use eq. (B.1) also for the boosted integrated eikonals.

Appendix C

PDF weights

The weights for the regions $\omega_{0,0}$, $\omega_{1,0}$, $\omega_{0,1}$ and $\omega_{1,1}$ are defined in eqs. 5.20-5.22. The remaining regions can be expressed as a linear combination of those, where $i_1, i_2 \in \{2, 3, 4, 5\}$:

$$
\begin{aligned}
\omega_{0,i_2} &= \frac{\log(1-x_2)^{(i_2-2)}}{1-x_2}\Big(\omega_{0,0} - (1-z_2)\omega_{0,1}\Big) + \frac{\log(1-z_2)^{(i_2-1)}}{i_2-1}\omega_{0,1}, \\
\omega_{i_1,0} &= \frac{\log(1-x_1)^{(i_1-2)}}{1-x_1}\Big(\omega_{0,0} - (1-z_1)\omega_{1,0}\Big) + \frac{\log(1-z_1)^{(i_1-1)}}{i_1-1}\omega_{1,0}, \\
\omega_{1,i_2} &= \frac{\log(1-x_2)^{(i_2-2)}}{1-x_2}\Big(\omega_{1,0} - (1-z_2)\omega_{1,1}\Big) + \frac{\log(1-z_2)^{(i_2-1)}}{i_2-1}\omega_{1,1}, \\
\omega_{i_1,1} &= \frac{\log(1-x_1)^{(i_1-2)}}{1-x_1}\Big(\omega_{0,1} - (1-z_1)\omega_{1,1}\Big) + \frac{\log(1-z_1)^{(i_1-1)}}{i_1-1}\omega_{1,1}, \\
\omega_{i_1,i_2} &= \frac{\log(1-x_1)^{(i_1-2)}\log(1-x_2)^{(i_2-2)}}{(1-x_2)(1-x_2)} \\
&\qquad \times \Big(\omega_{0,0} - (1-z_1)\omega_{1,0} - (1-z_2)\omega_{0,1} + (1-z_1)(1-z_2)\omega_{1,1}\Big) \\
&\quad + \frac{\log(1-x_1)^{(i_1-2)}\log(1-z_2)^{i_2-1}}{(i_2-1)(1-x_1)}\Big(\omega_{0,1} - (1-z_1)\omega_{1,1}\Big) \\
&\quad + \frac{\log(1-x_2)^{(i_2-2)}\log(1-z_1)^{i_1-1}}{(i_2-1)(1-x_2)}\Big(\omega_{1,0} - (1-z_2)\omega_{1,1}\Big) \\
&\quad + \frac{\log(1-z_1)^{i_1-1}\log(1-z_2)^{i_2-1}}{(i_1-1)(i_2-1)}\omega_{1,1}.
\end{aligned}
\tag{C.1}
$$

Bibliography

[1] G. Aad *et al.* [ATLAS Collaboration], Phys. Lett. B **716** (2012) 1 [arXiv:1207.7214 [hep-ex]].

[2] S. Chatrchyan *et al.* [CMS Collaboration], Phys. Lett. B **716** (2012) 30 [arXiv:1207.7235 [hep-ex]].

[3] G. Aad *et al.* [ATLAS Collaboration], Phys. Lett. B **726** (2013) 120 [arXiv:1307.1432 [hep-ex]]. G. Aad *et al.* [ATLAS Collaboration], Phys. Lett. B **726** (2013) 88 [Erratum-ibid. B **734** (2014) 406] [arXiv:1307.1427 [hep-ex]].

[4] V. Khachatryan *et al.* [CMS Collaboration], arXiv:1412.8662 [hep-ex].

[5] G. Aad *et al.* [ATLAS Collaboration], arXiv:1412.2641 [hep-ex]. G. Aad *et al.* [ATLAS Collaboration], Phys. Rev. D **90** (2014) 11, 112015 [arXiv:1408.7084 [hep-ex]]. G. Aad *et al.* [ATLAS Collaboration], Phys. Rev. D **91** (2015) 1, 012006 [arXiv:1408.5191 [hep-ex]]. G. Aad *et al.* [ATLAS Collaboration], Phys. Lett. B **738** (2014) 234 [arXiv:1408.3226 [hep-ex]]. G. Aad *et al.* [ATLAS Collaboration], Phys. Lett. B **738** (2014) 68 [arXiv:1406.7663 [hep-ex]].

[6] G. Aad *et al.* [ATLAS Collaboration], JHEP **1409** (2014) 112 [arXiv:1407.4222 [hep-ex]].

[7] F. Englert and R. Brout, Phys. Rev. Lett. **13** (1964) 321. P. W. Higgs, Phys. Lett. **12** (1964) 132. P. W. Higgs, Phys. Rev. Lett. **13** (1964) 508. P. W. Higgs, Phys. Rev. **145** (1966) 1156. G. S. Guralnik, C. R. Hagen and T. W. B. Kibble, Phys. Rev. Lett. **13** (1964) 585. T. W. B. Kibble, Phys. Rev. **155** (1967) 1554.

[8] F. Zwicky, Helv. Phys. Acta **6** (1933) 110. F. Zwicky, Astrophys. J. **86** (1937) 217. V. C. Rubin, D. Burstein, W. K. Ford, Jr. and N. Thonnard, Astrophys. J. **289** (1985) 81. Y. Sofue and V. Rubin, Ann. Rev. Astron. Astrophys. **39** (2001) 137 [astro-ph/0010594]. A. Bosma, Astron. J. **86** (1981) 1825. D. Fabricant and P. Gorenstein Astrophys. J. **267** (1983) 535. D. M. Wittman, J. A. Tyson, D. Kirkman, I. Dell'Antonio and G. Bernstein, Nature **405** (2000) 143 [astro-ph/0003014].

[9] H. Miyasawa, Prog. Theor. Phys. **36** (1966) 1266. P. Ramond, Phys. Rev. **D 3** (1971) 2415. Y. A. Golfand and E. P. Likhtman, JETP Lett. **13** (1971) 323 [Pisma Zh. Eksp. Teor. Fiz. **13** (1971) 452]. A. Neveu and J. H. Schwarz, Nucl. Phys. B **31** (1971) 86. A. Neveu and J. H. Schwarz, Phys. Rev. D **4** (1971) 1109. J. L. Gervais and B. Sakita, Nucl. Phys. B **34** (1971) 632. D. V. Volkov and V. P. Akulov, Phys. Lett. B **46** (1973) 109. J. Wess and B. Zumino, Phys. Lett. B **49** (1974) 52. J. Wess and B. Zumino, Nucl. Phys. B **70** (1974) 39.

[10] N. Arkani-Hamed, S. Dimopoulos and G. R. Dvali, Phys. Lett. B **429** (1998) 263 [hep-ph/9803315]. L. Randall and R. Sundrum, Phys. Rev. Lett. **83** (1999) 3370 [hep-ph/9905221].

[11] S. Weinberg, Phys. Rev. D **13**, 974 (1976). S. Weinberg, Phys. Rev. D **19** (1979) 1277. L. Susskind, Phys. Rev. D **20** (1979) 2619.

[12] K. G. Wilson, Phys. Rev. D **3** (1971) 1818. E. Gildener, Phys. Rev. D **14** (1976) 1667. S. Weinberg, Phys. Lett. B **82**, 387 (1979). G 't Hooft, in Proc. of 1979 Cargèse Institute on *Recent Developments in Gauge Theories*, p. 135, Plenum Press, New York 1980.

[13] M. Dittmar and H. K. Dreiner, Phys. Rev. D **55** (1997) 167 [hep-ph/9608317]. S. Asai, G. Azuelos, C. Buttar, V. Cavasinni, D. Costanzo, K. Cranmer, R. Harper and K. Jakobs *et al.*, Eur. Phys. J. C **32S2** (2004) 19 [hep-ph/0402254].

[14] ATLAS Collaboration Phys. Lett. **B 716** (2012) 62. S. Chatrchyan *et al.* [CMS Collaboration], Phys. Lett. B **710** (2012) 91 [arXiv:1202.1489 [hep-ex]].

[15] I. W. Stewart, F. J. Tackmann, [arXiv:1107.2117]. E. Gerwick, T. Plehn, S. Schumann, [arXiv:1108.3335].

[16] J. M. Butterworth, A. R. Davison, M. Rubin and G. P. Salam, Phys. Rev. Lett. **100** (2008) 242001 [arXiv:0802.2470 [hep-ph]].

[17] J.R. Ellis, M.K. Gaillard, D.V. Nanopoulos and C.T. Sachrajda, Phys. Lett. B **83** (1979) 339.

[18] F. Wilczek, Phys. Rev. Lett. **39** (1977) 1304;
M.A. Shifman, A.I. Vainshtein and V.I. Zakharov, Phys. Lett. B **78** (1978) 443;
T. Inami, T. Kubota and Y. Okada, Z. Phys. C **18** (1983) 69.

[19] R.K. Ellis, I. Hinchliffe, M. Soldate, and J.J. van der Bij, Nucl. Phys. **B297** (1988) 221;
U. Baur and E.W.N. Glover, Nucl. Phys. **B339** (1990) 38.

[20] D. Graudenz, M. Spira and P.M. Zerwas, Phys. Rev. Lett. **70** (1993) 1372;
M. Spira, A. Djouadi, D. Graudenz and P. M. Zerwas, Nucl. Phys. B **453** (1995) 17 [hep-ph/9504378];
A. Djouadi, M. Spira and P.M. Zerwas, Z. Phys. C **70** (1996) 427 [hep-ph/9511344];
M. Spira, Fortsch. Phys. **46** (1998) 203 [hep-ph/9705337].

[21] S. Dawson, Nucl. Phys. B **359** (1991) 283.

[22] R. V. Harlander, W. B. Kilgore, Phys. Rev. Lett. **88** (2002) 201801 [hep-ph/0201206];
C. Anastasiou, K. Melnikov, Nucl. Phys. **B646** (2002) 220 [hep-ph/0207004]; V. Ravindran, J. Smith, W. L. van Neerven, Nucl. Phys. **B665** (2003) 325 [hep-ph/0302135].

[23] C. Anastasiou, K. Melnikov, F. Petriello, Nucl. Phys. **B724** (2005) 197 [hep-ph/0501130];

[24] C. Anastasiou, G. Dissertori, F. Stockli, JHEP **0709** (2007) 018 [arXiv:0707.2373].

[25] M. Grazzini, JHEP **0802** (2008) 043 [arXiv:0801.3232].

[26] D. de Florian, M. Grazzini, Z. Kunszt, Phys. Rev. Lett. **82** (1999) 5209 [hep-ph/9902483];
V. Ravindran, J. Smith, W. L. Van Neerven, Nucl. Phys. **B634** (2002) 247 [hep-ph/0201114]. C. J. Glosser and C. R. Schmidt, JHEP **0212** (2002) 016 [hep-ph/0209248].

[27] R. V. Harlander, T. Neumann, K. J. Ozeren and M. Wiesemann, JHEP **1208** (2012) 139 [arXiv:1206.0157 [hep-ph]].

[28] V. Del Duca, A. Frizzo and F. Maltoni, JHEP **0405** (2004) 064 [hep-ph/0404013].

[29] L. J. Dixon, E. W. N. Glover, V. V. Khoze, JHEP **0412** (2004) 015 [hep-th/0411092];
S. D. Badger, E. W. N. Glover and V. V. Khoze, JHEP **0503** (2005) 023 [hep-th/0412275].

[30] S. D. Badger and E. W. N. Glover, Nucl. Phys. Proc. Suppl. **160** (2006) 71 [hep-ph/0607139]. L. J. Dixon, Y. Sofianatos, JHEP **0908** (2009) 058 [arXiv:0906.0008];
S. Badger, E. W. N. Glover, P. Mastrolia, C. Williams, JHEP **1001** (2010) 036 [arXiv:0909.4475];
S. Badger, J. M. Campbell, R. K. Ellis, C. Williams, JHEP **0912** (2009) 035 [arXiv:0910.4481].

[31] C. R. Schmidt, Phys. Lett. B **413** (1997) 391 [hep-ph/9707448].

[32] F.V. Tkachov, Phys. Lett. **100B** (1981) 65.

[33] K.G. Chetyrkin and F.V. Tkachov, Nucl. Phys. **B192** (1981) 159.

[34] T. Gehrmann and E. Remiddi, Nucl. Phys. **B601** (2001) 248 [hep-ph/0008287];

[35] T. Gehrmann and E. Remiddi, Nucl. Phys. **B601** (2001) 287 [hep-ph/0101124].

[36] T. Gehrmann, M. Jaquier, E. W. N. Glover and A. Koukoutsakis, JHEP **1202** (2012) 056 [arXiv:1112.3554 [hep-ph]].

[37] G. P. Lepage, J. Comput. Phys. **27** (1978) 192.

[38] S. Catani, M. Grazzini, Phys. Rev. Lett. **98** (2007) 222002. [hep-ph/0703012].

[39] S. Catani, L. Cieri, G. Ferrera, D. de Florian and M. Grazzini, Phys. Rev. Lett. **103** (2009) 082001 [arXiv:0903.2120 [hep-ph]]. S. Catani, G. Ferrera and M. Grazzini, JHEP **1005** (2010) 006 [arXiv:1002.3115 [hep-ph]].

[40] G. Ferrera, M. Grazzini and F. Tramontano, Phys. Rev. Lett. **107** (2011) 152003 [arXiv:1107.1164 [hep-ph]].

[41] S. Catani, L. Cieri, D. de Florian, G. Ferrera and M. Grazzini, Phys. Rev. Lett. **108** (2012) 072001 [arXiv:1110.2375 [hep-ph]].

[42] J. Gao, C. S. Li and H. X. Zhu, Phys. Rev. Lett. **110** (2013) 4, 042001 [arXiv:1210.2808 [hep-ph]].

[43] T. Binoth and G. Heinrich, Nucl. Phys. B **585** (2000) 741 [hep-ph/0004013], Nucl. Phys. B **693** (2004) 134 [hep-ph/0402265];
C. Anastasiou, K. Melnikov and F. Petriello, Phys. Rev. D **69** (2004) 076010 [hep-ph/0311311];
G. Heinrich, Int. J. Mod. Phys. A **23** (2008) 1457 [arXiv:0803.4177];
J. Carter and G. Heinrich, Comput. Phys. Commun. **182** (2011) 1566 [arXiv:1011.5493];

[44] C. Anastasiou, F. Herzog, A. Lazopoulos, JHEP **1103** (2011) 038. [arXiv:1011.4867]; [arXiv:1110.2368].

[45] C. Anastasiou, K. Melnikov and F. Petriello, Phys. Rev. Lett. **93** (2004) 262002 [hep-ph/0409088].

[46] K. Melnikov and F. Petriello, Phys. Rev. D **74** (2006) 114017 [hep-ph/0609070].

[47] M. Czakon, Phys. Lett. B **693** (2010) 259 [arXiv:1005.0274 [hep-ph]]. M. Czakon and D. Heymes, Nucl. Phys. B **890** (2014) 152 [arXiv:1408.2500 [hep-ph]].

[48] P. Bärnreuther, M. Czakon and A. Mitov, Phys. Rev. Lett. **109** (2012) 132001 [arXiv:1204.5201 [hep-ph]]. M. Czakon and A. Mitov, JHEP **1301** (2013) 080 [arXiv:1210.6832 [hep-ph]].

[49] A. Gehrmann-De Ridder, T. Gehrmann, E. W. N. Glover, JHEP **0509** (2005) 056 [hep-ph/0505111];

[50] A. Daleo, T. Gehrmann, D. Maitre, JHEP **0704** (2007) 016 [hep-ph/0612257];

[51] A. Daleo, A. Gehrmann-De Ridder, T. Gehrmann, G. Luisoni, JHEP **1001** (2010) 118 [arXiv:0912.0374];
R. Boughezal, A. Gehrmann-De Ridder, M. Ritzmann, JHEP **1102** (2011) 098 [arXiv:1011.6631];
T. Gehrmann, P. F. Monni, [arXiv:1107.4037].

[52] E. W. N. Glover, J. Pires, JHEP **1006** (2010) 096 [arXiv:1003.2824].

[53] A. Gehrmann-De Ridder, T. Gehrmann, E. W. N. Glover, G. Heinrich, JHEP **0711** (2007) 058 [arXiv:0710.0346].

[54] S. Weinzierl, JHEP **0907** (2009) 009 [arXiv:0904.1145];

[55] J. Currie, A. Gehrmann-De Ridder, E. W. N. Glover and J. Pires, JHEP **1401** (2014) 110 [arXiv:1310.3993 [hep-ph]].

[56] X. Chen, T. Gehrmann, E. W. N. Glover and M. Jaquier, Phys. Lett. B **740** (2015) 147 [arXiv:1408.5325 [hep-ph]].

[57] R. Boughezal, K. Melnikov and F. Petriello, Phys. Rev. D **85** (2012) 034025 [arXiv:1111.7041 [hep-ph]].

[58] M. Brucherseifer, F. Caola and K. Melnikov, JHEP **1304** (2013) 059 [arXiv:1301.7133 [hep-ph]].

[59] R. Boughezal, F. Caola, K. Melnikov, F. Petriello and M. Schulze, JHEP **1306** (2013) 072 [arXiv:1302.6216].

[60] H. Fritzsch, M. Gell-Mann and H. Leutwyler, Phys. Lett. B **47** (1973) 365. S. Weinberg, Phys. Rev. Lett. **31** (1973) 494.

[61] D. J. Gross and F. Wilczek, Phys. Rev. D **8** (1973) 3633.

[62] L. D. Faddeev and V. N. Popov, Phys. Lett. B **25** (1967) 29.

[63] S. L. Glashow, Nucl. Phys. **22** (1961) 579. A. Salam, in *Elementary Particle Theory*, ed. N. Svartholm, Almquist and Forlag, Stockholm (1968). S. Weinberg, Phys. Rev. Lett. **19** (1967) 1264.

[64] K. G. Chetyrkin, B. A. Kniehl and M. Steinhauser, Nucl. Phys. B **510** (1998) 61 [hep-ph/9708255].

[65] M. L. Mangano, S. J. Parke and Z. Xu, FERMILAB-CONF-87-078-T, C87-03-01.

[66] F. A. Berends and W. Giele, Nucl. Phys. B **294** (1987) 700. M. L. Mangano, S. J. Parke and Z. Xu, Nucl. Phys. B **298** (1988) 653.

[67] P. Cvitanovic, P. G. Lauwers and P. N. Scharbach, Nucl. Phys. B **186** (1981) 165. D. A. Kosower, Nucl. Phys. B **315** (1989) 391.

[68] M. L. Mangano, Nucl. Phys. B **309** (1988) 461.

[69] L. J. Dixon, Proceedings of TASI'94 "QCD & Beyond", ed. D. Soper, World Scientific, 1995, p. 539 [hep-ph/9601359].

[70] G. P. Korchemsky and G. F. Sterman, Nucl. Phys. B **437** (1995) 415 [hep-ph/9411211]. Y. L. Dokshitzer and B. R. Webber, Phys. Lett. B **352** (1995) 451 [hep-ph/9504219]. R. Akhoury and V. I. Zakharov, Phys. Lett. B **357** (1995) 646 [hep-ph/9504248]. P. Ball, M. Beneke and V. M. Braun, Nucl. Phys. B **452** (1995) 563 [hep-ph/9502300]. Y. L. Dokshitzer, G. Marchesini and B. R. Webber, Nucl. Phys. B **469** (1996) 93 [hep-ph/9512336]. E. Gardi, Nucl. Phys. B **622** (2002) 365 [hep-ph/0108222].

[71] J. B. Babcock and R. E. Cutkosky, Nucl. Phys. B **176** (1980) 113. A. Backer, Z. Phys. C **12** (1982) 161. J. Dorfan, Z. Phys. C **7** (1981) 349. H. J. Daum, H. Meyer and J. Burger, Z. Phys. C **8** (1981) 167. K. Lanius, H. E. Roloff and H. Schiller, Z. Phys. C **8** (1981) 251.

[72] S. D. Ellis and D. E. Soper, Phys. Rev. D **48** (1993) 3160 [hep-ph/9305266].

[73] M. Wobisch and T. Wengler, In *Hamburg 1998/1999, Monte Carlo generators for HERA physics* 270-279 [hep-ph/9907280]. M. Wobisch, DESY-THESIS-2000-049.

[74] M. Cacciari, G. P. Salam and G. Soyez, JHEP **0804** (2008) 063 [arXiv:0802.1189 [hep-ph]].

[75] N. N. Bogoliubov, O. S. Parasiuk and , Acta Math. **97** (1957) 227. K. Hepp, Commun. Math. Phys. **2** (1966) 301. W. Zimmermann, in Deser, et. al. (1970).

[76] W. A. Bardeen, A. J. Buras, D. W. Duke and T. Muta, Phys. Rev. D **18** (1978) 3998.

[77] M. Gell-Mann and F. E. Low, Phys. Rev. **95** (1954) 1300. E. C. G. Stueckelberg and A. Petermann, Helv. Phys. Acta **26** (1953) 499.

[78] H. D. Politzer, Phys. Rept. **14** (1974) 129.

[79] A. Bassetto, M. Ciafaloni and G. Marchesini, Phys. Rept. **100** (1983) 201. M. L. Mangano and S. J. Parke, FERMILAB-CONF-87-121-T, C87-06-25. F. A. Berends and W. T. Giele, Nucl. Phys. B **313** (1989) 595.

[80] G. Altarelli and G. Parisi, Nucl. Phys. B **126** (1977) 298.

[81] A. Gehrmann-De Ridder and E. W. N. Glover, Nucl. Phys. B **517** (1998) 269 [hep-ph/9707224].

[82] J. M. Campbell and E. W. N. Glover, Nucl. Phys. B **527** (1998) 264 [hep-ph/9710255].

[83] S. Catani and M. Grazzini, Phys. Lett. B **446** (1999) 143 [hep-ph/9810389].

[84] S. Catani and M. Grazzini, Nucl. Phys. B **570** (2000) 287 [hep-ph/9908523].

[85] Z. Bern, V. Del Duca and C. R. Schmidt, Phys. Lett. B **445** (1998) 168 [hep-ph/9810409].

[86] Z. Bern, V. Del Duca, W. B. Kilgore and C. R. Schmidt, Phys. Rev. D **60** (1999) 116001 [hep-ph/9903516].

[87] S. Catani and M. Grazzini, Nucl. Phys. B **591** (2000) 435 [hep-ph/0007142].

[88] S. Catani, Phys. Lett. **B427** (1998) 161 [hep-ph/9802439].

[89] G. Sterman and M. E. Tejeda-Yeomans, Phys. Lett. B **552** (2003) 48 [hep-ph/0210130]; T. Becher and M. Neubert, Phys. Rev. Lett. **102** (2009) 162001 [arXiv:0901.0722]; E. Gardi and L. Magnea, JHEP **0903** (2009) 079 [arXiv:0901.1091].

[90] T. Kinoshita, J. Math. Phys. **3** (1962) 650. T. D. Lee and M. Nauenberg, Phys. Rev. **133** (1964) B1549. E. C. Poggio and H. R. Quinn, Phys. Rev. D **14** (1976) 578. G. F. Sterman, Phys. Rev. D **14** (1976) 2123.

[91] V. N. Gribov and L. N. Lipatov, Sov. J. Nucl. Phys. **15** (1972) 438 [Yad. Fiz. **15** (1972) 781]. Y. L. Dokshitzer, Sov. Phys. JETP **46** (1977) 641 [Zh. Eksp. Teor. Fiz. **73** (1977) 1216].

[92] G. Curci, W. Furmanski and R. Petronzio, Nucl. Phys. B **175** (1980) 27. W. Furmanski and R. Petronzio, Phys. Lett. B **97** (1980) 437. E. G. Floratos, D. A. Ross and C. T. Sachrajda, Nucl. Phys. B **129** (1977) 66 [Erratum-ibid. B **139** (1978) 545]. E. G. Floratos, D. A. Ross and C. T. Sachrajda, Nucl. Phys. B **152** (1979) 493.

[93] F. A. Berends and W. T. Giele, Nucl. Phys. B **306** (1988) 759.

[94] T. Binoth, E. W. N. Glover, P. Marquard and J. J. van der Bij, JHEP **0205** (2002) 060 [hep-ph/0202266].

[95] Z. Xu, D. H. Zhang and L. Chang, Nucl. Phys. B **291** (1987) 392.

[96] F. A. Berends, R. Kleiss and S. Jadach, Nucl. Phys. B **202** (1982) 63; F. A. Berends, R. Kleiss, P. de Causmaecker, R. Gastmans, W. Troost and T. T. Wu [CALKUL Collaboration], Nucl. Phys. B **239** (1984) 382, **239** (1984) 395.

[97] C. Studerus, Comput. Phys. Commun. **181** (2010) 1293. [arXiv:0912.2546].

[98] S. Laporta, Int. J. Mod. Phys. A **15** (2000) 5087 [hep-ph/0102033].

[99] T. Gehrmann and E. Remiddi, Nucl. Phys. **B580** (2000) 485 [hep-ph/9912329].

[100] E. Remiddi and J.A.M. Vermaseren, Int. J. Mod. Phys. **A15** (2000) 725 [hep-ph/9905237].

[101] N. Nielsen, Nova Acta Leopoldiana (Halle) **90** (1909) 123; K.S. Kölbig, J.A. Mignaco and E. Remiddi, BIT **10** (1970) 38.

[102] T. Gehrmann and E. Remiddi, Comput. Phys. Commun. **141** (2001) 296 [hep-ph/0107173]; Comput. Phys. Commun. **144** (2002) 200 [hep-ph/0111255];

[103] J. Vollinga, S. Weinzierl, Comput. Phys. Commun. **167** (2005) 177. [hep-ph/0410259]; D. Maître, Comput. Phys. Commun. **174** (2006) 222 [hep-ph/0507152]; S. Bühler, C. Duhr, [arXiv:1106.5739].

[104] L.W. Garland, T. Gehrmann, E.W.N. Glover, A. Koukoutsakis and E. Remiddi, Nucl. Phys. B **627** (2002) 107 [hep-ph/0112081] and **642** (2002) 227 [hep-ph/0206067].

[105] A. Gehrmann-De Ridder, T. Gehrmann, E.W.N. Glover and G. Heinrich, Phys. Rev. Lett. **99** (2007) 132002 [arXiv:0707.1285]; JHEP **0712** (2007) 094 [arXiv:0711.4711]; Phys. Rev. Lett. **100** (2008) 172001 [arXiv:0802.0813]; JHEP **0905** (2009) 106 [arXiv:0903.4658].

[106] S. Weinzierl, Phys. Rev. Lett. **101** (2008) 162001 [arXiv:0807.3241]; JHEP **0906** (2009) 041 [arXiv:0904.1077]; JHEP **0907** (2009) 009 [arXiv:0904.1145]; Phys. Rev. D **80** (2009) 094018 [0909.5056]. Eur. Phys. J. C **71** (2011) 1565 [arXiv:1011.6247].

[107] T. Gehrmann and L. Tancredi, [arXiv:1112.1531].

[108] P. Nogueira, J. Comput. Phys. **105** (1993) 279.

[109] C.G. Bollini and J.J. Giambiagi, Nuovo Cim. **12B** (1972) 20.

[110] G.M. Cicuta and E. Montaldi, Nuovo Cim. Lett. **4** (1972) 329.

[111] G. 't Hooft and M. Veltman, Nucl. Phys. **B44** (1972) 189.

[112] J.A.M. Vermaseren, *New features of FORM*, math-ph/0010025; Nucl. Phys. Proc. Suppl. **183** (2008) 19 [0806.4080].

[113] T. Gehrmann and E. Remiddi, Nucl. Phys. B **640** (2002) 379 [hep-ph/0207020].

[114] R. V. Harlander and W. B. Kilgore, Phys. Rev. D **64**, 013015 (2001) [hep-ph/0102241].

[115] R. J. Gonsalves, Phys. Rev. D **28** (1983) 1542. G. Kramer and B. Lampe, J. Math. Phys. **28** (1987) 945. T. Gehrmann, T. Huber and D. Maitre, Phys. Lett. B **622** (2005) 295 [hep-ph/0507061]. P. A. Baikov, K. G. Chetyrkin, A. V. Smirnov, V. A. Smirnov and M. Steinhauser, Phys. Rev. Lett. **102** (2009) 212002 [arXiv:0902.3519 [hep-ph]]. T. Gehrmann, E. W. N. Glover, T. Huber, N. Ikizlerli and C. Studerus, JHEP **1006** (2010) 094 [arXiv:1004.3653 [hep-ph]].

[116] C. Duhr, T. Gehrmann and M. Jaquier, JHEP **1502** (2015) 077 [arXiv:1411.3587 [hep-ph]].

[117] J. M. Henn, Phys. Rev. Lett. **110** (2013) 25, 251601 [arXiv:1304.1806 [hep-th]].

[118] C. Duhr and T. Gehrmann, Phys. Lett. B **727** (2013) 452 [arXiv:1309.4393 [hep-ph]].

[119] G. Abelof and A. Gehrmann-De Ridder, JHEP **1104** (2011) 063 [arXiv:1102.2443 [hep-ph]]. G. Abelof and A. Gehrmann-De Ridder, JHEP **1204** (2012) 076 [arXiv:1112.4736 [hep-ph]]. G. Abelof and A. Gehrmann-De Ridder, JHEP **1211** (2012) 074 [arXiv:1207.6546 [hep-ph]]. G. Abelof, O. Dekkers and A. Gehrmann-De Ridder, JHEP **1212** (2012) 107 [arXiv:1210.5059 [hep-ph]].

[120] D. A. Kosower, Phys. Rev. D **57** (1998) 5410 [hep-ph/9710213].

[121] D. A. Kosower, Phys. Rev. D **71** (2005) 045016 [hep-ph/0311272].

[122] D. A. Kosower, Phys. Rev. D **67** (2003) 116003 [hep-ph/0212097].

[123] A. Gehrmann-De Ridder, T. Gehrmann, E. W. N. Glover and J. Pires, JHEP **1302** (2013) 026 [arXiv:1211.2710 [hep-ph]].

[124] J. Currie, E. W. N. Glover and S. Wells, JHEP **1304** (2013) 066 [arXiv:1301.4693 [hep-ph]].

[125] E. W. Nigel Glover and J. Pires, JHEP **1006** (2010) 096 [arXiv:1003.2824 [hep-ph]].

[126] J. F. Gunion and Z. Kunszt, Phys. Lett. B **161** (1985) 333.

[127] S. Dawson and R. P. Kauffman, Phys. Rev. Lett. **68** (1992) 2273.

[128] J. R. Ellis, M. K. Gaillard and D. V. Nanopoulos, Nucl. Phys. B **106** (1976) 292. M. A. Shifman, A. I. Vainshtein, M. B. Voloshin and V. I. Zakharov, Sov. J. Nucl. Phys. **30** (1979) 711 [Yad. Fiz. **30** (1979) 1368]. L. Okun, *Leptons and Quarks*, Ed. North Holland, Amsterdam 1982. M. B. Gavela, G. Girardi, C. Malleville and P. Sorba, Nucl. Phys. B **193** (1981) 257.

[129] A. Gehrmann-De Ridder, E. W. N. Glover and J. Pires, JHEP **1202** (2012) 141 [arXiv:1112.3613 [hep-ph]].

[130] M. R. Whalley, D. Bourilkov and R. C. Group, hep-ph/0508110.

[131] A. D. Martin, W. J. Stirling, R. S. Thorne and G. Watt, Eur. Phys. J. C **63** (2009) 189 [arXiv:0901.0002 [hep-ph]].

[132] R. D. Ball, V. Bertone, S. Carrazza, C. S. Deans, L. Del Debbio, S. Forte, A. Guffanti and N. P. Hartland *et al.*, Nucl. Phys. B **867** (2013) 244 [arXiv:1207.1303 [hep-ph]].

[133] G. Aad *et al.* [ATLAS Collaboration], JHEP **1409** (2014) 112 [arXiv:1407.4222].

[134] D. de Florian, M. Grazzini, Z. Kunszt, Phys. Rev. Lett. **82** (1999) 5209 [hep-ph/9902483]; V. Ravindran, J. Smith, W.L. Van Neerven, Nucl. Phys. **B634** (2002) 247 [hep-ph/0201114].

[135] C. Balazs and C.P. Yuan, Phys. Lett. B **478** (2000) 192 [hep-ph/0001103]; G. Bozzi, S. Catani, D. de Florian and M. Grazzini, Nucl. Phys. B **737** (2006) 73 [hep-ph/0508068]; V. Ahrens, T. Becher, M. Neubert and L. L. Yang, Eur. Phys. J. C **62** (2009) 333 [arXiv:0809.4283]; D. de Florian, G. Ferrera, M. Grazzini and D. Tommasini, JHEP **1111** (2011) 064 [arXiv:1109.2109]; JHEP **1206** (2012) 132 [arXiv:1203.6321].

[136] J. M. Campbell, R. K. Ellis and C. Williams, Phys. Rev. D **81** (2010) 074023 [arXiv:1001.4495 [hep-ph]].

[137] J. Alwall, R. Frederix, S. Frixione, V. Hirschi, F. Maltoni, O. Mattelaer, H.-S. Shao and T. Stelzer *et al.*, JHEP **1407** (2014) 079 [arXiv:1405.0301 [hep-ph]].